SURFACE FUNCTIONALISATION OF POLYMERS FOR TISSUE ENGINEERING: EFFICACY OF PHOSPHORYLATED POLY (HYDROXY ETHYL METHACRYLATE-CO-METHYL METHACRYLATE) FOR BIOMIMETIC MINERALIZATION OF CALCIUM PHOSPHATE PHASE AND ITS FUNCTIONALITY ASSESSMENT- *IN VITRO AND IN VIVO*

G. S. SAILAJA

for the award of the degree
of

DOCTOR OF PHILOSOPHY

SREE CHITRA TIRUNAL INSTITUTE FOR MEDICAL SCIENCES AND TECHNOLOGY
LIBRARY
THIRUVANANTHAPURAM

SREE CHITRA TIRUNAL INSTITUTE FOR MEDICAL SCIENCES AND TECHNOLOGY

THIRUVANANTHAPURAM – 695 012

JULY 2007

DECLARATION

I, G.S. SAILAJA, hereby declare that I had personally carried out the work depicted in the thesis entitled "Surface functionalisation of polymers for Tissue engineering: Efficacy of phosphorylated poly (hydroxy ethyl methacrylate-co-methyl methacrylate) for Biomimetic mineralization of calcium phosphate phase and its functionality assessment- *in vitro and in vivo*" under the direct supervision of Dr. H.K. VARMA, Scientist-In-charge, Bioceramics Laboratory, Biomedical Technology wing, Sree Chitra Tirunal Institute for Medical Sciences and Technology, Thiruvananthapuram, Kerala, India, except where external help sought are acknowledged.

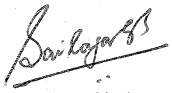

G.S. Sailaja

Tele: 0471-2340801
Fax : 0471-2341814

Grams: CHITRAMET
Telex : 0435-6290

श्री चित्रा तिरुनाल आयुर्विज्ञान तथा प्रौद्योगिकी संस्थान
बायो मेडिकल टैक्नोलॉजी विंग
पूजापुरा, तिरुवनन्तपुरम-695 012, इन्डिया

SREE CHITRA TIRUNAL INSTITUTE FOR MEDICAL SCIENCES AND TECHNOLOGY
BIO MEDICAL TECHNOLOGY WING
POOJAPPURA, THIRUVANANTHAPURAM-695 012, INDIA
(An Institute of National Importance under Govt. of India)

Ref:

Date: 20.07.07

CERTIFICATE

This is to certify that **Ms. G.S. Sailaja**, in the Bioceramic Laboratory of this institute, has fulfilled the requirements of the regulations relating the nature and prescribed period of research for the Ph.D degree of the Sree Chitra unal Institute for Medical Sciences and Technology, Thiruvananthapuram. The work relating to her thesis entitled **"Surface functionalisation of polymers for Tissue engineering: Efficacy of phosphorylated poly (hydroxy ethyl methacrylate-co-methyl methacrylate) for Biomimetic mineralization of calcium phosphate phase and its functionality assessment-** ***in vitro and in vivo*****"** was carried out under my direct supervision.

Dr.H.K.VARMA
(Research Supervisor)

The Thesis

Entitled

SURFACE FUNCTIONALISATION OF POLYMERS FOR TISSUE ENGINEERING: EFFICACY OF PHOSPHORYLATED POLY (HYDROXY ETHYL METHACRYLATE-CO-METHYL METHACRYLATE) FOR BIOMIMETIC MINERALIZATION OF CALCIUM PHOSPHATE PHASE AND ITS FUNCTIONALITY ASSESSMENT- *IN VITRO AND IN VIVO*

Submitted

by

G.S. Sailaja

for

Doctor of Philosophy

of

**SREE CHITRA TIRUNAL INSTITUTE
FOR
MEDICAL SCIENCES & TECHNOLOGY**

TRIVANDRUM

evaluated and approved
by

Dr. H. K. Varma
(Guide)

(Names of Thesis Examiner)

"Surface functionalisation of polymers for Tissue engineering: Efficacy of phosphorylated poly (hydroxy ethyl methacrylate-co-methyl methacrylate) for Biomimetic mineralization of calcium phosphate phase and its functionality assessment- in vitro and in vivo"

To

My husband...

CONTENTS

ACKNOWLEDGEMENTS

This work was carried out at the Bioceramics Laboratory of Sree Chitra Tirunal Institute for Medical Sciences and Technology (SCTIMST), Thiruvananthapuram, India under the financial support of CSIR, Govt. of India during the years 2002-2007. I take this opportunity to convey my sincere thanks to CSIR and SCTIMST for the financial support and infrastructure respectively.

It is my proud privilege to express my deepest gratitude to my supervisor, Dr. H.K. Varma for his optimistic and enthusiastic attitude towards research and his brilliant perception in the field of bone substitute materials that encouraged for me towards the successful completion of this work. I specially acknowledge him for his logical outlook, excellent sense of humour, and the infinite degree of freedom he has offered to me all the way through my research period.

I am obliged to Prof. K. Mohan Das, Director, SCTIMST for his whole- hearted, sincere and kind attitude towards me. I am grateful to Dr. G.S. Bhuvaneswhar, Head Biomedical Technology Wing, of SCTIMST for kindly providing me all the necessary support for accomplishing this venture. I am indebted to him further for his kind and wonderful guidance as my Doctoral Advisory Committee (DAC) member.

I am very much grateful to Dr. Mira Mohanty, Dr. P. Ramesh and Dr. K. Sreenivasan, my DAC members for their continuous support all through my PhD period.

I specially thank Dr. Mira Mohanty for being extremely kind towards me to teach the basics of histopathology and her earnest efforts in analyzing the histopathology results.

I bow my head before Dr. P. Ramesh, for introducing me to the fascinating world of biomaterials. I am exceptionally thankful to him for finding time for creative discussions, which helped me to mould my research outlook. Further, I am thankful to him for his critical and efficient review of this thesis.

I am really indebted to Dr. Balagopal N Nair for his enormous help and great suggestions in fulfilling this work as it is. I am much obliged to Mr. David Pritchard for his kind teaching and help in obtaining the UV-VIS and AAS results. Also my friends at Curtin University, Mr. T. Das and Ms. F. Lee are gratefully acknowledged for the AFM results.

I am sincerely indebted to Dr.Sunil.K.Narayanankutty for his kind inspiration throughout my life.

I am really thankful to Dr. T.V. Kumary for teaching me the fundamentals of cell culture and related aspects.

I am grateful to Dr. A.C. Fernandez for his sincere efforts in providing the experimental animals in time. I thank Dr. P.V.Mohanan for his honest efforts to conduct the bone-implantation surgeries in time.

I owe my heartfelt gratitude to Mr. S. Suresh Babu for his kind and sincere guidance in the analytical chemistry. I thank Dr. Manoj Komath and Mr. S. Vijayan for their immense help throughout this work. I thank my colleagues in Bioceramics Lab, Mr. Mohandas and Mr. Sreekanth for their fruitful co-operation.

I am thankful to Mr. Ramesh Babu and Mr. Rajalingam for their kind efforts for making moulds and Mr. R. Sreekumar for SEM analysis.

I am really grateful to Mrs. Sulekha baby for her sincere efforts to teach me histopathological work. I thank Mrs. Usha Vasudev for her help in cell culture works

I express my heartfelt thanks to my colleagues, Dr. Nirmala Simon, Dr Rekha M.R. , Mr. S. Sajeesh, Dr. P.R. Anilkumar, Ms. Divya, Ms. Viji Varghese, Ms. Bindu, Mr. Joseph, Mr. Tilak prasad, Mr. Giju Skaria, for their kind help in hard times.

I would like to thank my family- my parents for their great support. I feel myself lucky to have my parents for being so understanding and supporting all through my life.

Finally, I want to express my deepest gratitude to my husband without his never-failing love and motivation, this work would not have been accomplished. I am blessed to have a person like him as a constant inspiration throughout my life.

G.S. Sailaja

LIST OF FIGURES

LIST OF TABLES

ABBREVIATIONS

AAS	Atomic absorption spectroscopy
AFM	Atomic force microscopy
DMA	Dynamic mechanical analysis
DSC	Differential scanning calorimetry
DTA	Differential thermal analysis
EDS	Energy dispersive spectrum
EVA	Ethylene vinyl acetate
HAP	Hydroxyapatite
HEMA	2-Hydroxy ethyl methacrylate
HOS cells	Human osteosarcoma cells
MMA	Methyl methacrylate
PET	Poly(ethylene terephthalate)
PHEMA	Poly(hydroxy ethyl methacrylate)
PMMA	Poly(methyl methacrylate)
POLY(HEMA-CO-MMA)	Poly(hydroxy ethyl methacrylate-co methyl methacrylate)
PVA	Poly(vinyl alcohol)
SAED	Selected area diffraction pattern
SBF	Simulated body fluid
SEM	Scanning electron microscopy
TEM	Transmission electron microscopy
T_g	Glass transition temperature
TGA	Thermogravimetric analysis
XPS	X-ray photoelectron spectroscopy
XRD	X-ray diffraction pattern

SYNOPSIS

INTRODUCTION

Biomineralization is a natural process that gives rise to small as well as large inorganic based structures of life [1]. Biomimetic mineralization could be defined as '*mimicking the basic conditions required for biomineralization through synthetic approaches*'. The rationale behind applying this concept in the area of bone tissue engineering is the achievement of biomolecular or surface functional group recognition in the *in vivo* environment through surface or bulk modification of biomaterials [2]. It could be understood from several reports that, surface functionalization can serve as a solution towards imparting biomimetic growth of calcium phosphate on biocompatible polymeric substrates [3-6]. Hence this paradigm could be extended to develop biomimetic materials that can serve as a better functional bone graft material. The special research interest on the biomimetic mineralization of calcium phosphate on surface functionalized polymers has evolved from the basic understanding of the structure and composition of bone tissue. Bone is an organic-inorganic hybrid structure with 58% mineralized part, namely hydroxyapatite, the most stable form of calcium phosphate [7]. The clinical success of a bone implant requires the simultaneous achievement of a stable interface with host tissue and a matching of the mechanical properties between the implant and the host tissue [8].

Poly(methyl methacrylate), PMMA is a clinically significant polymer widely used as bone cement for the fixation of joint prostheses [9-11]. However, in the *in vivo* environment, PMMA is isolated from the surrounding tissues by a layer of fibrous tissue formed around it, which obviously eliminates bonding with

the host bone and eventually promotes stress shielding and implant loosening [12,13]. Hence it becomes a highly significant need to eliminate the fibrous tissue encapsulation of PMMA to improve its efficacy towards bone bonding. One of the versatile strategies to achieve biomimetic interface is through imparting active anionic functional groups such as Si-OH, -COOH, $-PO_4$ on the polymer surfaces that will help the nucleation and growth of calcium phosphate phase under simulated physiological fluid [14-17]. Moreover, the biomimetic surfaces have a significant role in enhancing viability and adhesion of cells [18,19]. However, the *in vivo* behaviour of functioanlized polymers is hardly explored.

It has been observed by several investigators that functionalized polymers with surface bound phosphate group induces *in vitro* nucleation of calcium phosphate crystals on their surface under simulated physiological environment [14, 20, 21, 22]. Tanahashi and Matsuda found that phosphate group has a higher potential to induce nucleation of hydroxyapatite compared to carbonate or hydroxyl groups [23]. However, many of the surface functionalized polymers require a calcium hydroxide/calcium chloride pretreatment for the *in vitro* mineralization of calcium phosphate [14, 20, 21, 22]. Moreover the popular surface phosphorylation techniques are done at higher temperature (>100 ^{0}C), using organic solvents and catalysts [14, 20, 21, 22].

OBJECTIVES AND SCOPE OF THE PRESENT WORK

The objective of the present work is biomimetic functional modification of PMMA to impart osseointegrative property and thereby preventing the formation of fibrous tissue at the bone-implant interface.

The aims of the present study are

i) To synthesize a copolymer of methyl methacrylate, MMA with a known biocompatible comonomer with an active hydroxyl (-OH) group, namely, 2-hydroxy ethyl methacrylate, HEMA, without affecting its favorable bulk properties

ii) To functionalize the copolymer, poly(HEMA-co-MMA) by surface phosphorylation using a a phosphorylating agent capable of surface phosphorylating biocompatible polymers with hydroxyl (-OH) group, at relatively lower temperatures (<100 ^{0}C)

iii) To assess the ability of the surface phosphorylated polymer, poly(HEMA-co-MMA) to induce *in vitro* nucleation of calcium phosphate was evaluated under accelerated simulated physiological environment using 1.5xSBF (simulated body fluid).

iv) To investigate the *in vitro* cytocompatibility and cell adhesion behaviour of phosphorylated poly(hydroxy ethyl methacrylate-co-methyl methacrylate) using human osteosarcoma (HOS) cell-line.

v) To investigate the *in vivo* toxicological response of the surface phosphorylated as well as *in vitro* calcium phosphate coated polymer as per ISO 10993

vi) To evaluate the efficacy of bone bonding by short-term bone implantation in rabbit as per ISO 10993-6: 1994(E): Test for local effects after implantation, *clause 6.0: Test method for implantation in bone* using'CMW1' poly(methyl methacrylate) radiopaque bone cement (DePuy, Johnson and Johnson, England) as control material.

MATERIALS AND METHODS

THE EXPERIMENT FLOW CHART

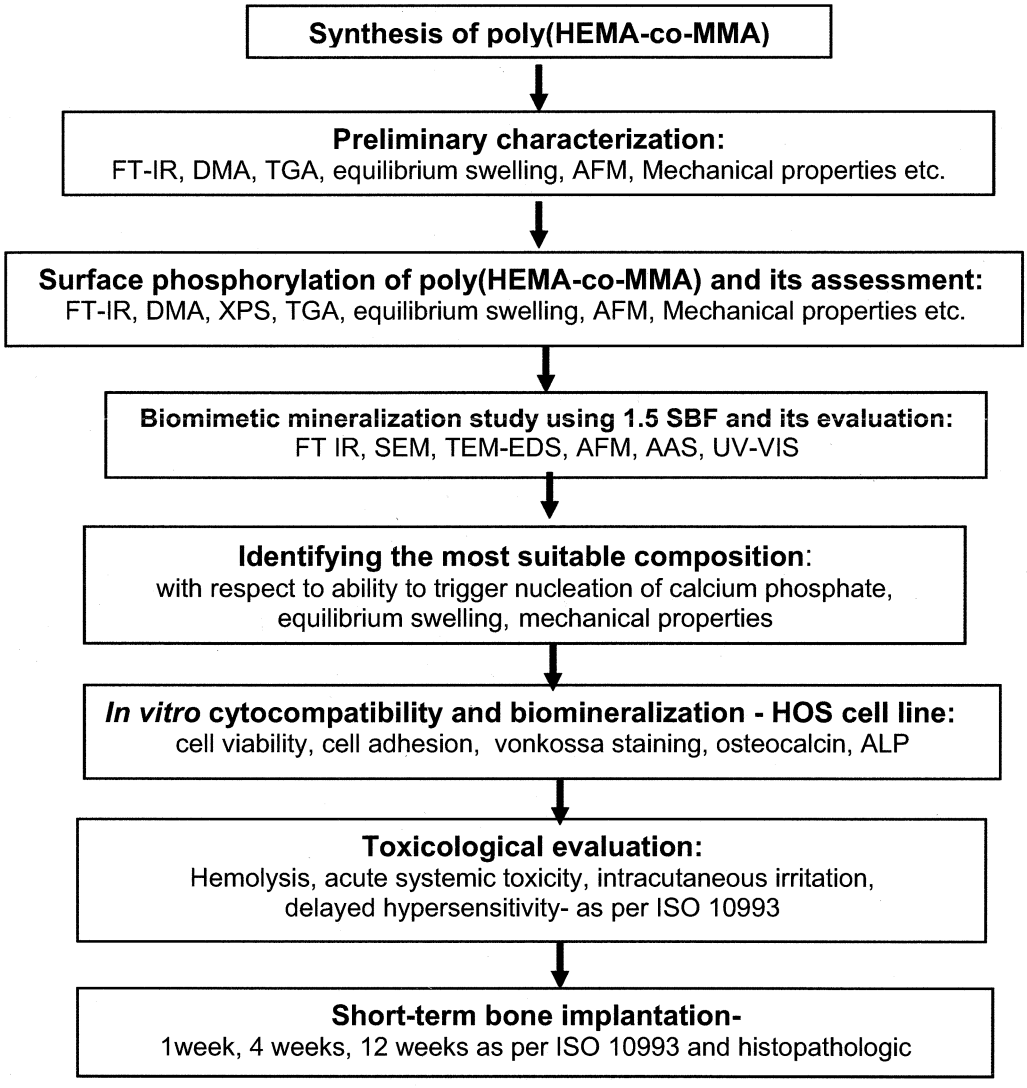

The chapter on materials and methods is divided into *three* sections.

Section I

Poly(2-hydroxy ethyl methacrylate-co-methyl methacrylate), poly(HEMA-co-MMA) was synthesized by free radical initiated bulk polymerization of the mixture of monomers, namely, 2-hydroxy ethyl methacrylate (HEMA) and methyl methacrylate (MMA) with varying molar ratio and simultaneously cross-linking by ethylene glycol dimethacrylate (EGDMA). The copolymers of HEMA: MMA with varying molar ratio such as 0.07:0.90, 0.19: 0.75, 0.38: 0.5, 0.57: 0.25 and 0.69: 0.10 represented as PH_1, PH_2, PH_3, PH_4 and PH_5 respectively were prepared as per the above-mentioned procedure.

FT-IR spectra of the samples were collected using Thermo Nicolet 5700 FT-IR microscope, Madison, WI. The glass transition temperature of PH_1 and its variation after surface phosphorylation has been assessed and compared with the neat polymers, PMMA and PHEMA using differential scanning calorimetry (DSC 2920, TA instruments Inc, USA) and storage modulus using Dynamic mechanical analyzer, (Tritec 2000 DMA machine) in tensile mode. The thermogravimetric analysis (simultaneous TGA and DTA) of the copolymers and the neat polymers, PMMA and PHEMA were performed using simultaneous DTA-TGA (model SDT 2960) TA Instruments, USA). A heating ramp of 20^0C/min from room temperature to a maximum temperature of 600^0C was used. The X-ray photoemission spectroscopy of PH_1 was performed in a KRATOS AXIS ULTRA system (Kratos Analytical, Manchester, UK). The conditions employed for wide scan are pulse energy: 80 eV, Anode: Al, emission current 12mA, scan time 120seconds, number: 4, HV: 11KV and step: 1eV. For the scanning of phosphorous peak, the conditions used are pulse energy: 20 eV, Anode: Al, emission current 12mA, scan time 60seconds, number: 4, HV: 11KV

and step: 0.1eV. The surface topography and roughness profile of PH_1 was acquired using atomic force microscope cantilevers (spring constant ≈ 0.58N/m) in the contact mode using Digital Instruments Multimode Nanoscope E, California, USA) with the software Nanoscope V 6.12 r2. The difference in the force of attraction between the unmodified polymer, surface phosphorylated polymer and the hydroxyapatite coated polymer as a function of hydrophilicity has been calculated.

Equilibrium swelling of the copolymers, PH_1, PH_2, PH_3, PH_4 and PH_5 were measured in phosphate buffer saline and compared with that of poly(HEMA). The swelling study was carried out for 336h and the equilibrium swelling degree at different intervals was calculated. The extent of cross-linking in PH_1 was varied by varying the concentration of EGDMA from 0.5 wt-% to 3.0 wt-% and the equilibrium swelling was determined. Compressive strength of PH_1 and phosphorylated PH_1 (PPH_1) was measured using Instron-3345 ,(Instron, UK) at a cross-head speed of 1mm/min (temperature $25^0 \pm 2^0$C, RH 50%). The samples were cylindrical in shape with 2mm diameter and 4 mm height.

Phosphorylation was done using 76% phosphorous pentoxide (P_2O_5). The kinetics of phosphorylation with respect to time and temperature was evaluated. The status of phosphorylation was qualitatively assessed with the help of Micro-FT-IR spectroscope while the surface bound phosphate group was quantitatively estimated using the UV-Visible spectrophotometer, Shimadzu UV mini –1240, Japan. The chemistry of surface bound phosphate group and the binding energy status of phosphorous on phosphorylated PH_1 was further studied using X-ray photoelectron spectrophotometry. The topographical variation of PH_1 as a result of phosphorylation was studied using optical microscopy, scanning electron microscopy and atomic force microscopy. Equilibrium swelling of the surface phosphoylated copolymers were measured in phosphate buffer saline and compared with that of phosphorylated poly(HEMA).

The ability of phosphorylated poly(2-HEMA-co-MMA) to induce *in vitro* mineralization of calcium phosphate under simulated physiological environment was observed with the help of accelerated conditions of simulated physiological environment, 1.5×SBF, ie., 1.5 times saturated simulated body fluid. The 1.5×SBF was prepared as per the procedure reported by Kokubo *et al* [24]. The phosporylated samples were immersed in 1.5×SBF in airtight glass containers and kept at 37^0C. The SBF solution was decanted and the bottles were filled with fresh solution after every 24h. The unmodified PH_1, poly(HEMA) and poly(MMA) were used as control samples. The samples were retrieved from SBF after 3, 10 and 15 days, washed well with deionized water and dried in an air oven at 50^0C.

The calcium phosphate coating was evaluated using scanning electron microscope (SEM Hitachi model S-2400, Japan) connected with energy dispersive X-ray analysis unit (OXFORD Link EDS system, UK) attached to SEM. Atomic force microscope (Digital Instruments Multimode Nanoscope E, California, USA) and Transmission electron microscope (Jeol 2000, Japan) coupled with Energy dispersive X-ray analysis system were used for the detailed examination of the nucleation, crystal growth profile, calcium phosphate phase and Ca/P ratio. The quantitative estimation of calcium phosphate coating was done with the help of Atomic absorption spectroscopy (Varian AA10 machine, UK) and UV-Visible spectroscopy. The calcium phosphate phase analysis was performed using wide-angle X-ray diffraction pattern using Siemens D5005 X-ray diffractometer UK).

Based on the results, the proposed method of surface phosphorylation was further investigated for the possibility phosphorylating other biocompatible polymers with inherent hydroxyl (-OH) group or modified polymers with hydroxyl group and their ability to nucleate calcium phosphate phase under accelerated simulated physiological environment. The polymers studied were Poly (vinyl alcohol) PVA, Ethylene vinyl acetate copolymer, EVA 2825 and

polyethylene terephthalate, PET. In the case of EVA 2825 and PET, controlled surface hydrolysis was carried out prior to phosphorylation in order to acquire the necessary –OH groups for phosphorylation reaction.

Poly(2-hydroxy ethyl methacrylate) is a highly hydrophilic polymer. Hence with increase in HEMA in the copolymer poly(HEMA-co-MMA), the swelling and mechanical properties of the copolymer is significantly affected . It was found that the composition with lowest HEMA content, represented as PH_1 with HEMA: MMA ratio 0.07:0.90, showed minimum degree of swelling. It was also observed that PH_1 was capable of nucleating calcium phosphate under accelerated condition of simulated physiological environment. Preliminary mechanical property evaluation also showed that PH_1 possess good compressive and tensile properties. Hence further advanced studies such as, *in vitro* cytocompatibility evaluation, toxicological evaluation and short-term bone implantation were mainly conducted only with the composition PH_1.

Section II

Section II mainly focuses on the *in vitro* cytocompatibility, biomineralization of phosphorylated poly (HEMA-co-MMA), represented as 'PPH_1' and poly (HEMA-co-MMA) coated with calcium phosphate for 15 days, represented as '$CaPH_1$' and compared with unmodified PH_1 as control material. Human osteosarcoma (HOS) cells were selected for evaluating in vitro cytocompatibility. The HOS cell-line was supplied by National Centre for Cell Sciences (NCCS), Pune, India. The ability of the polymer substrates in supporting the secretion of bone specific bone marker protein, osteocalcin was performed using biosourse h-OST EASIA kit, Europe). Alkaline phosphatase released by the cells into the medium was measured with a commercially available assay kit (Glaxo, 'Qualigens', India).

Section III

Section III solely concentrates on the biological evaluation of phosphorylated poly (HEMA-co-MMA), represented as 'PPH_1' and poly (HEMA-co-MMA) coated with calcium phosphate for 15 days, represented as '$CaPH_1$'. The hemolytic property of the material was evaluated by 'standard practice for assessment of hemolytic properties of materials as per ASTM F 756: 2000'. The intracutaneous (intradermal) reactivity assessment was performed as per ISO 10993: 2002 (E)-Biological evaluation of medical devices- part 10: test for irritation and delayed type hypersensitivity and additional tests: *clause B.2: Intracutaneous(intradermal) reactivity test.* The acute systemic toxicity was evaluated as per ISO 10993-11: 1993 (E) Test for systemic toxicity: Acute systemic toxicity: *clause 6.5.4 Acute intravenous application and clause 6.5.5 Acute intraperitoneal application.* The maximization test for delayed hypersensititvity was evaluated by ISO 10993-10: 2002 (E)-Biological evaluation of medical devices: part 10, Tests for irritation and delayed type hypersensitivity *clause 7.4: Maximization test for delayed hypersensitivity.* The efficacy of 'PPH_1' and '$CaPH_1$' towards osteointegration and bone regeneration under *in vivo* environment was evaluated by short-term bone implantation in rabbits as per ISO 10993-6: 1994(E): Test for local effects after implantation, *clause 6.0: Test method for implantation in bone*. The control material used was the clinically used 'CMW1' poly(methyl methacrylate) radiopaque bone cement (DePuy, Johnson and Johnson, England).

RESULTS AND DISCUSSION

The results and discussion part is further divided in to six chapters. The ***chapter 3.1*** describes the preliminary evaluation of the poly(HEMA-co-MMA) copolymers and the identification of suitable composition for detailed study. ***Chapter 3.2*** is about the assessment on the extent of phosphorylation by various techniques while ***chapter 3.3*** is assessment of the biomimetic mineralization of

the phosphorylated copolymers. ***Chapter 3.4*** illustrates how the proposed surface phosphorylation method can be extended to functionalize other biocomplatibile polymers like poly(vinyl alcohol), poly(ethylene) vinyl acetate copolymer and poly(ethylene terephthalate). ***Chapter 3.5*** explains the *in vitro* cytocompatibility evaluation using human osteoblast cell line and the role of surface phosphorylation in enhancing the secretion of bone specific proteins such as osteocalcin and alkaline phosphatase. The ***Chapter 3.6*** is dedicated to *in vivo* toxicological evaluation and new bone formation of the phosphorylated and calcium phosphate coated copolymers against commercially available PMMA based bone cement, CMW1 radiopaque, as the control material.

Chapter 3.1 Preliminary Characterization

The FT-IR spectra of poly(HEMA-co-MMA) compositions, PH_1, PH_2, PH_3, PH_4 and PH_5 showed the characteristic –C=O, -CH_3 and –OH peaks at 1706, 2922, 3375 cm^{-1} respectively. It is evident from the spectra that with increasing HEMA content in the composition, the intensity of the –OH peak increases. The thermogravimetric analysis of all the compositions shows similar degradation profile and the copolymers are thermally stable up to 150 ^{0}C, which offers them the required stability during phosphorylation.

The equilibrium swelling degree values demonstrate that the composition with lowest HEMA content (PH_1) showed minimum percentage of swelling i.e., <3%. However, when HEMA percentage was increased, the degree of swelling also increased PBS. For poly(HEMA) the equilibrium swelling value was found as 40% while for PH_2 (which has 25 wt-% HEMA) the equilibrium swelling was 23%. Hence, when compared to poly(HEMA), PH_1 has a very minimum swelling which is very vital aspect in determining the mechanical properties of the copolymer in the *in vitro* and *in vivo* environment. The compressive strength (stress at maximum load) of PH_1 was found as 153MPa and modulus 4.6 GPa.

Hence, based on the preliminary evaluation, the composition PH_1 was given special emphasis for further extensive studies.

Chapter 3.2 Assessment of phosphorylation

The phsophorylated poly(HEMA-co-MMA) series has shown the corresponding phosphate peak at 1073, 1023, 984 cm^{-1}, ensuring the surface coupling of phosphate group. The kinetics of phosphorylation with respect to time and temperature was evaluated by phosphorylating PH_1 at a range of time and temperature. It was observed from the FT-IR spectra that the phosphorylation begins at 15 minutes and that 60 minutes would be sufficient for the completion of the reaction. Even though the surface phosphorylation occurs at room temperature under prolonged time period, it was observed from the FT-IR spectra that the most suitable temperature for phosphorylation was at 60 ^{0}C.

The glass transition temperature (T_g) of PH_1 was found as 104.57 ^{0} using DSC. It is to be commented that the surface phosphorylation does not change the Tg of PH_1 significantly, though a very narrow shift to the lower temperature is observed (T_g of PPH_1= 103.17 ^{0}) corroborating that the basic properties of the copolymer has not changed due to surface phosphorylation. The storage modulus of PH_1 before and after phosphorylation measured using DMA illustrates that there was no variation after phosphorylation (1.75 GPa in both the cases). The presence of surface bound phosphate group was further evident from the XPS analysis. The surface topography of PH_1 has changed due to phosphorylation as viewed with atomic force microscope. The phosphate group on the polymer surface was quantitatively estimated using UV-visible spectrophotometer. It was observed that, with increase in HEMA content in poly(HEMA-co-MMA), the extent of surface bound phosphate group per surface area increased exponentially.

Chapter 3.3 Assessment of *biomimetic* mineralization

The *in vitro* mineralization was assessed qualitatively using scanning electron microscope attached with an EDS detector. The calcium phosphate coating was viewed as unique spheroid in morphology, which is characteristic feature of apatite crystals. The nucleation of the crystals begins in 3 days. Within 10 days, the surface was totally covered by a primary layer, and at the same time secondary nucleation begins. The apatite morphology was analogous to apatite structures formed on other surface functionalized biocompatible polymers [14, 15, 21, 25]. The secondary growth propagates and is complete within the next five days of immersion in SBF. It was noted that the calcium to phosphate ratio of the coating increases with increase in immersion time, which is in accordance with previous reports [14, 20]

The ultra-structural features of coating characteristics were then further evaluated using transmission electron microscopy coupled with an EDS detector. It was found that the spheroid type apatite clusters are in fact made up of nanometer size apatite rods. Another key observation with TEM was that the amorphous to crystalline phase transformation begins as early as at 3 days of immersion in SBF as viewed with the selected area diffraction pattern. Further it was also noted that initially a calcium rich apatite was formed. Kim *et al* found that on immersion in SBF, the synthetic HAP was found to induce the formation of bone-like apatite on its surface through the formation of calcium-rich amorphous calcium phosphate (ACP) in the early soaking period [26]. While comparing the present observation with this report, it could be postulated that similar event is occurring on phosphate coupled poly(HEMA-co-MMA) also. The observation with atomic force microscope showed that the crystals have an average size of 25 nm and there is an orientation in the growth of the crystals even in the early stage of 3 days. The calcium phosphate phase was confirmed as hydroxyapatite using wide angle X-ray diffraction pattern.

Chapter 3.4 **Surface phosphorylation of other biocompatible polymers**

The results proved that the surface phosphorylation of EVA-2825 and PET was possible after subjecting them to surface hydrolysis and directly in the case of PVA. It was found that the phosphorylated polymers could initiate nucleation of calcium phosphate crystals on their surface when exposed to accelerated simulated physiological condition.

Chapter 3.5 In vitro **cytocompatibility**

The HOS cells showed good viability with unmodified PH_1, phosphorylated PH_1 (PPH_1) and the apatite coated PH_1 (CaPH1) as observed qualitatively by optical micrographs at different time periods. The MTT assay performed at two different time periods, 7 days and 14 days corroborate the viability of the cells in contact with the substrates. The cells retained 70% viability. The cell adhesion behaviour was investigated using scanning electron microscope. The cell adhesion at three different time periods was observed and it was found that the all the three samples supported cell adhesion while PPH_1 retained better morphology of the cells for a longer time (14 days) compared to PH_1. The cells on PPH_1-15d formed as a cell layer which covered the apatite clusters within two weeks. The von kossa staining showed that *in vitro* mineralization of the cells was more on PPH_1 compared to PH_1.

The concentration of human osteocalcin was found to be increasing with time (7, 14 and 21 days) in all cases with highest value for PPH_1 at 21 days, which is in accordance with the specific activity profile of osteocalcin reported in literature [27]. The alkaline phosphatase activity was highest for PPH_1 at 7 days, which showed a decreasing trend in all cases. This is also in agreement with the reports showing that alkaline phosphatase is an early marker while osteocalcin is a later bone marker [28].

***Chapter 3.6 In vivo* evaluation**

Both the test materials, phosphorylated PH_1 (PPH_1) and apatite coated PH_1 ($CaPH_1$) passed the biological evaluation tests, namely hemolysis, acute systemic toxicity, intracutaneous (intradermal) irritation, maximization test for delayed hypersensitivity. The potential of negatively charged organic matrix to induce biomimetic mineralization is well documented [14, 15, 21, 25]. However, only very few reports are available on the functional evaluation and efficacy of bone bonding ability of surface functionalized materials. Goississ *et al* performed one of the significant investigations, on the biomimetic mineralization of negatively charged collagen matrix [29]. The polyanionic collagen matrix, which they have produced by hydrolysis of side chain amides of asparagines and glutamine, was capable of undergoing *in vitro* and *in vivo* mineralization (in rats).

The histopathological evaluation of the present study revealed early bone healing around the test materials, phosphorylated PH_1 (PPH_1) and apatite coated PH_1 ($CaPH_1$) compared to the control material. Macrophages and fibroblasts were present initially at one week post-implantation with evidence of new bone formation at the host bone-implant interface at four and twelve weeks of post-implantation. However, collageneous tissue with fibroblasts persisted at twelve weeks post-implantation at the host bone- control interface. However, none of the implants showed any inflammation or other toxic responses.

CONCLUSIONS

Based on the results of the present study, it could be put forwarded that the surface phosphorylation of poly(HEMA-co-MMA) enhances the nucleation and growth of calcium phosphate under simulated physiological condition. The composition with lowest HEMA content, designated as PH_1 having HEMA: MMA in the molar ratio 0.07:0.90 was found as the most suitable composition with respect to surface phosphorylation, *in vitro* nucleation of calcium phosphate,

extent of equilibrium swelling (i.e., minimum percentage swelling) and mechanical properties and hence selected for detailed evaluation. PPH_1 showed excellent cell viability and cell adhesion with HOS cells. PPH_1 also showed *in vitro* biomineralization in presence of HOS cells. Human osteocalcin and alkaline phosphatase estimation showed that the bone specific protein secretion is enhanced in the presence of PPH_1. Finally, the short term bone implantation results proved that fibrous tissue was absent at the interface of *PPH1-bone* and *$CaPH_1$- bone* and new bone formation around the implant was obvious especially at four and twelve weeks period with a better healing profile.

REFERENCES

1. S. Mann, Biomineralization: Principles and concepts in bioinorganic materials chemistry, Oxford university press, 2001, page: 3
2. H. Shin, S. Jo. A. G. Mikos, Biomimetic materials for tissue engineering, Biomaterials, 2003; 24: 4353-4364
3. A.S. Hoffman, in Biomaterials Science: An introduction to Materials in Medicine; B.D. Ratner, A. S. Hoffman, F.J. Lemons, Eds; Academic Press, San Diego, 1996; Chapter 2, page: 124
4. G. Goissis, S. Vargas da Silva Maginador and v.d.c.A. Martins, Biomimetic mineralization of charged collagen matrices: *in vitro* and *in vivo* study, Artif. Organs, 2003; 27 (5): 437- 443
5. M.Tanahashi and T. Matsuda, Surface functional group dependence on apatite formation on self-assembled monolayers in a simulated body fluid, J. Biomed. Mater. Res., 1997; 34: 305-315
6. W.L. Murphy and D.J. Mooney, Bioinspired growtht of crystalline carbonate apatite on biodegradable polymer substrate, J. Am. Chem. Soc., 2002; 124(9): 1910-1917

7. S.C. Marks Jr. and D.C. Hermey, 'The structure and development of bone' in principles of bone biology, Eds: John P. Bilezikian, Lawerence G. Raisz, Gideon A. Rodan, Academic Press, 1996
8. L.L. Hench, and June Wilson, An introduction to bioceramics, World scientific, 1993, page 13-14
9. R. P. S. Chaplin, A. J. C. Lee, R. M. Hooper and M. Clarke, The mechanical properties of recovered PMMA bone cement: A preliminary study, Journal of Materials Science: Materials in Medicine, 2006; 17 (12):
10. G. Lewis, Properties of acrylic bone cement: state of art Review, J. Biomed. Mater. Res., 1997; 38(1): 155-182
11. C. Lee, The Mechanical Properties of PMMA Bone Cement in The Well-Cemented Total Hip Arthroplasty, Springer Berlin Heidelberg, 2005
12. J.H. Boss, I. Sharawi, D.G. Mendes, The nature of the bone-implant interface. The lessons learned from implant retrieval and analysis in man and experimental animal, Med. Prog. Technol., 1994; 20 (3-4): 119-42
13. L.L. Hench, and June Wilson, An introduction to bioceramics, World scientific, 1993; page 13-14
14. H.K. Varma.,Y.Yokogawa, E.F.Espinosa, Y.Kawamoto, K. Nishizawa, F. Nagata,T. Kameyama, Porous calcium phosphate coating over phosphorylated chitosan film, Biomaterials, 1999; 20: 879-884
15. S.Li, Q. Liu, J. de Wijn, J. Wolke, B. Zhou, K. de Groot, In vitro apatite formation on phosphorylated bamboo, J. Mater. Sci. Mater. Med., 1997; 8: 543-549
16. W.L. Murphy and D.J. Mooney, Bioinspired growtht of crystalline carbonate apatite on biodegradable polymer substrate, J. Am. Chem. Soc., 2002; 124(9): 1910-1917

17. Y. Chen, A F T Mark, M. Wang, J. Li, Composite coating of bonelike apatite particles and collagen fibres on poly(L-Lactic acid) formed through an accelerated biomimetic coprecipitation process, J. Biomed. Mater. Research, Part B, Appl. Biomater. 2006; 77B: 315-322
18. A.J. Gracia, B.G. Keselowsky, Biomimetic surfaces for control of cell adhesion to facilitate bone formation, Crit Rev Eukaryot Gene Expr., 2002; 12(2): 151-62
19. A. Veis, M. Sharkey, I. Dickson, in: R.H. Wasserman (Ed.), Calcium binding proteins and calcium function, Elsevier, New York, 1977, page 408
20. H.K.Varma, K. Sreenivasan, Y.Yokogawa, A. Hosumi, In vitro calcium phosphate growth over surface functionalised PMMA film, Biomaterials, 2003; (24): 297-303
21. P.L.Granja, L. Pouysegu, D. Deffieux, G. Daude, B. De Jeso, C. Labrugere, C. Baquey, M. A. Barbosa, Cellulose phosphates as Biomaterials. II. Surface chemical modification of regenerated cellulose hydrogels, J. Appl. Polym Sci, 2001; (82): 3354-3365
22. P.L.Granja, B. De Jeso, R. Bareille, F. Rouais, C. Baquey, M. A. Barbosa, Cellulose phosphates as biomaterials. In vitro biocompatibility studies, Reactive and Functional polymers, 2006; 66: 728-739
23. M.Tanahashi and T. Matsuda, Surface functional group dependence on apatite formation on self-assembled monolayers in a simulated body fluid, J. Biomed. Mater. Res., 1997; 34: 305-315
24. T. Kokubo, S. Ito, Z. T. Huang, T. Hayshi, S. Sakka, T. Kitsugi, T. Yamamuro, Ca, P- rich layer formed on high strength bioactive glass ceramic A-W, J. Biomed. Mater. Res. 1990; 24(3): 331-343
25. A. Bigi, B. Bracci, G. Cojazzi, S. Panzavolta, K. Rubini, In vitro mineralization of gelatin-poly(acrylic acid) complex matrices, J. Biomater Sci, Polymer Edn. 2004; 15 (3): 243-254

26. H.M. Kim, T. Himeno, M. Kawashita, T. Kokubo and T. Nakamura, The mechanism of biomineralization of bone-like apatite on synthetic hydroxypatite: an *in vitro* assessment, J. R. Soc. Interface 2004; 1: 17-22

27. M.Yamauchi, T.Yamaguchi, H. Kaji, T. Sugimoto and K. Chihara, Involvement of calcium-sensing receptor in osteoblastic differentiation of mouse MC3T3-E1 cells, Am J Physiol Endocrinol Metab, 2005; 288: 608-616

28. P. Collin, J. R. Nefussi, A. Wetterwald, V. Nicolas, M. Boy-Lefevre, H. Fleisch and N. Forest, Expression of collagen, osteocalcin, and bone alkaline phosphatase in a mineralizing rat osteoblastic cell culture, 1992; 50 (2): 175-183

29. G. Goissis, S. Vargas da Silva Maginador and v.d.c.A. Martins, Biomimetic mineralization of charged collagen matrices: *in vitro* and *in vivo* study, Artif. Organs, 2003; 27 (5): 437-443

CHAPTER 1

INTRODUCTION

1.1. BIOMINERALIZATION IN NATURE

Biomineralization is a natural process that gives rise to small as well as large inorganic based structures of life [1]. Examples for biomineralized structures are corals, ivory, oyster shells, bone enamel etc. The biomineralized structures offer the organism various functions like protection, motion, cutting and grinding, buoyancy, optical and magnetic sensing and storage of elements [1]. The formation of inorganic functional structures occurs under controlled biological conditions. Some of the fascinating biomineralized structures are shown in figure 1.1.

(a) Limpet teeth
(b) Calcified coral
(c) Magnetic bacteria
(d) Coccolith
(e) Trumpet spines
(f) Coccosphere

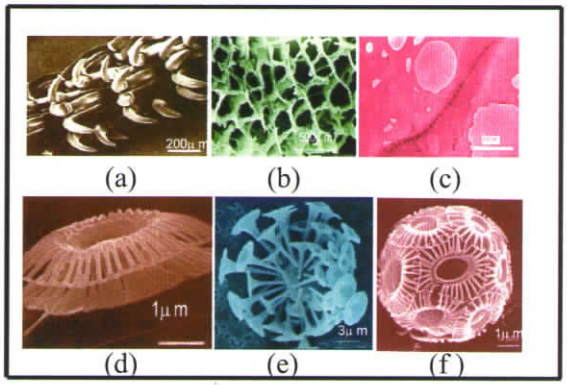

Figure 1-1Biomineralized structures in nature
Reference: *S. Mann, Biomineralization: Principles and concepts in bioinorganic materials chemistry, Oxford university press, 2001*

1.1.1. Biomineralization- Basic principles

Biomineralization is broadly classified into two, *biologically induced* mineralization and *biologically controlled* mineralization. In biologically induced mineralization, adventitious precipitation of the inorganic mineral occurs by the reaction of extraneous ions with metabolic products secreted across or into the cell wall. This leads to a heterogeneous structure with poorly defined shape, size, and composition. Example for biologically induced mineralization is the precipitation of calcium carbonate in certain algae from saturated calcium bicarbonate solution by metabolic removal of carbon dioxide during photosynthesis.

Biologically controlled mineralization is a highly regulated process for the production of structures with specific biological functions. Examples are bones, shells, teeth etc. Biominerals produced by this process are reproducible and possess species-specific crystallochemical properties like uniform particle size, complex morphology, preferential crystallographic orientation etc [2]. Biologically controlled mineralization could be further classified into intra cellular and extra cellular mineralization. Formation of lipid vesicles is an example for intracellular mineralization whereas construction of macromolecular framework such as bones, shells, teeth is effected by extracellular minerlization [1]. These processes are precisely regulated through the activity of specialized cells that seal off a space forming a compartment into which an organic matrix consisting of insoluble proteins and polysaccharides such as collagen or chitin respectively is secreted [3]. The mineral phase is then deposited in close association with the organic matrix. The diversity of biomineralization and its assorted functions are given in table 1.1. Biologically controlled mineralization is schematically illustrated in fig.1.2 [1].

Table 1-1 Biominerals and their function

Biomineral	Formula	Organism	Location	Function
Calcite	$CaCO_3$	Molluscs,Coccolithophore, Birds, Mammals, etc.	Cell wall scales, crab cuticle, egg shell, etc.	Exoskeleton, Protection, Mechanical strength, etc.
Aragonite	$CaCO_3$	Corals, Fish, Molluscs, etc.	Cell wall, shell, head, etc.	Exoskeleton, Buoyancy device, gravity receptor
Gypsum	$CaSO_4.2H_2O$	Jelly fish	Statoconia	Gravity receptor
Hydroxyapatite	$Ca_{10}(PO_4)_6(OH)_2$	Vertebrates	Bone, teeth	Protection, Mechanical strength, etc.
Whewellitite	$CaC_2O_4.H_2O$	Plants, fungi	Leaves, roots	Calcium store
Silica	Amorphous	Diatoms, radiolarians	Frustules, skeleton	Mechanical strength
Magnetite	Fe_3O_4	Bacteria, chitons	Intracellular, teeth, head	Magnetotaxis, grinding, etc

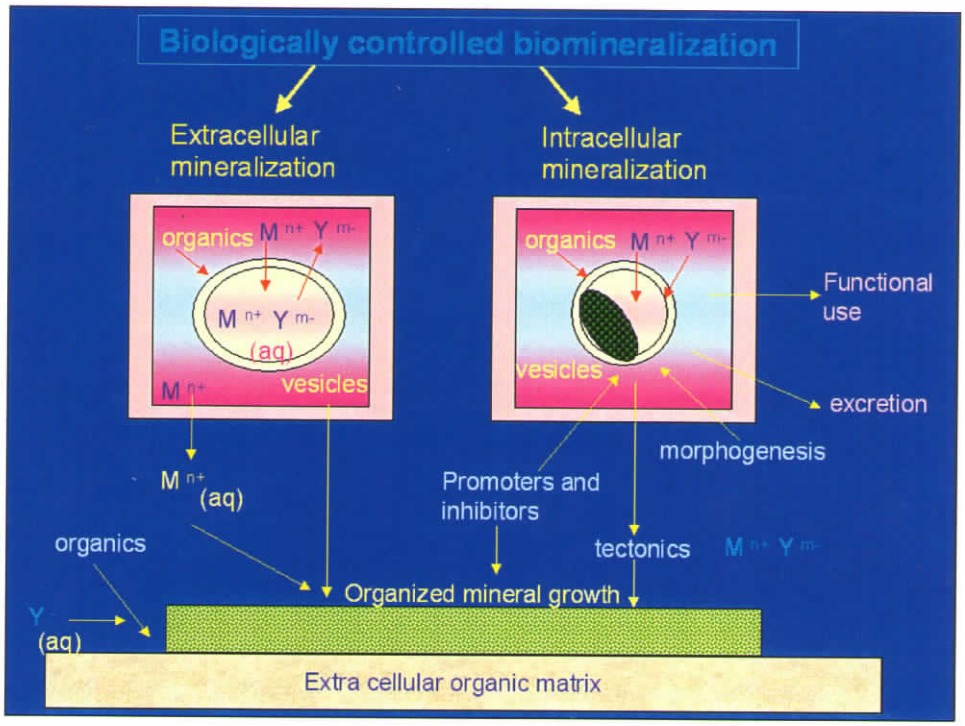

Figure 1-2 Types of biologically controlled biomieralization-schematic representation
Reference : *S. Mann, Biomineralization: Principles and concepts in bioinorganic materials chemistry, Oxford university press, 2001)*

1.1.2. Biomineralization- Salient and special features

Biomineralization offers the organisms to fulfill various functions such as protection, mechanical strength, cutting and grinding etc. The morphologic peculiarities of biominerals have remained a crystallographic paradox for decades [4]. Although the permanent association of organic compounds with biologically produced minerals have been documented for long time, no global concept was available until recent years that can explain the striking contrast between the morphologic diversity and astonishing specificity of biominerals [4]. Biomineralization is often controlled by the regulation of orientation, size, shape and assembly of the crystals. Control of biomineralization is implemented through specialized proteins capable of recognizing specific crystal surfaces during the

growth of the crystals. Recognition is based on molecular complementarities between the protein and the crystal structure on defined planes [5]. The control of crystal shape is one of the many puzzling features of biomineralization. Mineralized structures often have complex hierarchical structures, and many of them fulfill a mechanical function. In addition to this, biologically produced minerals appear as major sources of environmental information such as geological information [5]. Thus biologically conducted growth process becomes a leading factor that causes morphological diversity and compositional specificity of biominerals, and is also responsible for the specific geological behaviour they demonstrate during the fossilization process [4].

1.2. BIOMIMETIC MINERALIZATION

The term 'Biomimetics' is used to describe the concept of getting inspired by nature to improve and optimize properties of materials and for developing advanced technologies. The concept of biomimetics has been magnificently explored towards famous applications such as building of 'Eiffel Tower' by getting inspired from the intriguing trabecular structure of bone (offering it the greatest strength) or the development of novel dirt and water repellant paints based on the salient feature of lotus leaf to remain dirt repellant in the dirty polluted water, known as 'lotus effect'.

Biomimetic mineralization could be defined as 'mimicking the basic conditions required for inducing biomineralization under laboratory conditions through synthetic approaches'. Biomineralization usually occurs through specific or selective interaction between the organic moieties and the biomineral on the surface of organic templates like macromolecular frameworks, cell walls or lipid membranes. The rationale behind applying this concept in the area of bone tissue engineering is the achievement of biomolecular or surface functional group recognition in the biological milieu by surface or bulk modification of biomaterials [6].

1.2.1 Significance of biomimetic materials in bone tissue engineering

Bone formation is the result of sequential events that begin with recruitment and proliferation of osteoprogenitor cells from surrounding tissues, followed by osteoblastic differentiation, matrix formation and mineralization. The ability of a biomaterial scaffold to allow osteoprogenitor cell attachment and migration in the early stages of wound healing is crucial for later steps in the bone formation cascade [6]. It is known that many glycoproteins such as osteopontin, thrombospondin, osteocalcin and bone sialoproten in the extra cellular matrix are expressed during new bone formation [7,8]. The biomimetic materials facilitate the regulation and control of cellular interactions in the molecular level [9]. Suitable functionalization could be adopted as an efficient technique to trigger biomimetic mineralization of an organic matrix to improve its functionality and hence could be effectively proposed for bone tissue engineering applications.

1.2.2. Synthetic approaches towards biomimetic mineralization

A substrate coated with bioactive glass when immersed in simulated physiological fluid, will induce nucleation and growth of calcium phosphate. The bioactive glass coating is one of the popular methods to achieve calcium phosphate nucleation under simulated physiological conditions. The mechanism involved in this process is primarily associated with the increase in the ionic product of apatite in the surrounding body fluid caused by the dissolution of Ca^{2+} ions from the bioactive glass, which is in fact already supersaturated with respect to apatite. The hydrated silica formed on the surface acts as favourable sites for apatite nucleation and as a result, large number of apatite nuclei is formed on the surfaces of the bioactive glasses [10].

The bioactive glass coating can be achieved by different ways. One of the simple ways is as per the procedure reported by Riess *et al*, where they have pre-etched the substrate surface with 1M HCl for 15 minutes, and then rolled substrate on a bed of wet bioglass particles, followed by immersing in simulated body fluid

(SBF) [11]. The substrates they have used are high molecular weight polyethylene, biodegradable starch/ethylene vinyl alcohol blend (SEVA-C) and polyurethane foams with open cellular structure. They found that it is a simple method to impart apatite coating on bioinert substrates.

Surface modification of polymers by glow discharge technique is another potential approach, where the surface of the polymer is tailored as per the requirement, keeping the bulk properties intact. In one of the investigations, Tanahashi *et al* have modified the surface of polyether sulphone (PESF), with oxygen gas through glow discharge technique. The modified PESF substrate was coated with $CaO\text{-}SiO_2$ based bioactive glass [12]. The surface modified substrate, when subjected to SBF for 12 days, induced apatite coating. The apatite coated PESF polymer was then implanted in rabbit tibia for 8 weeks. The ultra-structural evaluation of the implant-host bone interface performed by TEM-EDS study showed that the apatite crystals in the host bone and the synthetic coating have more or less analogous structure. Another simple way of physical surface modification of surface is by grit blasting. Li has reported in 2003 that surface modification of titanium alloy (Ti6Al4V) by grit basting with alumina, followed by SBF treatment can induce nanoapatite coating, which helped better in the osteoblast adhesion and bone apposition compared to uncoated titanium samples [13].

Ozawa *et al* performed a first step towards the application of biomimetic apatite coating for micro cellular biosensing devices in 2002 [14]. They have proposed a method for the formation of micropattern of apatite by combination of a biomimetic process and transcription of resist pattern. The positive resist material was coated on alkali-free glass plates using a spin coater, pre-baked at 100 ^{0}C for 1 minute. Ultraviolet rays were irradiated on the surface after putting a photomask on areas of interest, which was then soaked in developing a solution. The UV exposed regions were dissolved off, leaving behind a resist pattern on the unexposed area. The substrate, after post-baking at 120 ^{0}C for 1 minute was immersed in bioactive glass followed by soaking in SBF offered an apatite coating.

The apatite coated resist pattern containing substrate on gentle washing with acetone offered an apatite micropattern transcribing the resist pattern.

Oliveira *et al* proposed sodium silicate as an alternative nucleating agent to bioactive glass-precursors [15]. They have taken biodegradable starch/ethylene vinyl alcohol blend (SEVA-C) as their system of investigation. The polymer was coated with sodium silicate gel (contains approximately 14% NaOH and 27% SiO_2 at a pH of 13). The viscosity of the gel was 6×10^{-2} Pa/s. The sodium silicate gel coated SEVA-C, when immersed in SBF induced calcium phosphate coating. The calcium phosphate coated SEVA-C showed good cell adhesion but their proliferation kinetics depends on the basic characteristics of the coating.

The deposition of calcium phosphates in bone and teeth involves an extracellular matrix, constituted of collagen fibrils and several non-collageneous proteins, rich in 'anionic aminoacids', which can interact with the growing crystal of calcium phosphate. Phosphophoryn, one of the major protein of dentin, and the bone phosphoprotein, osteonectin have found to bind to the (100) faces of hydroxyapatite [16,17]. Based on this, Bigi *et al* have studied the preferential oriented growth of hydroxyapatite on gelatin-poly(acrylic acid) matrix. The matrix was prepared by slow diffusion of poly(acrylic acid) into gelatin gels followed by uniaxial stretching and biomimetic mineralization was accomplished by SBF treatment [18].

The outstanding properties of biomineralized tissues are attributed to their organized structure and strong interfacial interactions between biomacromolecules and inorganic crystals. The functional group assisted inorganic crystal nucleation, and its kinetics is one of the interesting topics for researchers. Dalas and coworkers have tried the crystallization of calcium carbonate hexahydrate ($CaCO_3.6H_2O$) on acrylonitrile-butadiene styrene rubber (with -C≡N functional group) at 25 ^{0}C and atmospheric pressure by constant composition technique. The crystallization method based on constant composition was performed as follows [19].

The functionalized polymer was suspended in 0.1M calcium chloride solutions for 24 h under continuous stirring. The polymer samples were then washed with distilled water until the washings showed no calcium desorption. Two mechanically coupled burettes (connected to pH-stat (Metrohm Dosigraph with 614 Impulsomat) were filled with calcium nitrate and sodium carbonate titrants having the stoichiometry of the precipitating salt (calcium: carbonate=1:1). A pH drop as small as 0.005 pH units would be sufficient to trigger the addition of the titrant from the burettes. The concentration and ionic strength of the titrants, calcium nitrate, potassium nitrate and sodium bicarbonate was maintained constant throughout the precipitation process (and hence known as *constant composition technique*). The crystal growth rates were obtained from the recorder traces of the titrants (corresponding to the moles of $CaCO_3$ precipitating) as a function of time.

In one of the studies they have tried to investigate kinetics of hydroxyapatite crystallization on polymers containing -C≡N functional group, basically acrylonitrile copolymer rubber and poly(acrylonitrile) [20]. According to their observation, the critical nucleus is formed by the electrostatic attraction between -C≡N and Ca^{2+} ion, i.e., by the attraction of diffused PO_4^{3-} towards fixed Ca^{2+} ions. In another study they have pointed out the inhibitory effect of lysine on the crystallization kinetics of hydroxyapatite [21]. They claim that the adsorption of lyzin on HAP is due to the electrostatic attraction between the ε-aminogroup and the free phosphate groups of HAP surface. The α- carboxyl and α-amino group have a minor contribution as well. The extent of lyzin adsorption also depends on the solution pH (maximum at 8.5) and hence lyzin could be considered as a moderate calcification inhibitor. Amelogenin proteins are assumed to control the calcification of dental enamel with a nanoscale precision that facilitates the formation of fibrous apatite crystals with a remarkable microstructure. Habelitz *et al* observed that, recombinant full-length human amelogenin induces protein-guided mineralization and formation of an enamel-like composite material at specific chemical conditions [22]. The amelogenin bound specifically to

fluoroapatite crystals at a concentration similar to *in vivo* condition and a pH=8.0. The crystals are formed at 001 plane within 24h, forming layers up to 400nm high with an elongated structure.

Dousi *et al* have investigated the kinetics of calcite crystallization on polymers containing –C=O functional group. They found that the formation of calcite was initiated through the electrostatic interaction of Ca^{2+} ions with the negative end of the –C=O bond [23]. Grassmann and Lobmann further studied the effect of carboxylic group on biomimetic mineralization of calcite and vaterite [24]. They have incorporated carboxylate group by copolymerizing polyacrylamide hydrogels with acrylic acid and used as growth medium for $CaCO_3$ in a double-diffusion arrangement. The carboxylate functionalities in the gel network nucleated crystals of vatarite and calcite.

Chitin is one of the most important biomacromolecules in vertebrates, which influences the mineralization process of calcium carbonate in an essential way. Due to its insoluble property, most investigations are focused on the derivatives of chitin, for example chitosan and its functionally modified derivatives. Liang *et al* have modified chitosan into carboxy methyl chitosan and tried to use it as an additive for the precipitation of calcite [25]. They could see that the morphology of the calcite crystals varied with the concentration of carboxymethyl chitosan. The crystallization of calcium carbonate in the aragonite form was done by Dalas *et al* on styrene-butadiene rubber modified with $–SO_3H$ functional group [26].

1.3. SURFACE FUNCTIONALIZATION AS A TOOL

Surface modification offers a means to alter interfacial properties of a material leaving its bulk properties unaffected. Surface functionalization is an effective tool for modifying the chemical and topographical characteristics of a material. Properties altered are chemical functionality, surface charge, surface roughness and texture, surface wettability (hydrophilicity), cellular adhesion etc. [27].

Hence this paradigm could be extended to develop biomimetic materials that can serve as a better functional bone graft material.

1.3.1. Various surface modification techniques

There are different types of surface modification techniques available. Some of them are

i) Chemical etching

ii) Oxidative plasma treatment (typically for metals)

iii) Chemical and plasma enhanced vapour deposition

iv) Physisorption and chemisorption of block co-polymers and biopolymers

v) Coupling

a) Phosphate group

b) Silanol group

c) Calcium ion

vi) Surface hydrolysis to obtain free hydroxyl and carboxyl groups

1.3.2. Biomimetic mineralization of hydroxyapatite

1.3.2.1 Role of anionic charge on minralization

The immobilization of biomacromolecules on organic substrates via spacer groups in a temporary or permanent way is a potential approach towards the preparation of biomimetic polymers [28]. When the immobilization occurs via the spacer group, greater steric freedom and thus greater specific activity could be achieved. In the case of biomaterials, the immoblization of biomolecules is usually preceded by functional modification of the substrate to impart reactive functional groups (such as –OH, $-NH_2$, -COOH, $-PO_4$ etc.) capable of binding the biomolecules [28]. Moreover it has been demonstrated by several researchers that

imparting high anionic surface charge density would enhance nucleation and growth of apatite upon immersion in SBF [29, 30].

Biomineralization usually occurs through specific or selective interaction between the organic moieties and the biomineral on the surface of organic templates like macromolecular frameworks, cell walls or lipid membranes. It is well known that bone is formed by the mineralization of hydroxyapatite on collagen matrix. Goissis *et al* studied the biomimetic mineralization of charged collagen matrix [31]. The polyanionic collagen matrix was produced by hydrolysis of side chain amides of asparagines and glutamine. The polyanionic collagen matrix was capable of undergoing *in vitro* and *in vivo* mineralization (in rats). They have seen that the *in vitro* mineralization occurred as belts of two kinds. Chen *et al* performed a study on the accelerated precipitation of hydroxyapatite on poly (L-lactic acid) by using 5xSBF [32].

Tanahashi and Matsuda have studied the functional group dependence on apatite formation on self-assembled monolayers (SAMs) of alkanethiols having various functional groups in SBF [33]. In their study, self assembled monolayers of alkane thiols having $-CH_3$, $-PO_4H_2$, -COOH, $-CONH_2$, -OH and $-NH_2$ terminal groups formed on a gold surface (via sulphur attachment) were soaked in SBF up to 40 days. The effect of terminal functional groups on apatite formation was assessed by X-ray photoemission spectroscopy (XPS) and quartz crystal microbalance technique. The results showed that the growth rate of apatite crystals on the functionalized SAMs decreased in the order PO_4H_2>COOH>>$CONH_2$≅OH>NH_2>>CH_3. In their study, they could see that negatively charged groups strongly induced apatite formation but the positively charged group did not. Hence it could be said that the apatite formation is initiated via calcium ion adsorption upon complexation with a negative surface charged group is a dominant step in biomaterial calcification [33].

Most of the macromolecules known to promote surface nucleation provided they contain negatively charged functional groups at the crystallization pH. For example, acidic phospholipids such as phosphatidylserine (PS) and other phosphatides in matrix vesicles are believed to be the sites of nucleation in many tissues [34]. Moreover, polysaccharides containing sulphate groups, aspartic acid containing proteins and carboxyl group etc. found to promote surface nucleation [33].

1.3.2.2. Surface grafting

Surface grafting of the preferred functional group is one of the popular approaches for achieving calcium phosphate coating without altering bulk property of the organic matrix. One of the initial studies with this idea was performed by Tretinnikov and colleagues [35]. They have performed a comparative evaluation to understand the role of phosphate group and carboxylic group in inducing calcium phosphate phase. The functionalized matrices were prepared by surface grafting of high-density polyethylene with an organophosphate monomer, methacryloxyethyl phosphate (MOEP) as well as with acrylic acid respectively [35]. The deposition of apatite layer on the surface of modified HDPE was examined *in vitro* and they found that MOEP grafting was more efficient in inducing calcium phosphate coating compared to acrylic acid.

Surface hydrolysis of polyesters is another way to achieve surface functionality. Murphy and Mooney have studied the bioinspired growth of crystalline carbonate apatite on surface hydrolyzed poly (lactide-co-glycolide), PLGA films [36]. PLGA (85:15) films were subjected to surface hydrolysis to increase carboxylic and hydroxyl functional groups. This resulted in a substantial increase in the surface energy of the polymer from 42 to 49 dynes/cm^2. The surface hydrolysed polymers exhibited a 3-fold increase in heterogeneous growth of apatite upon SBF treatment. They have further examined the mechanism of heterogeneous carbonate apatite growth by ion-binding assays, which indicated that the calcium binding is mediated independently by the presence of soluble

phosphate counter-ions and surface functional groups. The apatite crystal size and morphology were dependent on the solution characteristics but not affected by the degree of surface-prehydrolysis. They claim that the impetus for mineral nucleation in this system appears more complicated than the simple electrostatic interactions. Peytcheva and Antonietti have studied the dependence of interfacial energy on the dissolution and growth behavior of hydroxyapatite crystal surfaces and they found that the interfacial energy was lowered in presence of poly (sodium aspartate) [37].

1.3.3 Biomimetic mineralization through bioactive molecules

Hartgerink *et al* reported a model for site directed nucleation and growth of hydroxyapatite [38]. They found that, the nucleation and growth of hydroxyapatite could be specifically controlled by designing a surfactant having self-assembled architecture of [38]. This was in fact designed for providing potential sites for cell adhesion. The surfactant molecule they have selected consists of a C_{16} alkyl chain to favour micelle formation, and a polar head group that was subdivided into blocks of different functional moieties. A block of four consecutive cystenic amino acids was chosen to promote robustness by intermolecular disulfide cross-linking and a phosphoserine was inserted to form a highly phosphorylated interface, which promoted HAP nucleation on the micelle. The amphiphile was terminated with Arg-Gly-Asp (RGD), which plays an important role in cell adhesion. The template molecule when exposed to simulated physiological fluid spontaneously formed coating of hydroxyapatite as oriented platelets.

Lu *et al* investigated the active involvement of bone morphogenic protein (BMP-7) to induce minerailzation of muscle-derived cells under *in vitro* [39]. They have found that BMP-7 delivered from PLGA matrix induced increased expression of bone markers and mineralization.

1.3.4 Mechanism of biomineral formation

The formation, remineralization and dissolution of hard tissues are complex process that involves numerous calcium phosphate phases [40]. Many biological mineralization processes involves the formation of metastable intermediates, which may subsequently transform into thermodynamically more stable phases. Kinetic study shows the precipitation of calcium phosphate involve formation of precursor phases such as dicalcium phosphate dihydrate and octacalcium phosphate, which eventually transforms into stable hydroxyapatite [40]. The other ions and molecules present in the physiological solution also have marked influence in the rate of mineralization and demineralization. However, the nature of phases that form depends upon the pH and the type of mineralization (normal or pathological) [40].

The control mechanisms in biomineralizatiton involve the regulation of chemistry, space, structure, morphology and construction of the minerals [1]. The four fundamental physicochemical factors that are involved in the formation of crystalline biominerals are [1]

i) Solubility

ii) Supersaturation

iii) Nucleation

iv) Crystal growth

The solubility factor determines the thermodynamic condition for precipitation while the supersaturation factor gives an idea about the extent to which a solution is out of equilibrium. This in turn influences the nucleation and growth of the crystal. The factors could be chemically controlled with the help of specialized molecules such as inhibitors/promoters for crystal growth or by regulating the ion transport.

Kim *et al* have recently proposed a mechanism for the formation of bone-like apatite on synthetic hydroxyapatite in the in vitro environment [41]. They have used hydroxyapatite polycrystalline samples with 5μm size to investigate the variation in surface composition, surface structure and surface potential of HAP in the process of biomineralization of apatite on its surface upon immersing in SBF. They found that on immersion in SBF, the synthetic HAP was found to induce the formation of bone-like apatite on its surface through the formation of calcium-rich amorphous calcium phosphate (ACP) in the early soaking period and calcium-poor ACP in the late soaking period. They claim that the formation of these two types of precursor phase of ACPs is sequential consequences of electrostatic interactions of the HAP surface with the calcium and phosphate ions in the SBF. On exposure to SBF, the HAP surface naturally reveals a negative charge, and thereby interacts with the positive Ca^{2+} ions in the fluid to form Ca-rich ACP. The Ca-rich ACP on the HAP has a positive charge and undergoes electrostatic interaction with negatively charged phosphate ions in the fluid to form the Ca-poor ACP, which eventually crystallizes into bone-like apatite. Therefore, the electrostatic interaction of HAP surface is the factor, which determines biomineralization [41]. Takadema *et al* have tried to explore the mechanism of apatite formation in Titanium metal (42) In another study they have tried to investigate the apatite formation on sodium silicate glass using TEM-EDS study (43)

Xin *et al* recently performed a comparative study of calcium phosphate formation on bioceramics in vitro and *in vivo* [44]. They have evaluated the formation of calcium phosphate on various bioceramic surfaces in vitro using simulated body fluid and *in vivo* by implantation in rabbit muscle. The bioceramics selected for the study were sintered porous solids of bioglass, glass-ceramics, hydroxyapatite, α- tricalcium phosphate and β-tricalcium phosphate. The ability of these materials to induce calcium phosphate was examined using single-crystal diffraction patterns in transmission electron microscopy. The results showed that these materials have similar ability to induce calcium phosphate both

in vitro and *in vivo*, with the exception of β-tricalcium phosphate. According to their observation, the calcium phosphate phase formed on the surfaces of bioglass, A-W glass, hydroxyapatite and α- tricalcium phosphate in vitro and *in vivo* was octacalcium phosphate. As per their observation, calcium phosphate formation on bioceramic surfaces is more difficult in *in vivo* than in *in vitro* and there is no difference in the calcium phosphate phase formed *in vitro* and *in vivo*.

The deposition of sparingly soluble salts on polymers is a significant phenomenon with respect to biomineralization. The first step of nucleation of inorganic minerals on the organic matrix is the formation of surface ion pairs [45]. Dalas observed that doubling or tripling the amounts of functionalized copolymers has no effect on the initial rates of crystallization [45]. However, subsequent growth rate increased with surpersaturation. Hence it could be suggested that the overgrowth of sparingly soluble salts is induced by organic matrix mediated heterogeneous nucleation.

As per Tanahashi *et al*, the mechanism of apatite formation on bioglass is as follows [12]. The Ca^{2+} ions dissolved from the glasses and glass ceramics increases the ionic product of the apatite in the surrounding body fluid, which is already supersaturated with respect to apatite. The hydrated silica formed on the surface provides favourable sites for apatite nucleation. As a result, a large number of apatite nuclei are formed on the surfaces of the glasses and glass-ceramics. Once the apatite nuclei are formed, they grow spontaneously consuming the calcium and phosphate ions from the surrounding fluid.

In general, the crystallization of insoluble salts involves the formation of metastable precursor phases. In the case of calcium phosphate, various metastable-phases with Ca/P molar ratio ranging from 1.00 to 1.67 have been identified. The metastable phases of calcium phosphate include dicalcium phosphate $CaHPO_4$ and dicalcium phosphate dihydrate (DCPD) $CaHPO_4$. $2H_2O$ with molar ratio 1.00,

octacalcium phosphate OCP Ca_8H_2 $(PO_4)_{6.5H2O}$ with molar ratio 1.33 and β-tricalcium phosphate (β-TCP) Ca_3 $(PO_4)_2$ with Ca/P ratio as 1.50 [46].

1.4. SIGNIFICANCE OF BIOMIMETIC MINERALIZATION OF CALCIUM PHOSPHATE

The special research interest on the biomimetic mineralization of calcium phosphate mineralization is quite evident from the basic understanding of the structure and composition of bone tissue. Bone, the unique connective tissue of vertebrates, is a living tissue because of its particular ability to undergo continual growth, dissolution and remodeling [47]. Bone is an organic-inorganic hybrid structure with 58% mineralized part and 25% organic matrix. The most stable form of calcium phosphate namely hydroxyapatite constitutes the inorganic part, while the organic part consists of 95% type I collagen and remaining 5% non-collageneous proteins [47]. It is essential to have adequate knowledge on the fundamental properties of bone and its mineralization for designing functional materials capable of inducing biomimetic mineralization.

1.4.1 Bone: Structural hierarchy

The primary functions of bone are as a protective shield for internal organs and marrow, to provide mechanical support without compromising mobility and to act as a storage device for essential ions necessary for normal functioning of the body. The properties of bone could be a thought of apparent contradiction such as, strong but not brittle, rigid but flexible, lightweight but solid enough to support tissues, mechanically strong but porous, stable but capable of remodeling. It is the different hierarchical levels of structure that offers bone these properties. There are mainly six levels of hierarchy in bone, which extends from molecular level to macroscopic level that is explained in table 1.2.

The four principal types of bones are long, short, flat and irregular. The long bones are primarily compact in nature and consist of a long shaft with two

bulky ends and a significant amount of spongy bone at the ends. Examples for long bones include bones of the thigh, leg, arm, and forearm.

Table 1-2 Structural Hierarchy in bone

Level	Size	Structure
1	1nm	Self assembly of collagen filaments
2	100nm	Collagen fibrils/hydroxyapatite nanocrystals
3	1μm	Organization of collagen fibrils into collagen sheets/woven texture
4	10μm	Self assembly of bone cells with adjacent layers (formation of lamellar bone) leading to the formation of concentric cylindrical structures called osteons
5	1mm	Formation of long bundles of osteons (Haversian bone)
6	>1mm	Formation of macroscopic bone microstructure

Reference: *S.Mann, Biomimetic materials chemistry, 1995*

1.4.2 Bone: Compact and Cancellous

The bone tissue can be basically classified into two, compact (dense) and cancellous or spongy (trabecular) based on the packing of the tissue. In compact bone, the haversian systems are closely packed together to form a solid mass [47]. The osteon or the haversian system consists of a central canal called the osteonic or haversian canal, which is surrounded by concentric rings called lamellae of the bone matrix. The matured bone cells (osteocytes) are located in spaces called lacunae, which is in between lamellae. The small channels called canaliculi radiate

from the lacunae to the haversian canal to provide passages through the hard matrix. The osteonic canals contain interconnected blood vessels that are parallel to the long axis of the bone with perforating canals towards bone surface.

Cancellous or spongy bone consists of plates (trabeculae) and bars of bone adjacent to small, irregular cavities that contain red bone marrow. In spongy bone, the canaliculi connect to the adjacent cavities, instead of a central haversian canal, to receive their blood supply. The trabeculae are arranged in a haphazard manner, but organized like braces in such a way that they follow the lines of stress. The trabeculae are capable of re-alignment with respect to stress changes to provide maximum strength. The trabecular bone is only 15-25% mineralized but is rich in bone marrow, blood vessels and connective tissue, making its primary role as metabolic rather than structural [47]. The macroscopic view of long bone and its structural hierarchy are shown in figure 1.3a and 1.3b respectively. The histological view of secondary level cortical bone structure is shown in figure 1.3c.

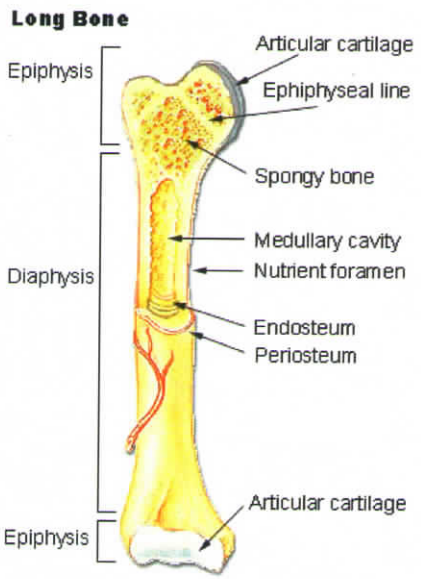

(a) **The macroscopic view of long bone**
Reference: *training.seer.cancer.gov/module_anatomy/unit3...*

Compact Bone & Spongy (Cancellous Bone)

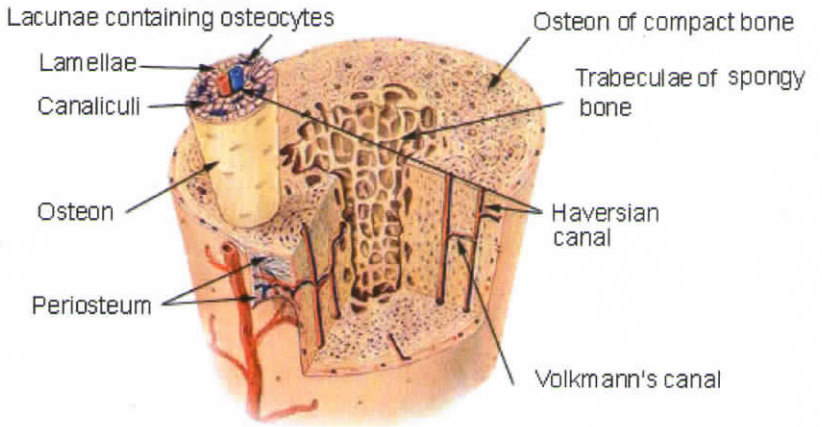

(b) The structural hierarchy in bone

Reference: *training.seer.cancer.gov/module_anatomy/unit3...*

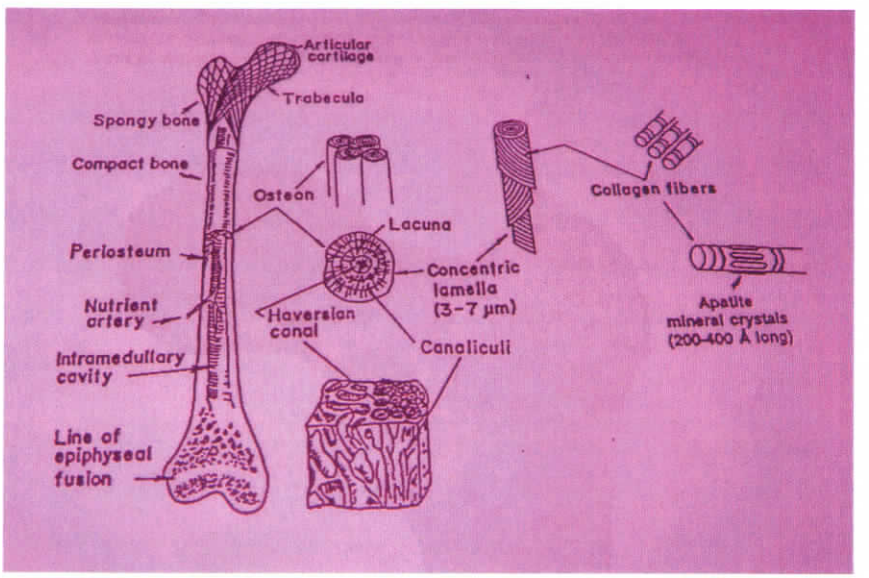

(c) Structural hierarchy in bone

Reference: *Biometrials: Principles and applications, J. B. Park, 2002.*

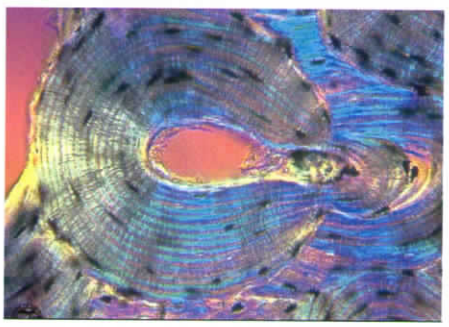

(d) Histological view of secondary level structure of cortical bone
Reference: http://medocs.ucdavis.edu

Figure 1-3 (a) The macroscopic view of long bone (b) The structural hierarchy in bone (c) Structural hierarchy in bone (d) Histological view of secondary level structure of cortical bone

1.4.3 Bone: Mechanical properties

The mechanical properties of bone vary as a function of age, location, mineral content, degree of hydration, temperature, sex etc. The most studied mechanical properties of bone are tensile strength, compressive strength, modulus, hardness and fracture-toughness. The values of mechanical properties reported by different investigators vary due to physical factors of bone such as microstructure, density, extent of mineralization, orientation (cortical bone is anisotropic in nature), sex and age. The physical variables are often inter-related. (e.g.: ageing and mineral content in the bone).

The Young's modulus reported for human bone ranges from 11 GPa-21GPa in the longitudinal direction (stress parallel to axis of osteon) and 5GPa to 13GPa in the transverse direction (stress perpendicular to osteon axis) [49]. The tensile strength is in the range 70MPa to 160MPa in the longitudinal direction and approximately 50MPa in the transverse direction [50]. The values of compressive strength vary as 70MPa to 280MPa in the longitudinal direction and while little data available in the transverse direction. The mechanical properties of cortical and trabecular bone are shown in tables 1.3 and 1.4 [49].

Table 1-3 Mechanical property of wet cortical bone

Property	Longitudinal	Transverse
Young's modulus (tension) GPa	17.7 ± 3.6	12.8 ±3.0
Young's modulus (compression) GPa	18.20±0.85	11.70±1.01
Tensile Strength MPa	133±15.6	53.0±10.7
Compressive strength, MPa	205.0±17.3	131.0±20.7
Shear strength, MPa	67.0±3.5	
Ultimate tensile strain, %	3.8±0.6	0.70±0.14
Ultimate compressive strain, %	1.9±0.3	5.0±1.1

Table 1-4 Mechanical properties of wet trabecular bone

Bone	Method of test	Young's modulus . GPa	Reference
Proximal femur	Buckling	11.4	Runckle and Pugh, 1975
Tibia	3-point bending	3.2	Ku *et al*, 1987
Tibia	4-point bending	5.4	Choi *et al* 1990
Femur	Ultrasonic	12.7 ±2	Ashman and Rho, 1998
Tibia	3-D finite element analysis	5.9	Van Rietenbergen *et al* 1995

1.4.4 Bone: Formation and growth

Bone is composed of two third inorganic phase constituted of hydroxyapaite and the remaining organic phase. The organic matrix is composed of 95% type I collagen, 5% proteoglycans, the high molecular weight complexes of proteins and polysaccharides (e.g.: glycosaminoglycan) and non-collageneous proteins. It is the organic-inorganic hybrid structure, which offers bone the high strength and rigidity with inherent flexibility. The three different types of cells that contribute to bone homeostasis are osteoblasts (bone-forming cells), osteoclasts (bone resorbing cells) and osteocytes (the mature bone cells) [48]. There is equilibrium between osteoblasts and osteoclasts, which maintains the bone tissue.

1.4.4.1 Development of bone cells

During the embryononic development, the embryo consists of three cell layers: the ectoderm, the endoderm and the mesoderm [51]. The cells of mesodermal layer eventually develop into several connective tissue types including muscle, blood, lymph tissue, bone, cartilage, tendon, ligament and fat. The cells of mesoderm are called mesenchymal stem cells and are found in the marrow of postnatal organisms. The development of bone cell can be simply divided into three stages: proliferation, extracellular matrix development and maturation and mineralization. There are mainly four stages of cell differentiation, osteoprogenitor cells, preosteoblasts, osteoblasts and osteocytes [48].

1.4.4.1.1 Osteoprogenitor cell

The osteoprogenitor cell, which represents the proliferate phase of bone development, has poorly defined morphological and molecular characteristics, but appears spindle-like, similar to fibroblast, and is located adjacent to the preosteoblast at the site of newly forming bone [48]. Osteoprogenitor cells are highly proliferative in nature, produces other osteoprogenitor cells as well as its

daughter cells. The most common bone marker, osteopontin is evident only at the later stages of osteoprogenitor cell.

1.4.4.1.2 Preosteoblasts

Preosteoblasts are the daughter cells of osteoprogenitor cells with cuboidal shape and found along the borders of newly forming bone. They could be identified *in vivo* by their ultra-structure and location [48]. Preosteoblasts produce type I collagen, alkaline phosphatase and ostopontin in limited amounts and are capable of dividing in a limited way. Preosteoblasts mark the end of proliferative phase and the beginning of the extracellular matrix development and maturation phase.

1.4.4.1.3 Osteoblasts

The differntiation of preosteoblasts gives rise to osteoblasts. Osteoblasts also appear as cuboidal in shape and found in more interior portion of the boundary of newly forming bone than preosteoblasts. Osteoblasts secrete the matrix, which eventually envelops them within new bone, and hence they are located much deeper into the bone layer [47]. They are capable of producing significant amount of alkaline phosphatase, osteopontin, and bone sialoprotein. They produce lesser amount of osteocalcin in the early stage of their development, but capable of producing more when they become matured. When matured osteoblasts produce collagen type I, for matrix development, proteoglycans, hormones, and growth factors for further matrix maturation and mineralization.

1.4.4.1.4 Osteocytes

Osteoblasts differentiate to form osteocytes and considered as post proliferative phase and are metabolically inactive. The osteocyte is a mature osteoblast within the bone matrix and is responsible for its maintenance [48]. They

are smaller than osteoblasts and have decreased or no alkaline phosphatase production. However, they produce osteocalcin, bone sialoprotein and ostepontin.

1.4.4.1.5 Osteoclasts

Osteoclasts are multinuclear giant cells and are responsible for bone resorption. They are differentiated from hematopoietic stem cells found in circulating blood [48]. Osteoblasts are characterized by two distinct plasma membranes, a ruffled border and a sealing zone. The clear or sealing zone forms a barrier known as resorption lacuna around the ruffled border, which is responsible for bone resorption [48]. The osteoclast synthesizes hydrochloric acid and collagenase that are excreted at the ruffled border at high extracellular concentrations. This highly acidic secretion dissolves the hydroxyapatite crystals. Then several enzymes and collagenase are released that destroy the collagen matrix. The degradation products are then removed from the resorption lacuna, or resorption pits, and released into the extracellular space. A schematic illustrations of osteoblast, osetocyte and osteoclast are shown in figure 1.4 a, b and c respectively.

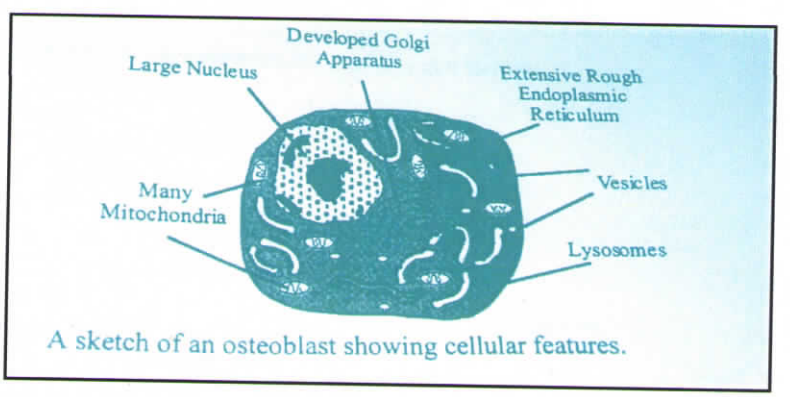

(a) Sketch of osteoblast

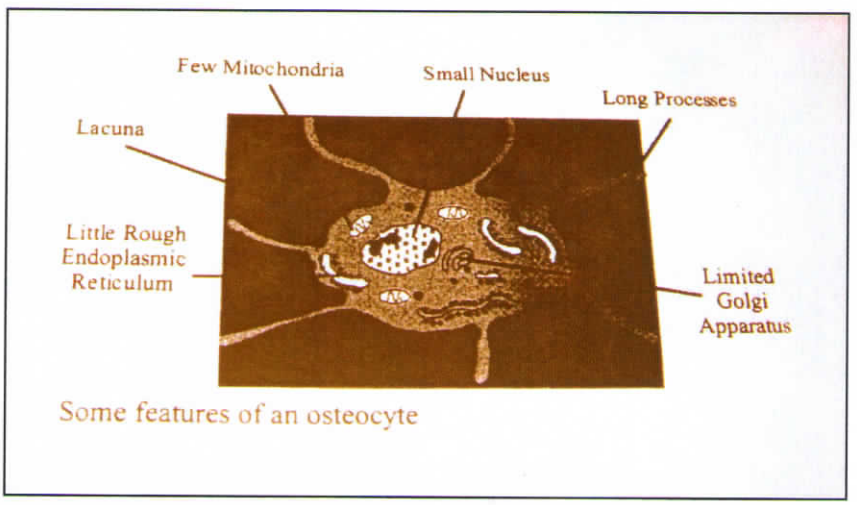

(b) Sketch of osteocyte

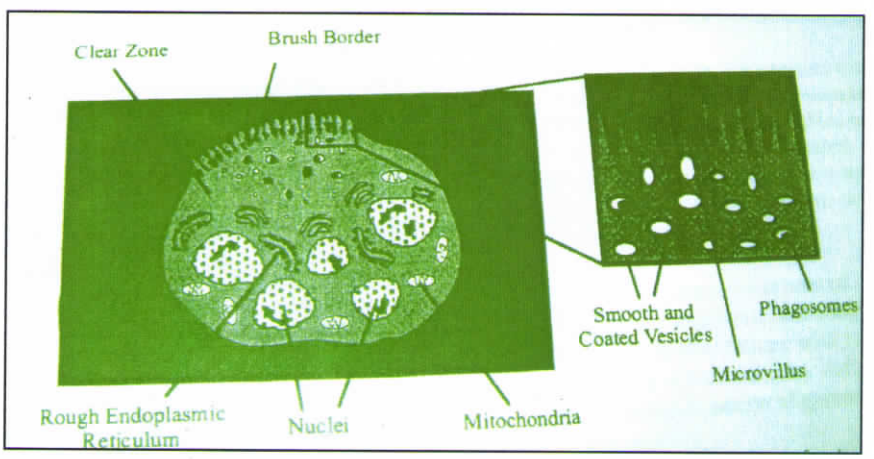

(c) Sketch of osteoclast

Figure 1-4 (a) Sketch of osteoblast (b) Sketch of osteocyte (c) Sketch of osteoclast
(Reference: *Ph.D thesis, H.Hung, University of London*)

1.4.4.2 Bone formation

The factors governing the functioning of bone cell are shown in figure 1.5. Once differentiated, osteoblasts secrete both type I collagen and the non-collageneous proteins necessary to produce the mineralized bone matrix [52]. Osteoblasts then secrete the necessary components for mineralization and eventually become surrounded by the mineralized extracellular matrix and transform to osteocyte. The osteocyte maintains the status of the mineralized tissue through formation and resorption of the matrix. The new bone is formed in concentric sheets known as lamellae surrounding the harvesion canals, which is responsible for blood and nutrient supply. As osteoblasts form new bone along the inner edge of these concentric circles, subsequent lamellae are migrated outward from the center. The canaliculi help in transferring nutrients from the newly formed lamellae to the older lamellae.

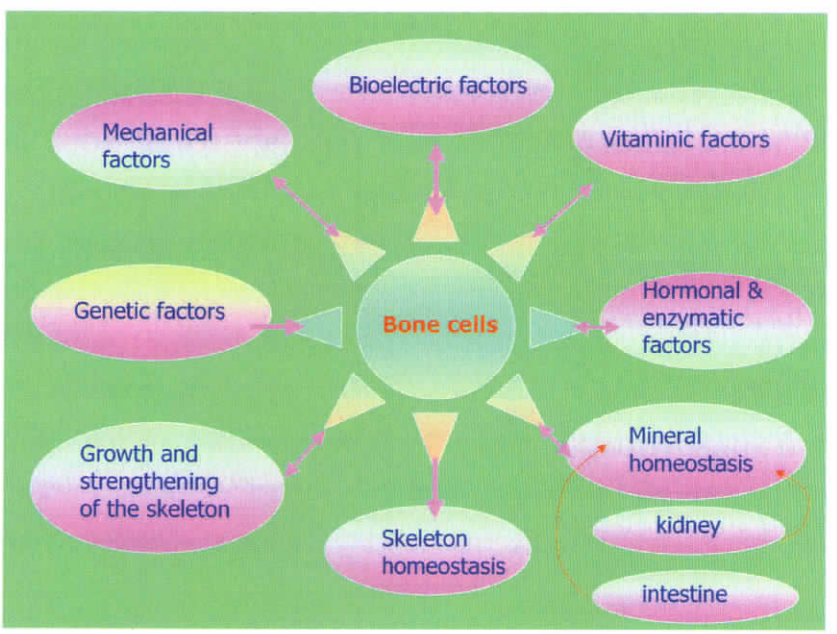

Figure 1-5 Factors governing the effective functioning of bone cells
(Reference: *H. Nakamura, Morphology, Function, and Differentiation of Bone Cells, Journal of Hard Tissue Biology, Vol. 16 (2007) , No. 1 pp.15-22)*

The formation of bone is known as osteogenesis or ossification. There are two types of ossification: intramembranous and endochondral [48]. Intramembranous ossifiction is considered as direct bone formation as it occurs during embryonic development; mesenchymal stem cells are directly differentiated into pre-osteoblasts and then osteoblasts [48]. There is no cartilage intermediate in this process. Bone formed by this method is characterized by collagen fibres forming irregular bundles with plenty of osteocytes, but not oriented as in the case of long bones. In this type of ossification, the replacement of sheet-like connective tissue membranes occurs with bony tissue and known as intramembranous bones. The future bones are initially formed as connective tissue membranes, where the osteoblasts migrate and deposit bony matrix around themselves leading to the formation of osteocytes. Examples are flat bones of the skull and some of the irregular bones.

The endochondral ossification, otherwise known as indirect bone formation involves the replacement of hyaline cartilage with bony tissue and known as endochondral bones [48]. Most of the bones of the skeleton are formed in this manner. In this process, the future bones are first formed as hyaline cartilage models. In the developing embryo, mesenchymal tissue takes the position and form of future bones, proliferates and differentiates into prechondroblasts and then chondroblasts which secrete a matrix and get embedded into the matrix resulting in the formation of chondrocytes. Unlike osteocytes, chondrocytes continue dividing, mineralizing and remodelling to form long bones. This process gradually replaces the cartilage cells by ostoblasts and ultimately mineralized bone tissue. As each of these mechanisms involve increase the length and width of the bone, the center of the bone is resorbed to form the marrow cavity.

1.4.5 Boundary-organized biomineralization in bone

Bone formation, when viewed as per the principles of boundary organized mineralization, occurs in a specialized fluid filled compartment, formed by the collective assembly of osteoblasts, which is separated from blood, and contains mineralized tissue [1]. The layer of cells is tightly packed so that the chemistry of the inner compartment is regulated by controlled diffusion of ions and molecules from the osteoblasts. At one side of the membrane, the osteoblasts are in direct contact with osteocytes, forming an interconnected network inside the bone and outside extracellular fluid, which is in equilibrium with blood. Thus, there exists a direct level of communication between the external and internal environments that enable bone to grow, remodel or remain in steady state depending on the hormonal signals from blood. The schematic illustration of this has been given in figure 1.6.

The parameters involved in boundary-organized biomineralization are

i) Spatial delineation: for controlling the size, shape, organization of mineral phase

ii) Diffusion limited ion flow: to control ionic activities, solution composition and supersaturation

iii) Mineral passivation: for surface stabilization of minerals against dissolution or phase transformation

iv) Ion accumulation and transport : for supplying chemicals to remote intra and extra cellular mineralization sites

v) Mineral nucleation: for regulating interfacial energies

vi) Mineral transportation: for moving mineralized structure to new construction sites

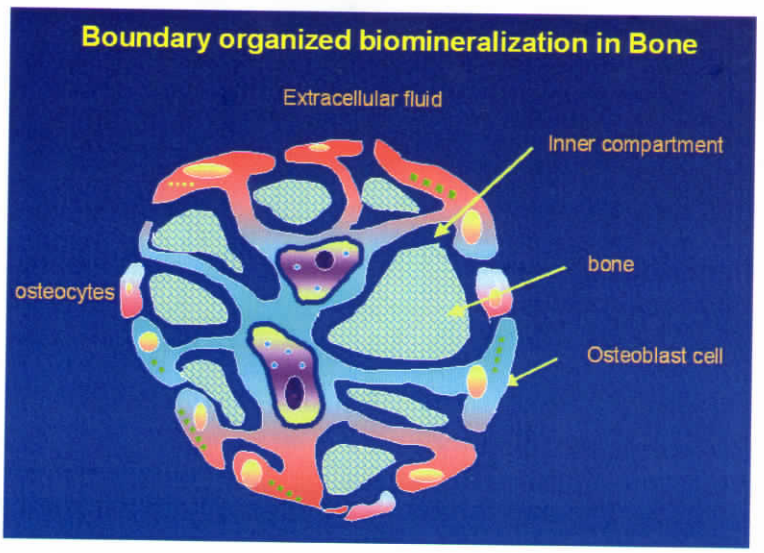

Figure 1-6 Boundary organized biomineralization in bone
(Reference: *S. Mann, Biomineralization: Principles and concepts in bioinorganic materials chemistry, Oxford university press, 2001)*

1.4.6 Bone specific markers

There is no protein that is exclusively produced by bone throughout its maturation process. However, there exists a small subset of proteins, which possess a specific combination in its presence elsewhere in the body with special reference to bone. Alkaline phosphatase is a commonly used indicator for normal osteoblastic development. It acts as a cell surface enzyme. Alkaline phospatase increases the local concentration of inorganic phosphate by hydrolyzing phosphate ester and promote the initial crystal formation of hydroxyapatite. Alkaline phosphatase is also believed to hydrolyze the calcification inhibitor, inorganic pyrophosphate and act as a transporter for inorganic phosphate and binds to Ca^{2+} to stimulate calcium phosphate precipitation [53].

Osteopontin, a member of sialoprotein family is basically a phosphorylated glycoprotein. It is believed that osteopontin is synthesized by preosteoblasts, osteoblasts and osteocytes into the bone and osteoid extracellular matrix [54]. It is

found abundant in areas, which undergo mineralization and promotes attachment and spreading of osteoblats. It has also a role in bone resorption in a dose dependent manner and is used as a control of mineralization and promoter of resorption. Bone sialoprotein, another member of sialoprotein family is found in mature osteoblasts and osteocytes, has a high affinity for Ca^{2+} and is an important component of bone. Another protein, osteonectin also possess high affinity to Ca^{2+} and regulates cellular progression.

Osteocalcin, one of the most abundant non-collageneous proteins in bone, is exclusively synthesized by bone and dentin and has a high affinity for Ca^{2+} [52]. Osteocalcin appears during the later stages of osteoblast differentiation and after the initiation of matrix synthesis. It is also capable of controlling mineral growth by recruiting osteoclasts.

1.5. FRACTURE HEALING MECHANISMS IN BONE

When bone met with a sustained injury, the resulting healing process has mainly three stages. In the event of bone fracture, the maintenance and functioning of blood supply becomes difficult and there are significant number of other tissues such as ligament, tendon and muscle, which may or may not be affected by the fracture. Hence the process of healing all these elements becomes a multidimensional event with an overlapping timeline. Even though the healing process is much complex, it could be mainly divided into three broad stages namely, inflammation, soft and hard callus formation, and bone remodeling [55].

1.5.1 Inflammation

The primary response to fracture is largely cellular in nature, with significant amount of hematoma at the injury site. Different types of cells such as platelets, macrophages, monocytes and polymorphonuclear neutrophils will arrive at the injury site and begin the repair process leading to inflammation. As a result of fracture, blood flow is interrupted which leads to cell death and bone necrosis at

the point of fracture. There is an elevated level of cell division after eight hours of injury, which continues for the first 24 hours not only on the injury site but also throughout the bone. The elevated cell division will minimize in a few days on majority of the bone, but continues at the injury site for a couple of weeks. The rebuilding process will then begin with the help of mesenchymal stem cells, osteoprogenitor cells, fibroblasts, and endothelial cells, which arrive at the fracture site from the medullary canal, periosteum or even from the soft tissue adjacent to the injury site, with the formation of new blood vessels as the primary step towards rebuilding [55].

1.5.2. Callus formation

As the inflammation subsides, fibrous tissue layer, known as callus is formed around the fracture. Remodelling of bone occurs within this callus over a period of several weeks. The primary callus formed is soft in nature and composed of a cartilaginous/bony tissue with cartilage at the edges of the callus and bone within the fracture site. The fibroblasts and osteogenic cells invade the soft callus. Fibroblasts produce collagen fibres, which connect broken ends of bone. The osteogenic cells in avascular areas, differntiate into chodroblasts and produce fibrocartilage [55]. This soft callus provides limited stability to the fracture site in compression but not rigid enough to prevent flexure of the fracture. In the formation of hard or bony callus, ostegenic cells near the capillaries differentiate into osteoblasts, which produces trabeculae. The fibrocartilageneous cartilage is then gradually transformed into bony callus. The mechanical rigidity of the site is increased with time by endochondral ossification of cartilage to woven bone direct transformation of mesenchymal stem cells and preosteoblasts within the callus.

1.5.3 Remodeling

In the final stage of fracture healing, the woven bone formed within the callus is slowly remodeled into lamellar bone [55]. The original diameter of the

bone and the medullary canal are slowly remodeled by the active involvement of the osteoclast in response to the stresses seen by the bone. The schematic illustration of bone remodeling is shown in figure 1.7.

Figure 1-7 Schematic illustration of bone remodeling
(Reference: *Stephen C. Cowin, Mechanical and Architectural Properties of Bone, Bone Mechanics Handbook*)

1.6. BONE GRAFTS

The need for bone graft arises due to multiple reasons such as congenital or acquired bone defects, developmental defects, trauma, presence of tumours etc. The worldwide demand for bone grafts is significantly increasing. As per the literature survey, the in the year 1998, nearly 300,000 bone graft procedures were performed in United States. In 2005, this figure exceeded 500,000 in US and world wide it is approximately 2.2 billion [56]. The incorporation of a bone graft is defined as 'the process of envelopment and interdigitation of the donor bone tissue with new bone deposited by the recipient' [57].

This process of interdigitation follows a multi-step cascade [57]. The primary response is the accumulation of inflammatory cells towards the bone graft. This follows a chemotaxis of host mesenchymal cells to the graft site. The primitive host cells then differentiate into chondroblasts and osteoblasts under the influence of various osteoinductive factors. The additional processes of bone graft

revascularization and necrotic graft resorption occur concurrently. Finally, bone production from the osteoblasts onto the three dimensional framework of graft occurs followed by bone remodeling in response to mechanical stresses [58]. The configuration and chemistry of the material plays an important role in dictating cell attachment and cell morphology [59].

1.6.1 Basic and preferred requirements

An ideal bone graft should provide both, the necessary elements for integration and new bone formation cascade, and lend structural support during this process. The ideal bone graft should possess the following properties [60]

i) An osteoconductive matrix that provides a nonviable three-dimensional framework amenable to the in-growth of blood vessels and osteoprogentor cells, required for bone formation

ii) Osteoinductive factors that recruit the recipient's mesenchymal cells through chemotaxis and then induce or modulate bone formation.

iii) Osteogenic cells with potential to differentiate into osteoblasts

iv) Structural integrity that provides mechanical support.

1.6.1.1 Osseointegration [61]

Osseointegration is the stable anchorage of an implant achieved by direct bone-to-implant contact. In craniofacial implantology, this mode of anchorage is the only one for which high success rates have been reported.

1.6.1.2 Osteoinduction [61]

Osteoinduction is the process by which osteogenesis is induced. It is a phenomenon regularly seen in bone healing process. Osteoinduction implies the recruitment of immature cells and stimulation of these cells to develop into

preosteoblasts. In a bone-healing situation such as fracture, the majority of bone healing is dependent on osteoinduction. Osteoinductivity is the ability of the graft to support attachment of new osteoblast and osteoprogenitor cells by providing an interconnected structure through which cell migration and blood vessel formation may take place.

1.6.1.3 Osteoconduction [61]

Osteoconduction means that bone grows on a surface. This phenomenon is regularly seen in the case of bone implants with the exception of implants with low biocompatibility.

Based on the basic material characteristics, bone grafts could be classified as autografts, allografts and synthetic biocompatible materials.

1.6.2 Autograft

Autograft is the patient's own bone, which is harvested usually from the iliac crest, but also from distal femur or proximal tibia to replace at the injury site. It is known as the gold standard of bone grafts, because it is ideal to be used as bone graft due to its inherent characteristics for new bone growth, such as osteoconductivity, osteogenicity and osteoinductivity [62]. However, autografts are associated with a few limitations as well. Harvesting of autografts inevitably needs an additional surgery at the donor-site, which can result its own complications offering short term or long term pain to the patient and these complications in total are known as donor-site morbidity (≈ 20% of all cases). An additional drawback is the specific limitation of the amount of bone tissue, which could be harvested from the patient.

1.6.3 Allograft

Allograft is the transplant of an organ or tissue from one individual to another of the same species with a different genotype. A transplant from one

person to another, but not an identical twin, is an allograft. Allograft is also known as allogenic graft or homograft. Allograft is the tissue obtained from donors or cadavers and is one of the alternatives to autograft, which helps to overcome the limitations of autograft, such as the donor-site morbidity and the limited supply [63]. However, there is a risk of immunogenic responses as well as disease transmission from the donor to the recipient. Although the allograft tissue is treated to minimize these types of risks, by tissue freezing, freeze drying, sterilization by γ-radiation/ ethylene oxide; the risk is not fully eliminated.

Even though autografts and allografts possess certain very important benefits to be used as bone grafts, their limitations focus towards the need for alternative grafts. Investigators have developed quite a variety of synthetic grafts, based on the basic needs anticipated for the grafts.

1.6.4 Synthetic grafts

Synthetic bone grafts could be basically classified as metals, polymers, ceramics, composites and biological grafts.

1.6.4.1.1 Metals and alloys [62]

The three main types of metallic implants used are austenitic stainless steel, cobalt-chromium and titanium (6 wt-% Al and 4 wt-% V). The 316L (ASTM F138, F139) having 60-65% Iron, alloyed with 17-19 % Chromium, 12-14% Nickel (and minor amounts of Mn, Mb, P, Si and S) is the most common type stainless steel used. The carbon content is particularly kept reduced (less than 0.030 wt-%) in order to minimize the possibility of *in vivo* corrosion.

Cobalt-based alloys include Haynes Stellite 21 and 25 (ASTM F75 and F90 respectively) forged Co-Cr-Mo (ASTM F799) and multiphase alloy MP 35N (ASTM F7562). The F75 and F799 alloys are virtually identical in composition with 58-69 wt-% Co and 26-30 wt-% Cr. The yield stress values for the materials are in the range 430-1028 MPa and the key difference is their composition and

processing history. The main advantage of Cobalt-Chromium alloys is their corrosion resistance in Chloride environments, which is related to its bulk composition and the surface oxide (normally Cr_2O_3).

Commercially pure titanium (CPTi) (ASTM F67 and Ti-6Al-4V alloy (ASTM F136) are two of the most common titanium based implant biomaterials. The oxygen content of the commercial purity titanium significantly affects its yield and fatigue strength. The outside oxide layer (TiO_2) offers corrosion resistance and better biological performance to these implant materials.

1.6.4.1.2 Ceramics and bioactive glasses

The most widely accepted bioactive materials for bone repair are hydroxyapatite, bioactive glasses and their composites. Hydroxyapatite holds its significance particularly due to its unique crystallographic similarity with the inorganic part of bone. However, for faster bone bonding and resorption, incorporation of bioactive glasses and tricalcium phosphate based composites are proposed.

Bioceramics such as hydroxyapatite exhibit bioactive behaviour and have been used as coatings on traditional metals for orthopaedic/dental implants. The long-term mechanical durability of some bioceramic coatings is still under debate [64]. Bioceramics are widely used as filler material for bone repair and as artificial bone matrix [65]. Clinical applications of bioceramics include artificial middle ear implants, maxillofacial implants, bone fillers, artificial iliac crests, artificial vertebrae, artificial intravertebral discs etc.

When placed in bone tissue, various bioceramics bond to bone physicochemically and in some cases, promote new bone formation leading to osseointegration [63-66]. Formation of calcium deficient (nonstochiometric) carbonate apatite on the surface of bioceramics is thought to be the crucial step in the osseointegration process [64-68]. The structure and composition of the

bioceramics determine the rate of formation and the chemical composition of apatite on these material surfaces [64-68]. The exact mechanisms by which bioceramics enhance bone formation and bonding have yet to be fully elucidated. The apatite or bone-like surface layer of bioceramics (not necessarily the bulk material), coupled with possible solution or substrate mediated local chemical conditions, is thought to be an important mediator of the 'bioactivity' of bioceramics [64].

Knowledge on the cellular/molecular processes on the surface layer of bioceramics will allow the strategic design of bioceramics which reliably enhance specific, clinically beneficial cellular functions while minimizing unwanted biological effects (for example, prolonged macrophage activation) [69]. Bioceramics that incorporate organic polymers (for example amino acids such as lysine) within a mineral network are described as organoapatites [70,71]. Organoapatites of poly(L-lysine), poly(L-sodium glutamate), and combined poly(sodium acrylate) and poly(L-lysine) have been investigated *in vivo* and exhibited apposition to bone after 35 weeks of implatation in canine and cortical bone [71].

1.6.4.1.3 Polymers

Biocompatible polymers used for orthopaedic applications are mainly poly(methyl methacrylate) PMMA as bone cement, ultra high molecular weight polyethylene (UHMWPE) as acetabular cup and biodegradable polyesters such as poly(lactic acid), poly(glycolic acid) and their copolymers as bone fixation plates and screws [72]. However, recently poly(ether ether ketone) PEEK has been used as a composite with bioactive ceramics for spinal fusion applications. The molecular characteristics of a material have a direct bearing on the local changes in pH and degradation *in vivo*.

An ideal orthopaedic/dental implant or fixation device made of biocompatible, degradable polymer should have adequate mechanical stability to

support and transfer loads known to exist in bone, allow cell adhesion and normal subsequent functions, support bone tissue regeneration and slowly degrade into nontoxic byproducts [73,74]. Poly(lactic acid) PLA, poly(glycolic acid) PGA and poly(DL lactic-co-glycolic acid) PLGA copolymer scaffolds degrade to products which can be eliminated from the body either through metabolic pathways such as the citric acid cycle or by renal excretion [75]. Poly(lactic acid) finds significant use in bone fixation devices such as bone plates and screws. Biodegradable polymeric scaffolds, seeded with living cells could be used as an alternative to traditional tissue graft materials [74,75]. Degradable polymeric materials could be transformed into proactive materials by controlling the porosity and chemical composition of the polymers, thus allowing the incorporation of bioactive substances such as growth factors, adhesive proteins, etc. [74].

1.6.4.1.4 Composites [62]

Some of the limiting factors of bioceramics like brittleness, low fracture-toughness etc. could be overcome by utilizing bioceramic composites. Biocompatible polymers such as poly(lactic acid) are suitably selected for preparing such composites, mainly with hydroxyapatite. The bioceramic is used as a filler for preparing such composites. Another option is obtaining a bioceramic coating on metals, preferably on titanium. The present trend of investigation is to explore the efficacy of biocompatible polymer-bioglass composites

1.7. BIOMIMETIC GRAFTS FOR BONE TISSUE REGENERATION

D.F Williams defined the concept of 'biocompatibility' in 1987 as follows. 'A biocompatible material is one which possess the ability to perform with an appropriate host response in a specific application'. Intelligent bone grafts are to be designed by engineering of biomimetic surfaces to modulate cellular responses. Imparting high anionic surface charge density would enhance nucleation and growth of apatite upon immersion in SBF.

The importance of surface functionalization arises from its unique characteristics that could be explored for the development of intelligent materials for tissue engineering applications. At the present time, numerous biomaterials are available as bone substitutes. They are used either in orthopaedic surgery (fillings of bone defects, hip prostheses, osteotomy etc.) in neurosurgery (vertebral fusion), in reconstructive surgery, in dental surgery especially in parodontology and implantology. Considering basic difficulties in harvesting the autografts and the lack of true osteoinduction capacities of many of the synthetic materials, there is a high demand for developing bimimetic materials that can help an increased adherence of osteoblasts onto the material surface, which can help *in situ* differentiation of osteoblast progenitor cells into active osteoblasts and an increased capacity for osteoblasts to produce larger amounts of bone matrix [76]. Bone tissue engineering has emerged as an alternative approach to circumvent the limitations associated with existing biological and synthetic grafts.

1.7.1 Biomaterial surface-tissue interactions

The clinical success of a bone implant requires the simultaneous achievement of a stable interface with host tissue and a matching of the mechanical properties between the implant and the host tissue.

1.7.1.1.1 Fibrous tissue formation

Fibrous tissue is a type of connective tissue, composed of polysaccharides, proteins and water with relatively high tensile strength due to a fairly high concentration of collagenous fibres [77]. The cells of fibrous tissue are mostly fibroblasts, the irregular branching cells that secrete strong fibrous proteins as an extracellular matrix. The most commonly secreted protein is collagen. The type and morphological appearance of the interface between the bone and the components of arthroplasties depend on multiple factors [78].

1.7.1.1.2 Stress shielding

The primary causes for the failure of an implant are interfacial loosening and stress shielding [79]. Metals and bioinert ceramics are too stiff and induce stress shielding. Stress shielding occurs when the implant prevents the bone from being properly loaded. The higher modulus of elasticity of the implant results in its tendency to carry nearly all the load. The interface between a stress shielded bone and the implant deteriorates as the bone is weakened. This results in the loosening and/or fracture of the bone at the interface or the implant. The presence of wear debris that often occurs in the artificial hip and knee joints accelerates the weakening of the stress-shielded bone. This is particularly due to the increased cellular activity occurs surrounding the host tissue- implant interface, for removing the foreign wear particles also attacks and destroys bone. The combination of stress shielding, wear debris and motion at an interface leads to the damage and failure of the implant.

1.7.2 Role of biomimetic calcium phosphate coating in biomaterial surface-tissue interaction

Successful incorporation of a prosthetic material in the human body depends on several factors such as biocompatibility, complete incorporation and maintenance of function [80, 81]. The influence of substratum free energy on growth and spreading of human fibroblasts in the presence and absence of serum proteins was studied by Schakenraad *et al* in 1986 [81]. They found that in the presence of serum proteins, cell spreading did not vary much with reference to surface energy, while in the absence of serum proteins, good spreading occurred only when the surface free energy was higher than approx. 57 ergs/cm^2. Grinner demonstrated the influence of extra cellular substrata on cell adhesiveness [82]. Schakenraad *et al* found that in the presence of serum protein cell growth increases with increase in surface free energy while Ginner found that in the absence of serum protein, there is a consistent cell growth with increase in surface free energy.

Van der valk *et al* demonstrated a sigmoid relationship between cell spreading and substratum surface free energy [83]. Hence the relationship between surface free energy and serum protein could be presumed as a complex one. However, the surface characteristics always have a relation to cell spreading and growth.

One of the requirements for an implant to show osseointegration is early stability. This can be achieved by suitable bioceramic coating on metallic implants. Advantages of titanium as a bone repairing material are it high fracture resistance, high ductility, and high specific strength. A porous structure is required to support the nutrients transport through cell growth. The problems associated with bioactive coatings of apatite on Ti and other metals are [84]

i) The coatings suffer from thickness non-uniformity

ii) Poor adhesion

iii) Low mechanical strength

The disadvantages of plasma-spray dried apatite coating are

i) Difficult to control its composition and structure

ii) May not be stable for a long period in the living body

iii) Moreover, the plasma-spray dried HA coating cannot cover the entire porous surface because of the line-of-sight nature of plasma spraying process. Additionally, the coating of HA on porous surface alters morphology of porosity by blocking the pores.

1.8. POLY(METHYL METHACRYLATE) AS BIOMATERIAL: BASIC NEED TO IMPART BIOACTIVITY

Poly (methyl methcrylate), PMMA is known for its orthopaedic applications mainly as bone cement for the fracture fixation of joint prostheses [85-88].

PMMA as antibiotic loaded microspheres finds a significant place mainly for the treatment of chronic osteomyelitis as well as for the repair of dental and infrabony defects [89, 90]. However PMMA when implanted leads to the formation of fibrous tissue at the bone-implant interface [91, 92]. The formation of fibrous tissue occurs because PMMA lacks osteoconductivity, which obviously eliminates bonding with host bone and eventually promotes stress-shielding and implant loosening. Hence it becomes a highly significant to eliminate the fibrous tissue encapsulation of PMMA for improving its efficacy towards bone bonding. Aseptic loosening of a cemented arthroplasty is a multifunctional phenomenon involving interfacial failure, bone failure, bone remodeling and cement failure [92]. There are mainly six drawbacks associated with PMMA bone cement. They are [92],

i) The high exothermic reaction (67-124 ^{0}C) at the center of the cement mantle, leading to the thermal necrosis of the bone, impaired local blood circulation, and predisposition to membrane formation at the cement-bone interface.

ii) Chemical necrosis due to release of unreacted methyl methacrylate

iii) Shrinkage of the cement during polymerization

iv) Large stiffness mismatch between cement and the adjacent bone

v) The three week-link zones namely the cement mantle, the implant-cement interface, the cement-bone interface

vi) Cement particles (debris) interact with surrounding tissues evoking inflammatory periprosthetic tissue responses and increasing bone destruction.

1.8.1 Active approaches

Investigations towards the development of bioactive cement has been undergoing actively for the past two decades. One of the popular approaches to achieve this goal was to use hydroxyapatite as filler in the methacrylate matrix [93]. In another approach, acrylic bone cement was modified by the addition of tricalcium phosphate, HEMA and EGDMA [94]. According to their observation, when acrylic bone cement contains TCP, with HEMA and EGDMA, the incompatibility between acrylic bone cement and TCP can be ameliorated. Another study to impart bioactivity was via modification with methacryloxy propyltri-methoxysilane and calcium acetate [95]. A recent one in this series is modification of PMMA based bone cement by gamma methacryloxy propyltrimethoxysilane (MPS) and calcium acetate by Tsukeka *et al* in 2006 [96]. Their investigation was mainly focused on handling, mechanical and histological properties and they found that the modified version of the bone cement exhibited osteoconduction, which the conventional PMMA lacked.

1.8.2 Functionalization as a method

The importance of surface functionalization arises from its unique characteristics that could be explored for the development of intelligent materials for tissue engineering applications. Surface functionalization helps to impart desired properties to the material without altering its bulk properties significantly. Surface functionalization of PMMA is an area, which is hardly explored, and hence only a few reports are available with this approach. One of them was coupling adenosine triphosphate (ATP) onto PMMA after surface hydrolyzing PMMA with NaOH [97]. However, a calcium hydroxide pretreatment is required for the nucleation of calcium phosphate on its surface. Other approaches are mainly oriented on the development of composites of PMMA [98, 99].

1.8.3 Role of surface phosphorylation to trigger nucleation of calcium phosphate on polymers

It has been described already in previous sections (1.3.2.1) that biocompatible polymers, rich in negatively charged groups, are capable of nucleating bone-like apatite under *in vitro* conditions [28-30]. Moreover, surface functionalization has been recognized as an important method to stimulate *in vitro* biomimetic deposition of calcium phosphate on various polymers or metallic substrates under simulated physiological conditions [100-105]. Studies have proved that the heterogeneous nucleation of apatite is greatly enhanced by terminal groups such as -Si-OH, -Ti-OH, -COOH, and phosphate groups [101-105]. Among these, surface phosphorylation has a higher potential to trigger calcium phosphate nucleation compared to many other groups [33].

A popular method of surface phosphorylation is using phosphoric acid and urea, which has been followed by many researchers [106-112]. The method involves refluxing the substrate with 98% orthophosphoric acid and urea (wt ratio = 1:5) in presence of dimethyl formamide at 120 ^{0}C for 60 to 120 minutes, based on the substrate property. Varma *et al* have explored this technique to induce porous calcium phosphate coating on phosphorylated chitosan [108]. In another investigation they could prove the growth of calcium phosphate phase on PMMA after coupling the surface with ATP molecule [97]. Li *et al* have used sodium hydroxide-phosphoric acid instead of urea-phosphoric acid method for phosphorylating bamboo [108].

Suzuki *et al* reported a method for phosphorylating poly(vinyl alcohol), PVA using 100 % phosphoric acid along with dicyanodiamide and urea in dimethyl formamide (DMF) at 130 ^{0}C [110].

Another method is using phosphoric acid and triethyl phosphate, used by Granja *et al* for phosphorylating regenerated cellulose [111]. In this process, the

regenerated cellulose was initially swelled in distilled water, followed by swelling in ethanol and then in hexanol for 24h prior to phosphorylation. The sample was dispersed in hexanol and a solution of phosphorous pentoxide (50g) in 37 mL of triethyl phosphate and 42 mL of 85% phosphoric acid was added portion-wise to the suspension. The reaction was allowed to proceed for time periods varying as 4h, 8h and 24h at room temperature. The *in vitro* biocompatibility evaluation of cellulose phosphates as biomaterials was further evaluated by using human bone marrow stromal cells (HBMSC), in terms of cytotoxicity, cell attachment, proliferation and immunohistochemistry [112].

1.8.4 Origin and specific attractions of the present method

It has been observed by several investigators that functionalized polymers with surface bound phosphate group induces in vitro nucleation of calcium phosphate crystals on their surface under simulated physiological environment. However many of these surfaces functionalized polymers require a calcium hydroxide/calcium chloride pretreatment for the in vitro mineralization of calcium phosphate [97, 108, 109, 111]. Moreover the popular surface phosphorylation techniques are done at higher temperatures (>100 ^{0}C), using organic solvents and catalysts, which may alter the basic polymer characteristics significantly [97, 108, 109, 111].

The surface phosphorylation technique adopted for the present work was based on a procedure, which does not involve any organic solvent and is expected to minimally alter the basic characteristic properties of the copolymer. The phosphorylating medium used was 76% phosphorous pentoxide (P_2O_5). The first reported use of this procedure was by Ferrel *et al* for phosphorylating proteins [113]. Pogell *et al* applied the methodology to phosphorylate fructose in 1953. However, use of this procedure for phosphorylating polymers was hardly found in literature. The present study uses this agent for surface phosphorylation of polymers with a free hydroxyl group.

1.9. EFFICACY OF SURFACE PHOSPHORYLATED POLY(2-HYDROXY ETHYL METHACRYLATE-CO-METHYL METHACRYLATE) FOR BIOMIMETIC MINERALIZATION

The commercially available PMMA based bone cement is a two component self- setting cement having PMMA powder mixed with initiator and an activator as one component and a monomer component (MMA). The two components when mixed together, gives paste like mass, which will undergo setting within 8 minutes [114]. In the present study, methyl methacrylate, MMA was initially copolymerized with a known biocompatible comonomer with an active hydroxyl (-OH) group, 2-hydroxy ethyl methacrylate, HEMA, in the molar ratio HEMA: MMA = 0.07:0.90. The active hydroxyl group (-OH) in the copolymer thus incorporated will facilitate the surface phosphorylation.

1.9.1 2-Hdroxy ethyl methacrylate (HEMA) as the comonomer

The monomer 2-hydroxy ethyl methacrylate is of great interest to biomedical researchers because of its unique properties

i) It could be easily polymerized and copolymerized

ii) It has a primary alcohol group which offers tremendous possibility of formation of new HEMA derivatives, leaving the double bond unchanged.

Poly(2-hydroxy ethyl methacrylate) has been widely recognized in the field of biomedical polymers mainly due to its biocompatibility and hydrophilicity [115]. Wichterle, in the pioneering work of poly(HEMA) showed that it can form hydrogels, which later led to the development of soft optical lenses [116]. The biomedical applications of poly(HEMA) is numerous, which includes use as histological embedding medium [117], in dentistry as bonding agent [118], for the immobilization of enzymes and drugs in pharmaceutical applications [119], as

composites of collagen for biodegradable implants [120] and as contact and intra-ocular lenses [121].

2-Hydroxy ethyl methacrylate is a less expensive commercially available monomer. One of the cost effective methods of synthesizing HEMA is a single step trans esterification process of methyl methacrylate (MMA) with ethylene glycol [122]. During this reaction, a second trans esterification occurs providing a divinyl monomer, ethylene glycol dimethacrylate (EGDMA) and a low percentage of methacrylic acid resulting from the hydrolysis of HEMA. The reaction scheme is shown below [115]

$$CH_2=C(CH_3)COOCH_3 + HOCH_2CH_2OH \longrightarrow CH_2=C(CH_3)COOCH_2CH_2OH + CH_3OH$$

MMA Ethylene glycol HEMA Methanol

$$CH_2=C(CH_3)COOCH_2CH_2OH + CH_2=C(CH_3)COOCH_3 \longrightarrow$$

MMA HEMA

$$CH_2=C(CH_3)COOCH_2CH_2OCOC(CH_3)=CH_2$$

EGDMA

The reaction of methacrylic acid with ethylene oxide is another common method to prepare HEMA [123]. Purification of HEMA is based on the solubility of the monomer in water or diethyl ether and its insoulubility in petroleum ether or hexane (EGDMA is soluble in hexane). Preliminary assessment of the purity of HEMA could be done by thin layer chromatography by using n-hexane –diethyl ether (1/1 v/v) as the solvent, silica gel as the absorbent and n-hexane as the counter-current solvent. Ethylene glycol dimethacrylate is removed by liquid-liquid continues extraction of aqueous solution of HEMA (water-HEMA ¼ v/v) containing 0.3% w/v t-butyl catechol as the polymerization inhibitor for a period of 14-15h. 2-Hydroxy ethyl methacrylate could be then recovered form aqueous

solution by salting out with sodium chloride after which separated HEMA was diluted again with 10 volumes of water and salting out could be repeated.

Uncross-linked polymer is insoluble in water but soluble in dimethyl sulfoxide (DMSO), dimethyl formamide (DMF), alcohols or diethylene glycol. The cross-linked polymer swells in water and the degree of swelling is high in polar organic solvents such as alcohols or ethylene glycol.

Copolymerization of HEMA with MMA

The Alfrey-Price parameters Q and e of HEMA are 1.75 and –0.39 respectively [124]. The value of reactivity ratios r1 and r2 with MMA are given as 1.05 (r1) and 0.30 (r2) for bulk polymerization using benzoyl peroxide as initiator [125]

HEMA-MMA copolymers were synthesized and studied for their potential to be used for microencapsulating various cells. For example, HEMA-MMA copolymer microcapsules were devised and evaluated for pancreatic islets by Crooks *et al* [126]. Wells *et al* have designed a copolymer of HEMA and MMA with 80 wt-% HEMA for encapsulating rat hepatocytes [127]. Another group has prepared thermoplastic copolymers of HEMA and MMA (75/2) with different amounts of ethylene glycol dimethacrylate (EGDMA) to investigate their suitability for encapsulating Chinese hamster ovary cells [128]. The Chinese hamster ovary cells survived the microencapsulation process and the metabolic activity of the encapsulated cells increased within the 14 days of observation. Another proposed application of HEMA-MMA-EGDMA copolymer is to be used as beads for size exclusion chromatography [129]. The copolymer was prepared by free radical suspension polymerization using azobiz isobutyronitrile (AIBN) as initiator at 70 ^{0}C. Most of the cases, HEMA component is higher in order to keep significant amount of hydrophilicity. However, copolymerization of MMA with HEMA, following surface funtionalization by phosphorylation is hardly reported.

1.10. OBJECTIVE AND SCOPE OF THE WORK

Congenital or acquired bone repair is one of the major concerns in human health care. Reviewing the contemporarily used bone graft materials, bioactive ceramics and glasses are popular for osteointegration and bone-bonding, but is associated with basic limitations such as brittleness and restricted processability. While biocompatible metals are known for their toughness, they significantly lack osteointegrative property. Polymers are known for their easiness in processing, but lack osteointegrative property. However, biofunctionality could be easily imparted to polymers through suitable biomimetic techniques. The significance of biomimetic bone graft materials arises from their unique capability in establishing smart interfaces by eliciting *in vivo* biomineralization and accelerates osteoinduction; thus could be suitably proposed as potential candidates for bone repair. One of the versatile strategies to achieve biomimetic interface is through surface functionalization of the polymers with active functional groups such as Si-OH, -COOH, $-PO_4$ etc.

It has been observed by several investigators that functionalized polymers with surface bound phosphate group induces in vitro nucleation of calcium phosphate crystals on their surface under simulated physiological environment. However, many of these surface functionalized polymers require a calcium hydroxide/calcium chloride pretreatment for the in vitro mineralization of calcium phosphate. Moreover the popular surface phosphorylation techniques are done at higher temperature (>100 ^{0}C), using organic solvents and catalysts, which may alter the basic polymer characteristics significantly.

The present work is focused on imparting biofunctionality and osteocompatibility to a clinically significant polymer, poly(methyl methacrylate), PMMA through an intelligent biomimetic approach. PMMA is clinically used as bone cement for the fixation of joint prostheses. The commercially available

PMMA based bone cement is a two component self- setting cement having PMMA powder mixed with initiator and an activator as one component and a monomer component (MMA), which when mixed with the powder undergoes setting within 8 minutes. However, in the *in vivo* environment, PMMA is isolated from the surrounding tissues by a layer of fibrous tissue formed around it. The formation of fibrous tissue occurs because PMMA lacks osteoconductivity, which obviously eliminates bonding with host bone and eventually promotes stress-shielding and implant loosening. Hence it becomes a highly significant need to eliminate the fibrous tissue encapsulation of PMMA to improve its efficacy towards bone bonding.

The objective of the present work is to prevent the formation of fibrous tissue, by imparting functionally active surface that can help bone growth.

The aims of the present study are

i) To synthesize a copolymer of methyl methacrylate, MMA with a known biocompatible comonomer with an active hydroxyl (-OH) group, namely, 2-hydroxy ethyl methacrylate, HEMA, without affecting its favorable bulk properties

ii) To functionalize the copolymer, poly(HEMA-co-MMA) by surface phosphorylation using a a phosphorylating agent capable of surface phosphorylating biocompatible polymers with hydroxyl (-OH) group, at relatively lower temperatures ($<100\ ^{0}C$)

iii) To assess the ability of the surface phosphorylated polymer, poly(HEMA-co-MMA) to induce *in vitro* nucleation of calcium phosphate was evaluated under accelerated simulated physiological environment using 1.5xSBF (simulated body fluid).

iv) To investigate the *in vitro* cytocompatibility and cell adhesion behaviour of phosphorylated poly(hydroxy ethyl methacrylate-co-methyl methacrylate) using human osteosarcoma (HOS) cell-line.

v) To investigate the *in vivo* toxicological response of the surface phosphorylated as well as *in vitro* calcium phosphate coated polymer as per ISO 10993

vi) To evaluate the efficacy of bone bonding by short-term bone implantation in rabbits as per ISO 10993-6: 1994(E): Test for local effects after implantation, *clause 6.0: Test method for implantation in bone* using'CMW1' poly(methyl methacrylate) radiopaque bone cement (DePuy, Johnson and Johnson, England) as control material.

CHAPTER 2

MATERIALS AND METHODS

This chapter on materials and methods is divided into *three* parts.

The first part deals with the synthesis of poly(2-hydroxy ethyl methacrylate-co-methyl methacrylate), poly(HEMA-co-MMA), its preliminary characterization, surface phosphorylation of poly(HEMA-co-MMA), kinetics of phosphorylation and its evaluation, in vitro mineralization of calcium phosphate on surface phosphorylated poly(HEMA-co-MMA) and its assessments by suitable characterization techniques.

The surface phosphorylation technique was further extended to selected biocompatible polymers containing hydroxyl (-OH) group (either naturally or induced by suitable techniques) using the same phosphorylating system, the ability of the surface phosphorylated polymer to induce *in vitro* nucleation of calcium phosphate was evaluated.

The second part focus on the in vitro cytocompatibility and the extent of in vitro biomineralization of surface-phosphorylated poly(HEMA-co-MMA) and its

ability to facilitate bone specific proteins such as osteocalcin and alkaline phosphatase using Human Osteosarcoma (HOS) cells.

The last part solely concentrates on biological evaluation of surface phosphorylated and in vitro hydroxyapatite coated poly(HEMA-co-MMA) as per ISO 10993 part X, XI and ASTM F 756 and the efficacy of these two test samples towards osteointegration and bone tissue regeneration under *in vivo* environment by short term bone implantation in rabbits using commercially available CMW1 bone cement as control sample according to ISO 10993 part VI.

2.1. SYNTHESIS OF POLY(HYDROXY ETHYL METHACRYLATE-CO-METHYL METHACRYLATE)

Poly(2-hydroxy ethyl methacrylate-co-methyl methacrylate), poly(HEMA-co-MMA) was synthesized by free radical initiated bulk polymerization of the monomers, 2-hydroxy ethyl methacrylate (HEMA) and methyl methacrylate (MMA) and simultaneously cross-linked by ethylene glycol dimethacrylate (EGDMA).

2.1.1. Materials

The monomers, 2-hydroxy ethyl methacrylate (HEMA) (Assay: 98%) and methyl methacrylate (MMA) (Assay: 99%) were procured from Aldrich chemical Co. USA while the cross-linker, ethylene glycol dimethacrylate (EGDMA) (Assay:98%) was from Fluka. Benzoyl peroxide (Assay: 98%), the free radical initiator used for the polymerization reaction was purchased from S.D.Fine India Ltd. The inhibitor removal column used for 2-hydroxy ethyl methacrylate was procured from Aldrich chemical Co., USA. Phosphorous pentoxide (Assay: 98+, ACS reagent) was procured from Aldrich chemical Co. USA. Other chemicals used were purchased from Ranbaxy India Pvt. Ltd. Poly(propylene) dishes used for casting the copolymer were purchased from Tarsons-India Pvt. Ltd.

Methyl methacrylate was made free of inhibitors by washing with aqueous sodium hydroxide solution (4%), followed by washing with distilled water and drying the inhibitor free monomer by placing over anhydrous magnesium sulphate. The monomer, HEMA was made free of inhibitor by passing through inhibitor remover column.

2.1.2. Polymerization

Poly(2-hydroxy ethyl methacrylate-co-methyl methacrylate) was synthesized by free radical bulk polymerization technique using 0.5 wt-% benzoyl peroxide as initiator. The monomers were taken in molar ratios varying from HEMA: MMA 0.07:0.90, 0.19: 0.75, 0.38: 0.5, 0.57: 0.25, 0.69: 0.10. PMMA and poly(HEMA) were also synthesized following the same conditions. The copolymers as well as the homopolymers were *in-situ* cross-linked using 1wt-% ethylene glycol dimethacrylate during polymerization.

A typical copolymerization reaction was conducted as follows. The inhibitor free monomers were taken out from refrigerator conditions and allowed to attain room temperature. The monomers were accurately weighed using an analytical balance as per the ratio and transferred in to a three-necked RB flask fitted with a condenser under nitrogen atmosphere. The RB flask with the contents was placed on a water bath kept on a magnetic stirrer (IKA, Germany). The initiator, benzoyl peroxide was carefully added to the contents in the RB flask under stirring, which was followed by addition of the cross-linker, ethylene glycol dimethacrylate. The temperature of water bath was set at 80 ^{0}C and the stirring rate 300 rpm. The polymerization was done under constant observation and just before gellation (approximately 12 minutes) the contents were transferred on to a clean poly(propylene) petri dishes. The polymerization was allowed to continue in a clean preheated air oven (set at 70 ^{0}C) for 24h. The copolymers with HEMA: MMA molar ratio varying as 0.07:0.90, 0.19: 0.75, 0.38: 0.5, 0.57: 0.25, 0.69: 0.10 were prepared as per the above-mentioned procedure. The compositions, their

representation, corresponding monomer ratio, amount of initiator and the amount of cross-linker used for preparing the copolymers are given in table 2.1.

Even though most of the characterization techniques prefer films, some of them prefer disc or cylinder shaped material with specific dimensions. In order to achieve the specific dimensions, samples were moulded using poly(propylene moulds with the required dimensions. Figure 2.1 illustrates the different shapes of the copolymer samples prepared. With the exception of microspheres all other shapes were prepared by free radical initiated bulk polymerization while the microspheres were prepared by free radical initiated suspension polymerization technique The poly(HEMA-co-MMA) microspheres were prepared by following a procedure reported elsewhere [130]. Briefly, the copolymer microspheres were prepared by using a free radical suspension polymerization using benzoyl peroxide (S.D. Fine, India Ltd, Mumbai) as initiator in presence of aqueous inorganic magnesium hydroxide gel medium prepared *in situ*. The microspheres were simultaneously cross-linked using ethylene glycol dimethacrylate.

Table 2-1 Composition of copolymers

Composition	PH_1	PH_2	PH_3	PH_4	PH_5
HEMA (moles)	0.07	0.19	0.38	0.57	0.69
MMA (moles)	0.90	0.75	0.50	0.25	0.10
Benzoyl peroxide (initiator), wt %	0.5	0.5	0.5	0.5	0.5
EGDMA (cross-linker), wt %	1.0	1.0	1.0	1.0	1.0

The homopolymers poly(HEMA) and poly(MMA) were also synthesized following free radical initiated bulk polymerization technique using benzoyl peroxide as initiator and ethylene glycol dimethacrylate as cross-linker. Similar to the copolymers, homopolymers were also cast on poly(propylene) petry dishes to obtain the films.

Poly(HEMA) being a highly hydrophilic polymer, increased amounts of HEMA in poly(HEMA-co-MMA) may severely affect the swelling and mechanical properties of the copolymer. Hence the equilibrium swelling of the copolymer with varying HEMA to MMA ratio was determined. Further, the ability to induce nucleation of calcium to phosphate was monitored for poly(HEMA-co-MMA) with varying HEMA concentration. It was found that the composition with lowest HEMA content, represented as PH_1 with HEMA: MMA ratio 0.07:0.90, showed minimum swelling and it was also capable of nucleating calcium phosphate under simulated physiological condition. Preliminary mechanical property evaluation also showed that PH_1 possess good compressive and tensile properties and hence the study was mainly focused on PH_1.

The effect of cross-linking on PH1 was further evaluated by varying the cross-linking density from 0.5 wt-% to 3 wt-%. The uncross-linked PH_1 was used as a reference for finding the effect of cross-linking in the degree of swelling.

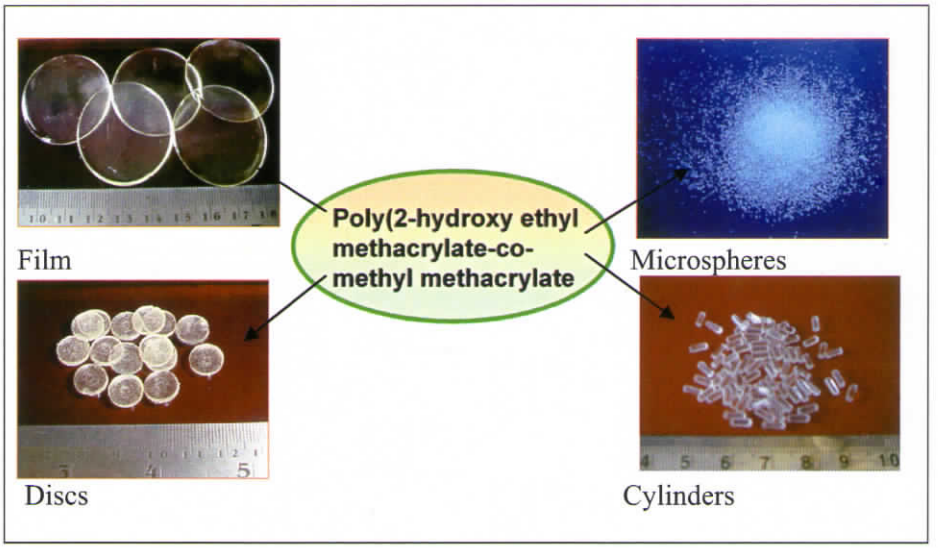

Figure 2-1 Poly(HEMA-co-MMA)- different shapes

2.2. CHARACTERIZATION

As the study mainly focuses on the composition PH_1, characterization techniques such as atomic force microscopy (AFM), X-ray photoemission spectroscopy (XPS), Dynamic mechanical analysis (DMA), and residual monomer analysis etc. were carried out only on this particular composition. However, preliminary characterizations such as Micro FT-IR, Thermogravimetric analysis, Percentage equilibrium swelling etc. were done for all the compositions.

2.2.1 Micro FT-IR analysis

FT-IR spectra of the samples were collected using Thermo Nicolet 5700 FT-IR microscope. Samples in the form of film were used for the analysis. All the poly(HEMA-co-MMA) compositions, PH_1, PH_2, PH_3, PH_4 and PH_5 were subjected to analysis.

2.2.2 Differential scanning calorimetry

The glass transition temperature (Tg) of PMMA, PHEMA and poly (HEMA-co-MMA) were determined using differential scanning calorimeter (DSC-2920) TA instruments Inc, USA based on ASTM E 1356-03, '*Determination of glass transition temperture of polymers by differential scanning calorimetry'*. The samples were pre-treated by a first heat cycle done from room temperature to 200 ^{0}C to get rid of any internal stress stayed back during the processing. For the determination of Tg, the heating rate was 5 ^{0}C /min and the purge gas was nitrogen.

2.2.3 Thermogravimetric analysis

The thermogravimetric analysis (simultaneous TGA and DTA) of poly(HEMA) poly(MMA) and PH1 before and after phosphorylation was performed as per ASTM E-1131-03 using simultaneous DTA-TGA (model SDT 2960) TA Instruments, Inc, USA. A heating rate of 10^{0}C/min from room temperature to a maximum temperature of 600^{0}C was used. Purge gas was Nitrogen.

2.2.4 Residual monomer analysis

The residual monomers present in poly(HEMA-co-MMA) was estimated by Gas chromatography following the headspace extraction of the sample using HS40 headspace sampler and 1022 GC, FID detecter (Perkin-Elmer, USA). A known weight of PH1 was Known weight of standard solutions of monomers, methyl methacrylate and hydroxy ethyl methacrylate in dioctyl phthalate (DOP) at very low concentration (10ppm) sealed in headspace vial and subjected to headspace GC analysis in an exhaustive manner. A blank analysis (DOP alone) was also performed. Similarly, a known weight of PH1 was analyzed separately until exhaustive extraction. The peak corresponding to 1.0610 1.07 min. was quantified using MMA analysis.

2.2.5 X-ray Photoemission Spectroscopy

The X-ray photoemission spectroscopy of PH_1 was performed in a KRATOS AXIS ULTRA system (Kratos Analytical, Manchester, UK) of Murdoch University, Perth, Western Australia. The conditions employed for wide scan are pulse energy: 80 eV, Anode: Al, emission current 12mA, scan time 120seconds, number: 4, HV: 11KV and step: 1eV. For the scanning of phosphorous peak, the conditions used are pulse energy: 20 eV, Anode: Al, emission current 12mA, scan time 60seconds, number: 4, HV: 11KV and step: 0.1eV.

2.2.6 Atomic Force Microscopy (AFM)

The surface topography and roughness profile of PH_1 was acquired using atomic force microscope cantilevers (spring constant =0.5 8N/m) in the contact mode using Digital Instruments Multimode Nanoscope E with the software Nanoscope V 6.12 r2. The difference in the force of attraction between the unmodified polymer, surface phosphorylated polymer and the hydroxyapatite coated polymer was calculated.

2.2.7 (a) Contact angle measurement

The surface hydrophilicity of PH_1 was measured by water contact angle using NRL contact angle goniometer (Rame's hart Inc, New Jersy, USA, model 100).

2.2.7. (b) Equilibrium swelling in Phosphate buffer saline (PBS)

Equilibrium swelling of the copolymers, PH_1, PH_2, PH_3, PH_4 and PH_5 were measured in phosphate buffer saline and compared with that of poly(HEMA). The swelling study was carried out for 336h. Circular specimens with dimensions 1 cm diameter x 0.5 cm thickness were prepared for the swelling studies using Teflon® moulds. Four specimens from each composition were taken for the study. Phosphate buffer saline (PBS) with pH 7.4 at 37^0C was prepared as per the composition designated in table 2.2. Each of these specimens was immersed in 15 mL of PBS in glass containers and kept in an incubator at 37 °C. The weight of the

samples and the pH were recorded at 12-h intervals for the first 48h and then at 96 h and at 336h.

Table 2-2 Composition of Phosphate Buffer Saline (PBS) solution

Chemical	Quantity (g)
Sodium chloride	8.0
Potassium chloride	0.2
Disodium hydrogen phosphate	1.15
Potassium dihydrogen phosphate	0.2
Made up to 1000 mL using deionized distilled water	

The equilibrium swelling degree was calculated as,

$$\text{Swelling degree (\%)} = \frac{W_w - W_d}{W_d}$$

Where, W_d and W_w are the weight of dry and swollen samples respectively.

2.2.8 Degree of cross-linking Vs Equilibrium swelling

The degree of cros-linking in PH_1 was varied by varying EGDMA concentration say from 0.5 wt- % to 3.0 wt-% and the equilibrium swelling of each specimen was determined as per the procedure mentioned in section 2.2.7.

2.2.9 Compressive strength

Compressive strength of PH_1 and phosphorylated ph1 (PPH1) was measured using Instron-3345, (Instron, UK) at a crosshead speed of 1mm/min (temperature $25^0 \pm 2^0$ C, RH 50%). The samples were cylindrical in shape with 2mm diameter and 4 mm height.

2.3. PHOSPHORYLATION

The surface phosphorylation technique adopted was based on a procedure, which does not involve any organic solvent and is expected to minimally alter the basic characteristic properties of the copolymer. The phosphorylating medium used was 76% phosphorous pentoxide (P_2O_5). The first reported use of this procedure was by Ferrel *et al* for phosphorylating proteins [113]. Pogell *et al* applied the methodology to phosphorylate fractose [131]. However, use of this procedure for phosphorylating polymers was hardly found in literature. The present study uses this agent for surface phosphorylation of polymers with a free hydroxyl group.

In a typical phosphorylation procedure, 1g of poly(2-hydroxy ethyl methacrylate-co-methyl methacrylate) film was taken in a RB flask fitted with the condenser. To this, 10 g of phosphorylating medium was added and heated at a temperature 80 $\pm$ 2^0C using a water bath and refluxed for 1h at 300 rpm. The contents in the flask were then allowed to cool to room temperature and then the film was taken out and washed with distilled water for several times to make free of excess reagents and then dried in an air oven at 70 $\pm$ 2^0C for analysis.

2.3.1 Description of the phosphorylating reagent

It is not a discrete molecular entity and considered as a mixture resulting from the partial hydration of P_2O_5. The resulting solution is a complex mixture of phosphoric acids consisting of orthophosphoric acid and linear phosphoric acid chains [113].

2.3.2 Kinetics of phosphorylation

The kinetics of phosphorylation with respect to time was performed by surface phosphorylation of PH_1 at different time periods (15 minutes, 30 minutes, 45 minutes, and 60 minutes).

Phosphorylation of poly(HEMA-co-MMA) compositions PH_2, PH_3, PH_4, PH_5 and poly(HEMA) were conducted in the same way as per the procedure described above. The extent of phosphorylation was quantitatively estimated and compared with phosphorylated PH_1.

2.4. ASSESSMENT OF PHOSPHORYLATION

The status of phosphorylation was qualitatively assessed with the help of Micro-FT-IR spectroscopy. The degree of phosphorylation was quantitatively estimated using UV-Visible spectroscopy. Phosphorylated poly(HEMA-co-MMA) samples: PPH_1, PPH_2, PPH_3, PPH_4 and PPH_5 and phosphorylated poly(HEMA) were subjected to analysis. The chemistry of surface bound phosphate group and the binding energy status of phosphorous on phosphorylated PH_1 was further estimated using X-ray photoemission spectrophotometry.

2.4.1 Assessment of phosphorylation by Micro-FT IR spectroscopy

The FT-IR spectra of the surface phosphorylated samples were collected using the machine Thermo Nicolet 5700 FT-IR (Madison, WI) microscope as per the procedure described in section 2.2.1 and compared.

2.4.2 Estimation of surface bound phosphate by UV-Visible spectroscopy

Estimation of the surface bound phosphate was done quantitatively by a procedure described in Environmental chemistry of Boston Harbor-IAP 2006, which is a modification of the procedure, by Strickland and Parsons (1968) [132]. The phosphate concentration is estimated in ppm using the UV-Visible

spectrophotometer, Shimadzu UV mini –1240. The basic principle involved in the procedure is the reaction between reactive phosphate group in the sample with a composite reagent containing ammonium paramolybdate, ascorbic acid and potassium antimonyl-tartarate. The orthophosphate in the sample react with molybdate to give phosphomolybdic acid and the phosphomolybdic acid is reduced by ascorbic acid to form a blue complex. The intensity of the blue colour at 885 nm is proportional to the phosphate concentration in solution.

Phosphate + Molybdate ⟶ Phosphomolybdic acid

Phosphomolybdic acid + Ascorbic acid ⟶ Reduced phosphomolybdate complex

The calibration graph was plotted by preparing standard potassium dihydrogen phosphate solutions of concentration varying from 2 to 10 mg/L and consequently reducing them to phosphomolybdate complex and measuring the absorbance at 885 nm.

The samples for phosphate estimation were prepared with dimensions as 1cm^2 area and 1mm thickness. The phosphorylated samples were refluxed with 1N HNO_3 for 8h at 100 ^{0}C and the extract thus obtained was used for the analysis.

2.4.3 Estimation of phosphate by X-ray photoelectron spectroscopy

The X-ray photoelectron spectroscopy of surface phosphorylated PH_1 (PPH_1) was performed as per the procedure described in section 2.2.5 and compared with PH_1.

2.4.4 Phosphorylation Vs Topographical changes

The topographical variation of PH1 as a result of phosphorylation was studied using optical, scanning electron and atomic force microscopy.

Table 2-3 Ionic concentration and pH of human blood plasma, SBF and 1.5 SBF

Ionic concentration (mM)									pH
	Na^+	K^+	Ca^{2+}	Mg^{2+}	Cl^-	HCO_3^-	HPO_4^{2-}	SO_4^{2-}	
Human Blood plasma	142.0	5.0	2.5	1.5	103.0	27.0	1.0	0.5	7.38
SBF	142.0	5.0	2.5	1.5	147.8	4.2	1.0	0.5	7.4
1.5 SBF	213.0	7.5	3.8	2.3	223.2	6.3	1.5	0.8	7.25

Evaluation of biomimetically mineralized of calcium phosphate phase was carried out by both qualitative and quantitative methods. The preliminary qualitative evaluation of the calcium phosphate coating was done by optical microscopy while scanning electron microscopy, atomic force microscopy and transmission electron microscopy coupled with energy dispersive X-ray analysis were used for the detailed examination of the nucleation, crystal growth profile, calcium phosphate phase and Ca/P ratio. The quantitative estimation of calcium phosphate coating was done with the help of atomic absorption spectroscopy and UV-Visible spectroscopy. The calcium phosphate phase analysis was performed using wide angle X-ray diffraction pattern.

2.5.1 Optical microscopy

The preliminary observation of the calcium phosphate coating was done using optical microscope (Lieca model: MZ6).

2.5.2 Scanning electron microscopy - Energy dispersive X-ray analysis

Scanning electron microscopic evaluation was carried out using scanning electron microscope (SEM Hitachi model S-2400, Japan) after coating the specimens by gold sputtering technique and energy dispersive X-ray analysis (EDS) was done on OXFORD EDS system attached to the SEM. The analysis was carried out for calcium phosphate coated phosphorylated poly(2-HEMA-co-MMA) samples, PPH_1, PPH_2, PPH_3, PPH_4 and and phosphorylated poly(HEMA). The coating formed at different time periods, such as 3 days, 10 days and 15 days were subjected to analysis. The control samples selected for the study were unmodified PH_1, poly(HEMA) and poly(MMA). The EDS patterns of the coating were also acquired.

2.5.3 Transmission electron microscopy and Energy dispersive X-ray (TEM-EDS) analysis

The ultrastructural features of the calcium phosphate coating, its transformation from amorphous to crystalline state and the calcium to phosphorous ratio has been understood with the help of transmission electron microscope, Jeol 2000, Japan of Nano Research Institute, Curtin University of Technology, Western Australia. The calcium phosphate coating formed on the surface of phosphorylated PH_1 at different time periods (3days, 10 days and 15 days) was dispersed in methanol, taken on carbon coated copper grid and observed. The amorphous to crystalline transformation was evident with the help of selected area electron diffraction patterns (SAED). The calcium to phosphorous ratio was calculated using the EDS detector attached to the TEM machine.

2.5.4 Atomic force microscopy

The coating morphology, calcium phosphate crystal size and the ultra structure of the mineralized structure were studied using Digital Instruments Multimode Nanoscope E with the software Nanoscope V 6.12 r2 as per the procedure described in section 2.2.6. The calcium phosphate coating formed on PPH_1 at two different time periods, 3 days and 15 days was subjected to analysis.

2.5.5 Wide angle X-ray diffraction

The calcium phosphate phase formed on the surface of phosphorylated PH_1 at different coating time periods was analyzed using wide angle X-ray diffraction patterns taken using D5005 X-ray diffractometer (SIEMENS, Germany) with scanning angle 2θ, from 5 to 50 and compared with hydroxyapatite PDF data.

2.5.6 Determination of Calcium by Atomic absorption spectroscopy

The quantitative estimation of calcium on the calcium phosphate coated samples were performed by with the help of atomic absorption spectroscopy using a Varian spectr AA10 machine (Varian Techtron, Victoria, Australia.).

In this study air –acetylene flame was used to ignite the sample. The light source for the experiment was a calcium hollow cathode lamp. The strongest absorption line for atomic calcium is at 422.7nm. Calibration curve was prepared with known-standard calcium solutions, followed by determination of the calcium concentration of the samples.

The amount of calcium in the coating formed on phosphorylated poly (HEMA-co-MMA) when subjected to simulated physiological environment with respect to time was measured. The effect of HEMA wt-% in the copolymer with respect to calcium uptake was determined by measuring the calcium content of the phosphorylated poly(HEMA-co-MMA) samples PPH_1, PPH_2, PPH_3, PPH_4 and PPH_5 immersed in 1.5SBF for 15 days and comparing with the calcium uptake of

phosphorylated poly(HEMA). The samples used for the estimation were of the same dimensions, 1 cm diameter and 1mm thickness. The coated samples were immersed in known quantity of 1M Nitric acid for 24h followed by ultrasonication for 30 minutes and the extract thus obtained was used for the analysis.

2.5.7 Determination of phosphate by UV-Visible spectroscopy

The quantitative estimation of the phosphate in the calcium phosphate coating was done using UV-Visible spectroscopic technique following the basic principle described in section 2.4.2. The same solution used for measuring calcium was taken for the phosphate estimation in order to get an idea of the calcium to phosphate ratio of the calcium phosphate coatings.

2.6. EXPLORING THE PHOSPHORYLATION TECHNIQUE FOR OTHER POLYMERS WITH HYDROXYL GROUP

It would be now inevitable to investigate the possibility of exploring the proposed phosphorylating procedure for other biocompatible polymers with hydroxyl (-OH) group and their ability to nucleate calcium phosphate phase under simulated physiological environment. The polymers selected for this study are

i) Poly (vinyl alcohol), PVA

ii) Ethylene vinyl acetate copolymer (EVA 2825) (after subjecting to surface hydrolysis)

iii) Poly (ethylene terephthalate) (After subjecting to surface hydrolysis)

2.6.1 Poly (vinyl alcohol)

Poly(vinyl alcohol) is a biocompatible polymer with hydroxyl group as side chain in its monomer unit, which could be easily phosphorylated. In the present study PVA has been selected as a simple model for studying the role of surface phosphorylation, which leads to the in vitro nucleation of calcium phosphate phase on its surface. Apart from this, the ability of surface

phosphorylated PVA in enhancing Human osteosarcoma (HOS) cell adhesion was also investigated.

2.6.1.1 Experimental

Hot water soluble PVA (average molecular weight 100000) was procured from Sigma Chemicals Co, St. Louis, USA. The chemical reagents used for phosphorylation are the same as that used for phosphorylating poly(HEMA-co-MMA).

2.6.1.2 Preparation of Phosphorylated PVA film

Casting of PVA film was done by dissolving 2g PVA in 100 ml deionised water at 80 ± 2^0C under stirring. The clear solution was poured into a glass petri dish and allowed to dry at room temperature (30 ^{0}C) initially for 24 h and further heated in an air oven at 50 ^{0}C to get a transparent film (shown in figure 2.2). Samples with dimension, 3 ×1 cm and a thickness of 0.3 mm were subjected to phosphorylation at room temperature for 6h. The phosphorylated samples were then washed extensively with distilled water and dried in an air oven at 50 ^{0} C.

Figure 2-2 Poly(vinyl alcohol) films

2.6.1.3 Characterization of the phosphorylated PVA film

The status of surface bound phosphate group was qualitatively assessed by Micro-FT-IR spectroscopy using Thermo Nicolet 5700 FT-IR microscope (Madison, WI).

2.6.1.4 Biomimetic mineralization

The ability of phosphorylated PVA to induce biomimetic mineralization of calcium phosphate under simulated physiological environment was observed by using 1.5x simulated body fluid (SBF) with ionic coincentrations similar to that of human blood plasma as per the procedure described in section 2.5. Unmodified PVA was selected as the control sample.

2.6.1.5 Evaluation of biomimetic mineralization

The morphological evaluation of calcium phosphate coating formed on the surface of phosphorylated PVA was carried out using Hitachi S 530 scanning electron microscope and a Horiba EMAX 2200 X- ray micro analyzer.

2.6.2 Ethylene vinyl acetate (EVA-2825)

Ethylene vinyl acetate (grade 2825) with vinyl acetate content of 28 wt-% and melt flow index 25 was used for the study.

2.6.2.1 Experimental

2.6.2.1.1 Materials

Ethylene vinyl aceteate (2825) was procured from National Organic Chemical Industries Ltd (NOCIL). The basic properties of the polymer, as supplied by the manufacturer is given in table 2.4. Potassium hydroxide used for hydrolysis of EVA 2825 was obtained from S.D.Fine India Ltd, Mumbai. Phosphorylating reagent was the same as that used for phosphorylating poly(HEMA-co-MMA).

Table 2-4 EVA 2825 –basic properties

Vinyl acetate (%)	28
Melt Flow Index (g/10 min)	25
Tensile strength at break (MPa)	9.0
Elongation at break (%)	800
Hardness (Shore A)	81
Density (g/cc)	0.95

2.6.2.1.2 Surface hydrolysis of EVA-2825

EVA 2825 obtained as beads were moulded in to a sheet of 0.5 mm thickness using a compression moulding hydraulic press (Santhosh Industries, Mumbai) at 100 ^{o}C under 10MPa pressure. The EVA sheet was then cut into small strips with dimensions 1cm length x 1cm breadth x 1mm height and washed with deionized water using an ultrasonicater for 30 minutes, 3 changes, each after 10 minutes. The small strips were then dried in an air oven at 50 ^{0}C for 24 h. The dried strips were then subjected to surface hydrolysis using 2 % potassium hydroxide at 50 ± 2^{0}C for 2h. The hydrolysed EVA sheets were then washed several times with distilled water, kept in deionized water for 24 h and then dried at 50 ^{0}C for 24h in an air oven.

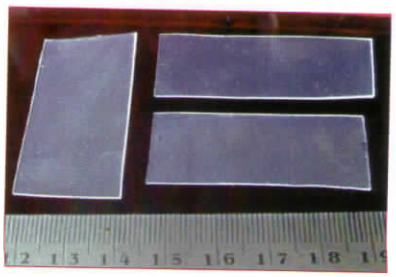

Figure 2-3 EVA sheets, compression moulded

2.6.2.1.3 Surface phosphorylation of EVA-2825

The surface hydrolysed EVA sheets were phosphorylated at 50 ^{0}C for 90 minutes as per the procedure used for poly(HEMA-co-MMA) described in section 2.3

2.6.2.2 Characterization of the phosphorylated EVA sheets

The status of surface bound phosphate group was assessed by Micro-FT-IR spectroscopy using Thermo Nicolet 5700 FT-IR microscope. The surface bound phosphate was estimated using UV-Visible spectroscopy technique at 885nm as per the procedure described in section 2.4.2 using Shimadzu UV-mini 1240. The samples for the phosphate estimation were with 1cm^2 area and 1mm thickness. The phosphorylated samples were refluxed with 1M HNO_3 at 70± 2^0 C for 8h and the extract thus obtained was used for the analysis.

2.6.2.3 Biomimetic mineralization

The ability of phosphorylated EVA to induce biomimetic mineralization of calcium phosphate under simulated physiological environment was observed by using 1.5x simulated body fluid (SBF) with ionic coincentrations similar to that of human blood plasma following the procedure described in section 2.5. Unmodified and hydrolysed EVA sheets were selected as control samples. The samples were retrieved from SBF after 3, 10 and 15 days, washed well with deionized water and dried in an air oven at 50 ± 2 ^{0}C.

2.6.2.4 Evaluation of biomimetic mineralization

The morphological evaluation of calcium phosphate coating formed on the surface of phosphorylated PVA was carried out using scanning electron microscope Hitachi model S-2400, Japan. Energy dispersive X-ray analysis (EDS) was done on OXFORD EDS machine attached to SEM. X-Ray diffraction pattern of the coating was taken using taken on Siemens D5005 X-ray diffractometer. The quantitative estimation of calcium phosphate coating was done with the help of atomic absorption spectroscopy and UV-Visible spectroscopy as per the procedure explaind in section 2.8.6 and 2.8.7.

2.6.3 Polyethylene terephthalate

2.6.3.1 Experimental

2.6.3.1.1 Materials

The polyethylene terephthalate samples used were woven texturized fabric made by wet spinning of staple fibres with a water permeability of 200+/- 100 mL/cm^2.

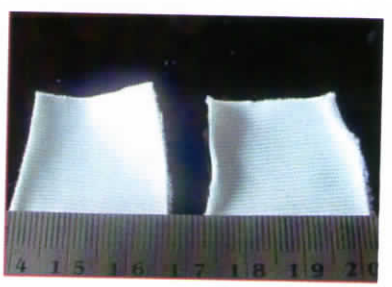

Figure 2-4 Polyethylene terephthalate fabric

2.6.3.1.2 Alkali hydrolysis of PET fabric

The alkali hydrolysis of PET fabric was conducted basically by treating with sodium hydroxide solution. In a typical experiment, PET fabric with $3cm^2$ area was immersed in 2% sodium hydroxide solution at 80 ^0C under stirring in a

water bath for 20 minutes. After 15 minutes, the fabric was washed several times with distilled water and ultrasonicated 3 times to remove traces of sodium hydroxide which could be adsorbed on the surface of the fabric and then dried at 70 ± 2^0C in an air oven. The kinetics of hydrolysis as a measure of weight loss was studied by

i) Varying the concentration of alkali from 1% to 4%

ii) Varying the time of hydrolysis from 15 minutes to 60 minutes

For each of the composition, 6 samples were taken and the average loss in weight (%) was calculated. The average breaking load and the burst pressure was calculated for both series of samples in a tensile testing machine, Instron -3345

2.6.3.1.3 Surface phosphorylation of PET fabric

From the preliminarly evaluation based up on the weight reduction of surface hydrolysed PET fabric with respect to time of hydrolysis, concentration of alkali used for hydrolysis and burst pressure measurements, the ideal composition selected for phosphorylation was HS-020, with time of hydrolysis as 15 minutes and concentration of alkali as 2%.

The PET samples were surface phosphorylated at 70 ^{0}C for 90 minutes as per the procedure explained in section 2.3. The phosphorylated samples were then washed extensively with distilled water and dried in an air oven at 50 ^{0} C.

2.6.3.2 Characterization of the phosphorylated PET fabric

The status of phosphorylation was qualitatively assessed by Micro-FT-IR spectroscopy using Thermo Nicolet 5700 FT-IR microscope. The state of surface bound phosphate group was estimated using UV-Visible spectroscopy technique at 885nm as per procedure explained in section 2.4.2. The samples for phosphate estimation were with area of 3cm^2. The phosphorylated samples were washed well

with distilled water and dried at 70 ^{0}C in an air oven. For estimating the phosphate group, the samples were refluxed with 1M Nitric acid at 70 ^{0}C for 8h and the extract thus obtained was used for analysis.

2.6.3.3 Biomimetic mineralization

The ability of phosphorylated PET substrate to induce biomimetic mineralization of calcium phosphate under simulated physiological environment was observed by using 1.5x simulated body fluid (SBF) with ionic coincentrations similar to that of human blood plasma as per the procedure described in section 2.5. The samples were retrieved from SBF after 3, 10 and 15 days, washed well with deionized water and dried in an air oven at 50^{0}C.

2.6.3.4 Evaluation of biomimetic mineralization

The morphological evaluation of calcium phosphate coating formed on the surface of phosphorylated PET was carried out using scanning electron microscope Hitachi model S-2400, Japan). Energy dispersive X-ray analysis (EDS) was done on OXFORD EDS machine attached to SEM. The estimation of calcium phosphate coating was done with the help of atomic absorption spectroscopy and UV-Visible spectroscopy as per the procedure described in section 2.5.6 and 2.5.7.

2.7. *IN VITRO* CYTOCOMPATIBILITY EVALUATION OF PHOSPHORYLATED POLY(2-HEMA-CO-MMA)

This part mainly focuses on the in vitro cytocompatibility, biomineralization of phosphorylated poly(HEMA –co-MMA), $PPH_1$and its ability to facilitate secretion of bone specific proteins such as osteocalcin and alkaline phosphatase was studied and compared with unmodified PH_1 and apatite coated PH_1 as control materials. Human osteosarcoma (HOS) cells were used for the study.

2.7.1 Human osteosarcoma (HOS) cells

Human osteosarcoma (HOS) cells are relatively slow growing cells and becomes growth arrested at a low density [133]. The cells are usually polygonal or stellate with large nuclei and multiple nucleoli, with occasional spindle shaped cells and rare multinucleated giant cells [133]. The cell-line is generally non-tumorogenic in nude mice. This characteristic and its low saturation density have made it useful for studies of transformation as well. Functional osteoblasts are obtained usually through bone or bone marriow biopsies, which can be difficult and painful for the patient. Moreover, these cells are limited in supply. Hence alternative cell source is tried.

The *in vitro* cytocompatibility evaluation includes in vitro cell viability and in vitro cell adhesion studies. Human osteosarcoma (HOS) cells (supplied by National Centre for Cell Sciences (NCCS), Pune, India) were selected for evaluating in vitro cytocompatibility.

2.7.2 Cell Viability by MTT assay

The principle of the assay is as follows. The cells in exponential phase of growth are exposed to a cytotoxic drug, MTT, 3-(4,5-dimethylthiazol-2-yl)-2,5,diphenyltetrazolium bromide. The number of surviving cells is then determined indirectly by MTT dye reduction at 569nm with a UV-Visible spectrometer. The graph with absorbance (y-axis) against concentration of drug (x-axis) was then plotted.

The MTT assay is based on the observation that a mitochondrial enzyme of viable cells has the ability to metabolise a water-sloble tetrazolium dye 3-(4,5-dimethylthiazol-2-yl)-2,5,diphenyltetrazolium bromide (MTT, Sigma) into an insoluble formazan salt. At the end of the incubation period, supernatants were discarded, cell layers rinsed twice in phosphate buffered saline (PBS), and then MTT was added (125μL per well of a 5mg/mL MTT solution in PBS). After 3h of

incubation at 37 °C, the MTT solution was removed and the insoluble formazan crystals formed were dissolved in 100μL dimethyl sulfoxide. Finally, the absorbance was measured at 540nm, using a microtitre plate spectrophotometer (Biotech, EL 311s, USA). The intensity of the blue colour obtained is directly proportional to the metabolic activity of cell populations, and inversely proportional to the toxicity of the extract.

Phosphorylated poly(HEMA-co-MMA), biomimetic calcium phosphate coated poly(HEMA-co-MMA), and unmodified poly(HEMA-co-MMA) (as control) were selected for the study. Eight samples per composition, each with dimensions 0.5 cm^2 area and 0.5 mm thickness were used for the assay after sterilizing by standard ethylene oxide (ETO) sterilization technique.

The cell viability assay was done for two different time intervals, 6h and 24h and the values were compared to understand the difference in the number of metabolically active cells on the unmodified, surface phosphorylated and calcium phosphate coated samples.

2.7.3 Cell adhesion

2.7.3.1 Sample preparation

The samples selected for the study were phosphorylated poly(HEMA-co-MMA) 'PPH_1', calcium phosphate coated poly(HEMA-co-MMA) '$CaPH_1$' and unmodified poly(HEMA-co-MMA), PH_1. The samples were in the form of films with dimensions as 0.5 cm^2 area and 1 mm thickness. In addition to films, poly (HEMA-co-MMA) microspheres were also selected for the study. Four specimens per each composition (in case of microspheres, 0.1g × 4 from each composition) were taken and carefully packed in sterilization pouches. The samples were then sterilized by standard ethylene oxide (ETO) sterilization technique at 56 ^0C for a period of 1h (gas exposure) followed by degassing for a minimum period of 12h.

2.7.3.2 Cell adhesion procedure

The culture medium used was Dulbecco's MEM (Sigma DMEM) supplemented with Foetal Bovine Serum (Sigma) and containing β glyceryl phosphate and ascorbic acid. Cell adhesion was done by seeding the cells at a concentration of 1×10^{3} onto the test samples. The cell-seeded samples were incubated at $37 \pm 2\ ^{0}C$ in a humidified atmosphere for two weeks and the cellular behaviour observed using Leica DMIL phase contrast inverted microscope at different time intervals.

The samples were then processed for scanning electron microscopic evaluation. The cells on the samples were rinsed with cucodylate buffer (pH = 7.2) and fixed using 2% gluteraldehyde solution at $4^{0}C$ for 30 minutes. The samples were again washed with cucodylate buffer and then dehydrated in ascending ethanol series (30 %, 50% and 70 %) two changes for 15 minutes each followed by two changes in 90 % and 100% for 30 minutes each. After keeping the samples in iso-amyl acetate for 10 minutes, they were subjected to critical point drying using liquid CO_2 to remove the final traces entrapped of water. The dried specimens were glued onto aluminum stubs, gold coated and viewed under the SEM.

2.7.4 *In vitro* mineralization of HOS cells by Von Kossa's staining method

Von kossa's staining method is used to detect the deposits of calcium on cells as well as on the body. The principle of the method is that when cells or tissue sections containing calcium deposits are treated with silver nitrate solution, calcium reduces silver nitrate to metallic silver in presence of strong light, commonly UV radiation.

The samples, phosphorylated poly(HEMA-co-MMA), calcium phosphate coated poly(HEMA-co-MMA), and unmodified poly(HEMA-co-MMA) as control were with dimensions as 0.5 cm^2 area and 0.5 mm thickness. Three samples per

each composition were taken sterilized by standard ethylene oxide (ETO) sterilization technique.

A 5% silver nitrate solution is used as the reagent for staining. The cells on the samples were rinsed with cucodylate buffer (pH = 7.2) and fixed using 2% gluteraldehyde solution at 4^0C for 30 minutes. The samples were again washed with cucodylate buffer. One drop of 5% silver nitrate solution was added on each of the sample, kept under UV light for 20 minutes. The samples were then observed under optical microscope.

2.7.5 Human osteocalcin

Human osteocalcin –ELISA was done using a kit [Biosourse h-OST EASIA], catalogue number KAP1381; Manufactured by BioSourse Europe S.A). The procedure was performed as per the instructions of the manufacturer's instruction leaflet.

The assay uses monoclonal antibodies (Mabs) directed against distinct epitopes of human osteocalcin. Standards and samples react with the captured monoclonal antibody (Mab 1) coated on the microtitre well and with monoclonal antibody (Mab 2) labeled with horseradish peroxidase (HRP). After an incubation period allowing the formation of a sandwitch: Coated Mab1-human osteocalcin-Mab2-HRP, the microtitre plate was washed to remove the unbound enzyme labeled antibody. Bound enzyme labeled antibody was measured thorugh a chromogenic reaction. Chromogenic solution (TMB) was added and incubated. The reaction was stopped with the addition of stop solution and the microtitre plate was read at Dual wavelength 450nm against a reference filter 630nm using a microplate reader (Biotech EL 311s USA). The amount of substrate turnover was determined colourimetrically by measuring the absorbance, which is proportional to the human ostocalcin concentration. The estimation was performed at three different time periods, 7days, 14 days and 21 days.

2.7.6 Alkaline phosphatase

Alkaline phosphatase released by the cells into the medium was measured with a commercially available assay kit (Glaxo, Qualigens diagnostics: product number 72011) India as per the manufacturer's instruction leaflet.

Principle of the test: The serum ALP hydrolyzes disodium phenyl phosphate into phenol and disodium hydrogen phosphate at pH 10. The phenol so formed reacts with 4-aminoantipyrine in alkaline medium in presence of oxidizing agent; potassium ferricyanide to form red coloured complex whose absorbance is proportional to the enzyme activity. The absorbance was read at 510 nm in a spectrophotometer.

2.8. *IN VIVO* EVALUATION OF PHOSPHORYLATED POLY(2-HEMA-CO-MMA)

This part solely concentrates on the biological evaluation of phosphorylated and calcium phosphate coated poly (HEMA-co-MMA), PPH_1 and $CaPH_1$ respectively as per ISO part X (intracutaneous irritation and maximization test), part XI (acute systemic toxicity) and ASTM F-756 (for hemolytic property evaluation). The efficacy of these two samples towards osteointegration and bone regeneration under *in vivo* environment was evaluated by short-term bone implantation in rabbits as per ISO 10993-part VI. The control sample selected for the bone implantation study was commercially available poly(methyl methacrylate) based bone cement, 'CMW1 bone cement'.

The biological evaluation was planned and performed based on the application of the material as per ISO 10993 protocols. The biological evaluation tests performed are

i) Hemolysis - ASTM F –756

ii) Acute systemic Toxicity - ISO 10993 –11; 1993 (E)

iii) Intracutaneous (intradermal) irritation - ISO 10993-10; 2002 (E)

iv) Maximization test for delayed hypersensitivity - ISO 10993-10; 2002 (E)

v) Implantation in Bone- ISO 10993 –6; 1994 (E)

The species made use for the study and the period of evaluation (ISO 109903) are given in table 2.5. Adult rabbits with 2-3 kg weight, and mice 17-23 g (gender F/M) were selected for the study.

Table 2-5 Species selected for Biological evaluation

Species	Evaluation	Period of study
Albino Rabbits	Assessment of hemolytic property	1 day
Albino Mice	Acute systemic toxicity test	7 days
Guinea pigs	Maximization test for delayed hypersensitivity	65 days
Albino Rabbits	Intracutaneous (intradermal) reactivity test	3 days
Albino Rabbits	Implantation in bone	1 week 4 weeks 12 weeks

2.8.1 Hemolytic properties of the material (ASTM F-756-2000)

Hemolytic property evaluation was done to determine the degree of red blood cell lysis and the release of haemoglobin. The test specimens were exposed to rabbit blood as per standard conditions according to ASTM F 756-2000 and the

increase in plasma haemoglobin was measured. Comparison was made with control materials under identical conditions.

2.8.2 Acute systemic toxicity test (ISO 10993 –11; 1993 (E) Clause 6.5.4 and 6.5.5)

Animals with adequate weight selected for the study. Extract of test as well as control materials was prepared and injected intravenously and intraperitonealy. Animals were observed for 72 hours and evaluated for biological/ toxic symptoms/ reactions or death.

2.8.3 Intracutaneous Reactivity Test (ISO 10993 –10; 2002 (E))

Healthy rabbits were selected and the fur was closely clipped and swabbed the skin with alcohol. The animal was restrained on a surgical table and the extract of the material injected intracutaneouly (0.2ml/site for 5 sites) along with control extract. The injection site was observed for immediate, 24, 48 and 72hrs for erythema, edema or necrosis and the scores were given.

2.8.4 Maximization test for delayed hypersensitivity (ISO 10993-10:2002(E))

The fur of guinea pig was closely clipped and the skin was swabbed with alcohol. The first application was intradermal injection using adjuvant. After 7 days, the extract of the material was applied topically. The challenge dose was given 14 days after topical application and skin responses were scored for erythema and edema.

2.8.5 Implantation in bone ISO 10993 – 6; 1994 (E)

Short-term bone implantation was performed as per ISO 10993-6; 1994 (E) in rabbits for three different time periods, 1 week, 4 weeks and 12 weeks. The test materials selected were PPH1 and CaPH1. The control sample used was conventional PMMA bone cement, CMW1 radiopaque.

2.8.5.1 Preparation of test samples for implantation

As per the standard, the test specimen for implantation should have a dimension, of 2mm diameter and 6mm length and the ends of the specimen should not have any sharp edges. The copolymer samples, PH1 with required dimensions were moulded using poly(propylene) tubes, and the ends were made blunt by polishing. After achieving the required dimension, the samples were well cleaned, dried and then phosphorylated. The phosphorylated PH1(PPH1) samples were washed with deionized water, ultrasonicated, dried and sterilized using ETO sterilization technique.

The calcium phosphate coated samples were prepared by immersing the phosphorylated PH1 samples in SBF for 15 days. The calcium phosphate coated samples were then washed with distilled water, dried and sterilized using ETO sterilization technique.

Figure 2-5 Samples for bone implantation (PPH1)

2.8.5.2 Preparation of control sample

The control sample used was PMMA based CMW1 radiopaque bone cement, manufactured by Johnnson and Johnson. The cement powder and the monomer in the packet were mixed as per manufacturer's instruction and extruded into 2mm diameter rods, kept for curing at 70 ^{0}C for 24 h, cut into 6mm long specimens, as per the instructions described in the ISO protocol. The ends of

samples were made blunt by polishing (Isomet). The control samples thus obtained were then washed by ultrasonication for 5 times using distilled water, dried at 70 ^{0}C and then sterilized using ETO sterilization technique.

2.8.5.3 Implantation procedure

The fur of selected animal was closely clipped. Animals were anaesthetized with atropine (0.5 mg/Kg body weight), ketamin (60 mg/Kg body weight) and xylaxin (5mg/Kg body weight). The skin was swabbed with alcohol and an incision was made along the dorsal aspect of femur. Skin and muscle were retracted and bone exposed. Periosteum was retracted and three defects were drilled, equidistant from each other along the diaphysis. Each defect measured 6mm. in depth and 2mm. in width. Test implant material was press fitted into each defect, periosteum and muscle replaced and skin flaps and sutured. Control material was implanted in the contralateral femur. Both test materials were implanted in separate animals. Hence, each animal had 3 test and 3 control implants. All implantation procedures were carried out following the rules of the Animal ethics committee of the Institute. The implantation procedure is shown in fig. 2-6.

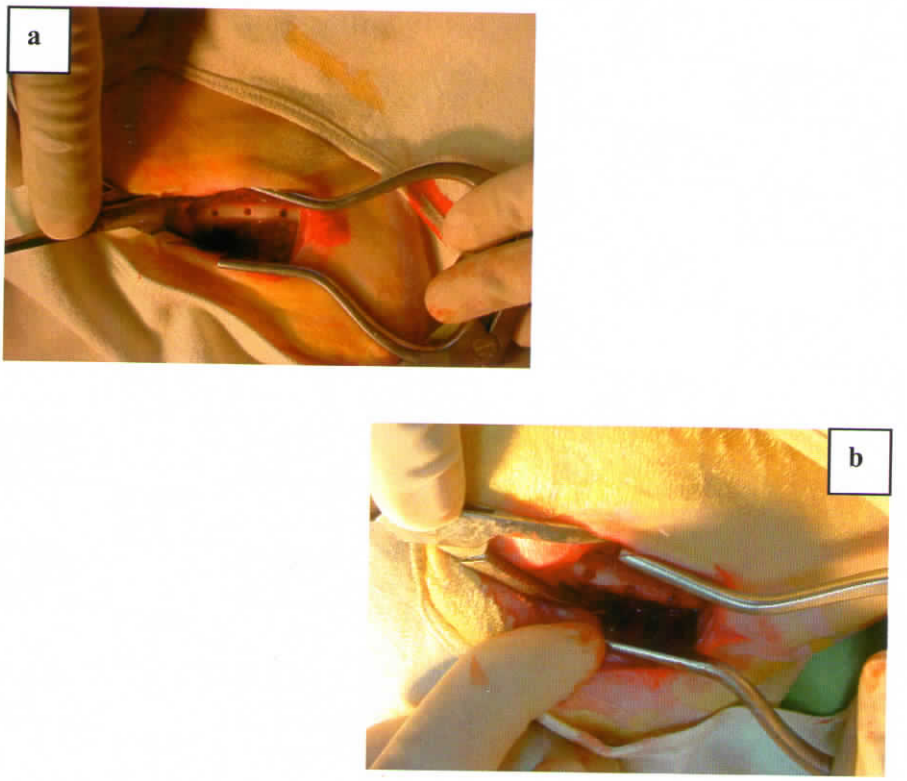

Figure 2-6 Implantation procedure (a) holes drilled for implantation (b) implants in position

Implantation was done for three different time periods, one week, 4 weeks and 12 weeks. A group of four rabbits were selected for each time period. The care and management of the experimental animals were performed following the ISO protocol and observed regularly. At the end of each implantation period animals are sacrificed and femur containing implant materials was retrieved, fixed in 10% formalin and prepared for histopathological analysis. The X-ray photographs of the implant sites were taken at the end of 3 months.

2.8.5.4 Retrieval of implants

Each group of animals were sacrificed at one week, 4 weeks and 12 weeks post implantation. Femur containing implant materials was retrieved and fixed in

10% formalin. Defects and bone were observed grossly and segments of bone with implant and surrounding bone was cut and fixed further using formalin.

2.8.6 Processing and embedding of retrieved bone with the implant

2.8.6.1 Processing of the tissue

The processing of the hard tissue with the implant is carried out following the different steps [134-136].

i) Dehydration of tissue: Dehydration of the tissue was done through ascending grades of alcohol at room temperature depending on size of the tissue, 70% alcohol (1-4 days), 80% alcohol (1-4 days), 96% alcohol (1-4 days), 100% alcohol (2 days), alcohol-acetone (1:1 v/v- one day, and 100% alcohol (1 day).

ii) Infiltration of tissue with monomer: The tissue was transferred into washed methyl methacrylate monomer and kept for 2-4 days in refrigerator followed by a second change of the monomer for the same period

iii) Embedding: Embedding solution was made by taking 1% recrystallized benzoyl peroxide mixed MMA and used within 15 minutes. Separate embedding bottle was used for each tissue and the cap is labeled. The embedding solution was poured into the bottle and the tissue was carefully oriented into the medium with cutting surface face down as specified in the grossing register, so that the tissue could be cut in the desired direction. The level of embedding medium should be at least 1cm higher than the tissue level to allow normal shrinkage of PMMA. The cap is loosely applied and vacuum was given for 30 minutes to one hour to remove entrapped air bubbles. The vacuum was then released slowly and the cap carefully tightened, without displacing the position of the tissue. Complete evacuation of oxygen in the chamber was ensured and polymerization was allowed to complete. The resultant blocks were obtained by breaking the glass bottles.

2.8.6.2 Cutting thin sections of PMMA blocks with implants

The equipment used is a high -speed precision saw with a diamond blade (4 inch diameter). The tissue with the implant embedded in PMMA was initially fixed in the chuck tightly. The chuck with the block was then fixed on the specimen arm and the block was oriented to get the cross section of the bone with the implant. The load set is between 150 to 300g and the rpm between 1500 and 3000. Thin sections were cut by advancing the specimen arm to a distance 0.4-0.5 mm. The sections thus obtained were glued on clean glass slides using cyanoacrylate glue.

2.8.6.3 Grinding and polishing

The sections were carefully glued on to glass slides and labeled. The sections were then subjected to grinding against waterproof abrasive papers of different grades in the Ecomet 3 – Buehler (Grinder/polisher) by placing the glass slide containing the sections firmly onto a slide holder. The speed is adjusted and the section thickness was occasionally measured using micrometer up to a thickness of 100μ. The thin sections were then polished carefully with the help of diamond paste to eliminate the scratches completely. The sections were washed carefully to remove the adhered diamond paste.

2.8.6.4 Staining

Staining of the sections was done with Stevenel's Blue and Van Gieson Picrofuschin stains.

i) Preparation of Stevenel's Blue

Materials:

Methylene Blue: 1g

Potassium permanganate: 1.5g

Distilled water: 150mL

Methylene blue is dissolved in 75 mL of distilled water. Potassium permanganate was dissolved in 75mL of distilled water and kept on a boiling water bath. To this, methylene blue was carefully added and heated until the precipitate formed was redissolved. This is a critical step in the procedure, as failure to do redissolve the precipitate completely gives a staining solution that tends to precipitate on the sections. The stain was then allowed to reach room temperature and then filtered. The stain remains stable for several months and does not require periodic filtration.

ii) Preparation of Van Gieson Picrofuschin

Materials:

Acid fuschin: 0.1g

Distilled water: 10 mL

Saturated aq. Picric acid: 100mL

Acid fuschin (0.1g) is dissolved in 10mL distilled water to make 1% solution. To this 100 mL of saturated picric acid was added and mixed well.

Staining procedure

The stevenel's Blue was taken in a beaker and kept in a water bath at 60 ^{0}C. The sections containing glass slide (dried) was carefully immersed in the stevenel's blue for 5 minutes. After 5 minutes, the slide was carefully taken out, washed with warm water, wiped carefully with tissue paper and made sure that the slide/sections doesn't contain any traces of water. The slide containing sections were then carefully immersed in Van Gieson picrofuschin stain, kept at room temperature for 5 minutes. After 5 minutes, the slide is taken out and wiped with tissue paper with extreme care. It is very important that after Van Gieson picrofuschin stain, the sections should not come into contact with water.

2.8.6.5 Light microscopic observation

The sections were scanned at 100X magnification to identify the implant site and the response. The extent of inflammation and fibrosis, severity of degeneration (determined by changes in tissue morphology) and presence of necrosis (determined by nuclear debris/or capillary wall breakdown) and graded. Implant site-tissue interface was examined for the presence of neutrophils, lymphocytes, plasma cells, eosinophils, macrophages and multinucleated cells, debris, fatty infiltration and granuloma. Presence of osteoblast cells, new bone formation, bone remodeling were also examined and compared.

CHAPTER 3

RESULTS AND DISCUSSION

The results and discussion part is divided in to six chapters. The ***chapter 3.1*** describes the preliminary evaluation of the poly(HEMA-co-MMA) copolymer series and the identification of suitable composition among them for further studies. ***Chapter 3.2*** is about the assessment on the extent of surface phosphorylation by various techniques while ***chapter 3.3*** deals with the assessment of the biomimetic mineralization of the phosphorylated poly(HEMA-co-MMA). ***Chapter 3.4*** illustrates how the proposed surface phosphorylation method could be extended to functionalize other biocomplatibile polymers like poly(vinyl alcohol), poly(ethylene) vinyl acetate copolymer and poly(ethylene terephthalate). ***Chapter 3.5*** explains the *in vitro* cytocompatibility evaluation using human osteoblast cell line and the role of surface phosphorylation in enhancing the secretion of bone specific marker proteins such as osteocalcin and alkaline phosphatase. The ***Chapter 3.6*** is dedicated to *in vivo* toxicological evaluation and the efficacy of phosphorylated as well as calcium phosphate coated poly(HEMA-co-MMA) to trigger new bone formation against a commercially available PMMA based bone cement, CMW1 radiopaque, as the control material.

CHAPTER 3.1

POLY (2-HYDROXY ETHYL METHACRYLATE-CO-METHYL METHACRYLATE): PRELIMINARY CHARACTERIZATION

3.1. PRELIMINARY CHARACTERIZATION

This chapter focus on the preliminary evaluation of poly(HEMA-co-MMA) by micro FT-IR spectroscopy, differential scanning calorimetry (DSC), simultaneous thermogravimetric-differential thermal analysis (TGA-DTA), dynamic mechanical analysis (DMA), degree of equilibrium swelling and compressive modulus.

3.1.1. Structure of poly(MMA), poly(HEMA) and poly(HEMA-co-MMA)

The structure of poly(MMA), poly(HEMA) and poly(HEMA-co-MMA) are shown as follows

i) Polymerization of MMA

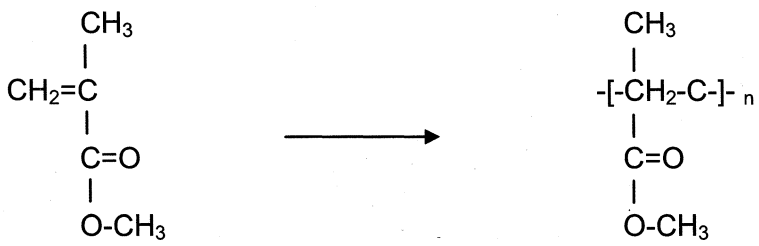

MMA POLY(MMA)

ii) Polymerization of HEMA

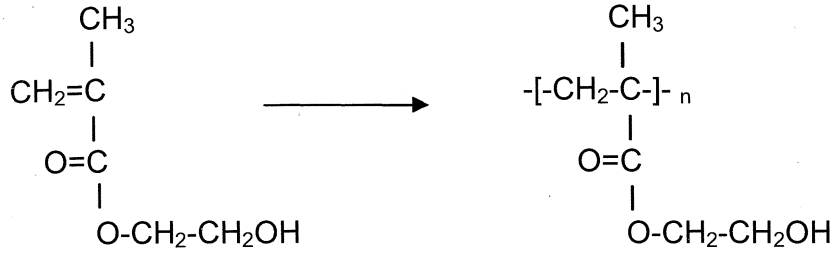

HEMA POLY(HEMA)

iii) Copolymerization of HEMA and MMA

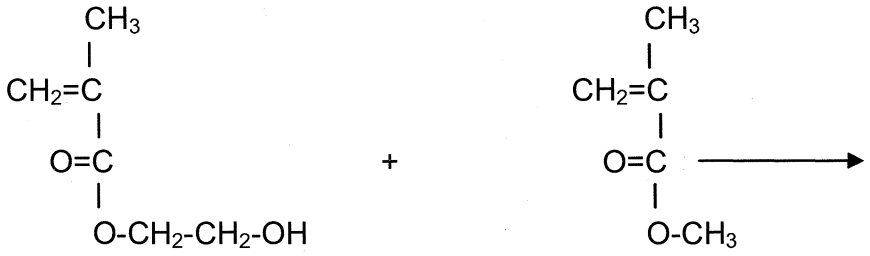

HEMA MMA

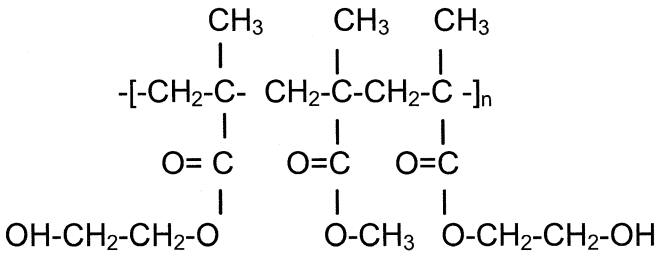

Poly (HEMA-co-MMA)

3.1.2. FT IR Spectroscopy

The FT-IR spectra of all the samples were taken in the attenuated total reflectance (ATR) mode. The ATR spectra of poly(HEMA-co-MMA) with HEMA:MMA ratio varying as 0.07:0.90, 0.57: 0.25, 0.69: 0.10 (represented as PH_1, PH_4 and PH_5 respectively) are shown in figure 3.1 (a).

The micro FT-IR spectrum of PH_1 is compared with that of PMMA in figure 3.1 (b). An overlay spectrum of PMMA, poly(HEMA) and PH1 is given as Fig. 3.1(c). It could be viewed from fig. 3.1(c) that the major peaks (-C=O, $-CH_3$, $-CH_2$) are closely matching in all the three samples, while the –OH peak is not visible at PH1 even though it contains 0.07 mole of HEMA.

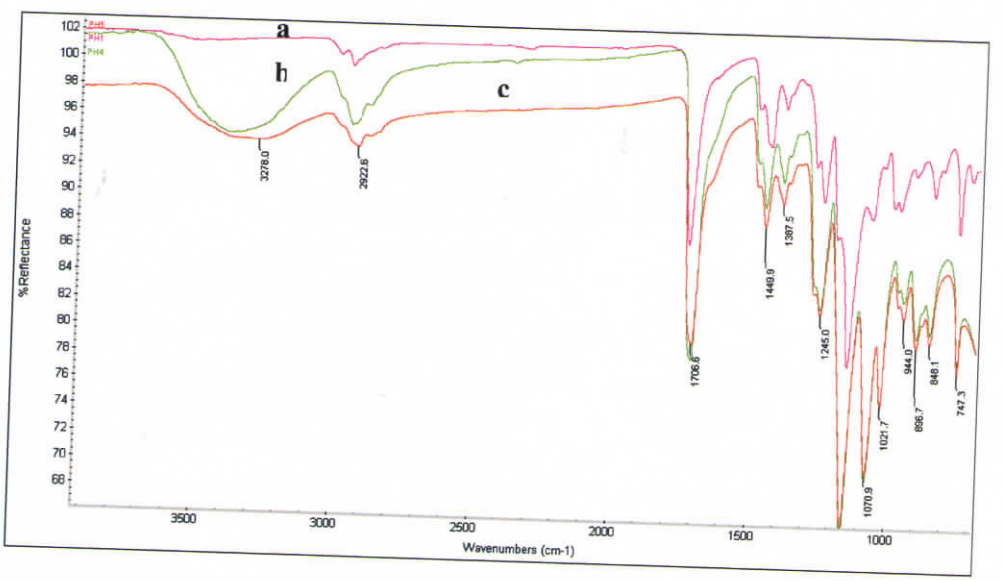

(a) Micro FT-IR spectra of PH_1, PH_4 and PH_5
a: PH_1 b: PH_4 c: PH_5

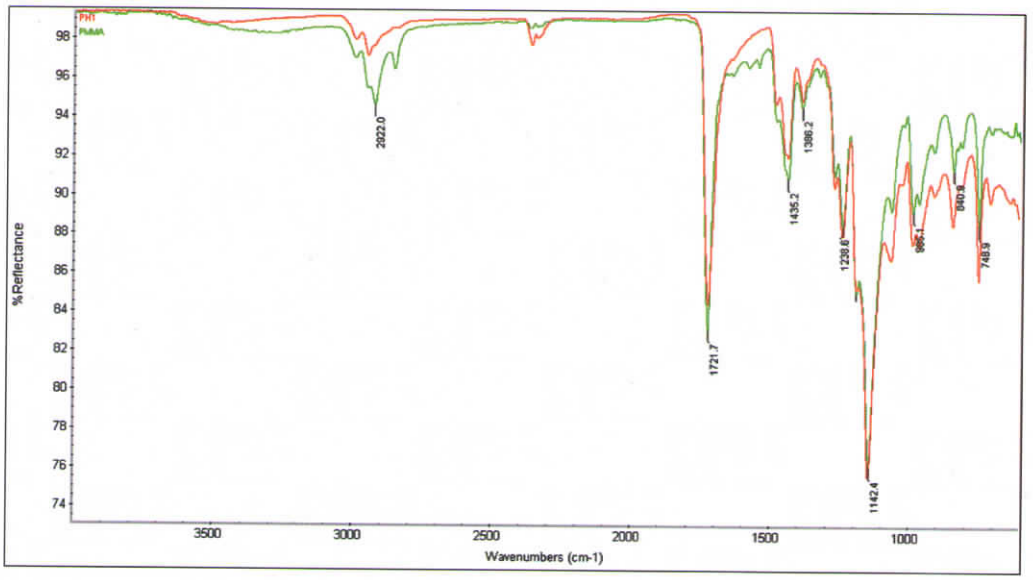

Fig. 3.1(b) Micro FT-IR spectrum of PH_1 and PMMA

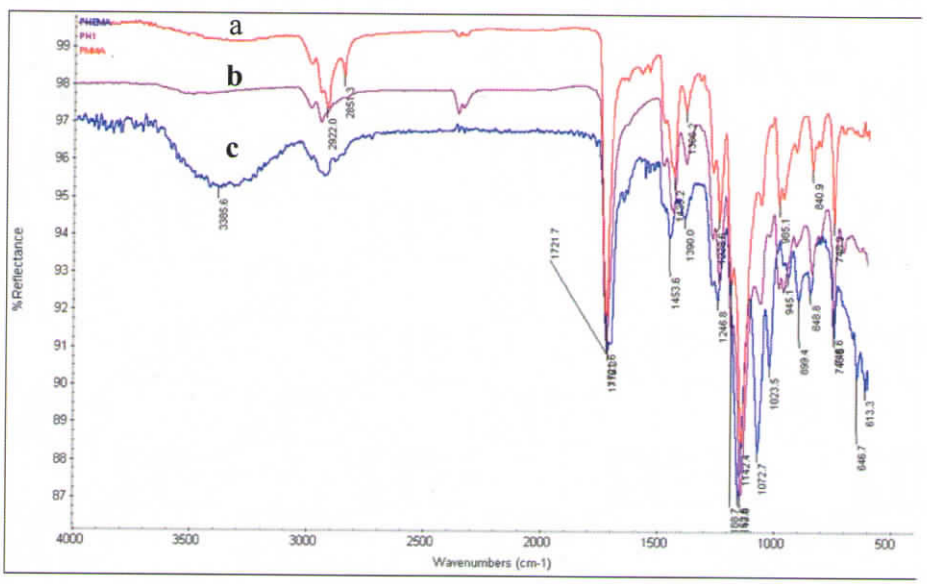

(c): FT-IR spectra of PMMA, poly(HEMA) and PH1
a: PMMA b: PH1 c: Poly(HEMA)

Figure 3-1 (a) Micro FT-IR spectra of PH_1, PH_4 and PH_5 (b) Micro FT-IR spectrum of PH_1 and PMMA (c): FT-IR spectra of PMMA, poly(HEMA) and PH1

Figure 3.1 (a) shows that all the compositions of poly(HEMA-co-MMA) namely PH_1, PH_4 and PH_5 showed the characteristic –C=O and -CH_3 peaks at 1706, 2922 cm^{-1} while PH_4 and PH_5 have –OH peak at 3375 cm^{-1}. It is obvious that poly(HEMA) also has the characteristic –C=O, -CH_3 and –OH peaks at 1706, 2922, 3375 cm^{-1} respectively. It is evident from the spectra that with increasing HEMA content in poly(HEMA-co-MMA), the intensity of –OH peak increases. Even though PH1 also has –OH groups, the FT-IR spectroscope could not recognize the presence of –OH peaks on it.

3.1.3. Differential scanning calorimetry (DSC)

The glass transition temperature (T_g) of PH_1 was found as 104.57. The T_g of PMMA and poly(HEMA) were observed as 99.77 and 98. 67 respectively. The overlay of the DSC curves is shown in fig. 3.2. The values were taken from the second run after heating the sample at a rate of 10 ^{0} C /min from room temperature to 150 ^{0}C and cooling. The appearance of a single T_g for the copolymer confirms that PH1 is a random copolymer.

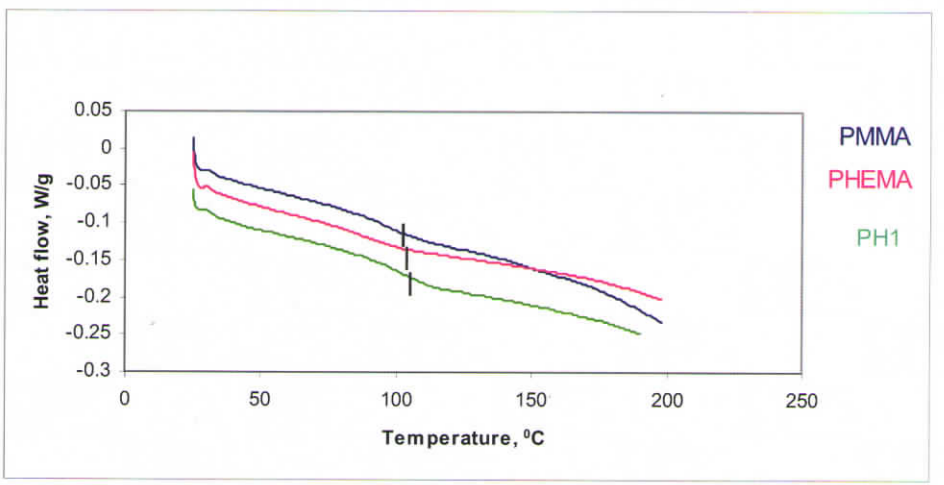

Figure 3-2 DSC curves of PMMA, PHEMA and PH1

PMMA, PHEMA and PH1 were synthesized under the same conditions, i.e., 0.5 % initiator (BPO) and 1% cross-linking agent (EGDMA). It could be noted that the T_g value of PMMA and PHEMA are very close to the reported values [137]. However, the small difference observed in this case is mainly due to cross-linking.

Polymers normally display broad melting endotherms and glass transitions. Both the glass and melting transitions are strongly dependent on processing conditions and dispersion in structural and chemical properties of plastics [137]. The glass transition temperature (T_g) is the onset of segmental mobility for a polymer, the temperature below which the polymer segments do not have sufficient energy to move past one another [138]. When the temperature is above the glass transition temperature the segments rearrange to relieve an externally applied stress, resulting in a heat flow and the values are characterized as an inflection point in the specific volume-temperature curve determined by DSC analysis. The T_g value for a polymer is important because it affects the mechanical properties at a particular temperature and determines the temperature range in which a polymer can be used effectively. The factors that affect the T_g are molecular weight, functionality, branching, and chemical structure [138].

The T_g value of PH1 has slightly shifted to the high temperature side compared to PMMA and PHEMA. This could be attributed to the restricted segmental mobility of the copolymer compared to the homopolymers. Methacrylates have a higher glass transition temperature than their chemically similar acrylate counter part. The stiff $-CH_3$ side group decreases mobility, increasing the T_g [137]. Conversely, flexible side groups increase chain separation, and the T_g decreases. Decreased mobility of polymer chains as well as increased chain rigidity results in higher T_g. The present situation leads to a cross-linked polymer and cross-linked polymers have higher T_g than uncross-linked counterparts due to the restricted chain mobility. Hence the cross-linked

homopolymers ((PMMA and poly(HEMA)) have a slightly higher T_g compared to the uncross-linked polymer.

3.1.4 Thermogravimetric analysis (TGA)

Figure 3.3 shows the TGA scans of PMMA, PHEMA and PH1.

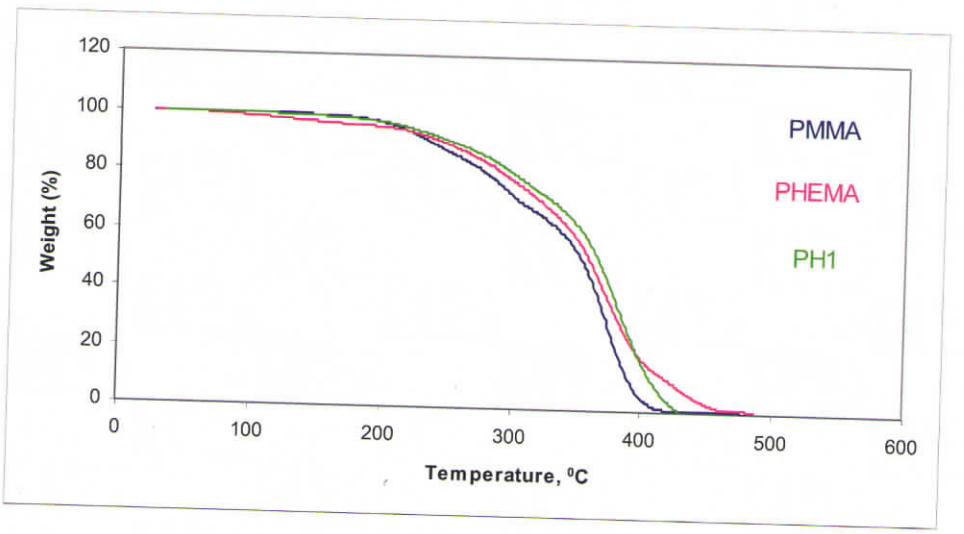

Figure 3-3 Thermograms of PMMA, PHEMA and PH1

It could be seen from fig. 3.3 that, for PMMA, the decomposition begins at 172.62 ^{0}C and the weight loss rapidly increases with increase in temperature. The weight loss after the first stage decomposition is 30.08 % and it reached 99. 55% after second stage decomposition. The weight remained at 592 ^{0}C was 0.20%. The temperature at 50% decomposition is 355.4 ^{0}C. Similar to PMMA, PHEMA also has a rapid burn out profile. However, the decomposition of PHEMA was initiated at a higher temperature, 200.85 ^{0}C. The weight loss after the first stage decomposition for PHEMA was 28.06 % and it increased to 84.16 % after second stage decomposition. The decomposition further continued with increase in temperature with a mass of 0.85 % remained at 524 ^{0}C. The temperature at 50% decomposition was 361.24 ^{0}C.

homopolymers ((PMMA and poly(HEMA)) have a slightly higher T_g compared to the uncross-linked polymer.

3.1.4 Thermogravimetric analysis (TGA)

Figure 3.3 shows the TGA scans of PMMA, PHEMA and PH1.

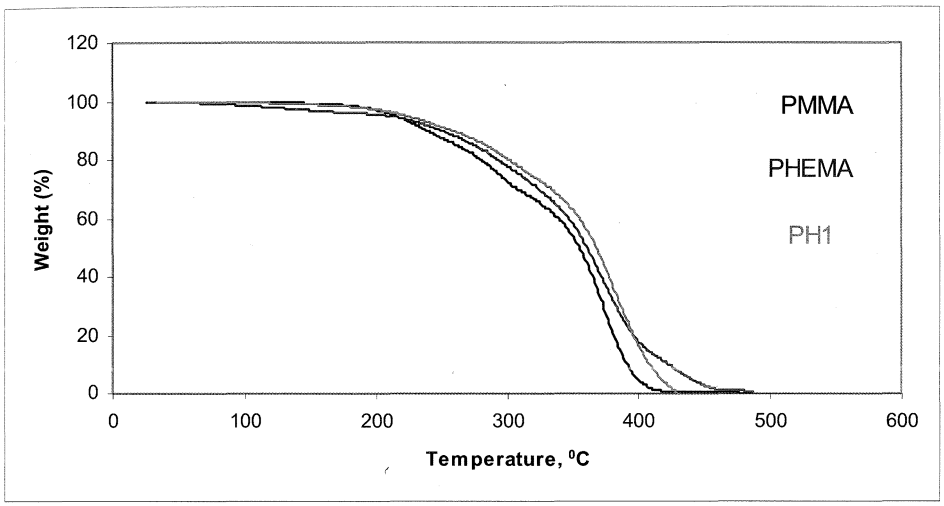

Figure 3-3 Thermograms of PMMA, PHEMA and PH1

It could be seen from fig. 3.3 that, for PMMA, the decomposition begins at 172.62 ^{0}C and the weight loss rapidly increases with increase in temperature. The weight loss after the first stage decomposition is 30.08 % and it reached 99. 55% after second stage decomposition. The weight remained at 592 ^{0}C was 0.20%. The temperature at 50% decomposition is 355.4 ^{0}C. Similar to PMMA, PHEMA also has a rapid burn out profile. However, the decomposition of PHEMA was initiated at a higher temperature, 200.85 ^{0}C. The weight loss after the first stage decomposition for PHEMA was 28.06 % and it increased to 84.16 % after second stage decomposition. The decomposition further continued with increase in temperature with a mass of 0.85 % remained at 524 ^{0}C. The temperature at 50% decomposition was 361.24 ^{0}C.

In the case of PH1, the decomposition has begun at 189.28 ^{0}C, which is a temperature in between that of PMMA (172.62 ^{0}C) and PHEMA (200.85 ^{0}C). However, the degradation profile for PH1 shows the same trend as that of PMMA and PHEMA. The weight loss after first stage decomposition is 24.14% and it declines further to 0% at 600 ^{0}C. The 50% of decomposition occurs for PH1 at a temperature 368.01 ^{0}C, which is slightly higher compared to that of PHEMA (361.24 ^{0}C) and PMMA (355.4 ^{0}C).

The thermograms show that there is no significant difference in the degradation profile of PMMA, PHEMA and PH1. However, PHEMA showed the highest thermal stability with an onset of degradation at 200.85 ^{0}C and PMMA the lowest (172.62 ^{0}C). As expected, PH1 stands in between with a thermal stability up to 189.28 ^{0}C. The thermograms thus ensure good thermal stability and assure a safe processing temperature range to PH1. It is to be noted further that the decomposition is not a spontaneous one, rather slow and hence no abrupt deterioration in property takes place.

It is to be mentioned that the decomposition profile of PMMA and PHEMA are quite similar to that of reported data [139]. Likewise, in the case of poly(HEMA-co-MMA, the degradation has a close match. The DTA curves shown in figure 3.4 (a) and 3.4 (b), further corroborate that there is no vital difference in the onset of decomposition between PMMA and PH1.

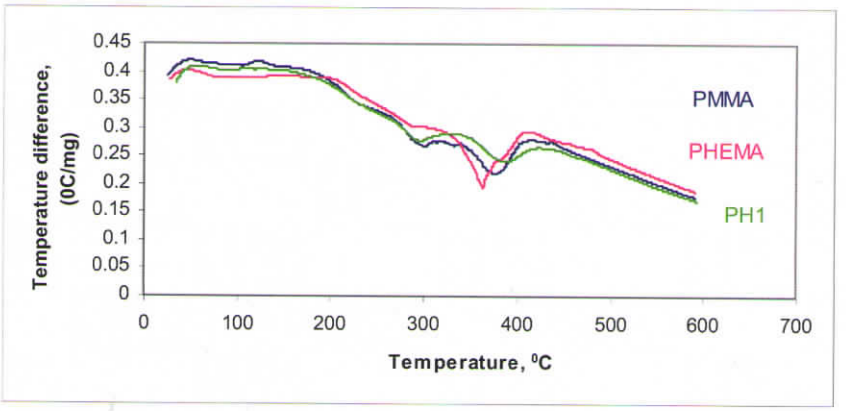

(a) Differential thermograms of PMMA, PHEMA and PH1

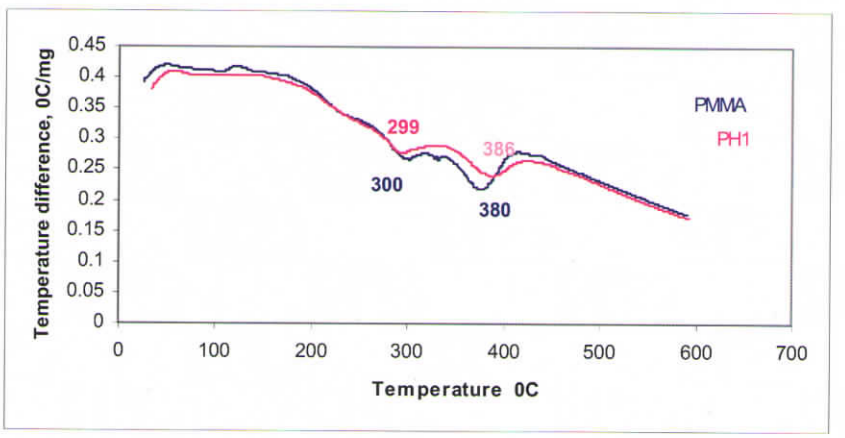

(b) Differential thermograms of PMMA and PH1

Figure 3-4 (a) Differential thermograms of PMMA, PHEMA and PH1
(b) Differential thermograms of PMMA and PH1

3.1.5. Residual monomer analysis

The residual monomer, MMA present in the sample was 3.71ppm.

3.1.6. Atomic Force Microscopy (AFM)

The figs 3.5 (a) and (b) show the surface topography images of PH1 at two different magnifications acquired using atomic force microscope.

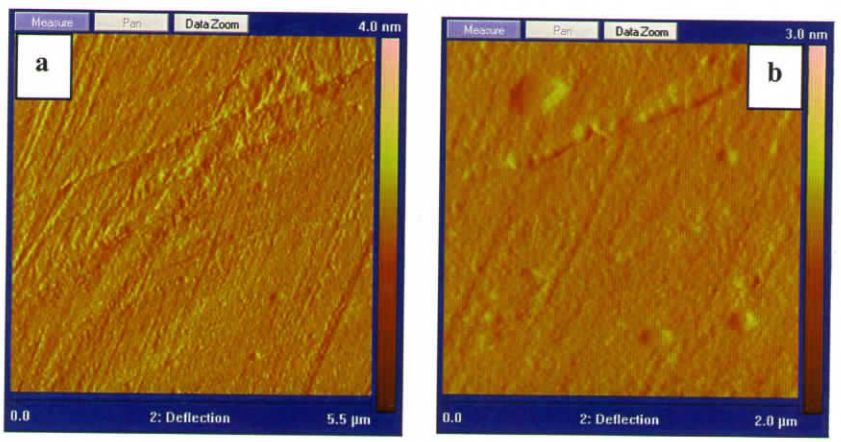

Figure 3-5 (a) and (b) AFM images of PH1

The measurement was made in contact mode where the tip scans the sample in close contact with the surface. The force on the tip is repulsive with a mean value of 10^{-9} N. This mode eliminates capillary forces and reduces Van der Waals' forces and hence suitable to study technologically and biologically important processes. It could be seen that the surface is smooth without much irregularities.

3.1.7. Contact angle measurement

The unmodified PH1 samples demonstrated a profoundly hydrophobic state with a contact angle of $u = 67.6^{0}$. The measured angles appeared stable and were closely reproducible.

3.1.8. Equilibrium swelling in Phosphate buffer saline (PBS)

The equilibrium swelling degree was calculated as,

$$\text{Swelling degree (\%)} = \frac{W_w - W_d}{W_d}$$

Where, W_d and W_w are the weight of dry and swollen samples respectively.

Figure 3.6(a) imparts information about the nature as well as extent of swelling of PH1, PH2, PH3 and PH4. The figure shows that the percentage of swelling increases with increase in HEMA content in poly(HEMA-co-MMA) leading to an equilibrium swelling represented by a plateau after 100h. Hence PH1 shows lowest and PH5 shows the highest percentage of swelling. At equilibrium, PH1(with HEMA:MMA = 0.07:0.90) shows a swelling of 2% while PH4 (HEMA:MMA = 0.57: 0.25) shows 39% swelling. It is worth to mention that PH2, the poly(HEMA-co-MMA) composition with HEMA:MMA = 0.19: 0.75, also shows a significant percentage of swelling of 24%. It is evident from the figure that poly(HEMA) has an exceptionally high degree of swelling i.e., 50%. Hence, when compared to poly(HEMA), PH_1 has a very minimum swelling which is very vital aspect in determining the mechanical properties of the copolymer in the *in vitro* and *in vivo* environment.

The dependence of swelling on cross-linking has been demonstrated by varying the amount of cross-linking agent, EGDMA as shown in fig. 3.6 (b) by selecting the composition PH1. The figure reflects the perception that with increase in the concentration of EGDMA, the extent of swelling decreases.

However, the equilibrium percentage of swelling for the uncross-linked PH1 as well as for PH1 cross-linked with 0.5 wt-% EGDMA are very close. Likewise for PH1 cross-linked with 1 wt-% and 3 wt-% EGDMA also have the similar extent of swelling. Further, for greater clarity, the percentage swelling at 336h for all the four compositions, PH1 cross-linked with 0.5 wt-%, 1 wt-% and 3 wt-% EGDMA as well as uncross-linked PH1 were plotted and shown in fig. 3.6 (c).

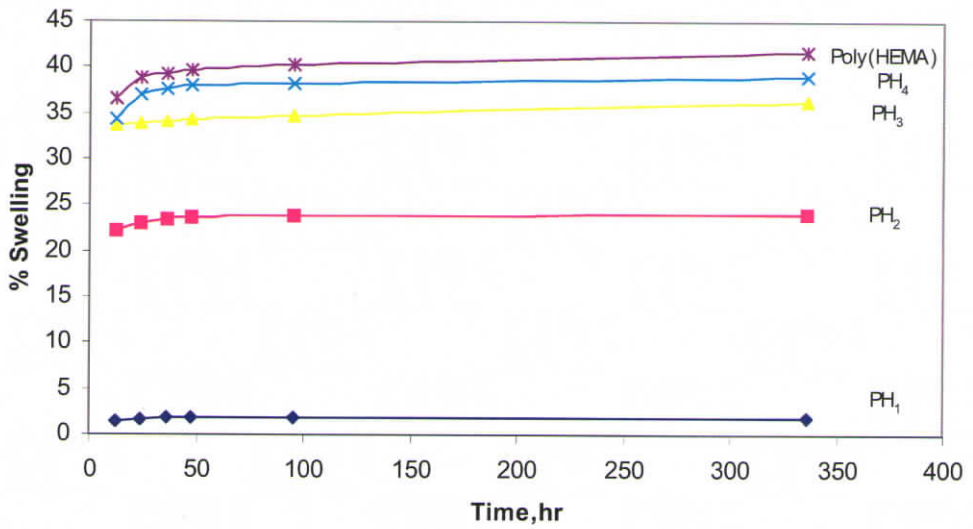

(a) Percentage equilibrium swelling of PH1, PH2, PH3, PH4 and poly(HEMA)

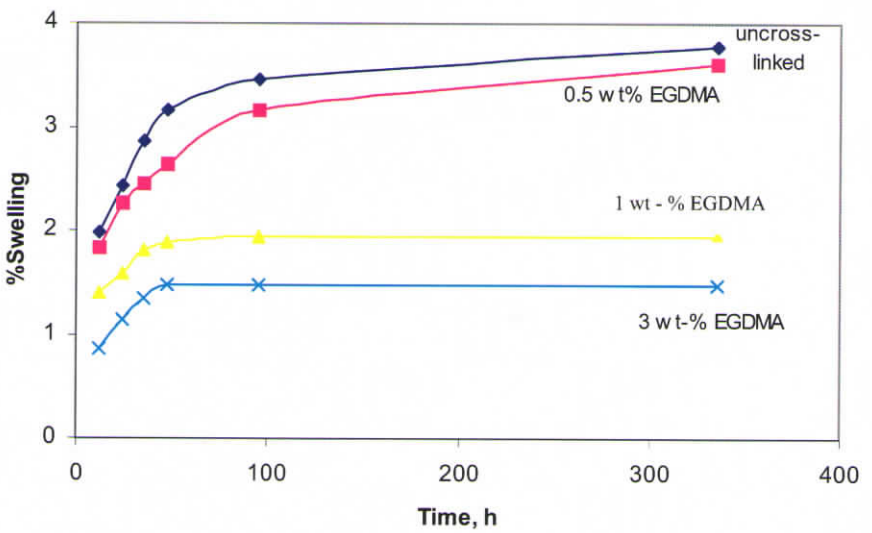

(b) Equilibrium swelling as a function of cross-linking agent

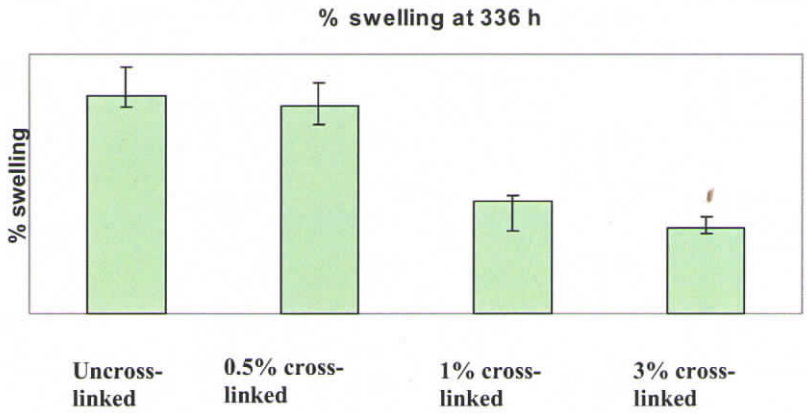

(c) Equilibrium swelling of PH1 at 336h as a function of cross-linking agent

Figure 3-6 (a) Percentage equilibrium swelling of PH1, PH2, PH3, PH4 and poly(HEMA) (b) Equilibrium swelling as a function of cross-linking agent (c) Equilibrium swelling of PH1 at 336h as a function of cross-linking agent

The extent of swelling of a hydrogel is favorably influenced by the osmotic potential, strong interactions with water, high free volume, high chain flexibility, and low cross-link density [140]. Because swelling leads to a less entropically desirable configuration, when the water enters the matrix, the chains extend a restrictive force and equilibrium swelling is reached when the restrictive force balances the osmotic force. Poly(HEMA) is a highly hydrophilic polymer and is known to form hydrogels [140]. Even though poly(HEMA-co-MMA) cannot be called as a hydrogel, the basic hydrophilicity of poly(HEMA) is reflecting in its swelling behaviour. Further, it is apparent from fig. 3.6 (b), that the cross-link density has an important role in determining the extent of swelling. As it is elucidated from fig. 3.6(b) that there is only marginal difference between PH1 cross-linked with 1 wt-% and 3 wt-% EGDMA, 1 wt-% EGDMA cross-linked PH1 was chosen for the detailed study.

3.1.9. Mechanical properties

(i) Compressive Modulus

The compressive strength (stress at maximum load) of PH_1 was found as 153MPa and modulus 4.6 GPa. The stress-strain curve of PH1 is given in fig. 3.7.

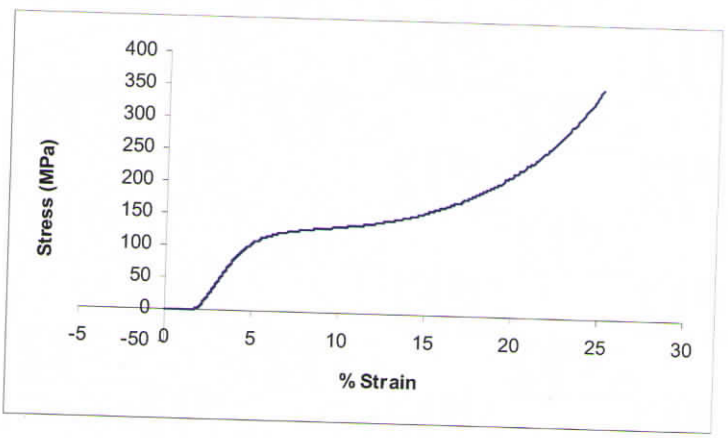

Figure 3-7 Stress-strain curve of PH1

(ii) Dynamic mechanical analysis

The storage modulus of PH1, measured using DMA is shown in fig. 3.8. The unmodified PH1 has a storage modulus of 1.75GPa at room temperature (25 ±2) ^{0}C.

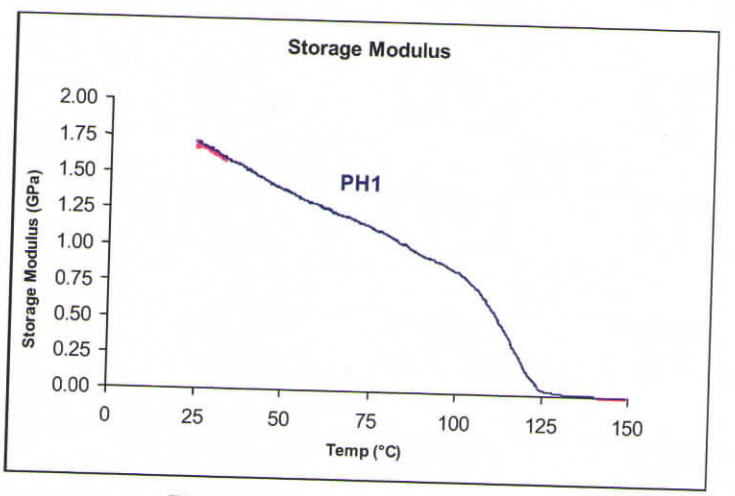

Figure 3-8 Storage modulus of PH1

3.1.9. Mechanical properties

(i) Compressive Modulus

The compressive strength (stress at maximum load) of PH_1 was found as 153MPa and modulus 4.6 GPa. The stress-strain curve of PH1 is given in fig. 3.7.

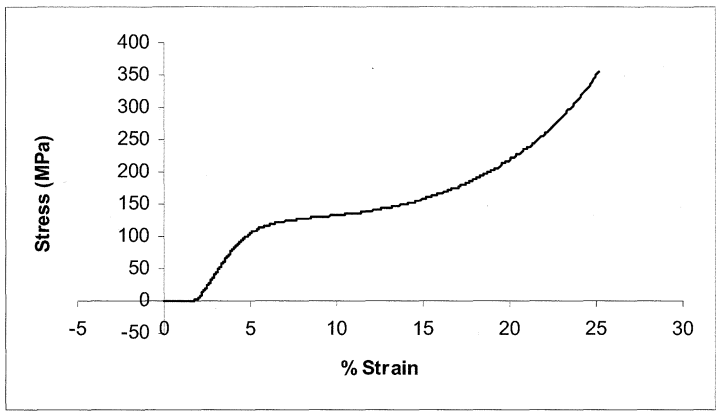

Figure 3-7 Stress-strain curve of PH1

(ii) Dynamic mechanical analysis

The storage modulus of PH1, measured using DMA is shown in fig. 3.8. The unmodified PH1 has a storage modulus of 1.75GPa at room temperature (25 ±2) ^{0}C.

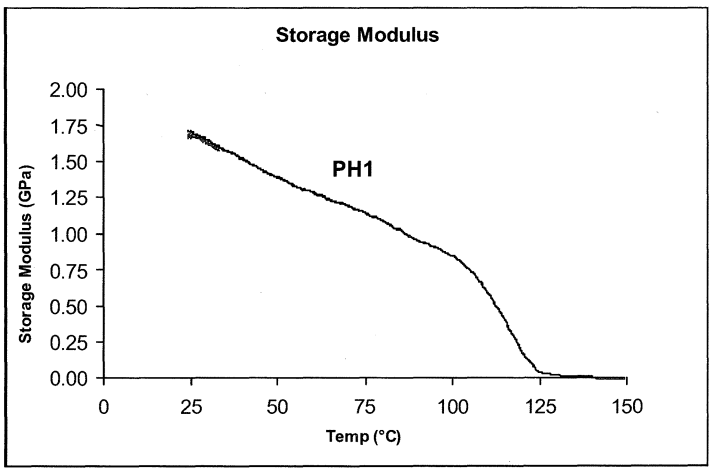

Figure 3-8 Storage modulus of PH1

Polymers are viscoelastic materials with strong time and temperature dependence to their mechanical properties. Temperature scans across the dynamic spectrum of mechanical absorptions are commonly required for the characterization of polymers [141]. Higher water content in poly(HEMA) will cause steep decrease in the tensile strength and tear resistance [142]. The same behaviour is expected for copolymers of poly(HEMA). Temperature indirectly influences the strength of poly(HEMA) copolymers, because it controls the extent of swelling. Deformations caused by stress are irreversible. Most importantly, the surface properties of poly(HEMA) is very pertinent as it has adjustable interfaces. Poly(HEMA) has a high index of refraction. However, refractive index does not vary with temperature. Like PMMA and poly(HEMA), PH1 can also be prepared in various forms and shapes.

3.1.10. Summary

The FT-IR results supports the formation of poly(HEMA-co-MMA) through the bulk polymerization reaction of HEMA and MMA. The DSC data ensures a single glass transition temperature (T_g) of 104.57 and thereby formation of random copolymer. The TGA results show that the degradation profiles for the copolymer as well as homopolymers are having a similar trend. Differential thermal analysis further supports the data. The residual monomer analysis performed using gas chromatography showed that the amount of residual monomer is 3.71 ppm. Equilibrium swelling study in PBS showed that with increase in HEMA content in the copolymer, the percentage of equilibrium swelling significantly increases and reaches a plateau after 100h. The AFM images show that the surface topography of PH1 is smooth. The PH1 surface-probe force of attraction value is 123.5. It has been observed that PH1 has good compressive strength value of 153MPa, modulus 4.6 GPa and good dynamic storage modulus value of 1.75 GPa at room temperature ($25\pm3\ ^{0}C$).

CHAPTER 3.2

ASSESSMENT OF PHOSPHORYLATION

3.2. ASSESSMENT OF SURFACE PHOSPHORYLATION

This chapter describes the assessment of surface phosphorylation of poly(HEMA-co-MMA). The preliminary analysis was done using micro FT-IR spectroscopy. The surface phosphate chemistry was understood with the help of X-ray photoemission spectroscopy (XPS) and quantitative phosphate analysis was performed using UV-Visible spectroscopy. Additionally, the topographical variations due to surface phosphorylation were identified with environmental scanning electron microscopy (ESEM) and atomic force microscopy (AFM). The variation in glass transition temperature (T_g) and thermal properties due to surface phosphorylation was examined by differential scanning calorimetry (DSC) and simultaneous thermogravimetric-differential thermal analysis (TGA-DTA) respectively. The amplification in the swelling behaviour was studied in phosphate buffer saline, PBS. Finally, the change in mechanical properties was evaluated.

3.2.1 Structure of phosphorylated poly(HEMA-co-MMA)

The structure of phosphorylated poly(MMA) and poly(HEMA-co-MMA) are shown as follows

i) Phosphorylation of HEMA

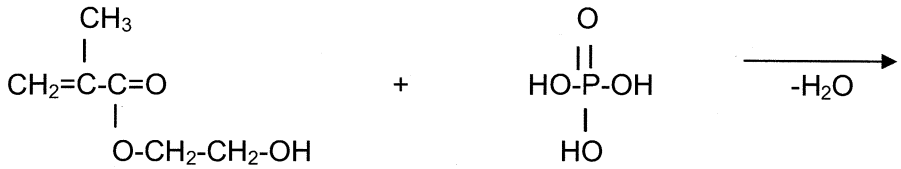

HEMA Phosphoric Acid

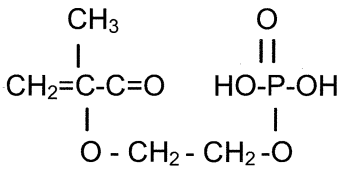

Phosphoric Acid ester of HEMA

iii) Structure of phosphorylated poly(HEMA-co-MMA)

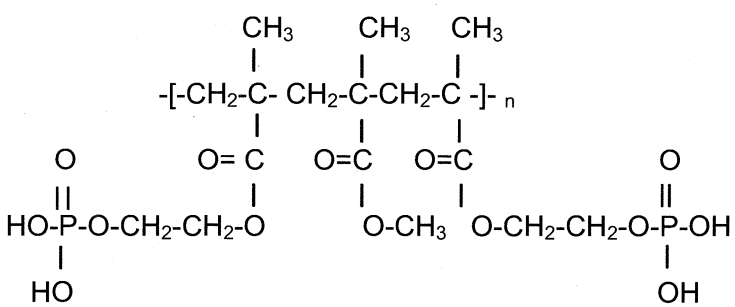

Structure of phosphorylated poly(HEMA-co-MMA)

3.2.2 Micro-FT IR spectroscopy

The FT-IR spectra of all the samples were taken in the ATR mode. The fig. 3.9 (a) illustrates an overlay spectrum of surface phsophorylated PH1 and virgin PH1, phosphorylated for 45 minutes. Fig. 3.9 (b) gives the FT-IR spectrum of PH1 phosphorylated at different time periods in comparison with neat PH1 and fig. 3.9 (c) is the overlay of the same series at a wavelength region of 600 to 2000 cm^{-1}.

The surface phsophorylated poly(HEMA-co-MMA) series has shown the peaks corresponding to phosphate group at 1060.9 and 962.3 cm^{-1}, ensuring the surface coupling. The kinetics of phosphorylation with respect to time is shown in figure 3.9 (b, c). It was observed from the FT-IR spectra that the phosphorylation begins at 15 minutes and that 45 minutes would be sufficient for the completion of the reaction. Even though the surface phosphorylation occurs at room temperature under prolonged time period, it was observed that the most suitable temperature for phosphorylation was at 80 ^0C.

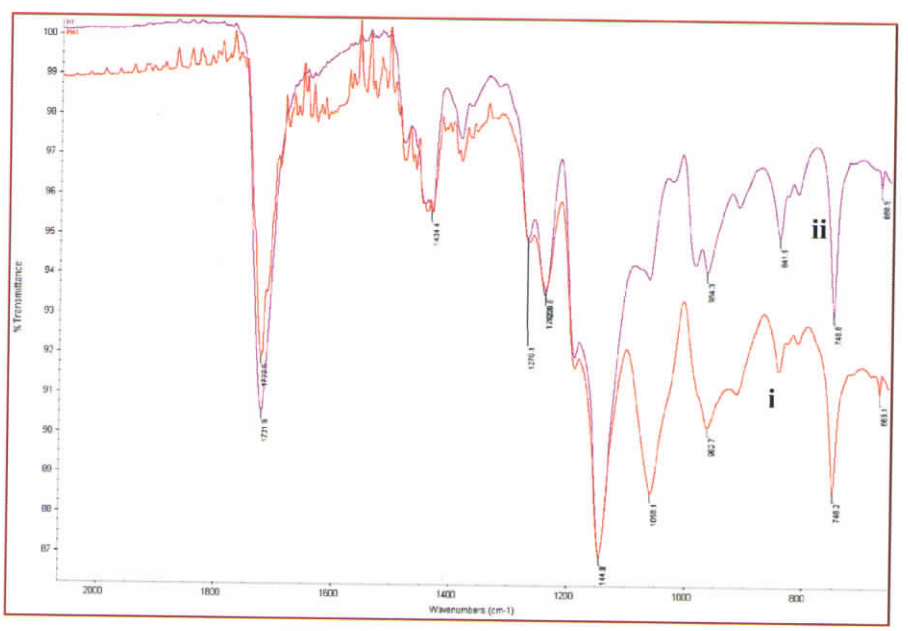

(a) surface phosphorylated PH1 (i) and virgin PH1 (ii)

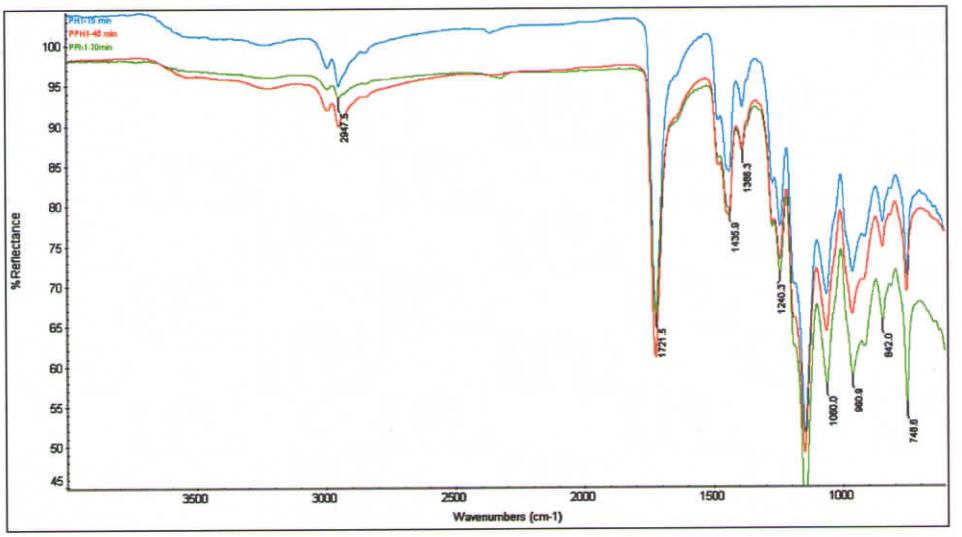

(b): Surface phosphorylated PH1 at different time periods

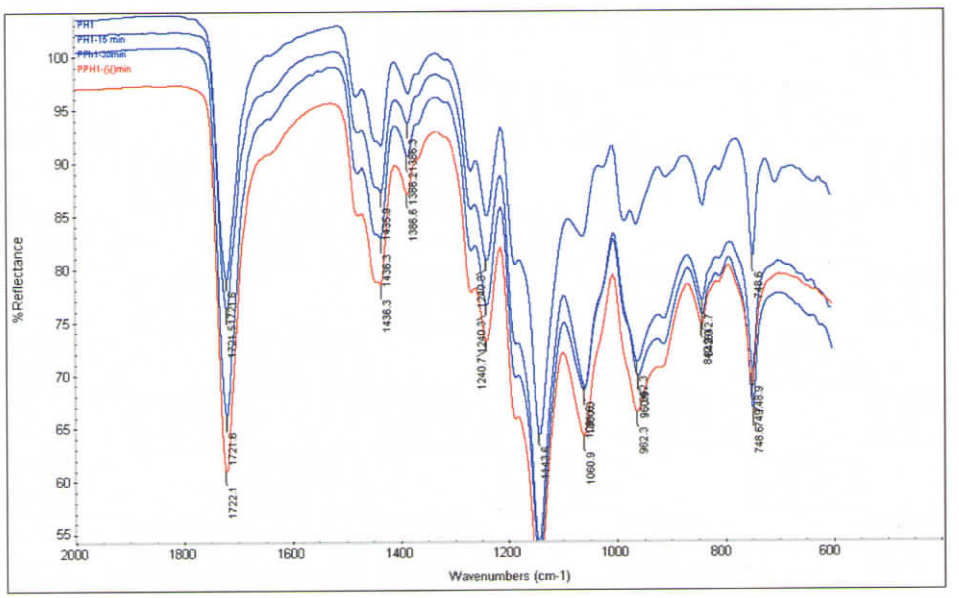

(c) Surface phosphorylated PH1 at different time periods in comparison with PH1 (2000 to 600 cm^{-1})

Figure 3-9 (a) Surface phosphorylated PH1 (i) and virgin PH1 (ii) (b): Surface phosphorylated PH1 at different time periods in comparison with PH1 (c): Surface phosphorylated PH1 at different time periods in comparison with PH1 (2000 to 600 cm^{-1})

3.2.3 Thermal properties

(a) Differential scanning calorimetry (DSC)

The glass transition temperature (T_g) of PPH_1 was found as 103.17. The T_g of PH1 was 104.57. The slight increase in Tg to the rubbery side may be attributed due to surface phosphorylation of PH1. The overlay of the DSC curves is shown in fig. 3.11. The values were taken from the second run after heating the sample at a rate of $10\ ^0$ C /min from room temperature to $150\ ^0$ C and cooling. Functionality is another factor affecting the T_g. Functionality and chemical structure act together to determine T_g characteristics. Monofunctional, aliphatic monomers, such as isooctyl acrylate, tridecyl acrylate, laurylacrylate, tend to exhibit low T_g value [138]. Higher functionality materials with similar molecular weights exhibit higher T_g as the crosslink density is higher.

(b) Thermogravimetric analysis (TGA)

Figure 3.10 shows the TGA scans of PMMA, PHEMA, PH1 and PPH1. The decomposition of PH1begins at 189 ^{0}C while for PPH1 the decomposition begins only at 206. 3 ^{0}C. All the samples show similar decomposition profile.

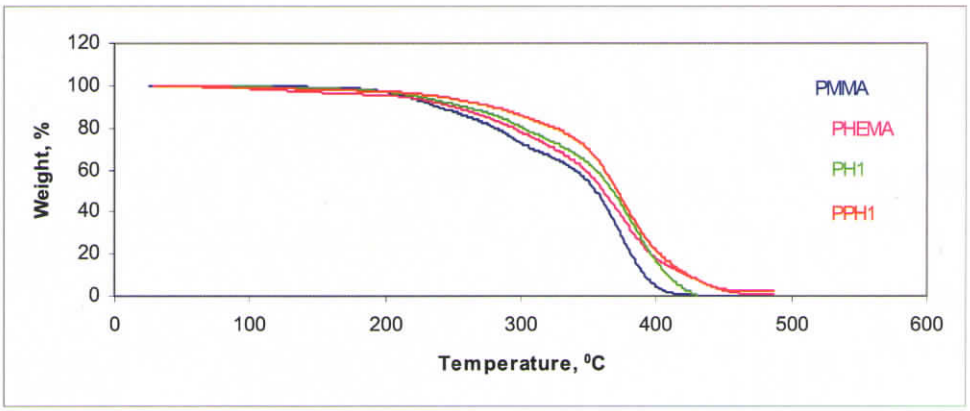

Figure 3-10 The overlay of the TGA curves- PMMA, PHEMA, PH1 and PPH1

It is apparent from the thermograms that there is a slight increase in the onset of decomposition for PPH1 compared to PH1. This could be attributed to surface phosphorylation. Phosphate group being more stable compared to –OH group, the initiation of decomposition is slightly delayed.

3.2.4 X-ray Photoelectron Spectroscopy

The survey spectrum of PH1 is shown in fig. 3.11 (a) while the overlay spectrum of PH1 and PPH1 are shown in fig 3.11 (b). It could be seen that the major peaks associated with PH1 and PPH1 are carbon and oxygen. It is noticeable that the broad spectrum of both PH1 and PPH1 are very similar. However, the narrow scan performed in the range 100 to 400 eV shows the slight spectral shift between the two. The individual difference between C 1s and O 1s of 'PH1' and 'PPH1' are shown in fig. 3.13 (a) and (b) respectively. The peak corresponding to P2p of PPH1 is viewed at 131. 5 (fig. 3.12 c).

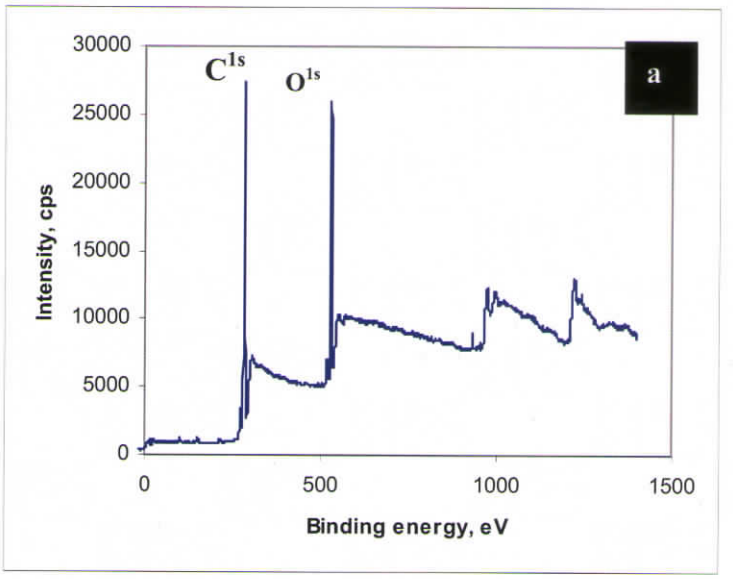

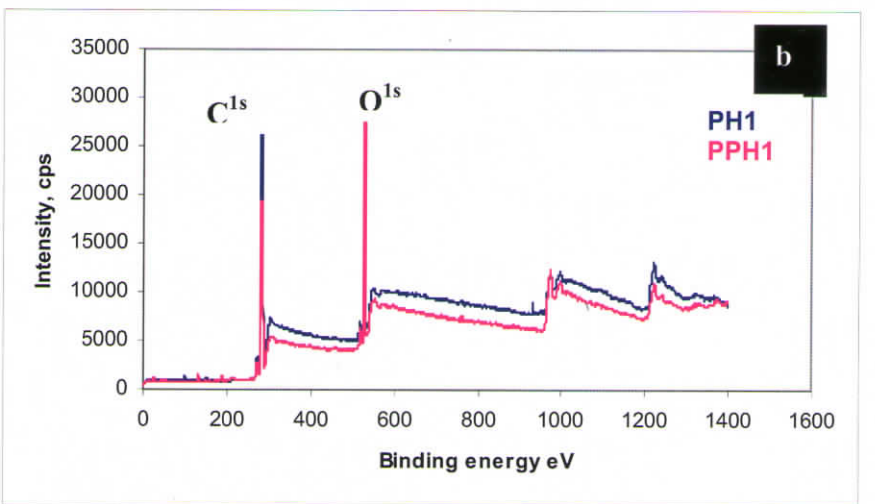

Figure 3-11 The survey spectrum of PH1 (a) and overlay spectrum of PH1 and PPH1 (b)

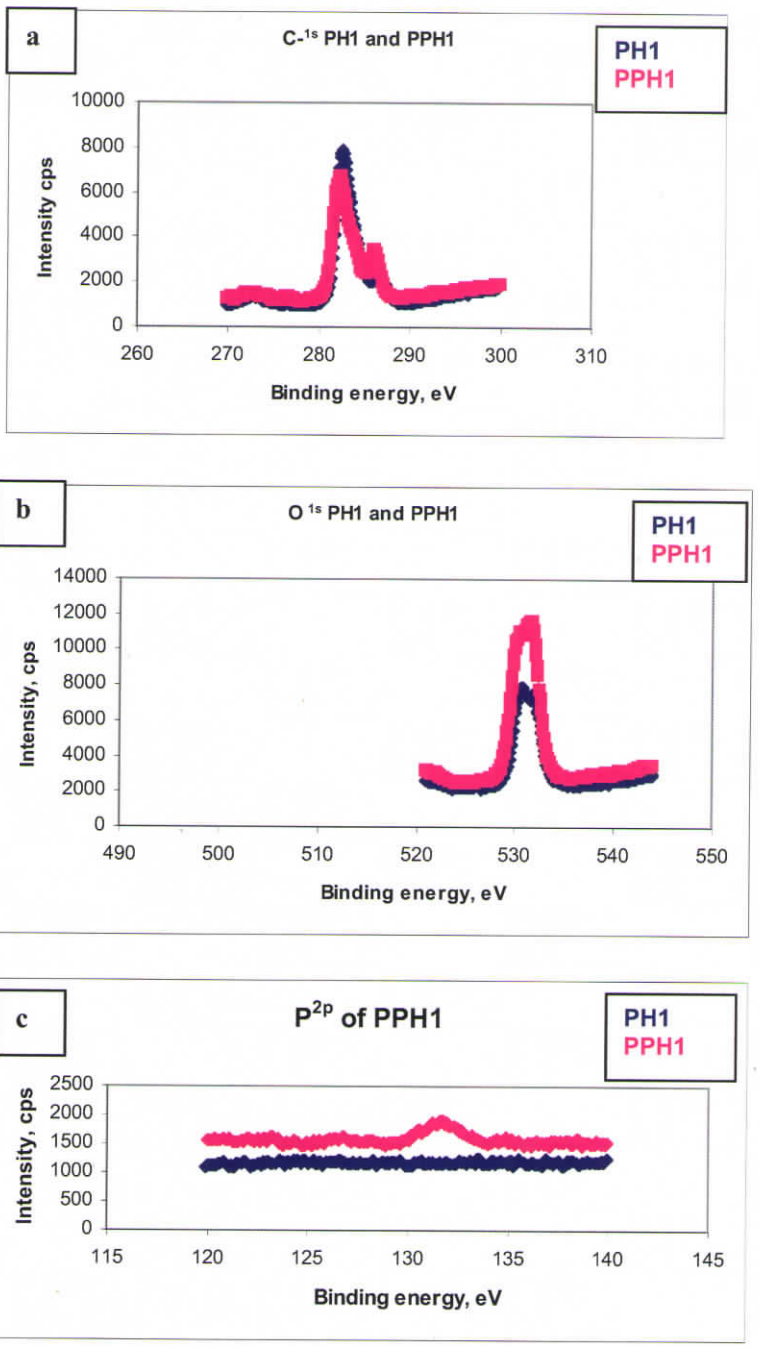

Figure 3-12 The XPS narrow scan comparison of PH1 and PPH1 (a): C 1s (b): O 1s (c): P 2p

The narrow scans of C1s shows that the peak values for PH1 and PPH1 are 282.6 and 282.2 respectively. A slight peak shift (0.4) was noted for PPH1 compared to that of PH1. At the same time, the O 1s peak has a significant difference between PH1 and PPH1 in both value and intensity. The O 1s peak values are 530.7 and 531.9 for PH1 and PPH1 respectively. The intensity of O 1s of PPH1 is significantly high compared to that of PH1. This could be attributed to the greater number of oxygen atoms associated with PPH1 due to surface phosphorylation. The increase in binding energy of O1s of PPH1 could be due to the strong P-O bond [143].

The P 2p peak of PPH1 is seen at 131.5 (fig. 3.13 c). The intensity of P peak is of one order less than that of the C and O peaks in the unmodified as well as surface phosphorylated PH1. Even though the amount of HEMA content in the PH1 is significantly less (0.07 moles), the particular ability of the copolymer to undergo a reversal of surface structure when transferred from air into the aqueous environment leads to the exposure of –OH group for phosphorylation [144].

Ratner *et al* have experimentally proved that many materials can undergo a reversal of surface structure when transferred from air into a water environment: i.e, hydroxylated polymers exhibits a surface rich in methyl groups (from the polymer chain backbone) in air, and a surface rich in hydroxyl groups under water [144]. That is why surface phosphorylation of PH1 occurs even at such a lower concentration of HEMA in the copolymer.

The XPS analysis thus proves the presence of surface bound phosphate group on PPH1. The study also throws light in confirming that there is no adverse change occurs to the polymer surface.

3.2.5 UV-Visible spectroscopy

The extent of phosphorylation as a function of HEMA content in poly(HEMA-co-MMA) is given in figure 3.13. It could be seen that the phosphate

concentration per surface area increases initially in a linear way and reaches to a plateau, at 50 wt-% of HEMA and then increases exponentially as it reaches 100% poly(HEMA).

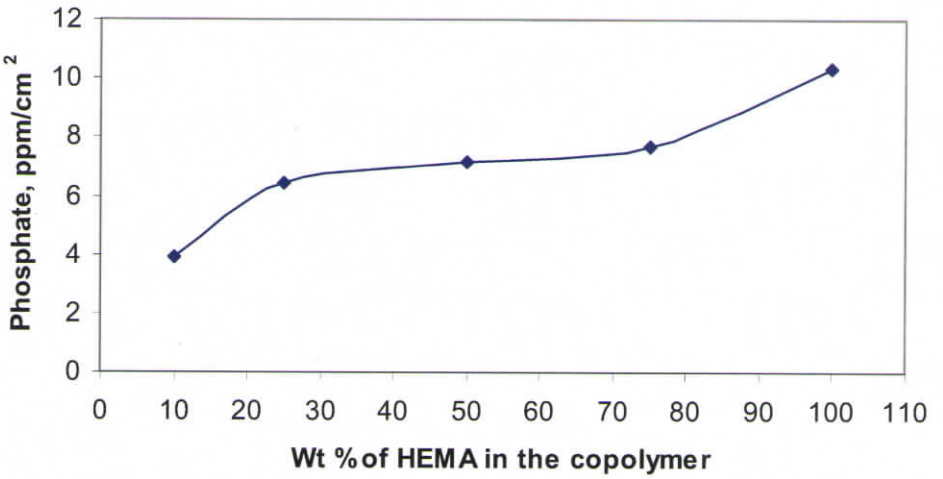

Figure 3-13 Extent of phosphorylation as a function of HEMA content in poly(HEMA-co-MMA)

It is clear from the above result that the extent of phosphorylation is directly proportional to the –OH group present in the copolymer, poly(HEMA-co-MMA). In the case of PH1, the phosphate concentration was identified as 4ppm/cm^2 and it increases to 7 ppm/cm^2 when HEMA concentration reaches 50 wt-%. For poly(HEMA) the phosphate concentration was 10.34 ppm/cm^2. The results shows that, surface phosphate concentration is significant even at 10 wt-% of HEMA when comparing the surface phosphate concentration of poly(HEMA). This could be very well correlated to the basic property of poly(HEMA) to undergo reversal of surface structure according to the environment (water or air) [144].

It could be assumed that the –OH groups of poly(HEMA-co-MMA) are very well get exposed to aqueous environment and thus actively facilitating the process of surface phosphorylation. It could be postulated that the surface phosphorylation of PH1 having very low HEMA content (HEMA: MMA =

concentration per surface area increases initially in a linear way and reaches to a plateau, at 50 wt-% of HEMA and then increases exponentially as it reaches 100% poly(HEMA).

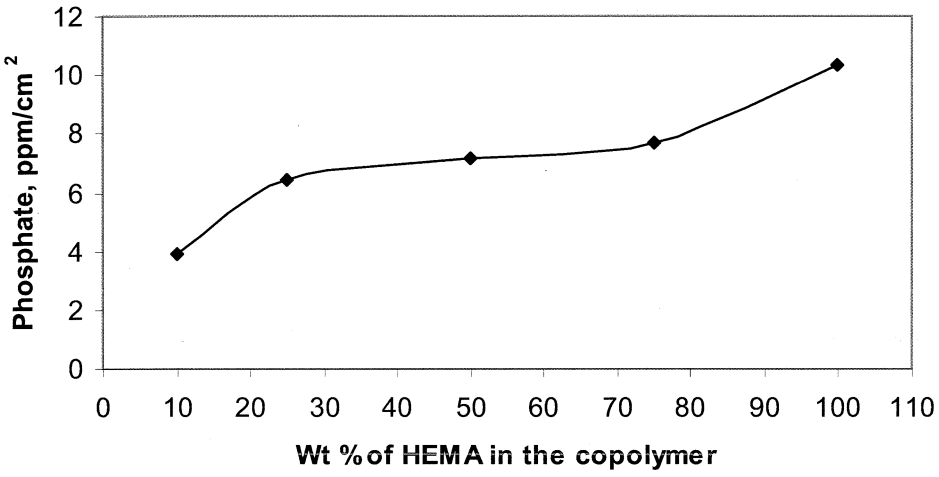

Figure 3-13 Extent of phosphorylation as a function of HEMA content in poly(HEMA-co-MMA)

It is clear from the above result that the extent of phosphorylation is directly proportional to the –OH group present in the copolymer, poly(HEMA-co-MMA). In the case of PH1, the phosphate concentration was identified as 4ppm/cm^2 and it increases to 7 ppm/cm^2 when HEMA concentration reaches 50 wt-%. For poly(HEMA) the phosphate concentration was 10.34 ppm/cm^2. The results shows that, surface phosphate concentration is significant even at 10 wt-% of HEMA when comparing the surface phosphate concentration of poly(HEMA). This could be very well correlated to the basic property of poly(HEMA) to undergo reversal of surface structure according to the environment (water or air) [144].

It could be assumed that the –OH groups of poly(HEMA-co-MMA) are very well get exposed to aqueous environment and thus actively facilitating the process of surface phosphorylation. It could be postulated that the surface phosphorylation of PH1 having very low HEMA content (HEMA: MMA =

0.07:0.90) is occurring principally due to this reason. Moreover, the comparative evaluation of phosphate content in poly(HEMA-co-MMA) series shows that the surface bound phosphate concentration for PH1 is more than half than that of PH3, which has 50 wt-% HEMA. This could be explained on the basis of the above hypothesis. The curve takes an exponential profile after 50 wt-% HEMA, which is basically owing to the extremely high concentration of exposed –OH group that could be phosphorylated easily.

Further more, the swelling of poly(HEMA-co-MMA) is also happening as a result of the above mentioned special characteristic of poly(HEMA). However, cross-linking has a significant role in determining the extent of swelling [145].

The macromolecular structures having highly repetitive patterns of anionic groups, such as phosphate and carboxylate, which lead to interactions between organic chains and mineral precursor ions can trigger nucleation of calcium phosphate under simulated physiological conditions [100-105]. Grafting of phosphorus-containing groups on polymer chains is a promising biomimetic approach for the deposition of calcium phosphate minerals in simulated body fluid (SBF) to synthesize the inorganic-polymer composite biomaterials [106-111]. Phosphorylated cellulose derivatives, chitin, chitosan, bamboo components, and other polymers, were found to be very effective for HA nucleation and its epitaxial growth [106-111]. All these studies were of surface modification of the materials, but little literature has reported the impact of phosphate-content on mineralization.

3.2.6 Phosphorylation Vs Topographical changes

The atomic force micrographs of surface phosphorylated PH1 is given in figure 3.14 (a) and (b). For easy comparison, the AFM images of unmodified PH1 are reproduced in this section also as 3.14 (c) and (d).

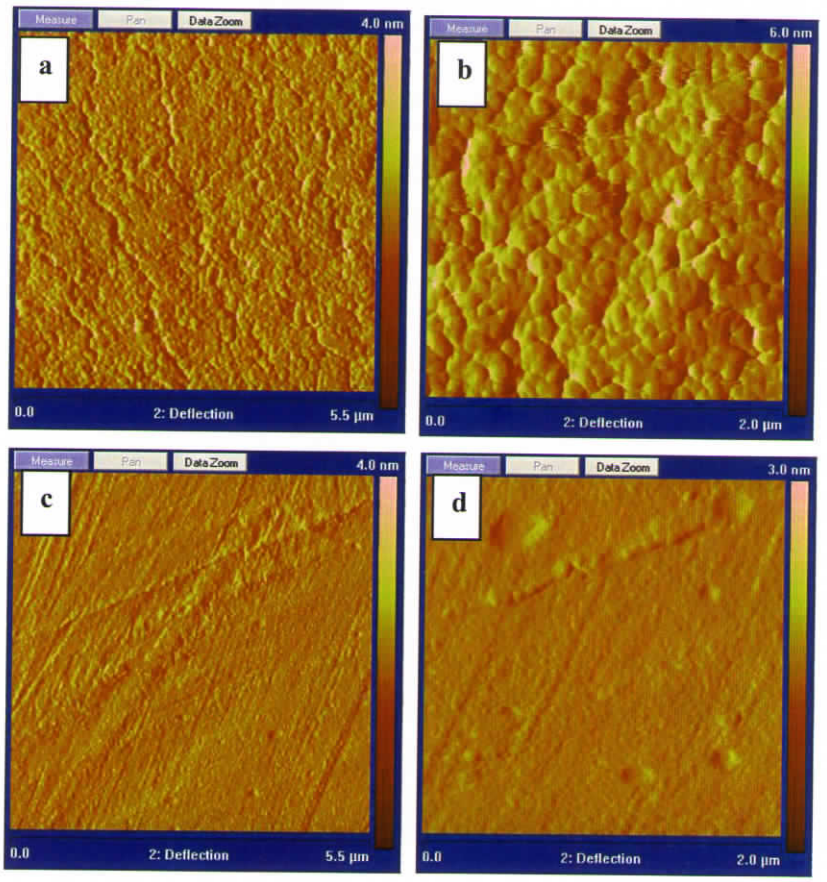

Figure 3-14 Atomic force micrographs of surface phosphorylated PH1 (a) and (b) unmodified PH1 (c) and (d)

The change in surface topography is apparent from the figures. It is clear that surface roughness of PH1 increases due to surface phosphorylation. This property also has a role in inducing the nucleation of calcium phosphate. As surface roughness increases, the surface energy also varies. It has been reported that surface energy has a prominent role in triggering crystal nucleation [146]. Here also the surface energy factor plays a significant role in determining the calcium phosphate nucleation. The basic requirement for crystal nucleation on a surface is the lowering of interfacial energy [147]. Mann *et al* proved that concave areas of a surface works as energy concentrated pockets and has the potential to accelerate crystal nucleation under simulated physiological fluids [147]. The

increase in surface roughness due to phosphorylation also thought to be a prominent factor in the induction of calcium phosphate nucleation.

3.2.7 (a) Phosphorylation Vs hydrophilicity

The unmodifiedPH1 samples demonstrated a profoundly hydrophilic state with a contact angle of 67.6 ^{0} while surface phosphorylation changes the contact angle significantly to 43.55 ^{0} leading to a deep wettability modulation. These measured angles appeared stable and were reproducible.

(b) Phosphorylation Vs degree of equilibrium swelling in Phosphate buffer saline (PBS)

The swelling behaviour of surface phosphorylated PH1, PH2, PH3 and PH4 are compared in fig. 3.15 (a). It could be viewed that the trend of swelling exhibited by the phosphorylated samples is similar to that of unmodified polymers (fig. 3.6(a)). The swelling of poly(HEMA) has been increased from 40 % to 54% is due to surface phosphate coupling. The equilibrium swelling profile of surface phosphorylated PH1 is compared with the virgin PH1 in figure 3.15 (b). It is imperative to state that surface phosphorylation significantly increases the degree of swelling as evident from the figure 3.15 (b). For neat PH1, the swelling degree was 2% while it has considerably increased to 8% for the phosphorylated PH1. An amplification of 4 times is obviously an indication of the increased hydrophilicity. This is merely attributed to the phosporylation. However, when a comparative evaluation is made between virgin and surface phosphorylated poly(HEMA) with that of PH1, it could be demonstrated that the degree of swelling is extremely less for PH1 (figure 3.15 (c)). Further, when equated with PH2 also, PH1 showed remarkably lower degree of swelling (fig. 3.15 (d)).

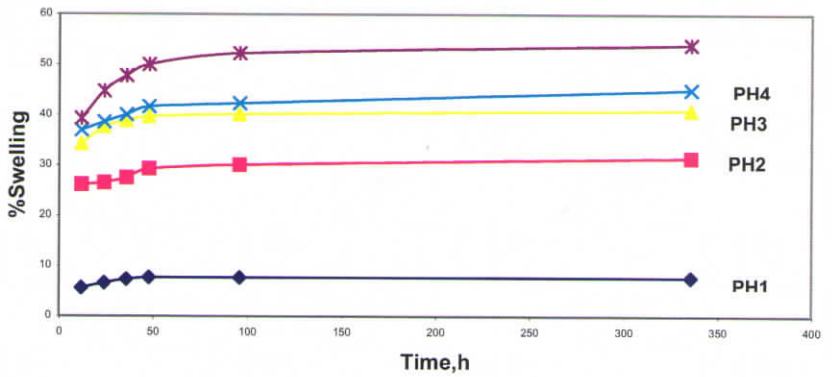

(a): Swelling behaviour of surface phosphorylated PH1, PH2, PH3 and PH4 and poly(HEMA)

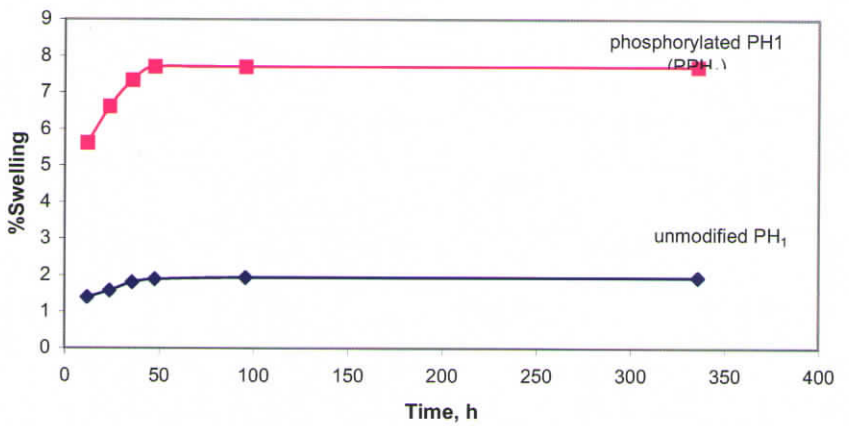

(b): Swelling comparison of surface phosphorylated PH1 with virgin PH1

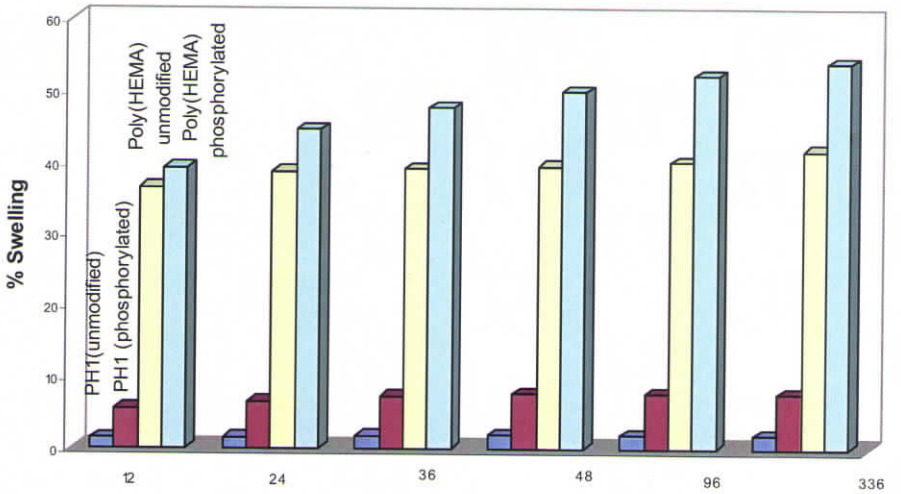

(c): Comparitive assessment of degree of swelling – PH1 Vs poly(HEMA)

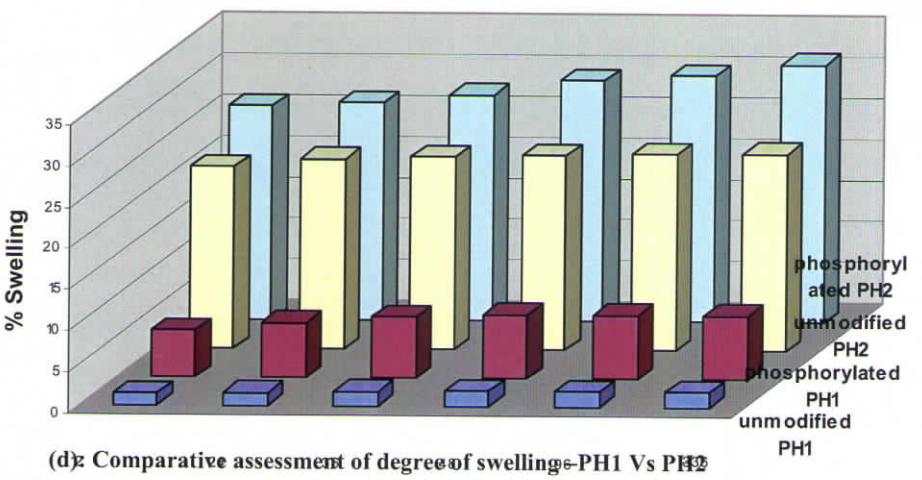

(d): Comparative assessment of degree of swelling –PH1 Vs PH2

Figure 3-15 (a): Swelling behaviour of surface phosphorylated PH1, PH2, PH3 and PH4 and poly(HEMA) (b): Swelling comparison of surface phosphorylated PH1 with virgin PH1 (c): Comparative assessment of degree of swelling –PH1 Vs poly(HEMA) (d): Comparative assessment of degree of swelling –PH1 Vs PH2

While analyzing the results, it could be understood that phosphate coupling imparts greater hydrophilicity to the system. This is in fact, the higher ability of the ester group to undergo ionization in the aqueous medium. The dipolar nature of water is well known [148]. The –OH group is undergoes esterification, during surface phosphorylation and this leads to greater hydrophilicity to the macromolecular chains.

Hermitte *et al* investigated the relationships between formulation, bulk properties, and surface properties of copolymers prepared with hydroxyethylmethacrylate (HEMA), methylmethacrylate (MMA), and ethylmethacrylate (EMA) [149]. The bulk water content, swelling ratio, and static (sessile drop and captive bubble) and dynamic (Wilhelmy plate technique) contact angles and the electrokinetic potential (streaming potential) were measured. The bulk water content and swelling ratio of HEMA copolymers were found to be proportional to the amount of HEMA and are linearly correlated to the contact angle hysteresis. Periodic instabilities in the wetting cycles, similar to Haines jumps, were observed with HEMA copolymers and support a bidirectional relaxation of the hydrophilic groups respectively towards external water and capillary water.

Poly(HEMA) in dry state are hard and glassy. However, when swollen, it is soft and flexible and possesses low surface friction. The swelling of poly(HEMA) is greatly dependent on temperature and the penetrating solution. The balance between hydrophilic/hydrophobic groups, the length between links, and the size and distribution of the mesh also determines the extent of swelling [142]. The equilibrium water content can be increased by copolymerization with a monomer more hydrophilic. Oxygen permeability coefficient increases exponentially with the water content [142].

3.2.8 Mechanical properties

(a) Compressive modulus

The compressive strength (stress at maximum load) for PPH_1 was found as 39.35MPa and modulus 1.6 GPa. The typical stress-strain curve of PPH1 is given in fig. 3.16.

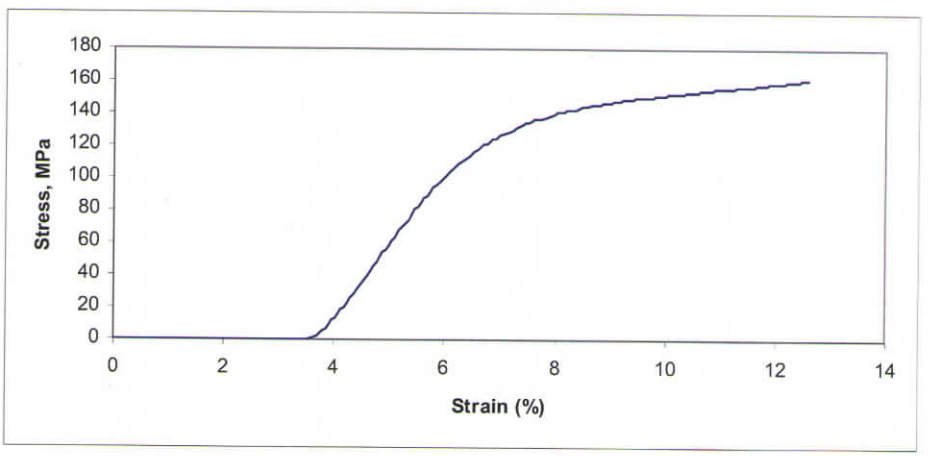

Figure 3-16 The typical stress-strain curve of PH1

(b) Tensile modulus (Dynamic)

The storage modulus of PPH1 is compared with that of PH1 in fig. 3.17 (a). It could be seen that the storage modulus of PPH1 is almost the same as that of PH1 at room temperature with a value of 1.75GPa. The storage modulus of PMMA and poly(HEMA) are 2.44 and 1.43 respectively (shown in fig. 3.17 (b)). It is obvious from the figure that PMMA has a higher modulus compared to poly(HEMA). The overlay of storage modulus curves for all the four polymer matrices is shown in fig. 3.17 (c). It is evident from fig. 3.17 (c) that the storage modulus value for PH1 is in between as that of PMMA and poly(HEMA).

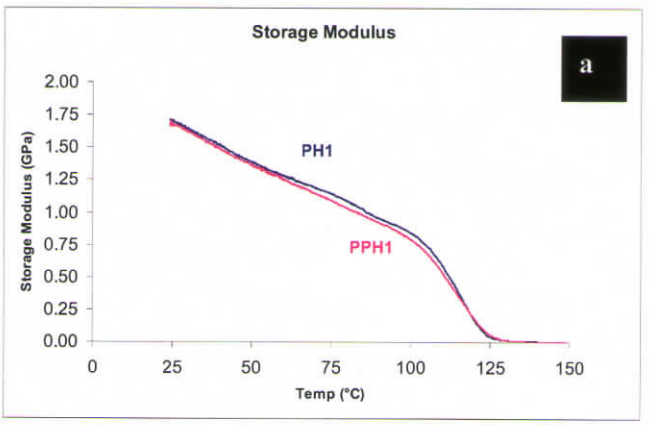

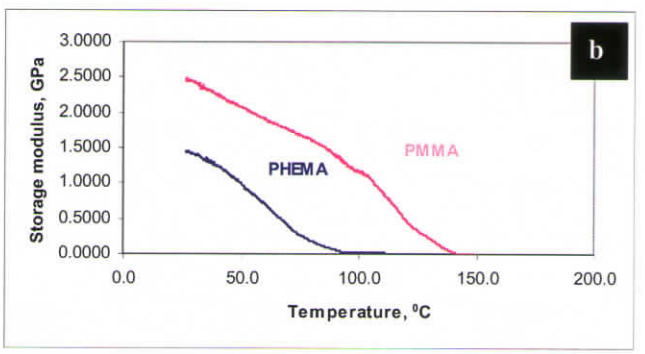

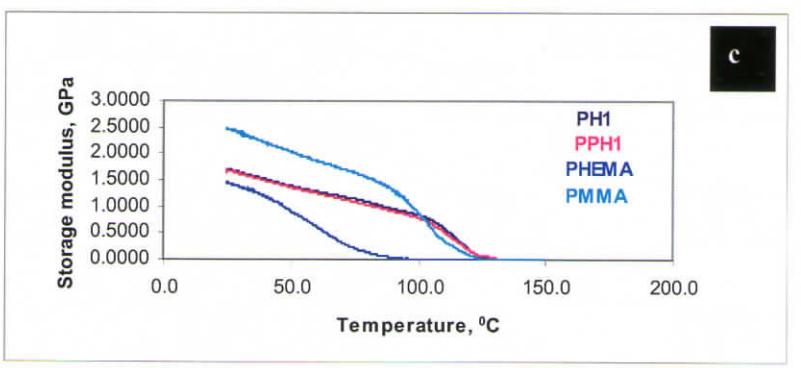

Figure 3-17: Storage modulus of PPH1 in comparison with PPH1 (a): Storage modulus of PMMA in comparison with Poly(HEMA) (b): Storage modulus of PPH1 in comparison with PPH1, PMMA and poly(HEMA) (c)

3.2.8 Mechanical properties

(a) Compressive modulus

The compressive strength (stress at maximum load) for PPH_1 was found as 39.35MPa and modulus 1.6 GPa. The typical stress-strain curve of PPH1 is given in fig. 3.16.

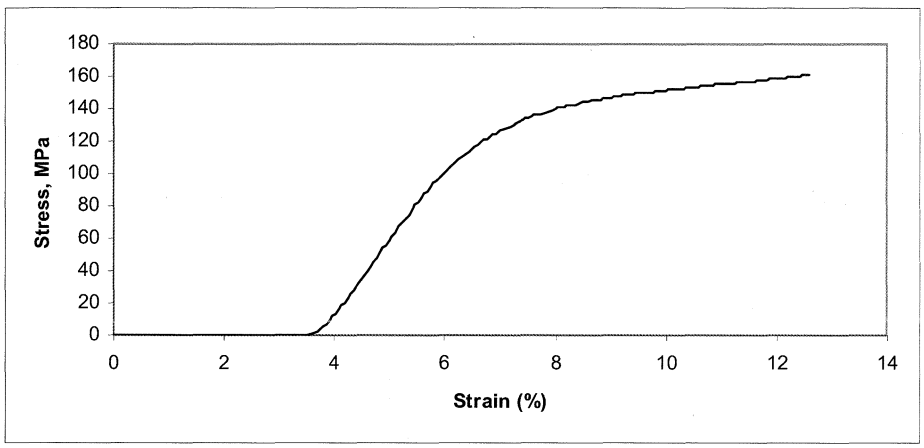

Figure 3-16 The typical stress-strain curve of PH1

(b) Tensile modulus (Dynamic)

The storage modulus of PPH1 is compared with that of PH1 in fig. 3.17 (a). It could be seen that the storage modulus of PPH1 is almost the same as that of PH1 at room temperature with a value of 1.75GPa. The storage modulus of PMMA and poly(HEMA) are 2.44 and 1.43 respectively (shown in fig. 3.17 (b)). It is obvious from the figure that PMMA has a higher modulus compared to poly(HEMA). The overlay of storage modulus curves for all the four polymer matrices is shown in fig. 3.17 (c). It is evident from fig. 3.17 (c) that the storage modulus value for PH1 is in between as that of PMMA and poly(HEMA).

The fundamental reason for poly(HEMA) to show a lower modulus compared to PMMA is specifically associated with the hydrophilic nature of poly(HEMA). The water molecules adsorbed by poly(HEMA) from the environment has a plasticizing action and offers greater flexibility to the polymer.

Even though there is no considerable change is associated with PH1 due to surface phosphorylation, its compressive strength as well as modulus of PH1 decreases significantly due to surface phosphorylation. The stress-strain curve of both PH1 and PPH1 shows that there is no breaking point during compression and hence no ultimate failure is observed. The curve reaches a plateau and further stress leads to an increased strain, but no breaking point. The diameter of the sample at this moment increases and height decreases, showing the rearrangement of the macromolecular chains.

3.2.9 Summary

The FT-IR results ensured surface phosphorylation of PH1 by the proposed method. The DSC results showed that the T_g of PH1 is not significantly altered due to surface phosphorylation. TGA data showed that the decomposition tempereture of surface phosphorylated PH1 (206.3 ^{0}C) is slightly higher than that of unmodified PH1 (189 ^{0}C), which shows that surface phosphorylation slightly improves the thermal stability. The equilibrium swelling data showed that surface phosphorylation of poly(HEMA-co-MMA) significantly increases the hydrophilicity. This is further supported by the contact angle values (unmodified PH1=67.6, surface phosphorylated PH1= 43.55). The AFM study showed that surface roughness of PH1 increased due to phosphorylation. The compressive strength of PH1 (153 MPa) decreased significantly due to surface phosphorylation (39.35 MPa). The compressive modulus also decreased from 4.6 GPa to 1.6 GPa. However, dynamic storage modulus (1.75 GPa) value is not altered due to surface phosphorylation. The UV-Visible analysis showed that extent of surface phosphorylation was proportional to HEMA content in poly(HEMA-co-MMA).

CHAPTER 3.3

EVALUATION OF BIOMIMETIC MINERALIZATION

3.3 EVALUATION OF BIOMIMETIC MINERALIZATION

The biomimetic mineralization was preliminarily assessed with micro FT-IR spectroscopy. The coating morphology was evaluated using scanning electron microscope attached with an energy dispersive X-ray (EDS) detector. The ultra-structural features of coating characteristics were evaluated using transmission electron microscope coupled with an EDS detector and the results were compared with the observations obtained through an atomic force microscope. The amount of calcium and phosphorous in the calcium phosphate coating was quantitatively estimated as a function of time using atomic absorption spectroscopy and UV-Visible spectroscopy respectively. The amount of calcium phosphate formed as a function of HEMA content in poly(HEMA-co-MMA) was also estimated. The calcium phosphate phase was confirmed as hydroxyapatite using wide angle X-ray diffraction pattern.

3.3.1 Micro FT-IR spectroscopy

The micro FT-IR spectrum of calcium phosphate coating formed after 15 days immersion in SBF is shown in figure 3.18 (a). The overlay spectrum of PPH1 with the calcium phosphate coated PH1 is shown in fig.3. 18 (b) while an overlay spectrum of calcium phosphate coated PH1 with synthetic sintered hydroxyaptatite is shown in fig. 3.18 (c).

The spectrum (fig. 3.18 (a)) shows peaks corresponding to inorganic phosphate group at 1071 and 582 cm^{-1}. The broad band 3435 cm^{-1} corresponds to

the –OH group of hydroxyapatite. The spectrum of surface phosphorylated polymer matrix and the inorganic phosphate coated polymer matrix are significantly different (shown in fig. 3.18 (b)). A comparative evaluation of calcium phosphate coated PH1 and synthetic hydroxyapatite is done in spectrum 3.18 (c). It is apparent in fig. 3. 18 (c) that the –OH peak is very sharp and this could be attributed to the crystalline nature HAP acquired due to sintering. The phosphate bands are closely matching for both HAP (1074, 565 cm^{-1}) and the calcium phosphate coated PH1 sample (1071 cm^{-1} and 582 cm^{-1}).

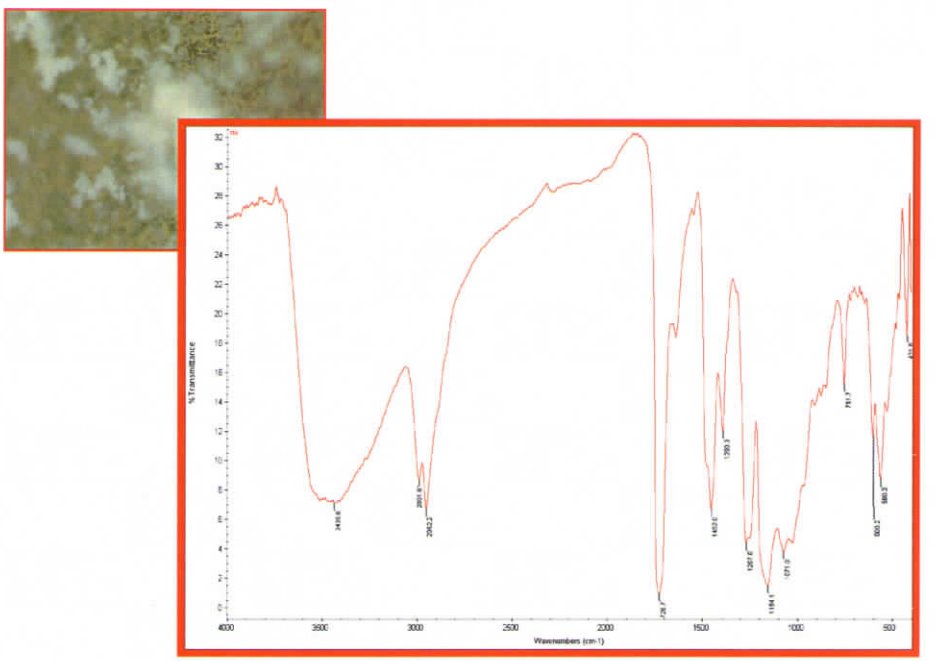

(a): Micro FT-IR spectrum of calcium phosphate coated PH1 (after 15 days immersion in SBF)

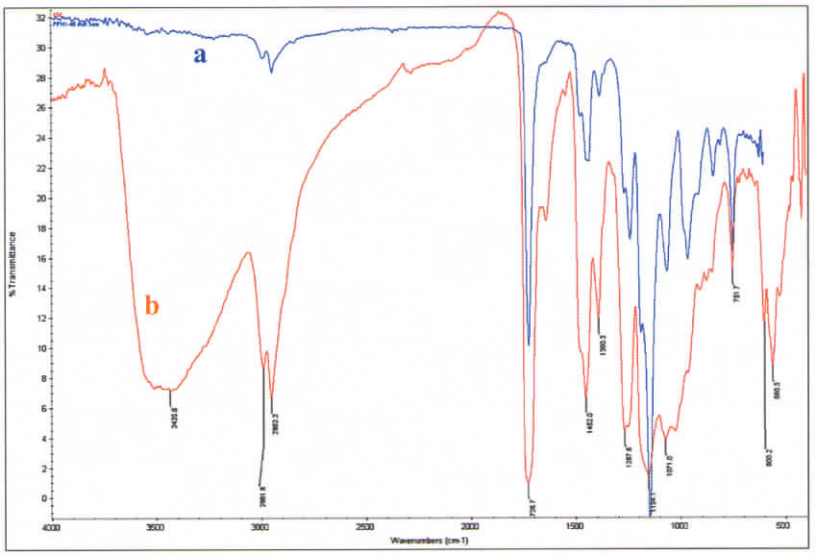

(b): Micro FT-IR spectra of PH1 with phosphorylated PH1 (a) and calcium phosphate coated PH1(b)

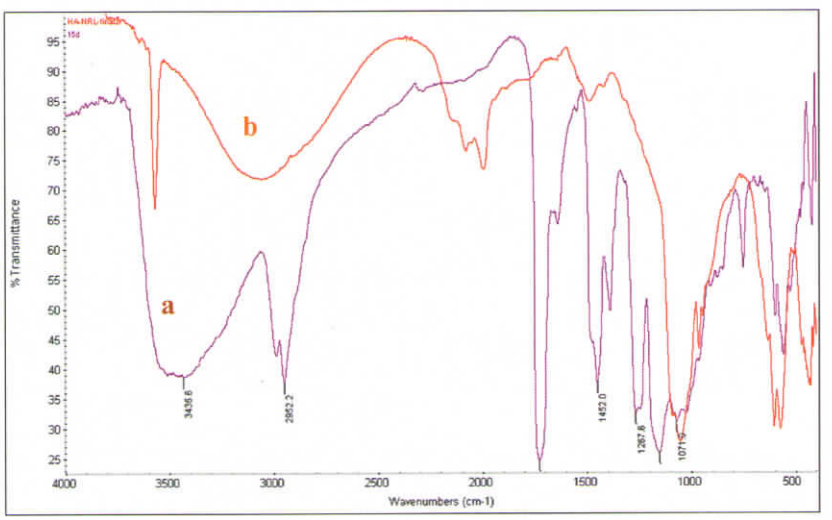

(c) Micro FT-IR spectra of calcium phosphate coated PH1 and synthetic hydroxyapatite

Figure 3-18 (a): Micro FT-IR spectrum of calcium phosphate coated PH1 (after 15 days immersion in SBF) (b): Micro FT-IR spectra of PH1 with phosphorylated PH1 (a) and calcium phosphate coated PH1(b) (c): Micro FT-IR spectra of calcium phosphate coated PH1 and synthetic hydroxyapatite

FT IR analysis of PPH1 and calcium phosphte coated PH1 (fig. 3.18 (c)) showed that characteristic peaks of PH1 progressively disappear, owing to the formation of a surface coating of calcium phosphate and new peaks appear corresponding to the ones of P-O stretching (1154 and 1071 cm^{-1}) and P-O bending (560 cm^{-1}) vibration modes, thus suggesting that the method is effective in promoting the formation of a surface phosphate layer.

3.3.2 Scanning electron microscopy - Energy dispersive X-ray analysis

The scanning electron micrographs showing the nucleation and growth of calcium phosphate on phosphorylated PH1 upon immersion in SBF at different time periods are shown in figures 3.19 (a -f). The nucleation begins at 3 days (fig. 3.19 (a) and (b)). Within 10 days, the surface was totally covered by a primary layer, and at the same time secondary nucleation begins (fig. 3.19 (c) and (d)). The micrographs show that, the calcium phosphate coating is having unique spheroid morphology, which is a characteristic feature of hydroxyapatite crystals. The secondary growth propagates and is complete within the next five days of immersion in SBF (fig. 3. 19 (e) and (f)). The EDS spectra of the coating at 3, 10 and 15 days are given in figs. 3.20 (a), (b) and (c). It is apparent from the figures that, the calcium to phosphate ratio of the coating increases with increase in immersion time.

The high magnification view of the hydroxyapatite crystals formed on phosphorylated PH1 is shown in fig. 3.21. The spheroid like superstructure of hydroxyapatite is in fact composed of fine network of tiny apatite crystals. A few void-like appearances could also be noted in the high magnification image. Fig. 3.22 (a) and (b) are the high magnification scanning electron micrographs of calcium phosphate coating formed on phosphorylated PH3 and phosphorylated poly(HEMA) respectively. It is evident from the micrographs that the morphology of these coating closely resembles to that formed on PH1. The coating formed on phosphorylated poly(HEMA) has a flower like appearance (fig. 3.22 b). However, the spheroid-like clusters seen in both cases are made up of tiny apatite crystals as in the case of PH1.

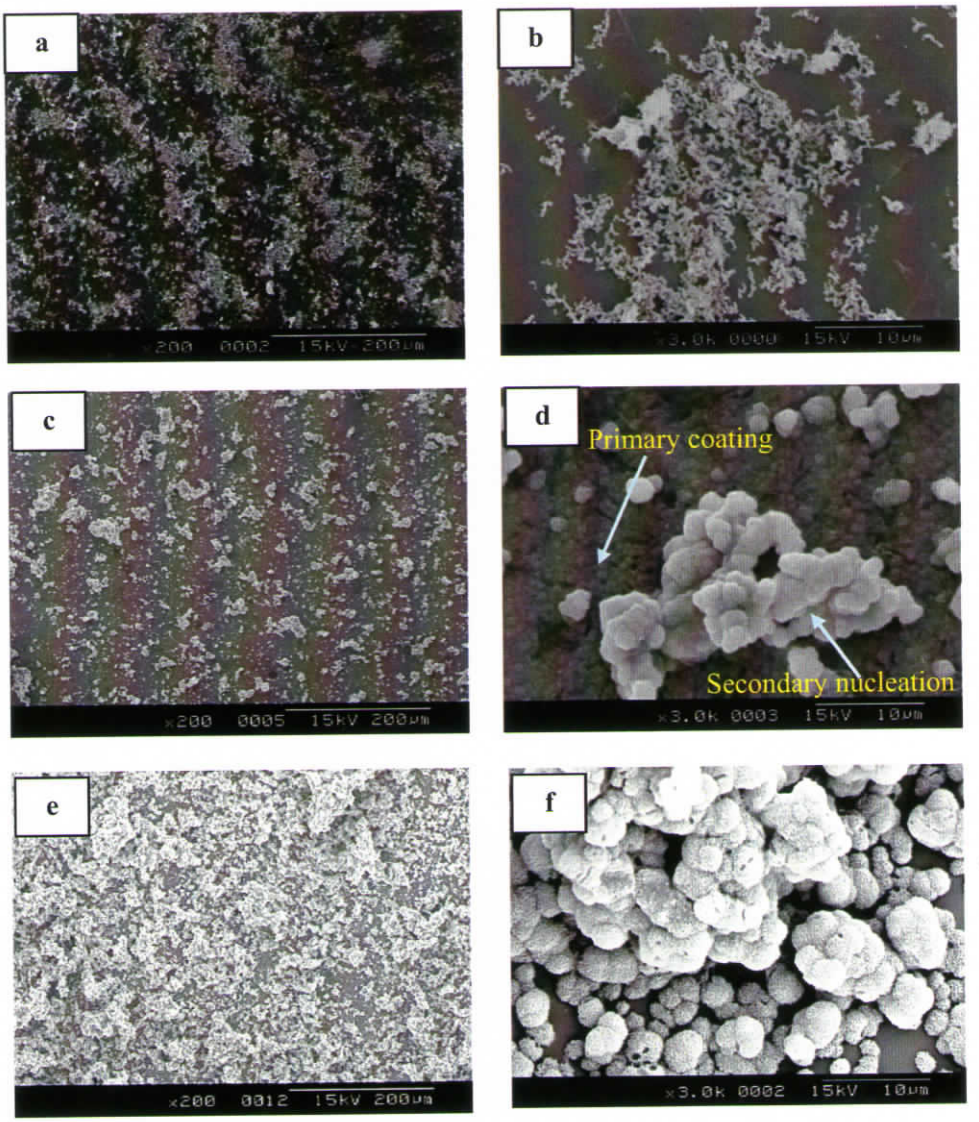

Figure 3-19 The nucleation and growth of calcium phosphate on phosphorylated PH1 at different time periods on immersion in SBF

(a) and (b): 3 days

(c) and (d): 10 days

(e) and (f): 15 days

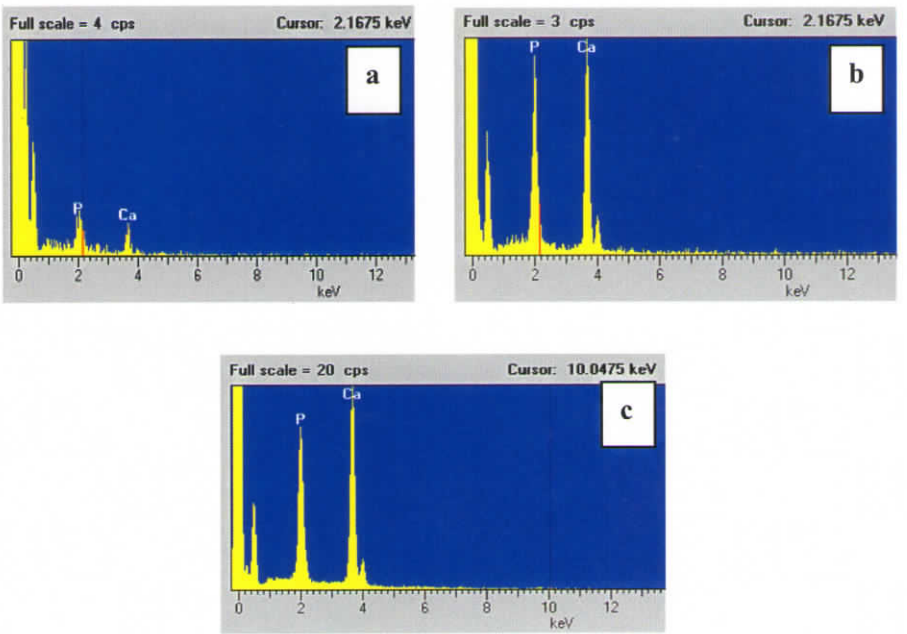

Figure 3-20 The Energy dispersive spectrum of calcium phosphate on phosphorylated PH1 at different time periods on immersion in SBF

(a) 3 days (b) 10 days (c) 15 days

Figure 3-21 Calcium phosphate coating formed on phosphorylated PH1 at 15 days-magnified view

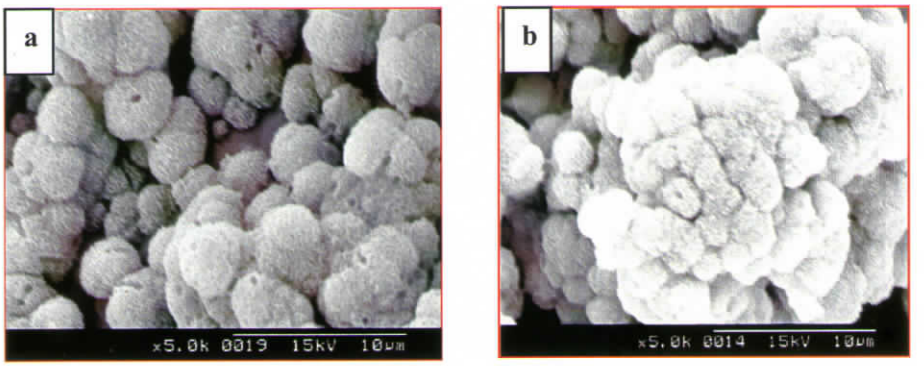

Figure 3-22 Calcium phosphate coating formed on phosphorylated PH3 (a) and phosphorylated poly(HEMA) (b) at 15 days-Magnified view

The SEM images of the control samples are shown in fig. 3. 23 (a) virgin PH1, (b) poly(HEMA) and (c) PMMA. The absence of calcium phosphate coating is apparent in all the three samples.

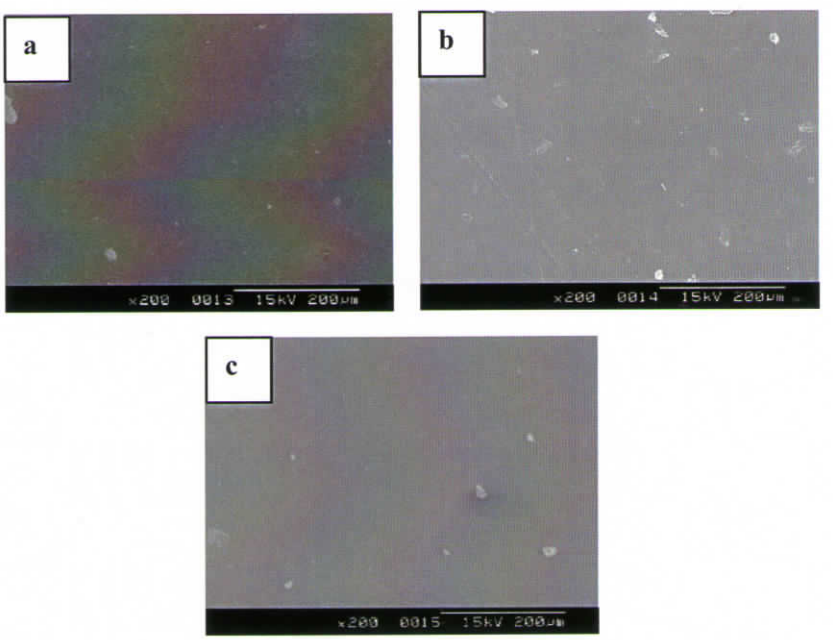

Figure 3-23 The scanning electron micrographs of control samples after immersion in SBF for 15 days (a):PH1, (b) PHEMA, (c) PMMA

The ionic activity product (IP) of the apatite in the SBF solution has been considered to be key to the formation of apatite on the surface of the substrate. The increase in the calcium ion concentration can result in the increase in the IP of the apatite and is beneficial to the precipitation of apatite on the surface of the substrate [150]. Many of the proteins directly involved in control of biomineral nucleation and growth contain acidic domains that are rich in aspartic acid and glutamic acid and phosphorylated serines [151, 152]. Li *et al.* have applied a 'charged surface'theory to explain the reaction of bioactive glass in simulated physiological solution and it is believed that precipitation of apatite on the surface of the bioactive glass soaked in SBF is due to the formation of an electric double layer in the glass-solution system [153].

The properties of calcium phosphate crystal formed by biomimetic way is different from those of biological apatite [154-157]. The properties that vary are chemical composition, Ca/P ratio, crystallinity, particle size, etc. This arises due to the following differences between *in vivo* and in vitro crystallization conditions [154-157].

(i) In vitro crystallization from supersaturated aqueous solutions normally occurs at permanently depleting concentrations of calcium and phosphate, while the concentrations of these ions are kept strictly constant during biological mineralization (the same is valid for the solution pH)

(ii) Chemical crystallization is a fast process (time scale of minutes and hours), while the biological process is usually slow (time scale of weeks to years)

(iii) Many organic, biological, and polymeric compounds are present in biological liquids (blood plasma, serum, saliva). Each of these compounds can have an influence (either positive or negative) on the *in vivo* crystallization of calcium phosphates.

Likewise surface phosphorylated poly(HEMA-co-MMA) film, surface phosphorylated poly(HEMA-co-MMA) microspheres also induced biomimetic growth of calcium phosphate on their surface when subjected to simulated physiological condition. The SEM images as well as the EDS spectra of the coating are shown in fig. 3.24.

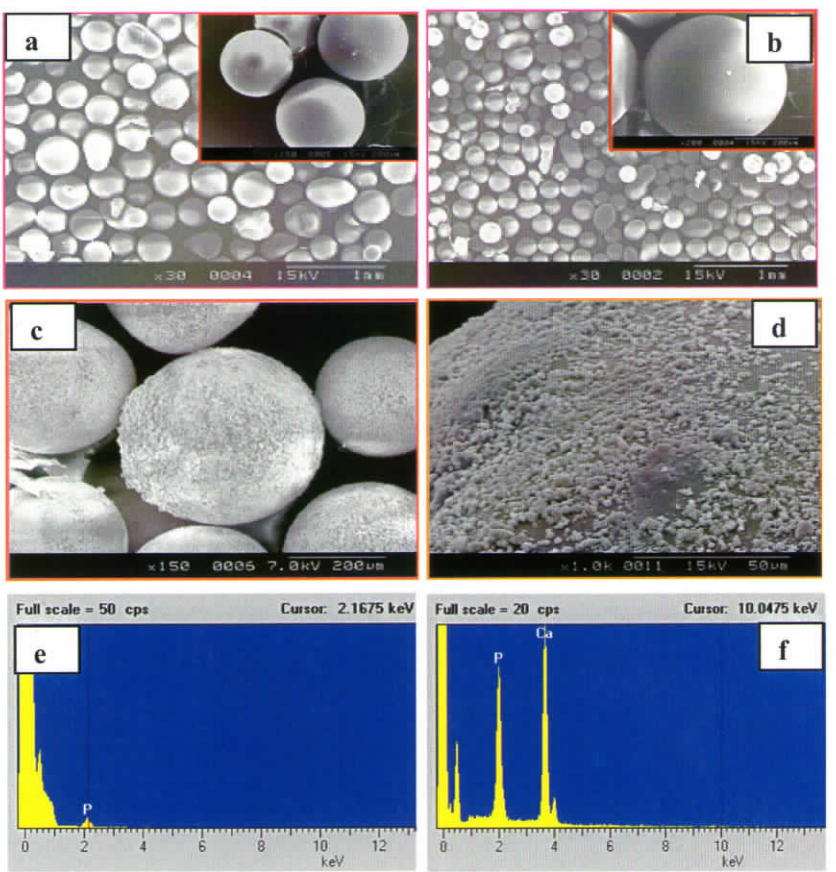

Figure 3-24 Scanning electron micrographs of PH1 microspheres before (a) and after phosphorylation (b) Figs. (c) and (d) calcium phosphate coating formed on the microspheres after 15 days immersion in SBF Figs. (e) and (f): EDS spectra of phosphorylated and calcium phosphate coated PH1 respectively

In biomineralization, inorganic precipitates form under the full control of an organic tissue matrix. This control includes manipulation of local concentrations of the precipitants, the presence of nucleating surfaces and the presence of inhibitors in solution which can bind to specific faces on the growing mineral. The matrix regulates the particle size, shape and orientation of the mineral. Even though there are certain differences in the crystallization behaviour between biomineralization and biomimetic mineralization, the biomimetic approach can be compared with biomineralization processes due to some potential similarities and would definitely provide greater control of particle morphology and distribution compared to conventional blending or deposition methods [158].

3.3.3 Transmission electron microscopy and Energy dispersive X-ray (TEM-EDS) analysis

The transmission electron micrograph of the calcium phosphate crystals formed on PH1 upon 3days immersion in SBF is shown in fig. 3.25. The ultra-structural features of coating are revealed in the micrograph. It is interesting to notice that the spheroid-like apatite clusters are in fact made up of nanometer size apatite rods. Another key observation is the transformation of calcium phosphate from amorphous state to crystalline phase begins at an early period of 3 days. This was recognized with the help of selected area electron diffraction (SAED) pattern of the crystalline region shown at the left corner of the micrograph. The EDS spectra of the crystalline and amorphous regions are shown in fig. 3.26(a) and (b) respectively. It is clear from the EDS spectra that initially calcium rich apatite was formed.

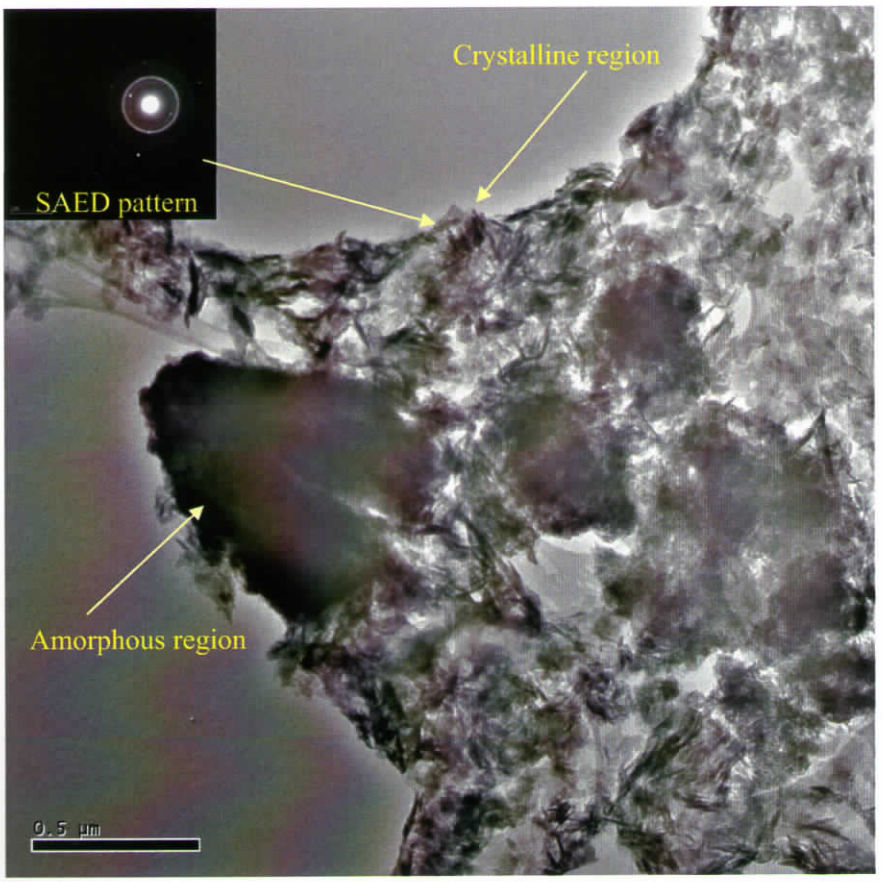

Figure 3-25 Transmission electron micrographs of calcium phosphate coating formed on phosphorylated PH1 after 3 days immersion in SBF

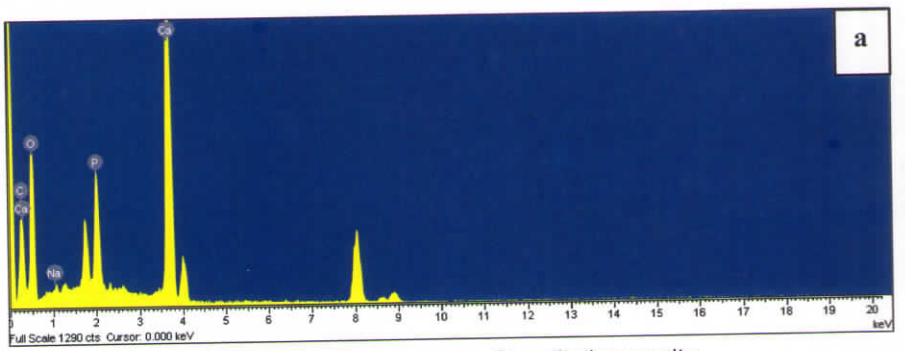

Element	Weight%	Atomic%
C K	12.41	24.40
O K	23.56	34.78
Na K	0.83	0.85
P K	15.66	11.94
Ca K	47.55	28.03
Totals	100.00	

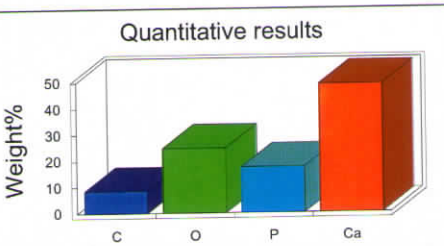

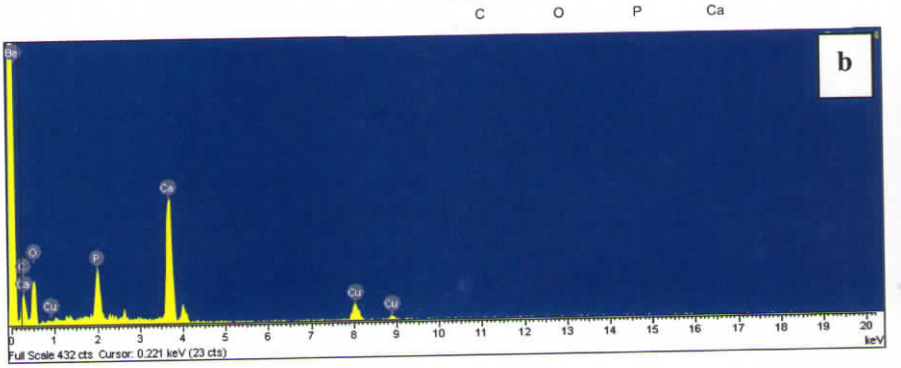

Element	Weight%	Atomic%
C K	11.69	25.14
O K	17.99	29.04
P K	15.30	12.76
Ca K	44.98	28.98
Cu K	10.03	4.08
Totals	100.00	

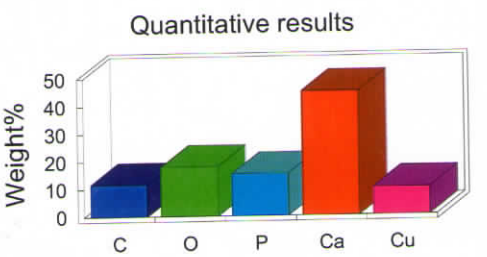

Figure 3-26 Energy dispersive spectrum of the *crystalline region* (a) and amorphous region (b) of the calcium phosphate coating formed on phosphorylated PH1 upon 3 days immersion in SBF

The rod-like structure of apatite crystals are better viewed in the higher magnification images, shown in figs. 3.27 (a) and (b). The apatite rods are of 20 to 40nm in length and 100 to 300 A^0 in diameter (fig. 3.27 b).

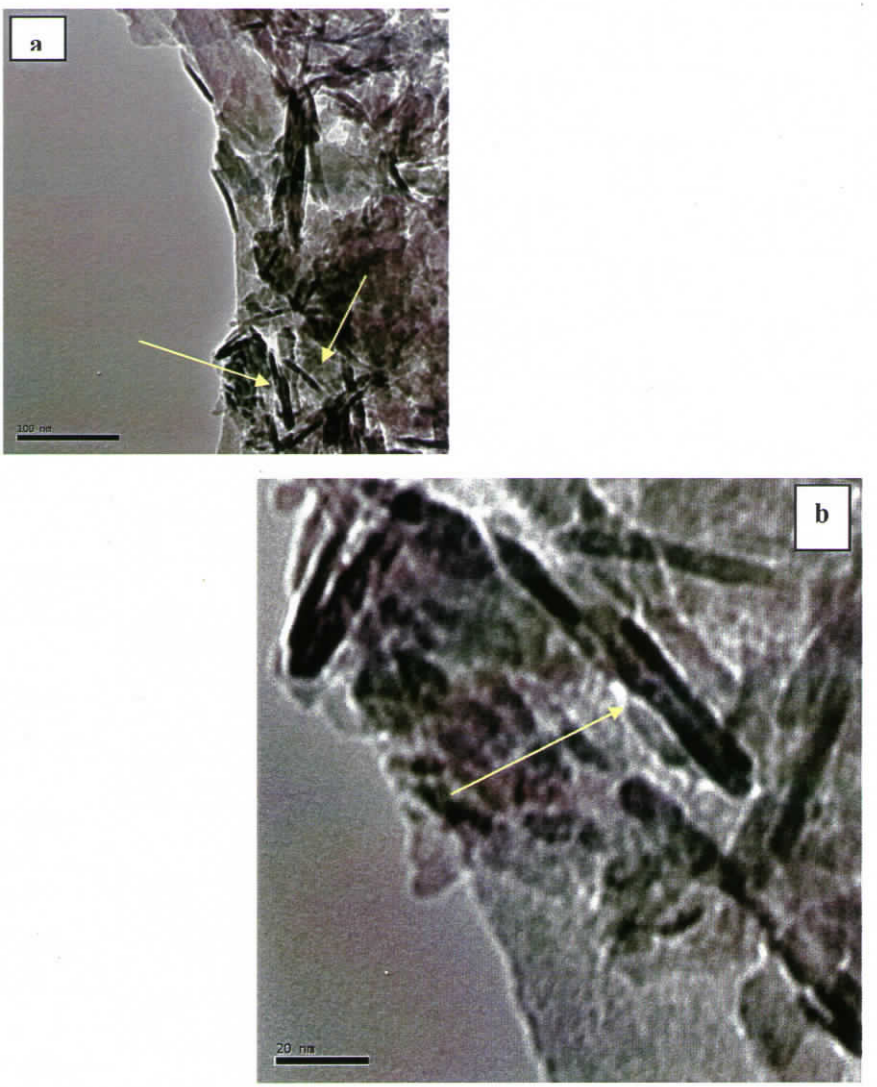

Figure 3-27 (a) and (b): TEM image rod-like structure of apatite crystals-higher magnification

The ultra-structural features of the calcium phosphate coating formed on phosphorylated PH1 after 10 and 15 days are shown in figs.3.28 and 3.29 respectively. It could be seen from the SAED pattern of both samples that the coating is of polycrystalline in nature, as obvious from the continuous rings seen in the pattern. The TEM images of both samples appeared as clusters of calcium phosphate. However, the calcium to phosphate ratio obtained from the EDS patterns indicates the calcium phosphate as calcium rich apatite.

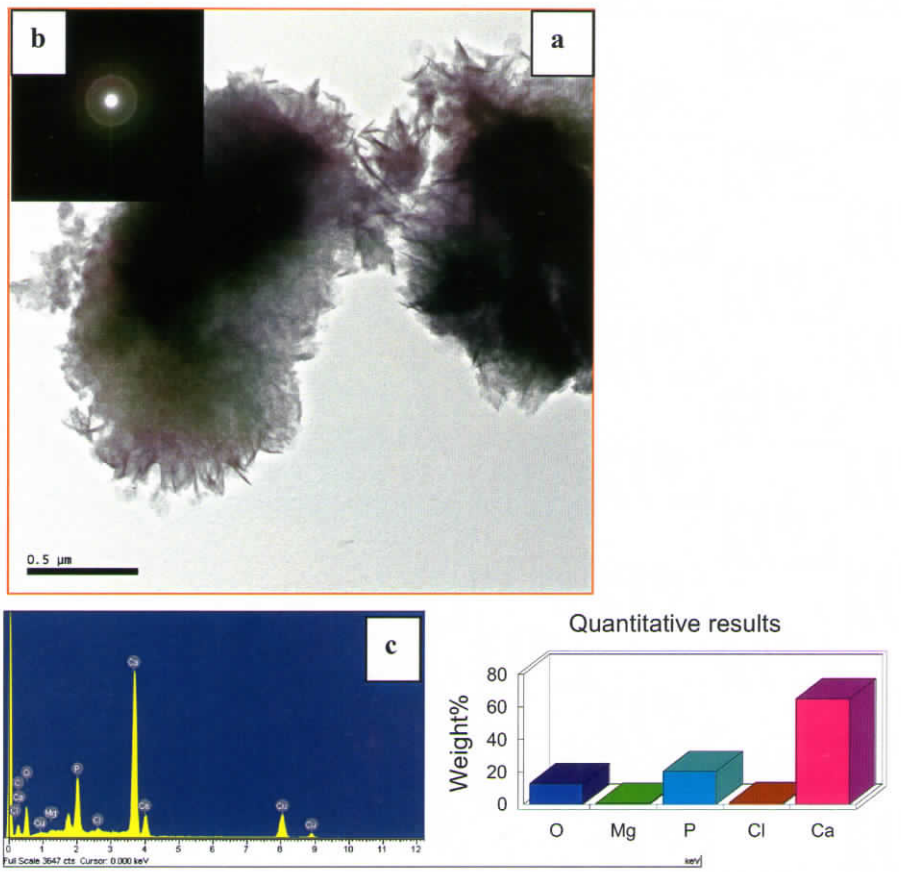

Figure 3-28 The ultra-structural features of the calcium phosphate coating formed on phosphorylated PH1 after 10 days (a): TEM image (b): SAED pattern (c): EDS spectrum

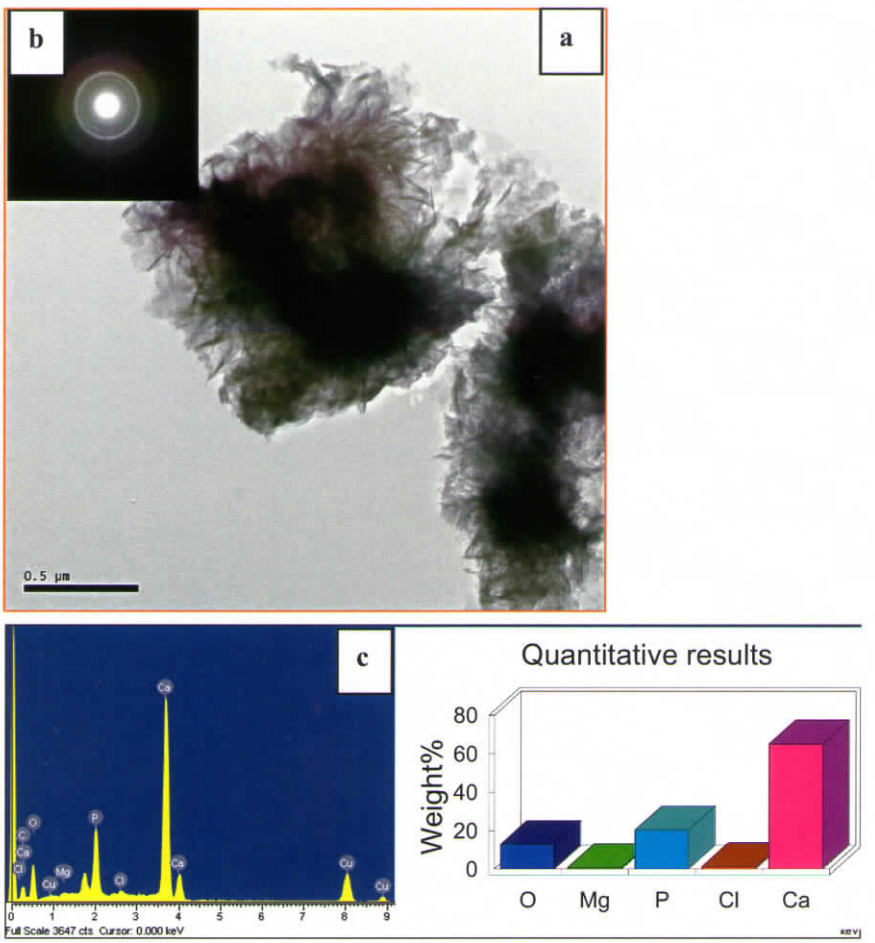

Figure 3-29 The ultra-structural features of the calcium phosphate coating formed on phosphorylated PH1 after 15 days

Kim *et al* found that on immersion in SBF, the synthetic HAP was found to induce the formation of bone-like apatite on its surface through the formation of calcium-rich amorphous calcium phosphate (ACP) in the early soaking period [41]. While comparing the present observation with this report, it could be postulated that similar event is occurring on surface phosphorylated poly(HEMA-co-MMA) also.

3.3.4 Atomic force microscopy

The AFM images (both height and deflection modes) of calcium phosphate coated PH1, immersed in SBF for 3days is given in fig. 3.30 (a) and (b) respectively. The three dimensional view of the same area is given as 3.30(c).

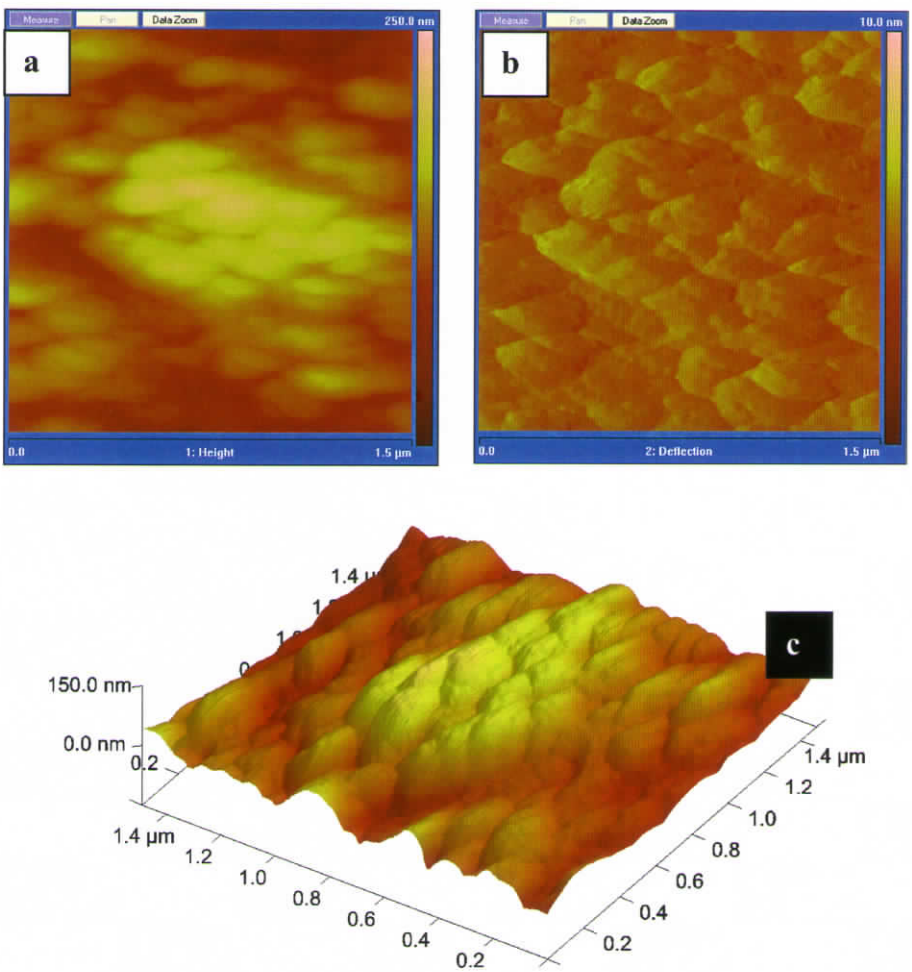

Figure 3-30 AFM image of 3 day calcium phosphate coating (a): Height (b): deflection (C): 3-dimensional view

The AFM images of calcium phosphate coated PH1, immersed in SBF for 10 days is given in fig. 3.31 (a), (b) and (c). The three-dimensional view of region showed in 3.31 (c) is given as 3.31(d).

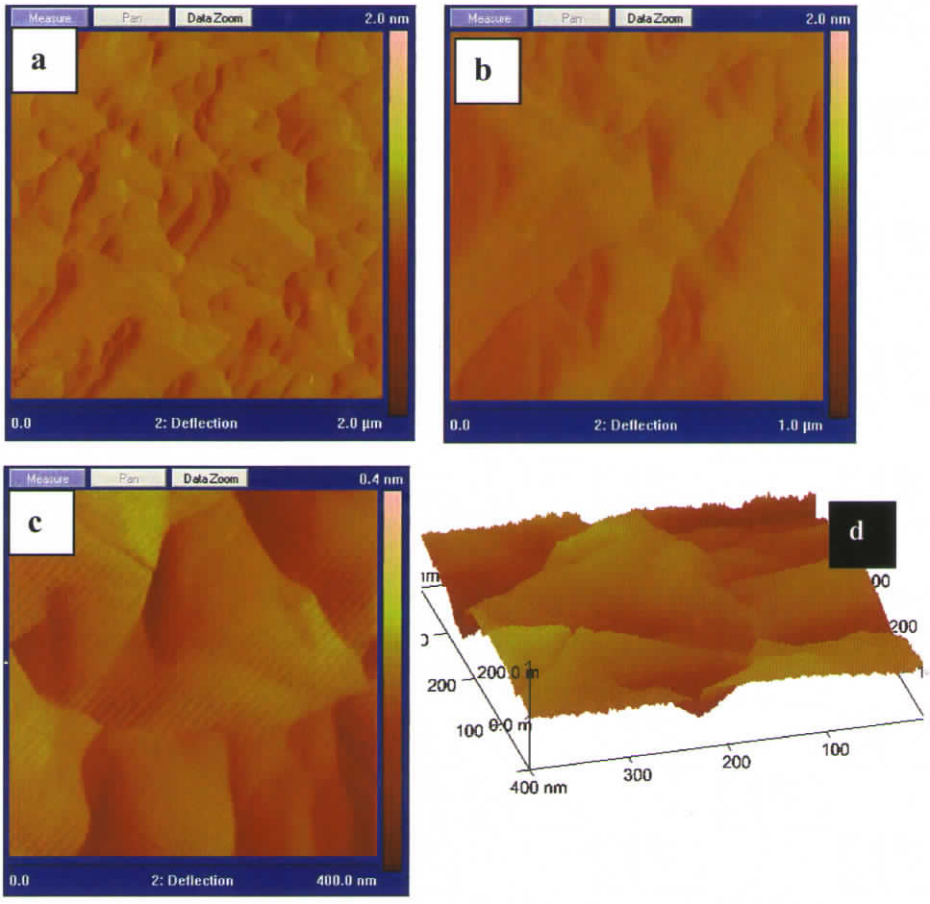

Figure 3-31 AFM images of calcium phosphate coated PH1 immersed in SBF for 10 days ((a), (b) and (c)) The three-dimensional view of region showed in 3.32 (c) is given as (d)

The AFM images show that the crystals are of approximately 200 nm in size. The crystals are seem to have < 20 nm thick during the initial stage of 3 days. They have a specific orientation in growth as seen from fig. 3.31(b). However, on further immersion in SBF, the crystal size increases to 400 to 600 nm. The observations are in accordance with transmission electron microscopic studies.

TEM also reveals that formation of nanosized rod like single crystals with preferred orientation. These experimental results support the three-dimensional growth of the calcium phosphate crystals. Noam *et al* report similar crystal dimension for hydroxyapatitie but with a different morphology [159]. However, they have used electrochemical process for the nucleation and growth of HAP and used a real-time electrochemical atomic force microscopy to analyze the ultra-structural features. In their work, highly crystallinehydroxyapatite was electrodeposited on pure titanium and Ti-6Al-4V alloy. *In situ* and *ex situ* imaging, coupled with potentiostatic and potentiodynamic measurements, was conducted by means of electrochemical atomic force microscopy.

The apatite crystals deposited by *in vitro* method are one order of magnitude larger than those of biological apatites. This implies that the conditions *in vivo* limit the progressive nucleation stage and three-dimensional growth of apatite crystals. Epitaxy, or oriented overgrowth, is a special case of heterogeneous nucleation in which the growth of the nuclei on the substrate follows a specific orientation. When the substrate and the deposit are made of different materials, the term heteroepitaxy is commonly used. Specifically organized organic surfaces have already been reported to induce growth of specifically oriented inorganic thin films either catalytically or epitaxially [151]. However, in the present study, no selfassembled organic templates or surfactants were used. The pH that raises during deposition makes the formation of HAP more favorable thermodynamically, compared to other calcium phosphate phases. It has already been argued that homogeneous nucleation of particles in the solution will only dominate at relatively high levels of supersaturation where the precipitation process becomes kinetically controlled [151]. On the other hand, formation of the inorganic phase directly on a substrate (i.e., heterogeneous nucleation) is the dominant precipitation mechanism in the case of thermodynamically controlled systems.

Interestingly, for bone mineralization in a given species, the average crystal size is smallest at formation and increases to maturity [152]. The conditions in the human body apparently limit the growth of HAP *in vivo*. The effects of specific molecules on the crystal growth of HAP has been reported Moreno *et al* [154]. The most effective inhibitors seem to be polyanions, particularly polyphosphates or polyphosphonates. It was observed that salivary peptides and proteins, such as statherin and PRPs (praline-rich proteins), respectively, are powerful inhibitors. These macromolecules appear to prevent the precipitation of calcium phosphate phases in saliva in spite of the supersaturation of this secretion with respect to HAP. The inhibiting mechanism was related to their adsorption onto the surface of apatite seeds [154]. Proteoglycans, even at low concentrations, can delay or prevent apatite formation.

The atomic force values between the various substrates (unmodified PH1, phosphorylated PH1 and calcium phosphate coated PH1) and the probe tip are shown in table 3.1.

Table 3-1Atomic force values between the various substrates and the probe tip

Sample	Force value
Unmodified PH1	123.5
Phosphoryated PH1	67.53
Calcium phosphate coated PH1	32.55

It could be seen from the table that the force value is the highest for unmodified. Surface phosphorylation decreases the force value and apatite coating further decreases it. This could be correlated to the hydrophilicity of the polymer due to different surface modifications. The hydrophilicity increases with surface phosphorylation and also due to calcium phosphate coating. An increase in this

force would indicate a larger surface charge per unit area if the force is caused mainly by electrostatics.

3.3.5 Wide angle X-ray diffraction

Fig. 3.32 gives the X-ray diffractogram of the calcium phosphate coating formed on phosphorylated PH1 after 15 days immersion in SBF. The diffractogram shows two very broad peaks at 26 ^{0} 2θ and 31–34 ^{0} 2θ that are typical for a poorly crystalline (nanocrystalline) apatite.

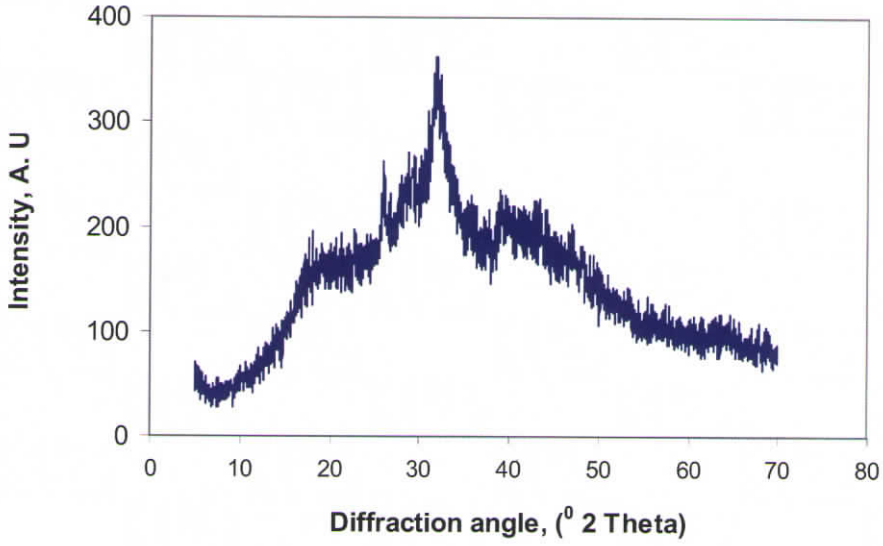

Figure 3-32 The X-ray diffractogram of the calcium phosphate coating formed on phosphorylated PH1 after 15 days immersion in SBF

3.3.6 Determination of Calcium by Atomic absorption spectroscopy (AAS)

Fig.3.33 gives the amount of calcium in the calcium phosphate coating deposited on phosphorylated PH1 estimated as a function of time using AAS. The figure shows that the calcium concentration increases linearly with time. The amount of calcium in the coating estimated as a function of HEMA content in

force would indicate a larger surface charge per unit area if the force is caused mainly by electrostatics.

3.3.5 Wide angle X-ray diffraction

Fig. 3.32 gives the X-ray diffractogram of the calcium phosphate coating formed on phosphorylated PH1 after 15 days immersion in SBF. The diffractogram shows two very broad peaks at 26 ^{0} 2θ and 31–34 ^{0} 2θ that are typical for a poorly crystalline (nanocrystalline) apatite.

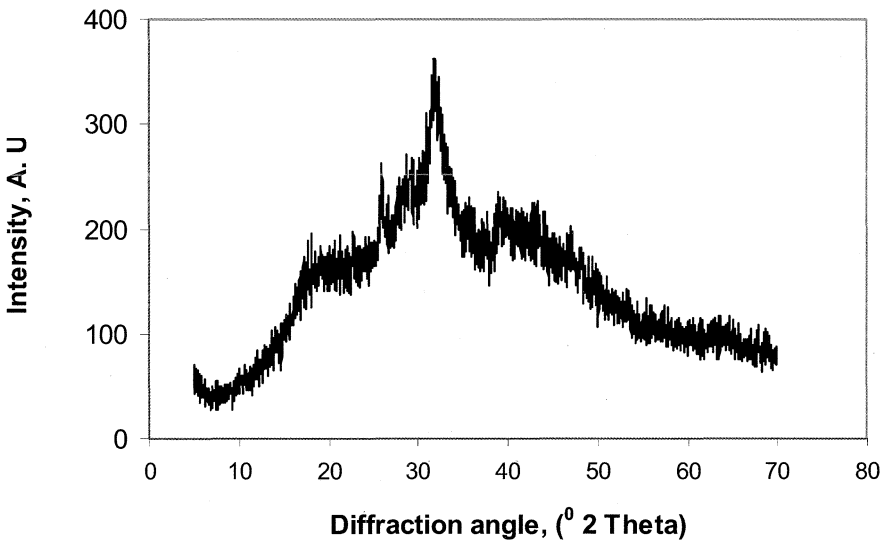

Figure 3-32 The X-ray diffractogram of the calcium phosphate coating formed on phosphorylated PH1 after 15 days immersion in SBF

3.3.6 Determination of Calcium by Atomic absorption spectroscopy (AAS)

Fig.3.33 gives the amount of calcium in the calcium phosphate coating deposited on phosphorylated PH1 estimated as a function of time using AAS. The figure shows that the calcium concentration increases linearly with time. The amount of calcium in the coating estimated as a function of HEMA content in

poly(HEMA-co-MMA) is shown in fig. 3.34 The graph indicates an exponential increase in the amount of calcium concention after 75 wt-% of HEMA in the copolymer.

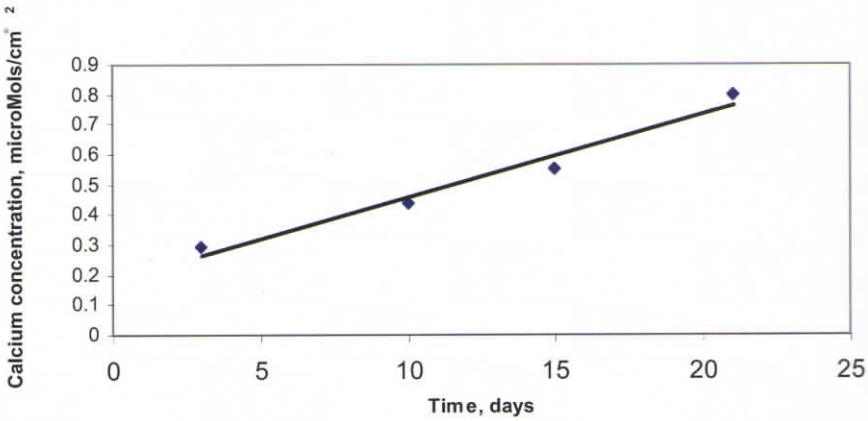

Figure 3-33 Amount of calcium in the calcium phosphate coating deposited on phosphorylated PH1 estimated as a function of time

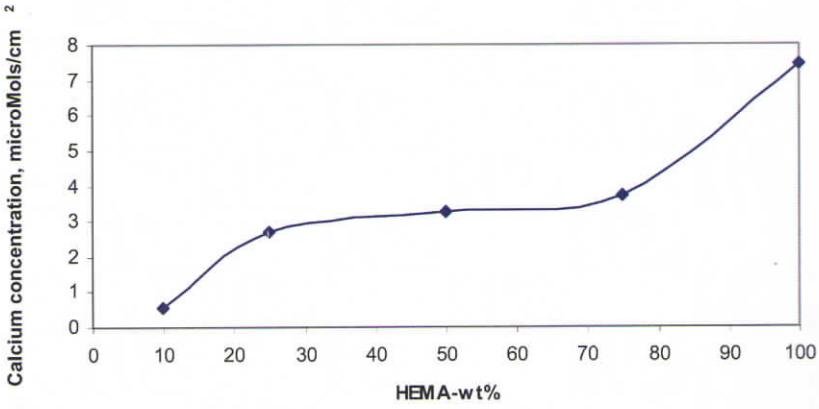

Figure 3-34 Amount of calcium in the coating estimated as a function of HEMA content in poly(HEMA-co-MMA)

The trend of linear increase in calcium in the calcium phosphate coating is according to expectation. It was clear from the SEM micrographs that the deposition of calcium phosphate increases with increase in time. The primary layer of calcium phosphate coating was complete within 10 days and secondary nucleation begins afterwards. The secondary coating is complete within two

poly(HEMA-co-MMA) is shown in fig. 3.34 The graph indicates an exponential increase in the amount of calcium concention after 75 wt-% of HEMA in the copolymer.

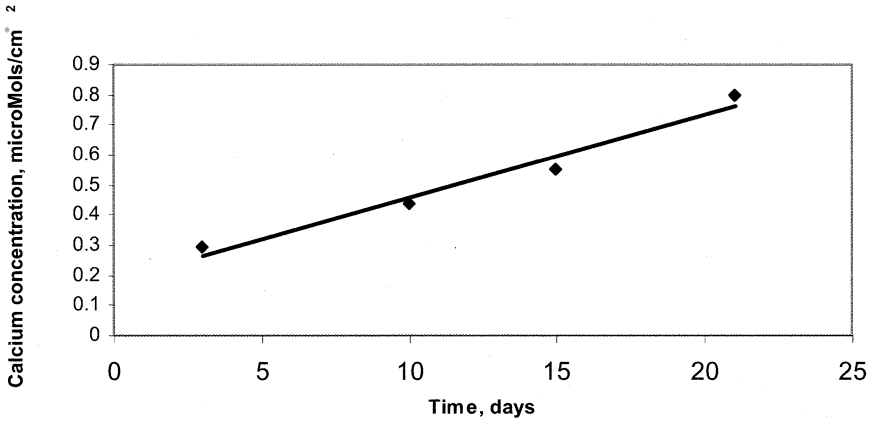

Figure 3-33 Amount of calcium in the calcium phosphate coating deposited on phosphorylated PH1 estimated as a function of time

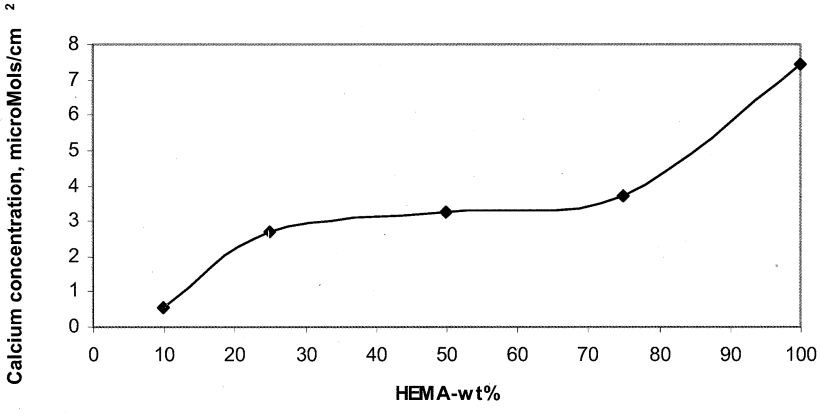

Figure 3-34 Amount of calcium in the coating estimated as a function of HEMA content in poly(HEMA-co-MMA)

The trend of linear increase in calcium in the calcium phosphate coating is according to expectation. It was clear from the SEM micrographs that the deposition of calcium phosphate increases with increase in time. The primary layer of calcium phosphate coating was complete within 10 days and secondary nucleation begins afterwards. The secondary coating is complete within two

weeks. Varma *et al* have reported similar observation tetra ethoxysilane treated cotton and phosphorylated chitosan showing that the SBF soaking time has a significant role in determining the Ca/P ratio [102, 108].

Since the medium for mineralization used is accelerated physiological medium at a highly super saturated condition, possibility of heterogeneous nucleation is significantly high. The nucleation of the mineral occurs due to the influence of negatively charged phosphate ions, exposed to the medium. Once the nucleation begins, the growth of crystals occurs depending on the supplement of calcium and phosphate ions in the medium. The continual growth of the mineral occurs as a result of adequate supply of calcium and phosphate ions through the replenishment of fresh SBF at a regular interval of 24h.

The trend of calcium concentration with increase in HEMA content in poly(HEMA-co-MMA) initially has a linear profile (up to 25 wt-% HEMA) , leading to a plateau (after 50 wt-%) and terminates in an exponential way for poly(HEMA). This could be correlated to the basic behaviour of poly(HEMA) explained in section 3.2.3, the extent of phosphorylation as a function of HEMA content in the copolymer. It has been described in section 3.2.3 that poly(HEMA) belongs to the class of materials one of the polymers which show can undergo a reversal of surface structure when transferred from air into a water environment: i.e, hydroxylated polymers exhibits a surface rich in methyl groups (from the polymer chain backbone) in air, and a surface rich in hydroxyl groups in water [144]. The curve representing the estimation of phosphorous as a function of HEMA shows an exponential profile after 50 wt-% HEMA, which is basically owing to the extremely high concentration of exposed –OH group that could be phosphorylated easily. Another main differences between chemical and biological crystallization is the rate of precipitation. Usually in chemistry, precipitation occurs fast whereas in biology the crystals need days, weeks, or months to grow. A suitable simulation of this process, especially in the presence of (bio)organic additives, must therefore slow down the crystallization [160].

From the above discussion it is clear that the fundamental reason of calcium phosphate nucleation on phosphorylated poly(HEMA-co-MMA) is the surface bound phosphate group. Hence the number of phosphate group is proportional to the degree of nucleation of calcium phosphate on the surface of phosphorylated PH1.

3.3.7 Summary

The FT-IR results confirmed the formation of calcium phosphate coating on surface phosphorylated PH1 under accelerated physiological environment. The scanning electron microscopic studies depicted the morphology of the coating as spheroid like clusters of hydroxyapatite. The SEM micrographs further revealed that nucleation of calcium phosphate begins at 3 days. Primary coating was complete by 10 days while secondary coating was complete by two weeks. The energy dispersive spectra showed that the calcium to phosphate ratio increased with time. Transmission electrons microscopic studies showed that the spheroid like apatite clusters found in SEM are in fact composed of needle like apatite rods with 20-40 nm diameter and approximately 100 nm length. The selected area diffraction patterns of the coating proved that the amorphous to crystalline transformation of the calcium phosphate phase is occurring within 3 days of immersion in SBF. The EDS spectra showed that the coating is initially composed of a calcium rich apatite. The AFM images showed that the calcium phosphate coating formed on 3 days of immersion in SBF itself has an orientation in growth. The AFM observations regarding the size of apatite crystals are supported by the TEM results. The X-ray diffraction pattern confirmed that the calcium phosphate phase is hydroxyapatite. The AAS data showed that the calcium concentration of the coating increased linearly with time of exposure of surface phosphorylated PH1 in accelerated physiological fluid. The study also proved that the calcium concentration increased with increase in HEMA content in poly(HEMA-co-MMA).

CHAPTER 3.4

SURFACE PHOSPHORYLATION OF OTHER BIOCOMPATIBLE POLYMERS

3.4 SURFACE PHOSPHORYLATION OF OTHER BIOCOMPATIBLE POLYMERS

Based on the previous results, the proposed method of surface phosphorylation was further investigated for the possibility phosphorylating other biocompatible polymers with inherent hydroxyl (-OH) group or modifying polymers with appropriate functional groups so as to obtain hydroxyl groups and assessing their ability to nucleate calcium phosphate phase under accelerated simulated physiological environment. The polymers studied are poly (vinyl alcohol) PVA, ethylene vinyl acetate copolymer (EVA having 28% vinyl acetate and melt flow index value 25) and polyethylene terephthalate, PET. In the case of EVA and PET, controlled surface hydrolysis was carried out prior to phosphorylation in order to acquire the necessary –OH groups for phosphorylation reaction.

3.4.1 Poly (vinyl alcohol)

3.4.1.1 FT-IR spectroscopy

The ATR spectra of unmodified (a) and surface phosphorylated PVA (b) are shown in fig. 3. 35. A strong peak characteristic of P-O stretching could be seen in phosphorylated PVA at 989 cm^{-1}, confirming the presence of surface bound phosphate group.

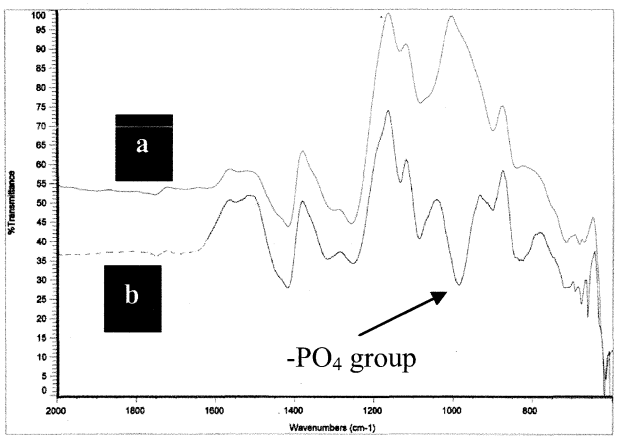

Figure 3-35 ATR spectra of unmodified (a) and surface phosphorylated PVA (b)

3.4.1.2 Evaluation of biomimetic mineralization

Fig.3. 36 (a) and (b) show the scanning electron micrographs of PVA and phosphorylated PVA. The SEM images of calcium phosphate coating formed on phosphorylated PVA when immersed in SBF are given in figs 3.37 (a) to (e). Fig. 3.37 (a) and (b) shows the nucleation of calcium phosphate crystals appeared at 3 days immersion in SBF. The growth is observed uniform all over the entire surface. Fig 3. 37 (c) to (e) show the surface morphology of PPVA sample immersed in SBF for 10 days. The spheroidal morphology of the hydroxyapatite crystals is apparent in all the images. At higher magnification, the primary layer of calcium phosphate coating is clearly visible on which the secondary spheroidal clusters are growing (fig. 3. 37 e).

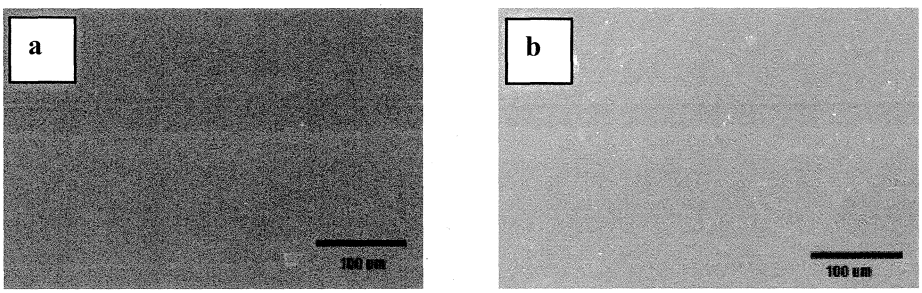

Figure 3-36 scanning electron micrographs of PVA (a) and phosphorylated PVA (b

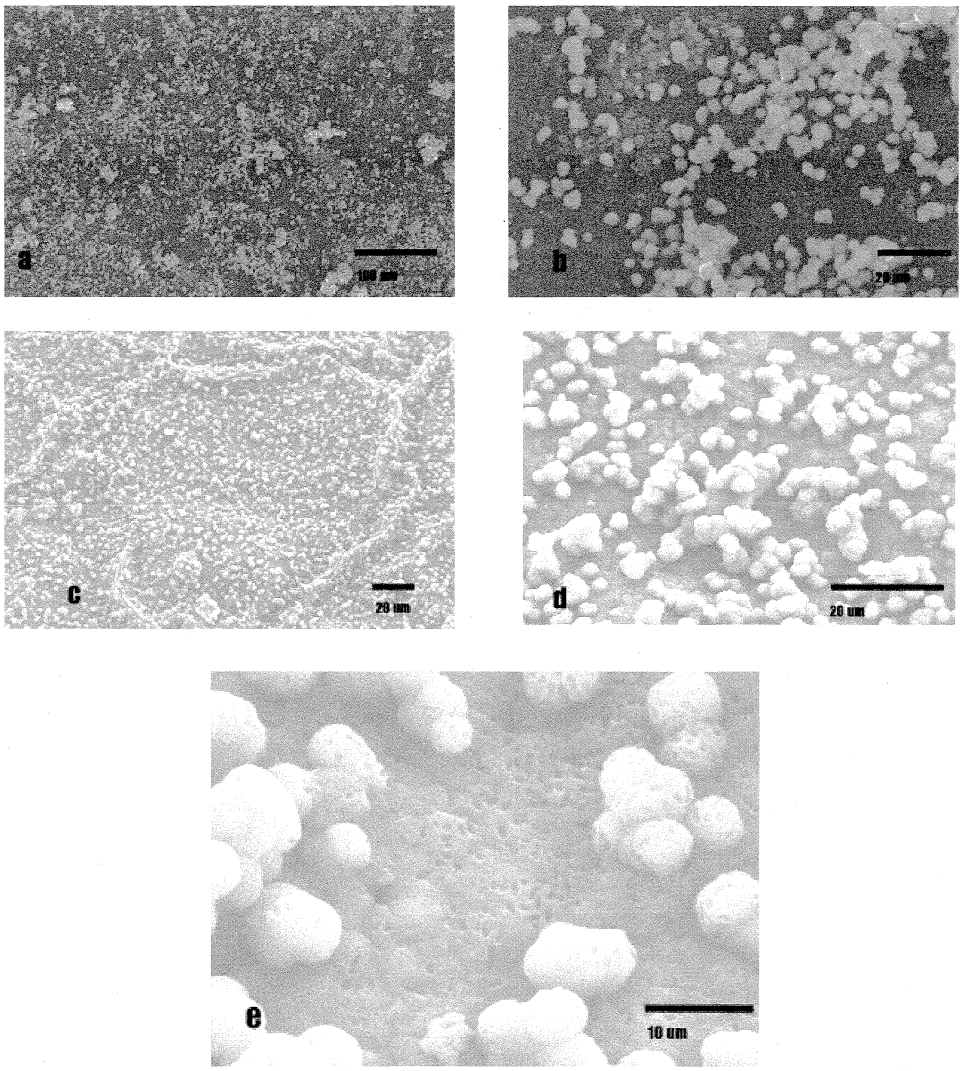

Figure 3-37 The SEM micrographs showing the morphology of calcium phosphate coating formed on phosphorylated PVA when immersed in SBF for 3 days (a and b) and10 days (c, d and e)

The EDS spectra of PVA and phosphorylated PVA are shown in figs.3.38 (a) and (b). The PVA shows only those peaks corresponding to C and O while PPVA shows an additional peak characteristic of phosphorous at 2.01eV. The figs. 3.39 (a) and (b) represent the EDS spectra correspond to the calcium phosphate coated areas observed under the SEM shown as fig. 3.37 (a) and (d) respectively i.e., the spectra corresponding to 3 and 10 days respectively. Both spectra show peaks corresponding to Oxygen, Calcium and phosphorous in addition to the peak of carbon due to the polymeric backbone. As the coating thickness increase, the carbon peak disappears. The calcium to phosphorous ratio is 1.6 for the 3 day immersed sample while the ratio increases to1.69 for the sample immersed in SBF for 10 days.

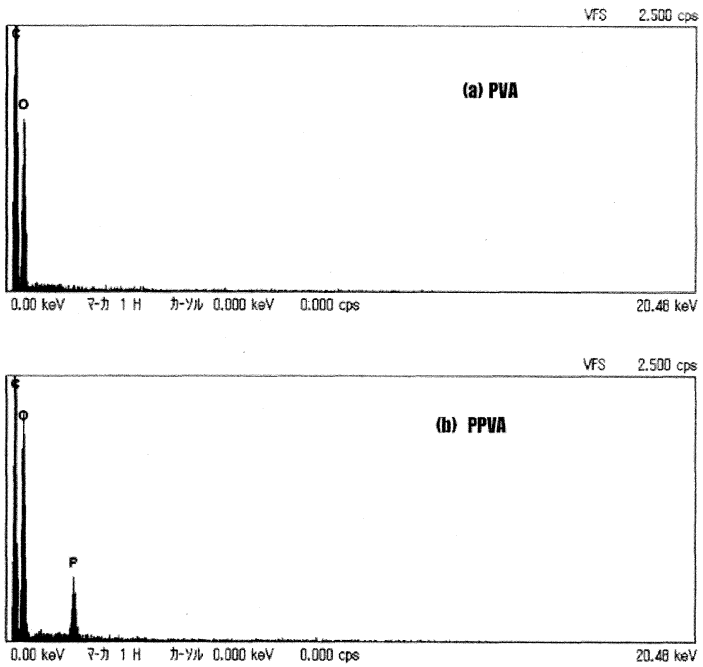

Figure 3-38 EDS spectra of PVA (a) and phosphorylated PVA (b)

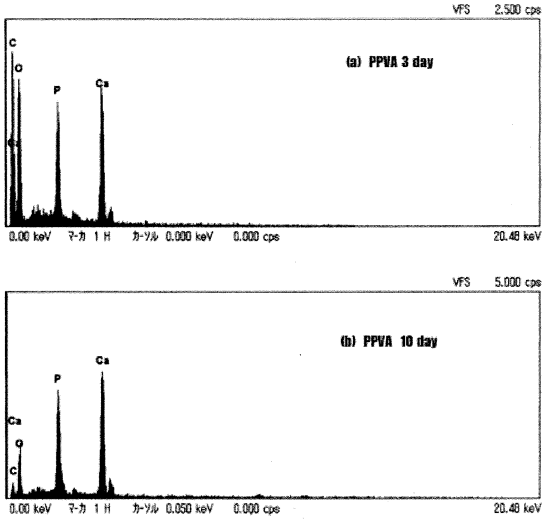

Figure 3-39 EDS spectra of calcium phosphate coating (a): 3 days (b): 10 days

The SEM images of PVA hollow tubes and the calcium phosphate coating formed on its surface upon SBF immersion is shown in fig. 3.40 (a) – (d).

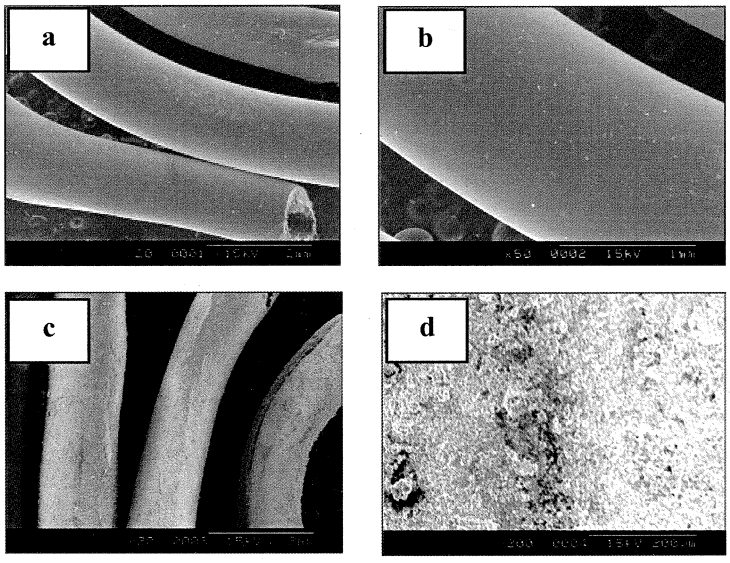

Figure 3-40 The SEM images of PVA hollow tubes (a), surface phosphorylated PVA (b) and the calcium phosphate coated PVA (c) and (d)

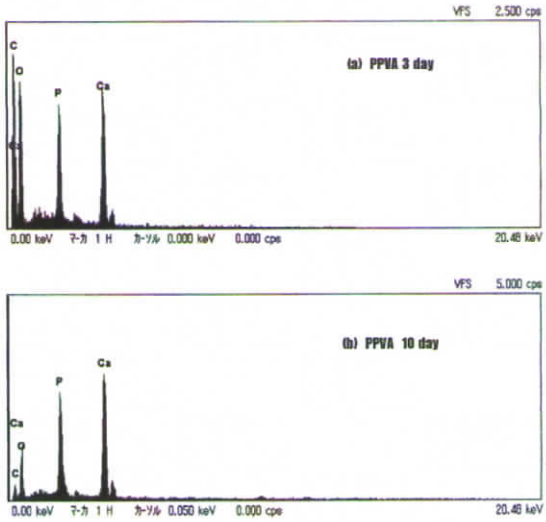

Figure 3-39 EDS spectra of calcium phosphate coating (a): 3 days (b): 10 days

The SEM images of PVA hollow tubes and the calcium phosphate coating formed on its surface upon SBF immersion is shown in fig. 3.40 (a) – (d).

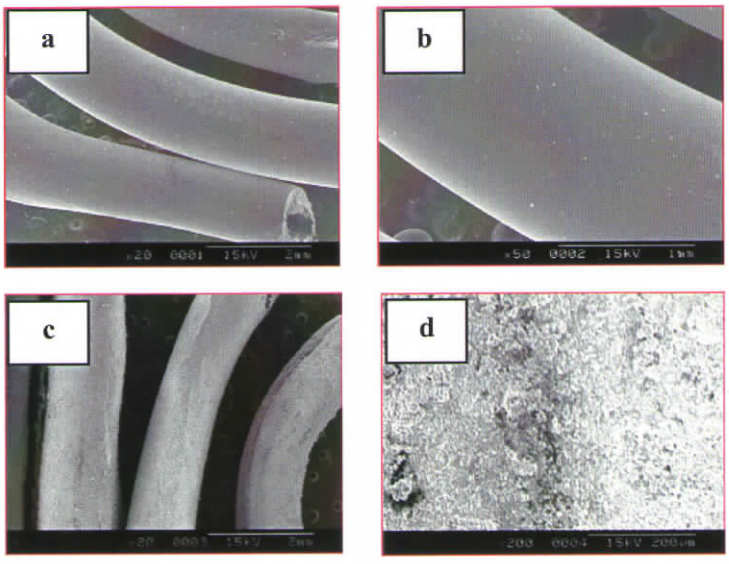

Figure 3-40 The SEM images of PVA hollow tubes (a), surface phosphorylated PVA (b) and the calcium phosphate coated PVA (c) and (d)

The FT-IR spectrum of calcium phosphate formed on the surface of phosphorylated PVA is given in fig. 3.41. The spectrum (fig. 3.41) shows peaks corresponding to inorganic phosphate group at 1019 and 583 cm^{-1}. The broad band 3455 cm^{-1} corresponds to the –OH group of hydroxyapatite.

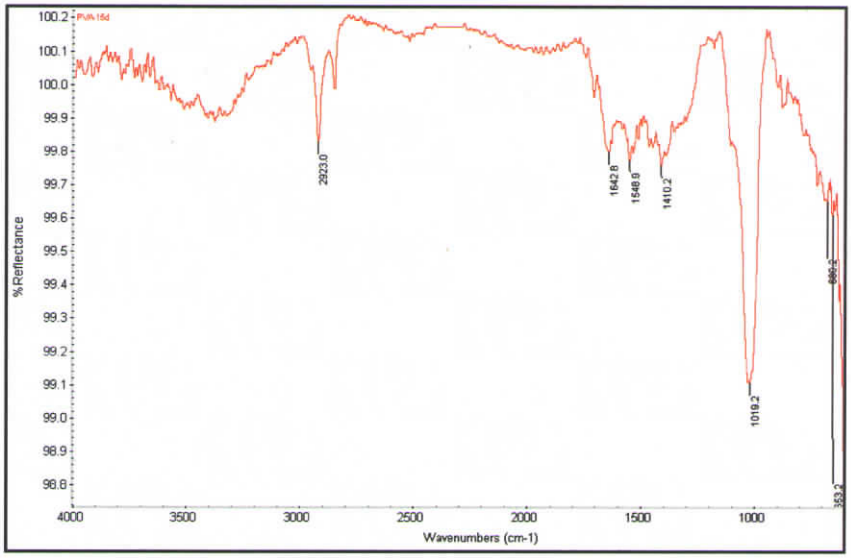

Figure 3-41 FT-IR spectrum of calcium phosphate coating on phosphorylated PVA

3.4.2 Ethylene vinyl acetate (EVA)

3.4.2.1 Assessment of phosphorylated EVA sheets

The FT-IR spectrum of EVA, surface hydrolyzed EVA and surface phosphorylated EVA are shown in fig.3.42. Ethylene vinyl acetate contains 28% vinyl acetate. In order to make EVA feasible for surface phosphorylation, surface hydrolysis is inevitable. The –OH group formed through surface hydrolysis is proportional to the ester group present in the copolymer. The surface phosphorylation of the hydrolysed EVA was performed at 70 ^{0}C for 90 minutes.

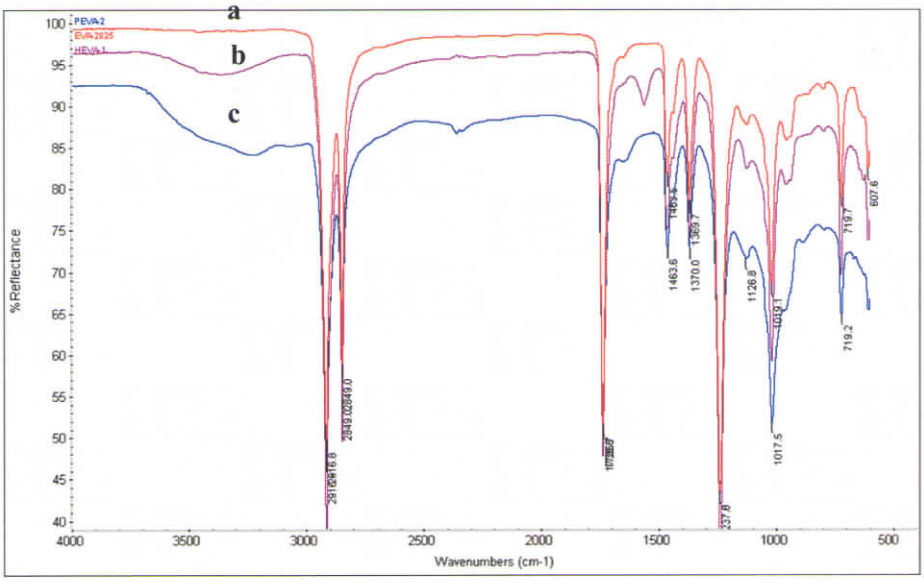

Figure 3-42 FT-IR spectrum of EVA (a), surface hydrolyzed EVA (b) and surface phosphorylated EVA (c)

3.4.2.2 Evaluation of biomimetic mineralization

The FT-IR spectrum of calcium phosphate formed on the surface of phosphorylated EVA is given in fig. 3.43 (a). The overlay spectrum of EVA and calcium phosphate coated EVA is shown in fig. 3.43 (b). The peaks corresponding to inorganic phosphate group could be viewed at 1073 and 555 cm^{-1} (fig. 3.43 a). The overlay spectrum of EVA and calcium phosphate coated EVA clearly indicates the reduction in the intensity of CH_2 and C=O groups (fig. 3.43 b).

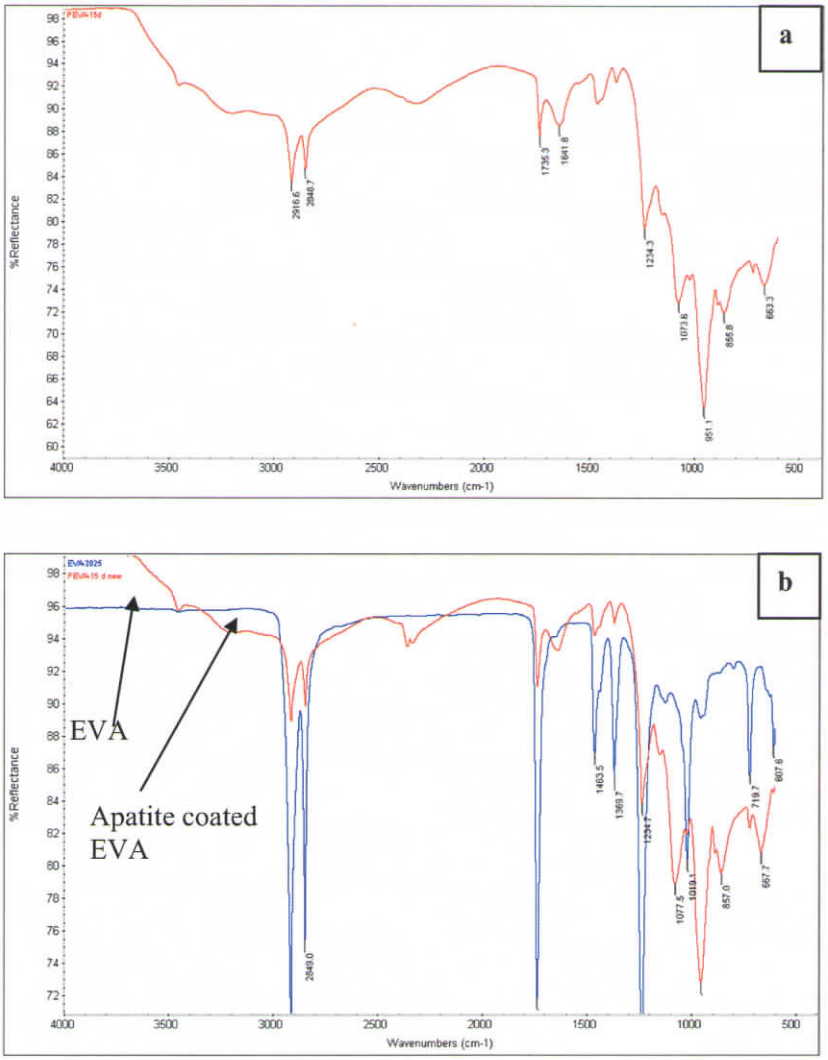

Figure 3-43 (a) FT-IR spectrum of calcium phosphate coated EVA (b) FT-IR spectra of EVA and calcium phosphate coated EVA

Fig.3. 44 (a) and (b) show the scanning electron micrographs of EVA and phosphorylated EVA respectively. The SEM images of calcium phosphate coating formed on phosphorylated EVA up on immersing in SBF are given in figs 3.45 (a) to (d). Fig. 3.45 (a) and (b) shows the calcium phosphate crystals nucleated at 3

days immersion in SBF. The growth is seen as homogeneous all through the surface. The surface morphology of PEVA sample immersed in SBF for 15 days is shown in fig 3. 45 (c) and (d). The distorted spheroid like morphology of the hydroxyapatite crystals is visible at higher magnification (fig. 3.45 (d)). Multiple layers of mineral growth is apparent in the images.

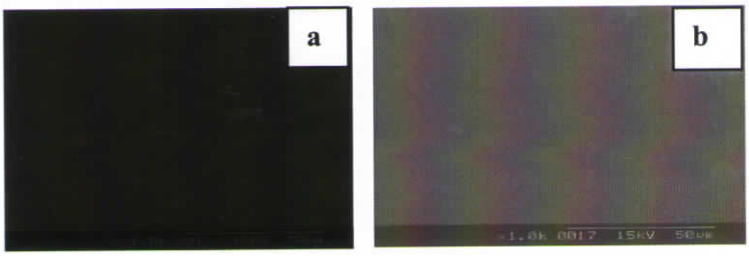

Figure 3-44 Scanning electron micrographs of EVA (a), phosphorylated EVA (b)

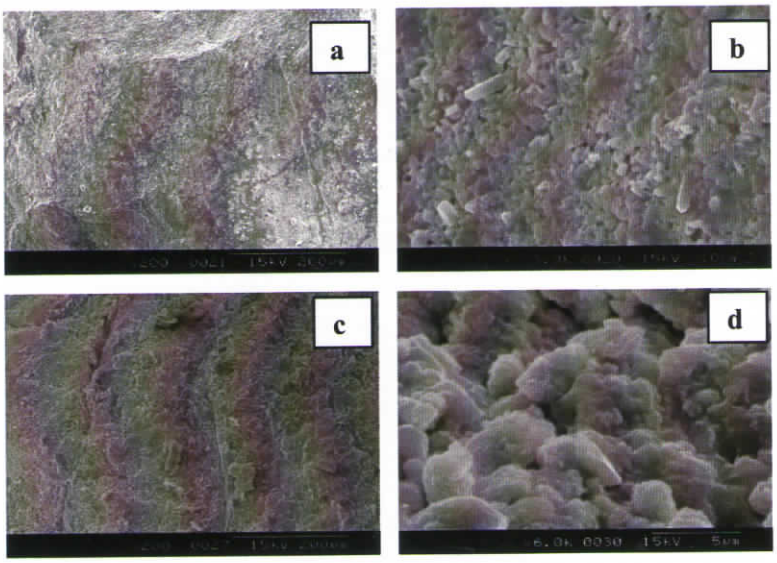

Figure 3-45 Nucleation and growth of the calcium phosphate crystals on phosphorylated EVA. (a) and (b): 3 days (c) and (d): 15 days

The EDS spectrum of phosphorylated EVA is shown in fig.3.46 (a). The figs. 3.46 (b) and (c) represent the EDS spectra of to the calcium phosphate coated EVA representing 3 and 15 days immersion in SBF respectively. Here also the calcium to phosphorous ratio increases with time.

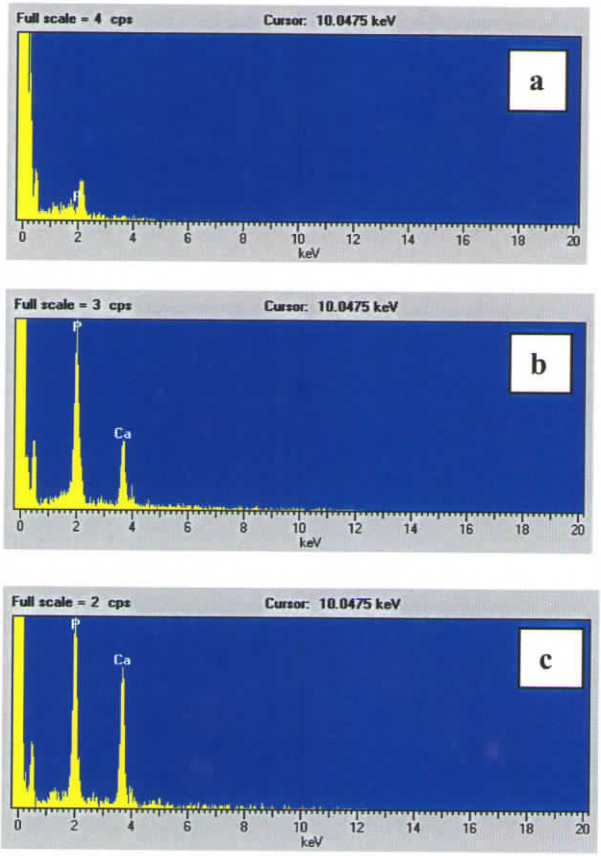

Figure 3-46 (a) The EDS spectra of phosphorylated EVA (b) EDS spectra of to the calcium phosphate coated EVA- 3 days (c) 15 days

days immersion in SBF. The growth is seen as homogeneous all through the surface. The surface morphology of PEVA sample immersed in SBF for 15 days is shown in fig 3. 45 (c) and (d). The distorted spheroid like morphology of the hydroxyapatite crystals is visible at higher magnification (fig. 3.45 (d)). Multiple layers of mineral growth is apparent in the images.

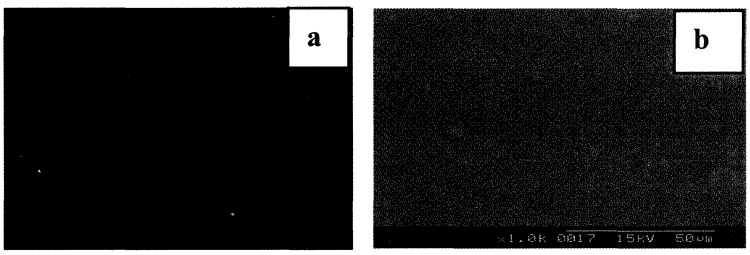

Figure 3-44 Scanning electron micrographs of EVA (a), phosphorylated EVA (b)

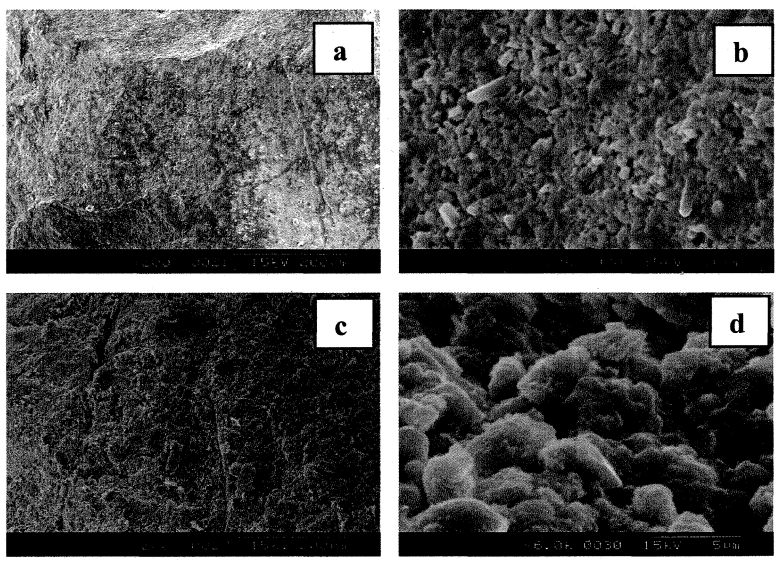

Figure 3-45 Nucleation and growth of the calcium phosphate crystals on phosphorylated EVA. (a) and (b): 3 days (c) and (d): 15 days

The EDS spectrum of phosphorylated EVA is shown in fig.3.46 (a). The figs. 3.46 (b) and (c) represent the EDS spectra of to the calcium phosphate coated EVA representing 3 and 15 days immersion in SBF respectively. Here also the calcium to phosphorous ratio increases with time.

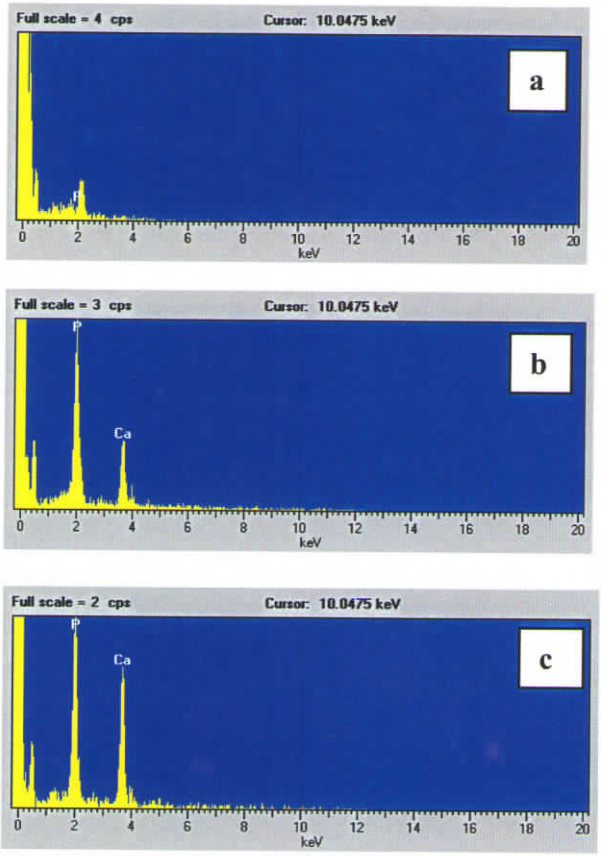

Figure 3-46 (a) The EDS spectra of phosphorylated EVA (b) EDS spectra of to the calcium phosphate coated EVA- 3 days (c) 15 days

3.4.3 Polyethylene terephthalate

3.4.3.1 Alkali hydrolysis of PET fabric

Surface hydrolysis is inevitable for obtaining the necessary –OH groups required for phosphorylation. The –OH group formed through surface hydrolysis is proportional to the ester group. The kinetics of hydrolysis as a measure of weight loss was studied by varying the concentration of alkali from 1% to 4% (sample representation given in table 3.2) and by varying the time of hydrolysis from 15 minutes to 60 minutes (sample representation given in table 3.3). The burst strength recorded for the samples at varying concentration of alkali, while keeping constant time for the surface hydrolysis (time of surface hydrolysis = 30 minutes) is given in table 3.4. Table 3.5 shows the burst strength of the samples measured when 2% alkali is used for hydrolysis at different time periods (15, 30. 45 and 60 minutes).

Table 3-2 Variation of Hydrolysis time (concentrtion of alkali kept constant)

Sample code	Time of treatment (minutes)
HS-000 (Control)	----
HS-010	15
HS-020	30
HS-030	45
HS-040	60

Table 3-3 Hydrolysis Vs concentration of alkali time (time kept constant)

Sample code	Concentration of alkali (%)
HS-000 (Control)	----
HS-010	1.0
HS-020	2.0
HS-030	3.0
HS-040	4.0

Table 3-4 Burst strength of samples at constant time of hydrolysis

Sample code	Time of treatment (minutes)	% wt-reduction (mean)	Max load at Break (N) (mean)	S.D (max. load at break)
HS-000 (control)	----	----	303	0.010
HS-010	30	0.84	273	0.013
HS-020	30	1.64	288	0.019
HS-030	30	1.71	275	0.008
HS-040	30	2.84	280	0.004

Table 3-5 Burst strength of samples at constant concentration of alkali

Sample code	Time of treatment (minutes)	% wt-reduction (mean)	Max load at Break (N) (mean)	S.D (max. load at break)
HS-000 (control)	----	----	303	0.010
HS-020 (a)	15	0.45	306	0.005
HS-020 (b)	30	1.64	288	0.19
HS-020 (c)	45	1.49	277	0.012
HS-020 (d)	60	5.03	235	0.04

Table 3.4 shows that, when time of hydrolysis kept constant, the weight reduction increases linearly with increase in alkali concentration. It is to be noted that even though the weight loss increases, the maximum load at break does not vary much compared to the control. Table 3.5 shows that even at constant alkali concentration, the weight reduction drastically increases with time. Further, the breaking load also decreases significantly with increase in hydrolysis time. Hence it becomes clear that the time of hydrolysis is more important than the concentration of alkai in determining the breaking load for the specimen. The surface hydrolysis was therefore performed for 15 minutes, keeping the alkali concentration 2%.

3.4.3.2 Characterization of the phosphorylated PET fabric

The FT-IR spectrum of PET, surface hydrolyzed PET and surface phosphorylated PET are shown in fig.3.47. The surface phosphorylation of the hydrolysed PET was performed at 80 ^{0}C for 90 minutes. It could be seen that there is no apparent difference between the spectra. It could be assumed due to the very

low percentage of hydrolysis that is occurring as the hydrolysis is performed for a minimum time period of 15 minutes. This was in order to prevent reduction in mechanical properties.

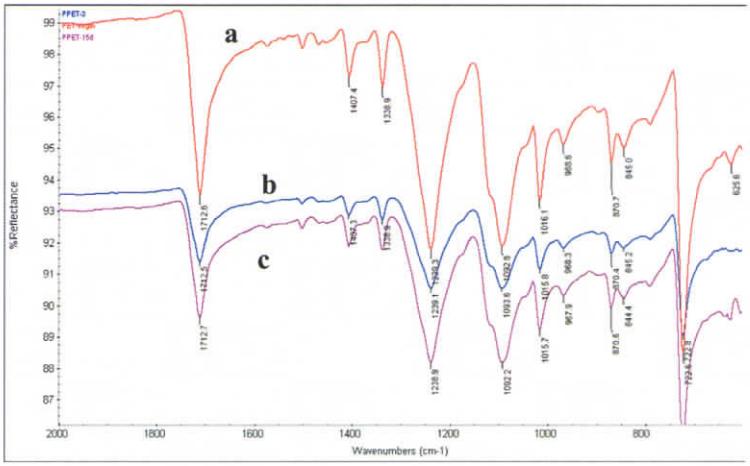

Figure 3-47 FT-IR spectrum of PET, surface hydrolyzed PET and surface phosphorylated PET

3.4.3.3 Evaluation of biomimetic mineralization

Figs.3. 48 (a) and (b) show the scanning electron micrographs of PET control sample (surface phosphorylated PET immersed in SBF for 10 days) and calcium phosphate coated PET upon immersion in SBF for 10 days. Fig. 3.48 (b) shows a homogeneous layer of calcium phosphate coating on PET surface. The figs. 3.48 (c) show the EDS spectra of the calcium phosphate coated PET. The PET substrates were initially placed on granular particles of a $CaO\text{-}SiO_2$-based glass in simulated body fluid (SBF) to form apatite nuclei on their surfaces (first treatment). It was followed by soaking in modified SBFs, the ion concentrations of which were changed to give a variation in ionic activity product of apatite (IP), in order to make the apatite nuclei grow (second treatment). They found that the apatite formed in 1.00 SBF showed a Ca/P ratio of 1.51 and lattice constants *a* of 9.432 Å and *c* of 6.870 Å. The Ca/P ratio and lattice constant *c* were smaller and

the lattice constant '*a*' was larger than those of the bone apatite; its Ca/P ratio and its lattice constants *a* and *c*, were 1.65, 9.419 Å, and 6.88 Å, respectively. According to them this is attributed to the lower content (2.64 wt%) of the CO_3^{2-} ion substituting for the PO_4^{3-} ion sites of the apatite compared to that of the bone apatite (5.80 wt%). The lower content of the CO_3^{2-} ion in the apatite might be caused by the lower concentration of HCO_3^- ion in 1.00 SBF compared to that in human blood plasma.

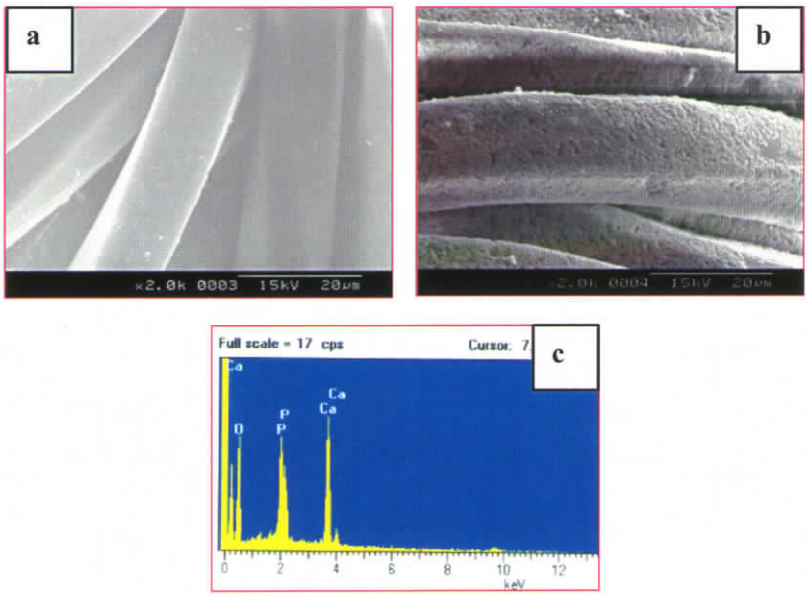

Figure 3-48 SEM image of (a) PET (control sample) (b) SEM image of calcium phosphate coated PET for 10 days (c) EDS spectra of calcium phosphate coated PET

The results show that the surface phosphorylation method used for poly(HEMA-co-MMA) could be extended to PVA, but altering the necessary conditions such as time and temperature, according to the fundamental properties of the polymer. In the case of EVA and PET, surface hydrolysis was essential for the availability of –OH groups required for phosphorylation. However, the other conditions for surface phosphorylation were almost same.

3.4.4 Summary

The proposed method of surface phosphorylation was extended to other biocompatible polymers with inherent hydroxyl (-OH) group like poly(vinyl alcohol) and by modifying other polymers like EVA and PET having appropriate functional groups to impart free –OH group. The surface phosphorylation of PVA was performed as such while, for EVA and PET, controlled surface hydrolysis was carried out prior to phosphorylation in order to acquire the necessary –OH groups for phosphorylation reaction. The surface phosphorylated PVA, surface phosphorylated EVA and surface phosphorylated PET induces in vitro nucleation of calcium phosphate under accelerated physiological condition.

CHAPTER 3.5

IN VITRO CYTOCOMPATIBILITY EVALUATION

3.5 *IN VITRO* CYTOCOMPATIBILITY EVALUATION OF PHOSPHORYLATED POLY(HEMA-CO-MMA)

The *in vitro* cytocompatibility conventionally performed using L929 mouse fibroblast cells. In the presence study, the surface phosphorylated poly (HEMA-Co-MMA) is proposed for bone tissue regeneration. Hence cytocompatibility evaluation HOS cell line would be more appropriate form the functional biomaterial developed in the study.

The in vitro cell viability was determined by MTT assay. In vitro cell adhesion study was monitored using SEM. The von kossa staining method was used for understanding *in vitro* biomineralization of HOS cells.

The secretion of bone specific markers such as human osteocalcin and alkaline phosphatase was quantitatively estimated to assess the *in vitro* functional activity of HOS cells.

In vitro conditions do not replicate *in vivo* situations, due to the involvement of a large number of factors. It is, however, possible to determine the basic cell reactions for a single cell type *in vitro*. While this would not represent fully the cell reactions *in vivo* it could give an idea of how different cell types might respond. As a part of a cytocompatibility repertoire of tests, these methods could be used to reduce the number of *in vivo* experiments.

3.5.1 Cell adhesion

(a) Light microscopic observations

The light microscopic images of HOS cells in contact with PH1, PPH1 and calcium phosphate coated PH1 (CaPPH1) after 24h are shown in fig. 3.49 (a), (b) and (c) respectively. The images show that the cell density is more or less same around all the three samples and the cells retain their typical morphology and hence the materials do not show any cytotoxic response after 24h.

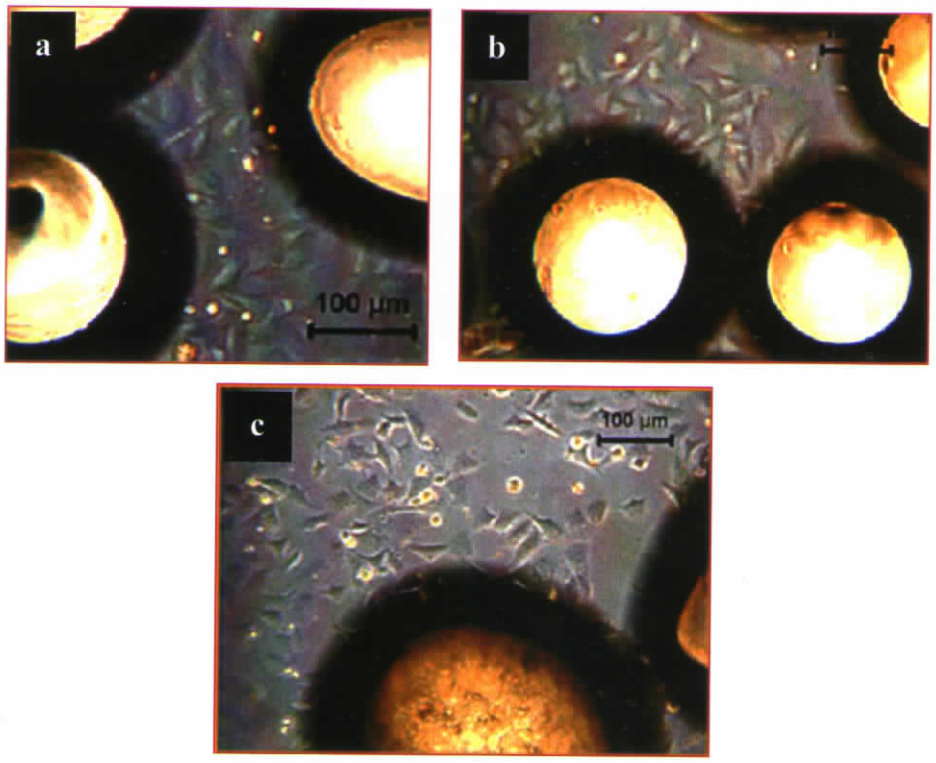

Figure 3-49 Light microscopic images of HOS cells in contact with PH1, PPH1 and CaPH1 after 24h (a): PH1, (b):PPH1, (c)CaPH1

(b) MTT assay

The results of MTT assay after 7d and 14 d are shown in Fig. 3.50. The number of metabolically active cells adhered on the samples after 14days is significantly higher than the cells at 7days as seen from the figure. The number of metabolically active cells on PPH1 and CaPH1 after 14d were considerably more compared to the number of viable cells on PH1. However, there was a slight increase in the number of active cells adhered on CaPH1 compared toPPH1 at both time periods. The Student's *t*-test was performed and it was found that the result obtained was statistically significant ($P<0.0005$). From the figure, it is evident that PPH1 and CaPH1 have a greater potential for favouring cell attachment and cell adhesion than PH1.

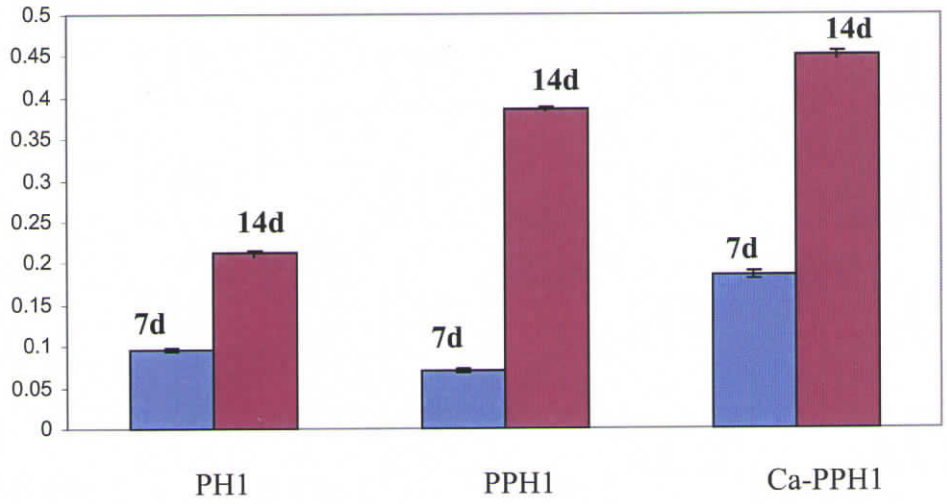

Figure 3-50 MTT assay of HOS cells in contact with PH1, PPH1 and CaPH1 after 7 and 14 days

From the results, it could be viewed that surface phosphorylation and apatite coating favour cell adhesion and viability. Even though the unmodified PH1 also support cell attachment, the degree of the same is lower than that of the functionalized and apatite coated samples. This could be attributed mainly to three important aspects. Firstly, the surface topography of the surface phosphorylated sample as well as calcium phosphate coated PH1 are different from that of

unmodified PH1 as revealed by the atomic force microscopic images (figs. 3-14, 3-30, 3-31). The surface phsophorylation offers a microtextured surface to PPH1. Similarly the apatite coating also changes surface topography of PH1. Moreover, the hydrophilicity of the three samples are different, as observed from the water contact angle values, swelling data and the atomic force values (shown in table 3-1). The third aspect is the surface energy of the three samples. The surface bound phosphate group lowers the surface energy and hence induces nucleation of calcium phosphate under physiological conditions. Moreover, the phosphate group imparts a negative charge to the surface. Calcium phosphate coating also acquires a negative charge on the surface under aqueous environment [41].

There are several reports on cell responses to topography [161,162]. The ability to control cell adhesion and response is desirable in cell engineering and is anticipated to have an important role in the development of next-generation materials [161]. Nanoscale topography is of great importance when considering how cells respond to their environment, and certainly appears to alter significantly the morphology of endothelial cells, epithelial cells, macrophages, osteoblasts and fibroblasts (Dalby *et al.*, Andersson *et al.*) [161, 162, 163, 164]. Several studies have identified that surface roughness has a major contribution to the development of cell-material interface and proved that rough surface promotes osteoblast cell attachment than a smooth surface [165-168].

The surface chemistry and thus surface energy of materials have a significant effect on cell spreading and migration [169, 170]. Harris *et al* found that surface with lower surface energy promoted greater cell growth [170].

From the above discussion it could be seen that surface phosphoryation and apatite coating increases the cell adhesion and growth due to their unique characteristics such as greater surface roughness, greater hydrophilicity and lower surface energy.

3.5.2 Cell adhesion

The ESEM images of HOS cells adhered on PH1, PPH1 and CaPH1 after 48h is shown in fig.3.52 (a), (b) and (c) respectively.

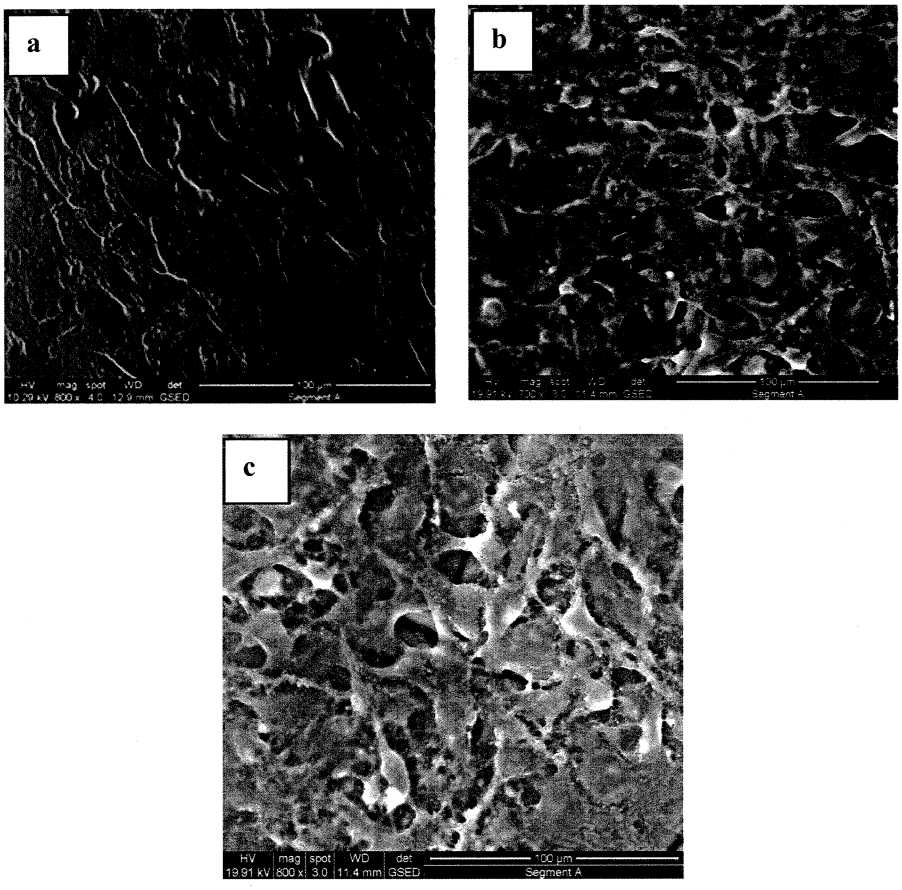

Figure 3-51 ESEM images of HOS cells adhered on PH1, PPH1 and CaPH1 after 48h (a): Unmodified PH1, (b): Surface phosphorylated PH1, (c) Apatite coated PH1

The SEM images of HOS cells adhered on PH1, PPH1 and CaPH1 after 7 days and 14 days are shown in figs.3.53 and 3.54 respectively. Fig. 3.55 shows the SEM image of the HOS cells adhered on PH1, PPH1 and apatite coated microspheres after 7 days.

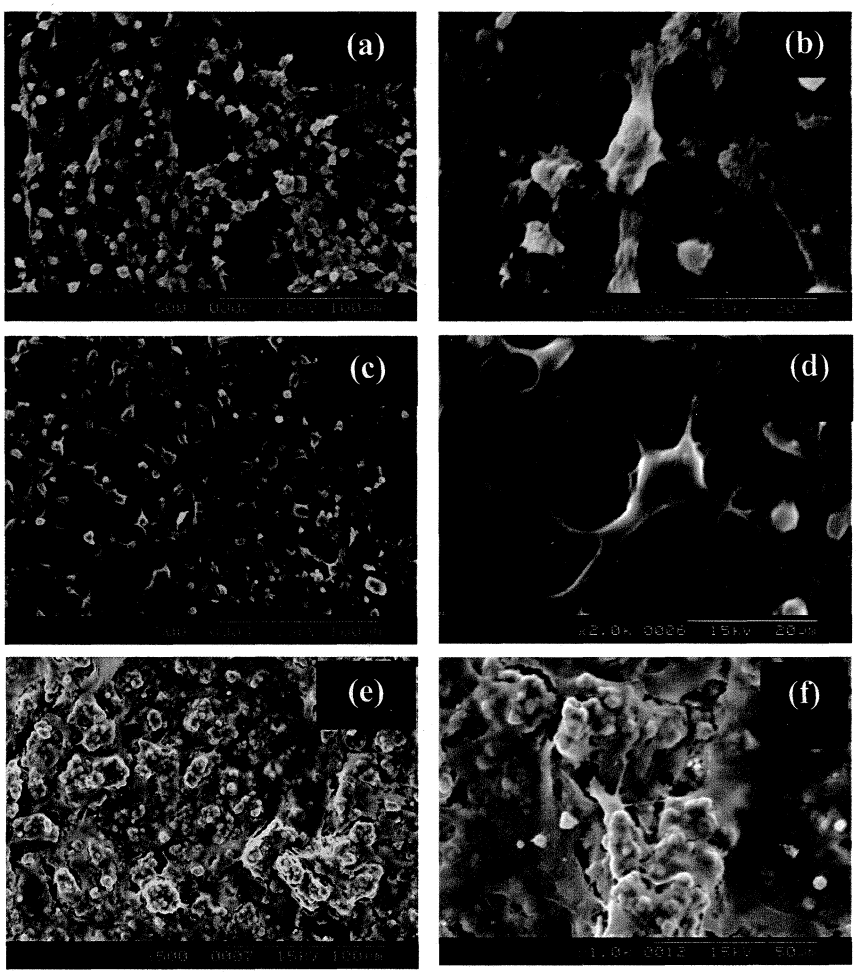

Figure 3-52 SEM images of HOS cells adhered on PH1, PPH1 and CaPH1 after 7 days (a), and (b): PH1(c) and (d): PPH1 (e) and (f): CaPH1

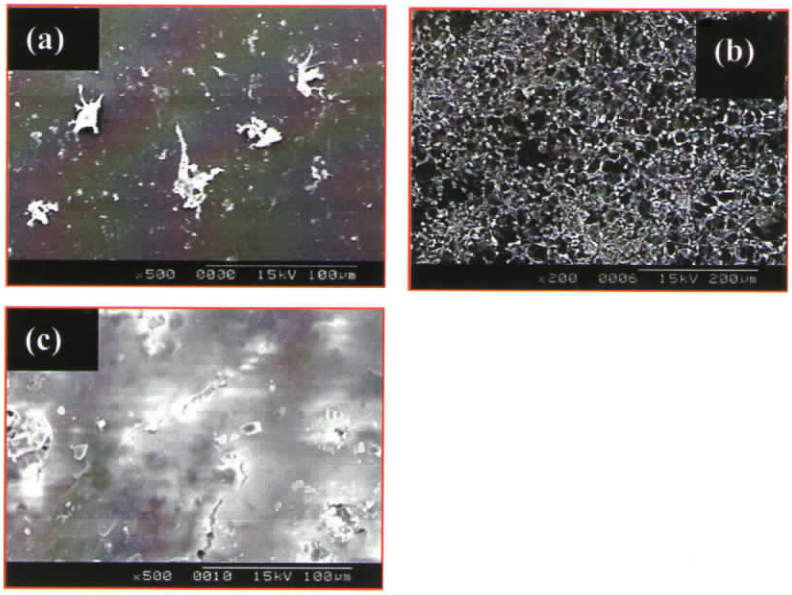

Figure 3-53 SEM images of HOS cells adhered on PH1, PPH1 and CaPH1 - 14 days (a): PH1 (b): PPH1 (c): CaPH1

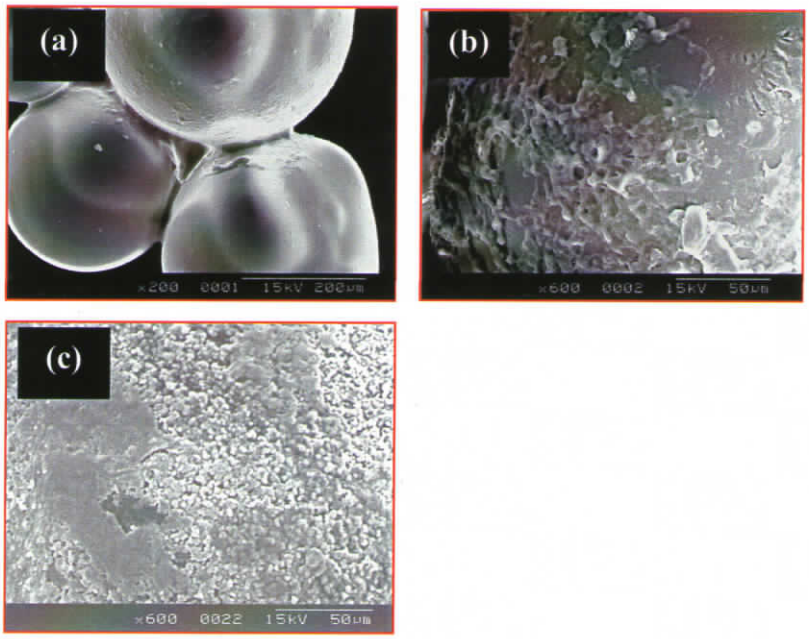

Figure 3-54 SEM image of the HOS cells adhered on PH1 (a), PPH1 (b) and CaPH1 (c) after 7 days

It is apparent from the figures that the cells attached and spread over the surfaces of all the three samples. However, the cell density seemed to be slightly greater on PPH1 and CaPH1, as multiple layers of cells are visible in the ESEM images. The cells exhibited flat morphology with long and short filopodia or lamellipodia. Even though the cells showed minor differences to their reactions to each of the different substrates, their morphology was more or less similar. As mentioned in the previous section, the cell-spreading pattern depends on surface roughness, surface energy and hydrophilicity of the substrate.

Smooth surface found to produce round or flat cells that are randomly oriented while grooved surfaces found to stimulate linearly oriented cellular morphology (known as contact guidance) [171]. The presence of an 'ordering' topography will stimulate bone cell outgrowth in a direction parallel to the surface topography with little correlation to the magnitude of the topographic features [171]. The focal contacts are individual mechanosensors whose elongation reveals the local balance between the force generated by the cell and ECM rigidity [172,173].

Dalby *et al* performed in vitro response of osteoblast-like cells on PMMA-HA composites [174]. In their study, PMMA discs having varying HAP volume percentage were examined using primary human osteoblast-like cells (HOBs). They could observe a synergy between increasing focal contact formation, cytoskeletal organisation, cell proliferation and expression of phenotype with increasing HA volume. Preferential anchorage of HOBs to HA rather than PMMA was a prominent observation. Thus it becomes clear that the cells have preferential orientation and growth even when a composite substrate is used. However, surface morphology does not significantly influence the production of collageneous or non-collageneous proteins [171].

The results of cell adhesion at three different time periods shows that the all the three samples supported adhesion and growth of cells while PPH_1 retained better morphology of the cells for a longer time (14 days) compared to PH_1. The cells on CaPH1 formed as a cell layer, which covered the apatite clusters within two weeks.

3.5.3 *In vitro* mineralization of HOS cells by Von Kossa's staining method

Von kossa staining method confirmed calcium deposition and the initiation of in vitro mineralization. Fig. 3.55 (a) and (b) are the light microscopic images of typical biomineralized regions of PH1and PPH1 in presence of HOS cells cultured for one week observed by von kossa staining method. The dark regions visible in the figures are due to calcium phosphate phases. It is clear from the figures that accelerated biomineralization has occurred on PPH1 (fig. 3.55 (b)) in presence of HOS cells, while such areas are not predominant in PH1 (fig. 3.55 (a)).

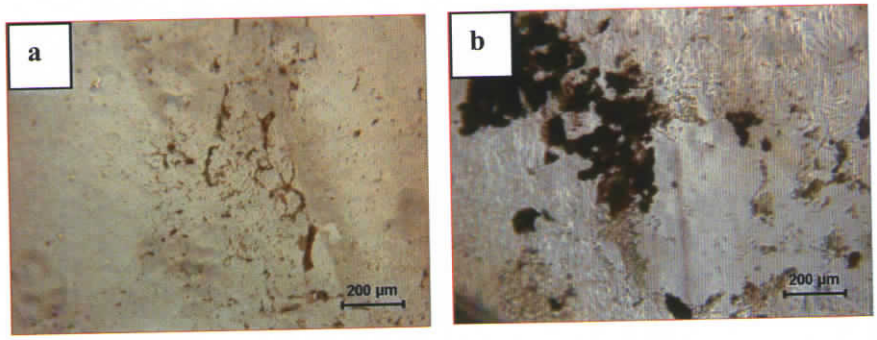

Figure 3-55 Biomineralized regions of PH1 (a) and PPH1 (b) in presence HOS cells cultured for one week- Von kossa staining.

3.5.4 Estimation of Human osteocalcin

The osteocalcin released by the HOS cells in the medium on culturing with PH1, PPH1 and CaPH1 at 7, 14 and 21 days are given in fig. 3.56. The osteocalcin expression of the cells cultured on culture plate was taken as control.

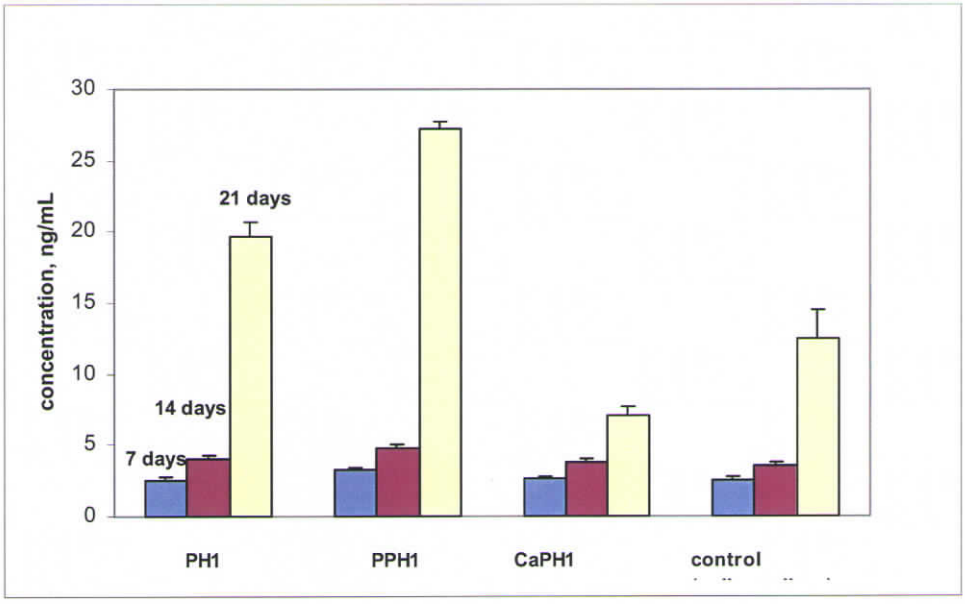

Figure 3-56 Osteocalcin expression of HOS cells on PH1, PPH1 and CaPH1

A steady increase in osteocalcin concentration was observed with time in all cases, and reached a maximum value at day 21. The trend is similar for all the samples as well as for control. The osteocalcin expression observed was in accordance with the specific activity profile of osteocalcin reported in literature [175]. The highest value was noted for PPH1. The figure also shows that PH1 and surface phosphorylated PH1 promotes cellular activity and accelerates osteocalcin release compared to control or calcium phosphate coated sample.

Osteocalcin is associated with extracellular matrix mineralization [48]. It is produced by mature osteoblasts during mineralization and found in fully developed mineralized matrices. The decrease in osteocalcin expression on apatite coated sample could be due to the increased local concentration of calcium. It is known that a calcium-rich environment stimulates calcium entry and increases intra-cellular calcium storage, whereas increase pH can promote calcium release from the intracellular pools in osteoblasts [176, 177].

3.5.5 Alkaline phosphatase (ALP) activity

The ALP activity of the HOS cells upon culturing with PH1, PPH1 and CaPH1 at 7, 14 and 21 days are given in fig. 3.57. The activity of the cells cultured on culture plate was plotted as the control.

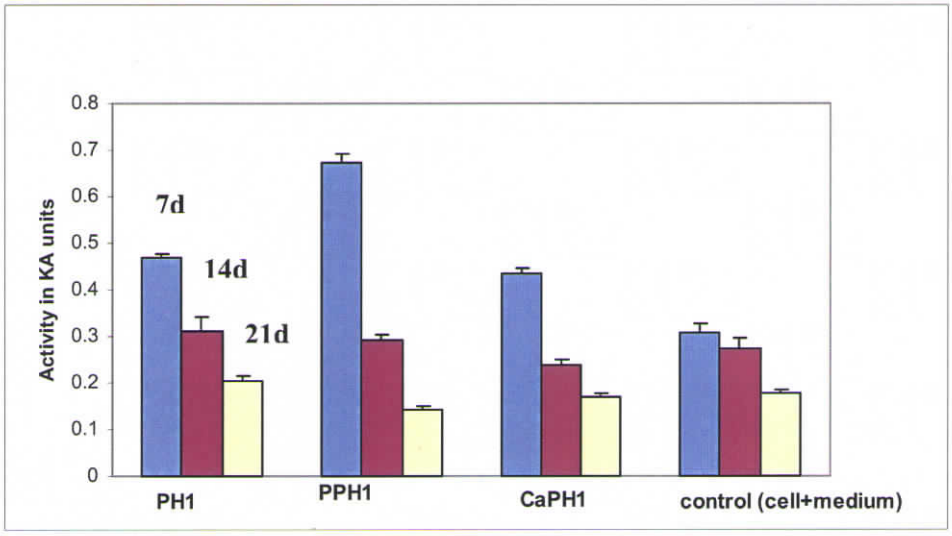

Figure 3-57 The ALP activity of the HOS cells on PH1, PPH1 and CaPH1 at 7, 14 and 21 days

The figure shows that the activity decreases with time with a maximum value observed at 7 days and then decreases. The trend is same in all cases. The highest activity is observed for PPH1. Alkaline phosphatase has been reported as

an early marker of osteoblastic differentiation [178]. It is evident from the figure that surface phosphorylation accelerates osteoblast differentiation and mineralization *in vitro*. However, the activity is found to be lower for apatite coated PH1. This could be attributed to the rough surface as well as the high calcium concentration of the sample. Even though rough surface promotes cellular attachment, a rough surface is reported to result in down regulation of ALP expression by osteoblast like and human bone cells [179,180]. CaPH1 has a greater surface roughness due to apatite coating as seen from AFM image. Moreover, increase in local calcium concentration with an elevated pH and the presence of apatite crystals accelerates matrix mineralization [166]. Hence the cells might have responded at a very early stage and ALP activity must have shown at its peak in the beginning stage itself. Cowles *et al* reported that the ALP activity on HAP/soluble calcium phosphate composite was obtained at 3days of incubation and the activity decreased on day 7 [178].

ALP activity is one of the representative markers of the osteoblast phenotype. It is generally accepted that increased specific activity of ALP in a population of bone cells reflects a shift to a more differentiated state [168]. Furthermore, ALP appears to have a crucial role in the initiation of matrix mineralization as the expression of this enzyme is down regulated after mineralization starts [181,182, 183].

Zhu *et al* performed ALP activity assessment and mineralization assay of phosphorylated chitosan. They found that water-soluble phosphorylated chitosan has excellent cytocompatibility compared to the chitosan without phosphorylation. Phosphorylated chitosan concentrations as high as 2% had a significant influence on cytocompatibility and osteoinduction [184].

3.5.6 Summary

The light microscopic images of HOS cells in contact with PH1, PPH1 and CaPH1 retained their normal cellular morphology after 24h which ensured that the test material are not cytotoxic in nature. The MTT assay performed for the quantitative estimation of metabolically active cells proved that the number of metabolically active cells adhered on PPH1 and CaPH1 after 14d was considerably more compared to the number of viable cells on PH1. Further, the number of active cells adhered on CaPH1 was a slightly more compared toPPH1 at both time periods. It is apparent from the SEM images that the cells attached and spread over the surfaces of all the three samples. However, the cell density seemed to be slightly greater on PPH1 and CaPH1, as multiple layers of cells are visible in the ESEM images after 48h. The cells exhibited flat morphology with long and short filopodia or lamellipodia. Even though the cells showed minor differences to their reactions to each of the different substrates, their morphology was more or less similar. The difference in cell-spreading pattern is attributed to the variation in surface roughness, surface energy and hydrophilicity of the substrate. Von kossa staining method confirmed calcium deposition and the initiation of in vitro mineralization. It is clear from the images that accelerated biomineralization has occurred on PPH1 in presence of HOS cells, while such areas were not predominant in PH1.

A steady increase in osteocalcin concentration was observed with time for PH1, PPH1 and CaPH1, and reached a maximum value at day 21. The trend was similar for all the samples as well as for control. The highest value was noted for PPH1. The *results* also showed that PH1 and surface phosphorylated PH1 promotes cellular activity and accelerates osteocalcin release compared to control or calcium phosphate coated sample. The alkaline phosphatase activity of the samples decreased with time with a maximum value observed at 7 days and then decreased. The trend was same in all cases. The highest activity was observed for PPH1.

CHAPTER 3.6

IN VIVO EVALUATION

3.6 *IN VIVO* EVALUATION

This section solely concentrates on the biological evaluation of phosphorylated poly (HEMA-co-MMA), represented as 'PPH_1' and poly (HEMA-co-MMA) coated with calcium phosphate for 15 days, represented as 'PPH_1 –15d'. The *in vivo* evaluation is divided into two parts. The initial part comprises the toxicological evaluation and the final part is the short-term bone implantation study.

3.6.1 Toxicological Evaluation

The hemolytic property of the material was evaluated by 'standard practice for assessment of hemolytic properties of materials as per ASTM F 756: 2000'. The intracutaneous (intradermal) reactivity assessment was performed as per ISO 10993: 2002 (E)-Biological evaluation of medical devices- part 10: test for irritation and delayed type hypersensitivity and additional tests: *clause B.2: Intracutaneous(intradermal) reactivity test.* The acute systemic toxicity was evaluated as per ISO 10993-11: 1993 (E) Test for systemic toxicity: Acute systemic toxicity: *clause 6.5.4 Acute intravenous application and clause 6.5.5 Acute intraperitoneal application.* The maximization test for delayed hypersensititvity was evaluated by ISO 10993-10: 2002 (E)-Biological evaluation of medical devices: part 10, Tests for irritation and delayed type hypersensitivity *clause 7.4: Maximization test for delayed hypersensitivity.*

3.6.1.1 Hemolytic properties of the material (ASTM F-756-2000)

The hemolytic property of the material was evaluated by 'standard practice for assessment of hemolytic properties of materials as per ASTM F 756: 2000'. As per the results, both materials were found to be non-hemolytic in nature.

3.6.1.2 Acute systemic toxicity test (ISO 10993 –11; 1993 (E) Clause 6.5.4 and 6.5.5)

The acute systemic toxicity was evaluated as per ISO 10993-11: 1993 (E) Test for systemic toxicity: Acute systemic toxicity: *clause 6.5.4 Acute intravenous application and clause 6.5.5 Acute intraperitoneal application.*

The physiological saline extract as well as the cotton seed extract of test materials injected intravenously in the animals did not show any abnormalities or loss in body weight during the observation period and suggest that the extract of the materials meet the requirements for acute intravenous and intraperitoneal applications

3.6.1.3 Intracutaneous Reactivity Test (ISO 10993 –10; 2002 E)

The intracutaneous (intradermal) reactivity assessment was performed as per ISO 10993: 2002 (E)-Biological evaluation of medical devices- part 10: test for irritation and delayed type hypersensitivity and additional tests: *clause B.2: Intracutaneous(intradermal) reactivity test.*

The results indicated that the test materials did not produce any irritation following intradermal injection of physiological saline and cotton seed oil extract of the test material. Hence the test materials meet the requirements for the intracutaneous reactivity test.

3.6.1.4 Maximization test for delayed hypersensitivity (ISO 10993-10:2002 E)

The maximization test for delayed hypersensititvity was evaluated by ISO 10993-10: 2002 (E)-Biological evaluation of medical devices: part 10, Tests for

irritation and delayed type hypersensitivity *clause 7.4: Maximization test for delayed hypersensitivity.*

The results indicated that none of the animals in the test materials showed any adverse skin reaction during the induction or challenge period. The extract of the test material induced a numerical grading of '0' for erythrema and oedema. Hence the physiological saline extract of the material meets the requirements for the test.

3.6.2 Implantation in bone ISO 10993 – 6; 1994 E

The efficacy of 'PPH_1' and 'PPH_1 –15d' towards osteointegration and bone regeneration under *in vivo* environment was evaluated by short-term bone implantation in rabbits as per ISO 10993-6: 1994(E): Test for local effects after implantation, *clause 6.0: Test method for implantation in bone.* The control material used was the clinically used 'CMW1' poly(methyl methacrylate) radiopaque bone cement (DePuy, Johnson and Johnson).

All animals survived throughout the experiment. Gross examination of the implant sites did not show infection or any other gross abnormality. The radiological view of the implant sites of PPH1 and its control after 3 months is shown in fig. 3.58. The defects appeared closed as the control samples are radiopaque. The test materials are not radiopaque and hence they appeared as uncovered holes.

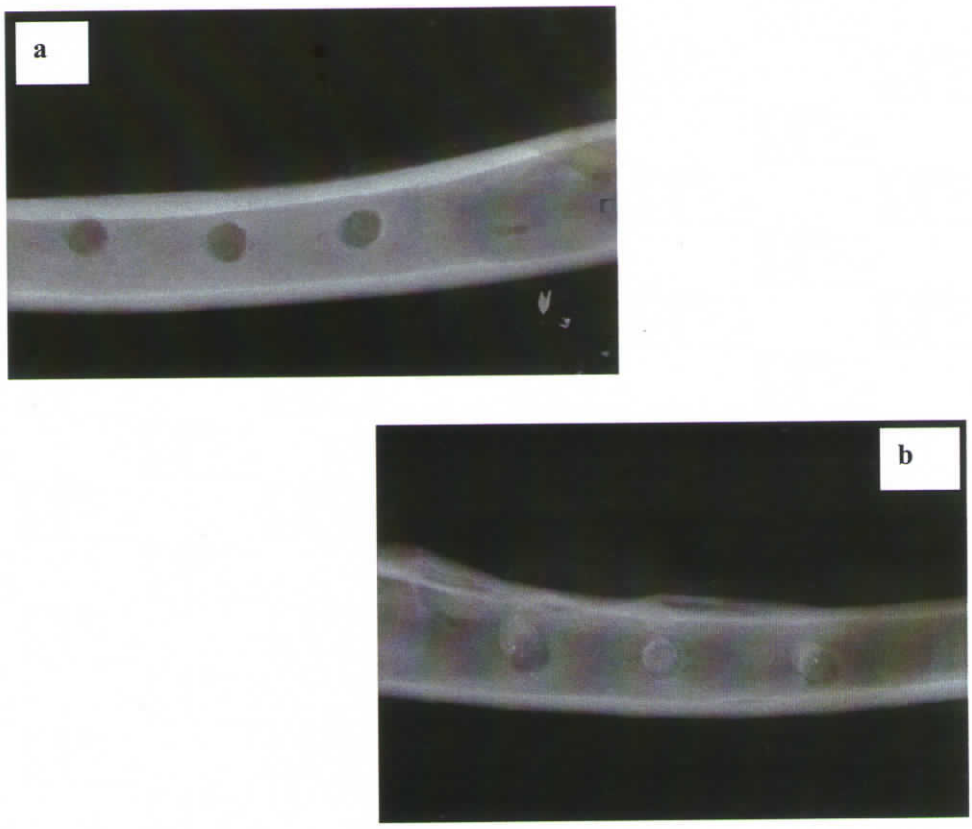

Figure 3-58 Radiological view of implant sites after 3 months (a) PPH1 (b) control

Histopathological results showed that the control implants were absent in all sections examined. Defects were noted in the cortical bone, opening into medullary cavity. Defects were an empty space in all sections. The empty space is due to dissolution of the control samples during the embedding process as reported by (CMW1 PMMA) during the embedding process in PMMA for obtaining undecalcified sections [185]. In order to reconfirm this observation a control experiment was conducted. The control samples and the test samples were subjected to all the processing steps that is performed for the implant sample and finally embedded. The samples with the same dimension, inserted in silicone tubes

were selected for the study. It was observed that the control samples started dissolving in 80% alcohol itself and completely dissolved in absolute alcohol.

3.6.2.1 Control

In the case of control samples at one-week post implantation, inflammatory cells predominantly macrophages, fibroblasts and fibrocytes were observed at the cortical margins around the defect. Occasional cases, this layer was a thin, except at endosteal and periosteal end where multilayering was observed. Moderate new woven bone trabeculae lined by osteoblasts were observed along the endosteal aspect of host cortical bone on either side of defect and extending into the medullary cavity (fig. 3.59).

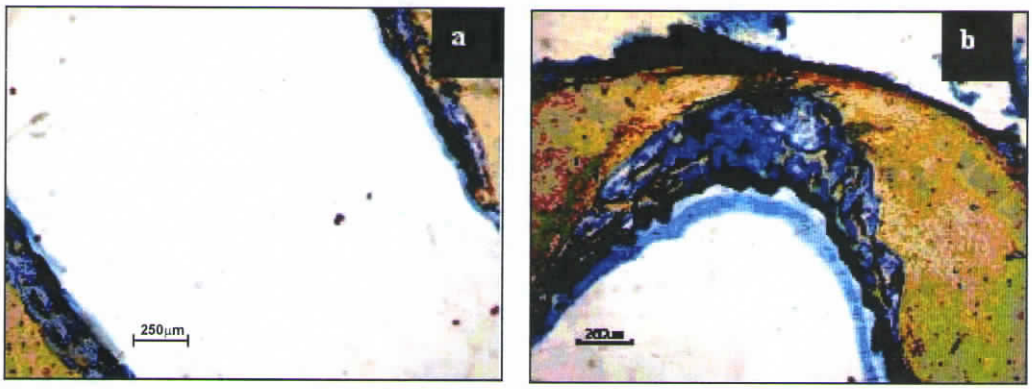

Figure 3-59 Light microscopic images of the stained sections of control material retrieved after one week.

At four weeks post implantation, repair was seen along both margins of the defect with deposition of new woven bone (fig. 3. 60). Fibroblasts were noted at the interface with implant space. Remodelling of this bone was evident with resorption bays. In some cases, the openings of the defects, either endosteal or periosteal were bridged with trabeculae of woven bone.

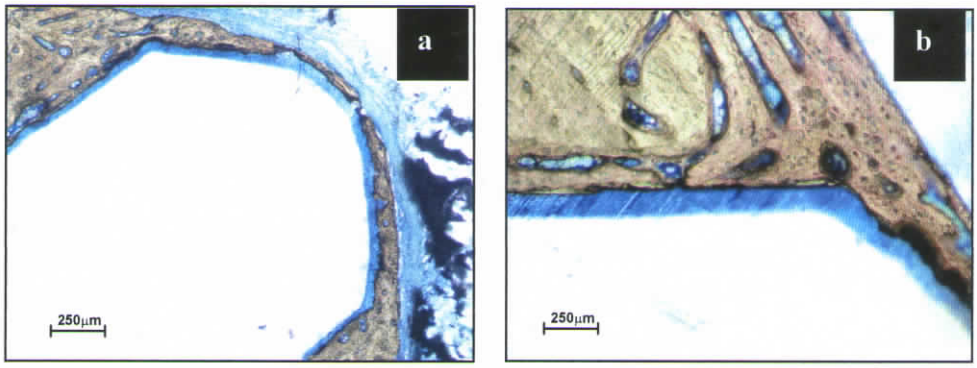

Figure 3-60 Light microscopic images of the stained sections of control material retrieved after 4 weeks

At twelve weeks post implantation, half of the defects were closed on periosteal surface with bone trabeculae, some of them being closed on endosteal aspect also (fig. 3-61). Remodelled bone was present along both margins of defect, some of them in direct contact with defect and some of them separated by fibrous tissue. The cortical bone at the interface did not show any reaction to the implants at any time period. Fibroblasts and fibrocytes were seen around the empty space in the medullary cavity in all cases at four and twelve weeks post implantation.

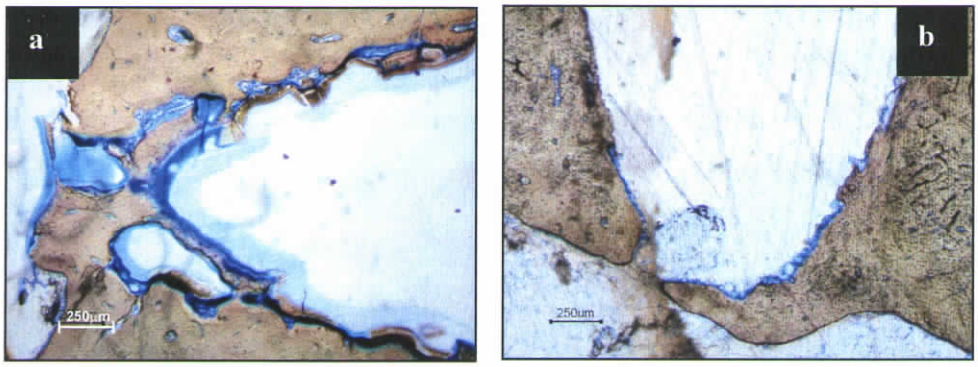

Figure 3-61 Light microscopic images of the stained sections of control material retrieved after 12 weeks

3.6.2.2 Test materials-

I: Surface phosphorylated PH1 (PPH1)
II: Apatite coated PH1 (CaPH1)

Remnants of test implant materials; both PPH1 and CaPH1 were observed in the defect at all time periods, in most sections. They were of a glassy morphology in globular or sheet form and mostly seen loose in the defect. The defects in the cortical bone, opened into medullary cavity. Early inflammation was followed by repair around both types of implants.

At one-week post implantation the histological picture resembled that seen around the control implants, with slight bone formation at edges of the openings in the defect (fig. 3.62).

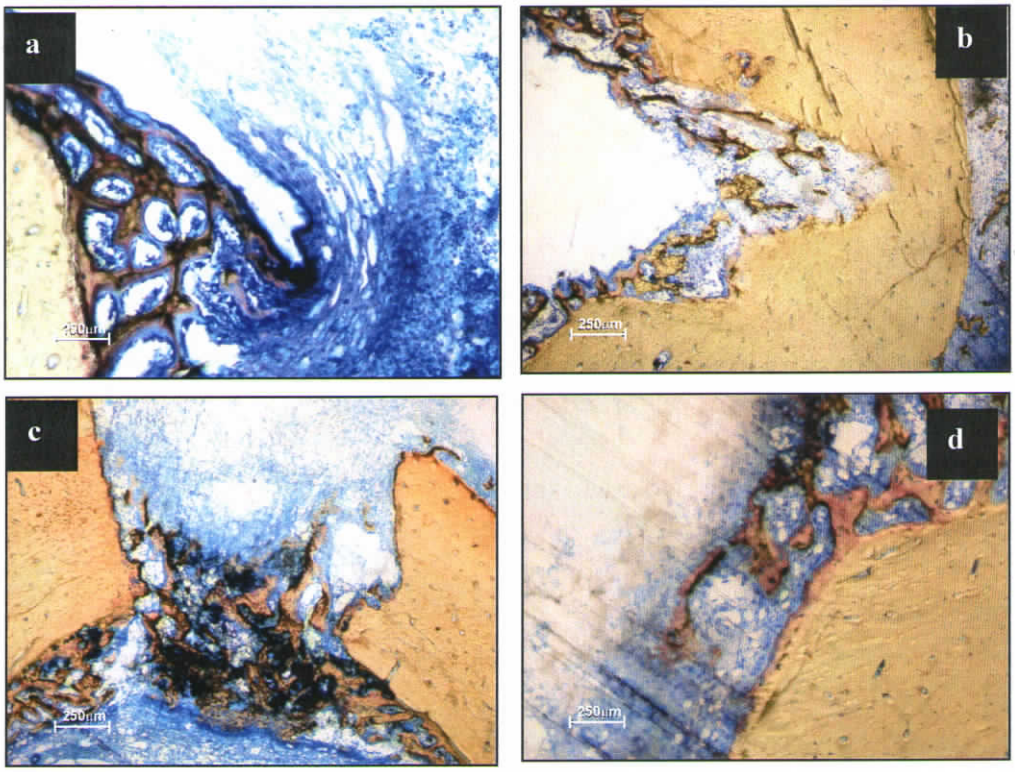

Figure 3-62 Light microscopic images of the stained sections of PPH1: (a), (b) and CaPH1: (c), (d) retrieved after one week

At four weeks post implantation, most defects were bridged with woven bone. Formation of new bone with remodelling was also observed along both margins of the defect (fig. 3. 63). In occasional cases, fibrous tissue was observed in between defect space and bone.

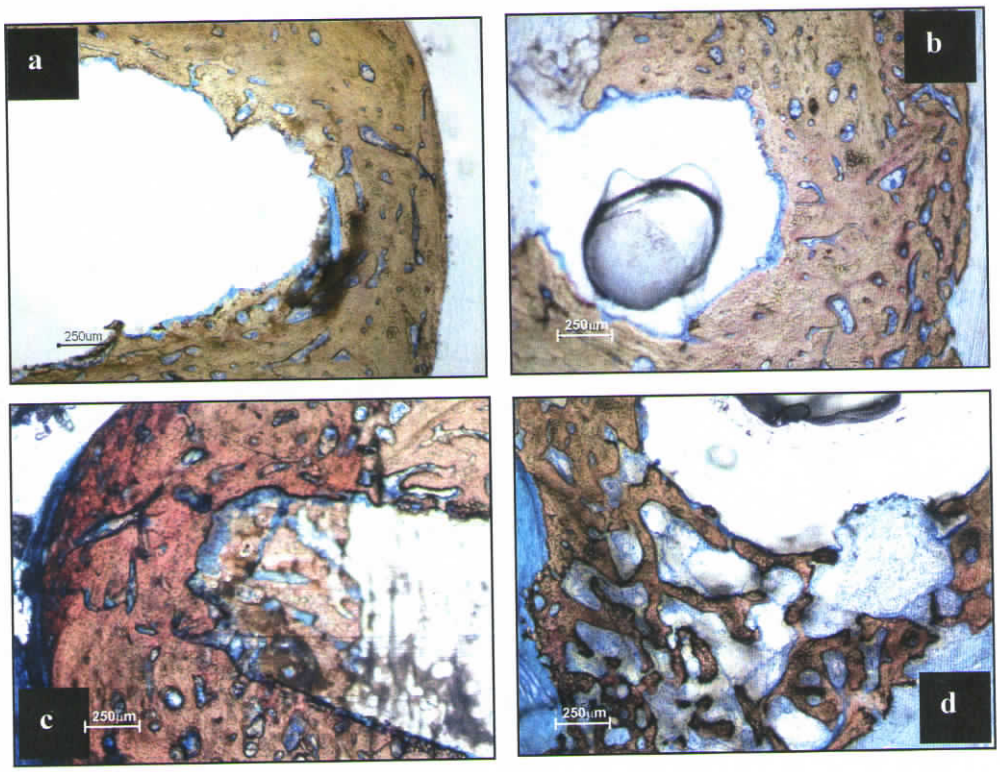

Figure 3-63 Light microscopic images of the stained sections of PPH1: (a), (b) and CaPH1: (c), (d) retrieved after four weeks.

At twelve weeks post implantation, peri-osteal and endosteal openings of defect were closed with woven bone in most cases around PPH1 as compared to a few cases in CaPH1 (fig. 3. 64). Fibroblasts and fibrocytes were seen around the empty space in the medullary cavity in all cases at four and twelve weeks post implantation.

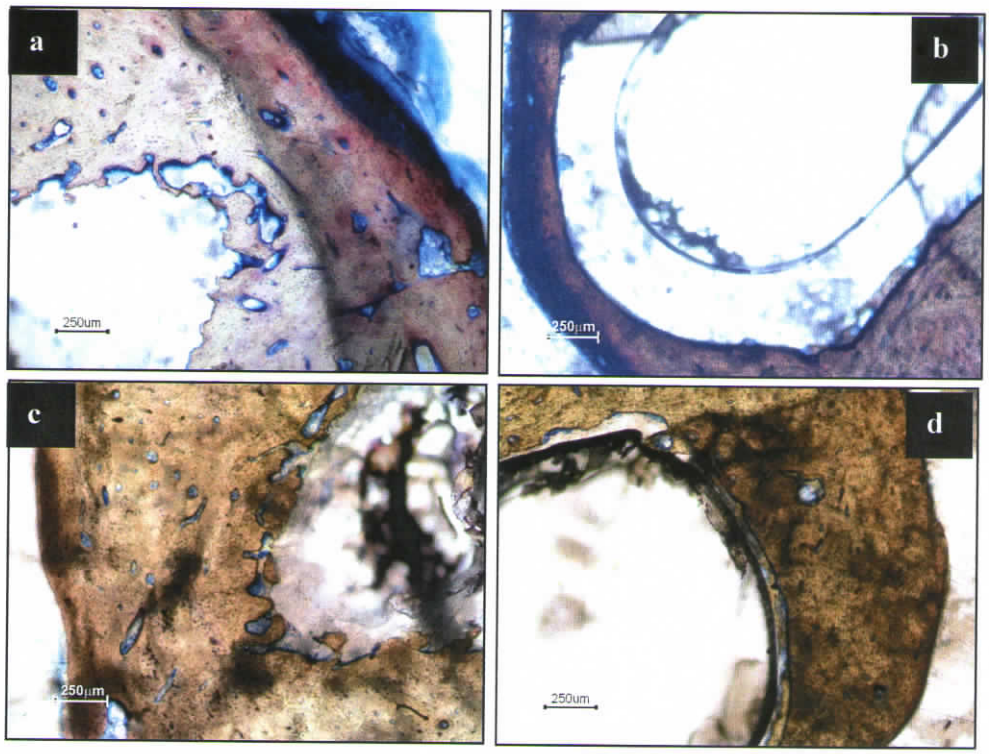

Figure 3-64 Light microscopic images of the stained sections of PPH1: (a), (b) and CaPH1: (c), (d) retrieved after 12 weeks

The response to material implantation is similar in both, control and test materials (PPH1 and CaPH1) at one week post-implantation. At four and twelve weeks post-implantation, repair with bone formation is observed in more cases around the test materials as compared to the control. Deposition of new bone was found in more cases around PPH1 as compared to that around CaPH1.

3.6.3 Summary

All animals survived throughout the experiment. Gross examination of the implant sites did not show infection or any other gross abnormality. The response to material implantation is similar in both, control and test materials (surface phosphorylated PH1 and apatite coated PH1) at one week post-implantation. At four and twelve weeks post-implantation, repair with bone formation is observed in more cases around the test materials as compared to the control. Deposition of new bone was found in more cases around surface phosphorylated PH1 as compared to that around apatite coated PH1.

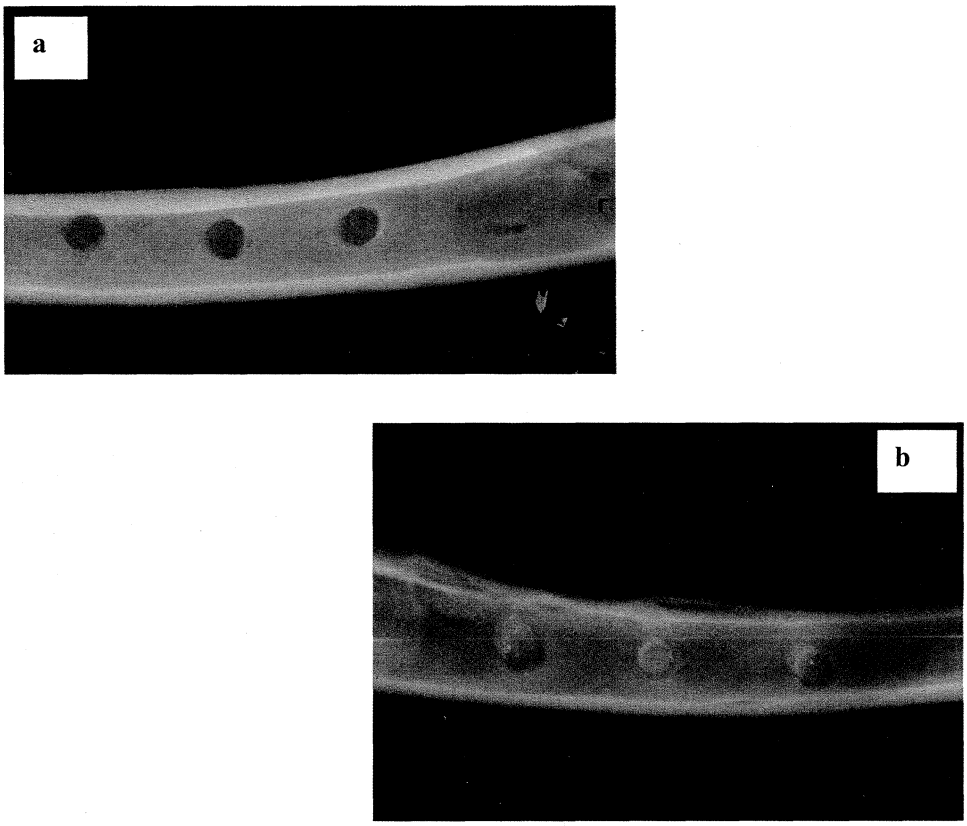

Figure 3-58 Radiological view of implant sites after 3 months (a) PPH1 (b) control

Histopathological results showed that the control implants were absent in all sections examined. Defects were noted in the cortical bone, opening into medullary cavity. Defects were an empty space in all sections. The empty space is due to dissolution of the control samples during the embedding process as reported by (CMW1 PMMA) during the embedding process in PMMA for obtaining undecalcified sections [185]. In order to reconfirm this observation a control experiment was conducted. The control samples and the test samples were subjected to all the processing steps that is performed for the implant sample and finally embedded. The samples with the same dimension, inserted in silicone tubes

CHAPTER 4

SUMMARY AND CONCLUSIONS

4.1SUMMARY

The present work is on biomimetic functional modification of PMMA through copolymerization of methyl methacrylate (MMA) with a comonomer, 2-hydroxy ethyl methacrylate (HEMA) followed by surface phosphorylation to achieve osseointegrative property and support new bone formation. HEMA was selected as the comonomer as it possess an active hydroxyl group (-OH), that can be easily functionalized. Further, poly(HEMA) is a known biocompatible polymer.

Poly(HEMA-co-MMA) with varying HEMA:MMA ratio was synthesized by bulk polymerization of the monomers using benzoyl peroxide as initiator and *in situ* cross-linked using ethylene glycol dimethacrylate (EGDMA). Surface functionalization of poly(HEMA-co-MMA) was performed by phosphorylation using P_2O_5 at 80 ^{0}C. The ability of the surface phosphorylated poly(HEMA-co-MMA) to induce *in vitro* nucleation of calcium phosphate was evaluated under accelerated simulated physiological environment using 1.5xSBF (simulated body fluid).

The preliminary characterization supported the formation of a random copolymer of MMA and HEMA. The FT-IR results showed the formation of poly(HEMA-co-MMA) through the bulk polymerization reaction of HEMA and MMA. The FT-IR spectra of surface phosphorylated poly(HEMA-co-MMA) ensured that the proposed method could be used for surface phosphorylating copolymers of MMA and HEMA with varying ratio. The composition with lowest HEMA content, designated as PH_1 having HEMA: MMA in the molar ratio 0.07:0.90 was found as the most suitable composition with respect to surface phosphorylation, *in vitro* nucleation of calcium phosphate, extent of equilibrium swelling (i.e., minimum percentage swelling) and mechanical properties and hence selected for detailed evaluation.

The DSC data ensured a single glass transition temperature (T_g) of 104.57 and thereby formation of random copolymer. The DSC data further showed that the T_g of PH1 is not significantly altered due to surface phosphorylation. The TGA results demonstrated that the degradation profiles for the copolymer as well as homopolymers are having a similar trend. Differential thermal analysis further supports the data. TGA data also showed that the decomposition temperature of surface phosphorylated PH1 (206.3 ^{0}C) is slightly higher than that of unmodified PH1 (189 ^{0}C), which shows that surface phosphorylation slightly improves the thermal stability. The residual monomer analysis performed using gas chromatography showed that the amount of residual monomer is 3.71 ppm. The XPS spectra analysis ensured the presence of surface bound phosphate group on surface phosphorylated PH1.

The equilibrium swelling study in PBS illustrated that with increase in HEMA content in poly(HEMA-co-MMA), the percentage of equilibrium swelling significantly increases and reaches a plateau after 100h. The study also ascertained that surface phosphorylation of poly(HEMA-co-MMA) significantly increases the hydrophilicity. All the different compositions of poly(HEMA-co-MMA) as well as

poly(HEMA) showed the same trend. The increase in hydrophilicity with respect to surface phosphorylation was further supported by the contact angle values (unmodified PH1=67.6, surface phosphorylated PH1= 43.55).

The AFM images showed that the surface topography of PH1 is smooth. The PH1 surface-probe force of attraction value is 123.5. The AFM study showed that surface roughness of PH1 increased due to phosphorylation. It has been observed that PH1 has good compressive strength value of 153MPa, modulus 4.6 GPa and good dynamic storage modulus value of 1.75 GPa at room temperature (25±3 ^{0}C). The compressive strength of PH1 (153 MPa) decreased significantly due to surface phosphorylation (39.35 MPa). The compressive modulus also decreased from 4.6 GPa to 1.6 GPa. However, dynamic storage modulus (1.75 GPa) value is not altered due to surface phosphorylation. The UV-Visible analysis showed that extent of surface phosphorylation was proportional to HEMA content in poly(HEMA-co-MMA).

The biomimetic nucleation and growth of calcium phosphate on surface phosphorylated poly(HEMA-co-MMA) was preliminarily assessed with micro FT-IR spectroscopy. The coating morphology was evaluated using scanning electron microscope attached with an energy dispersive X-ray detector. The ultra-structural features of coating characteristics were evaluated using transmission electron microscope coupled with an EDS detector and the results were compared with the observations obtained through an atomic force microscope. The amount of calcium and phosphorous in the calcium phosphate coating was quantitatively estimated as a function of time using atomic absorption spectroscopy and UV-Visible spectroscopy respectively. The amount of calcium phosphate formed as a function of HEMA content in poly(HEMA-co-MMA) was also estimated. The calcium phosphate phase was confirmed as hydroxyapatite using wide angle X-ray diffraction pattern.

The FT-IR results confirmed the formation of calcium phosphate coating on surface phosphorylated PH1 under accelerated physiological environment. The scanning electron microscopic studies depicted the morphology of the coating as spheroid like clusters of hydroxyapatite. The SEM micrographs further revealed that nucleation of calcium phosphate begins at 3 days. Primary coating was complete by 10 days while secondary coating was complete by two weeks. The energy dispersive spectra showed that the calcium to phosphate ratio increased with time. Transmission electrons microscopic studies showed that the spheroid like apatite clusters found in SEM are in fact composed of needle like apatite rods with 20-40 nm diameter and approximately 100 nm length. The selected area diffraction patterns of the coating proved that the amorphous to crystalline transformation of the calcium phosphate phase is occurring within 3 days of immersion in SBF. The EDS spectra showed that the coating is initially composed of a calcium rich apatite. The AFM images showed that the calcium phosphate coating formed on 3 days of immersion in SBF itself has an orientation in growth. The AFM observations regarding the size of apatite crystals are supported by the TEM results. The X-ray diffraction pattern confirmed that the calcium phosphate phase is hydroxyapatite. The AAS data showed that the calcium concentration of the coating increased linearly with time of exposure of surface phosphorylated PH1 in accelerated physiological fluid. The study also proved that the calcium concentration increased with increase in HEMA content in poly(HEMA-co-MMA).

The proposed method of surface phosphorylation was extended to other biocompatible polymers with inherent hydroxyl (-OH) group like poly(vinyl alcohol) and by modifying other polymers like EVA and PET having appropriate functional groups to impart free –OH group. The surface phosphorylation of PVA was performed as such while, for EVA and PET, controlled surface hydrolysis was carried out prior to phosphorylation in order to acquire the necessary –OH groups for phosphorylation reaction. The surface phosphorylated PVA, surface

phosphorylated EVA and surface phosphorylated PET induces *in vitro* nucleation of calcium phosphate under accelerated physiological condition.

The *in vitro* cytocompatibility and cell adhesion behaviour of surface phosphorylated as well as apatite coated poly(HEMA-co-MMA was investigated and compared with unmodified poly(HEMA-co-MMA) using human osteosarcoma (HOS) cell-line, supplied by National Centre for Cell Sciences (NCCS), Pune, India. The ability of the test materials in supporting the secretion of bone specific bone marker protein, osteocalcin was performed using biosourse h-OST EASIA kit, Europe). The alkaline phosphatase activity of the cells in contact with the test materials was measured with a commercially available assay kit (Glaxo, Qualigens diagnostics, India).

The light microscopic images of HOS cells in contact with PH1, PPH1 and CaPH1 retained their normal cellular morphology after 24h which ensured that the test materials are not cytotoxic in nature. The MTT assay performed for the quantitative estimation of metabolically active cells proved that the number of metabolically active cells adhered on PPH1 and CaPH1 after 14d was considerably more compared to the number of viable cells on PH1. Further, the number of active cells adhered on CaPH1 was a slightly more compared toPPH1 at both time periods. It is apparent from the SEM images that the cells attached and spread over the surfaces of all the three samples. However, the cell density seemed to be slightly greater on PPH1 and CaPH1, as multiple layers of cells are visible in the ESEM images after 48h. The cells exhibited flat morphology with long and short filopodia or lamellipodia. Even though the cells showed minor differences to their reactions to each of the different substrates, their morphology was more or less similar. The difference in cell-spreading pattern is attributed to the variation in surface roughness, surface energy and hydrophilicity of the substrate. Von kossa staining method confirmed calcium deposition and the initiation of *in vitro* mineralization. It is clear from the images that accelerated biomineralization has

occurred on PPH1 in presence of HOS cells, while such areas were not predominant in PH1.

A steady increase in osteocalcin concentration was observed with time for PH1, PPH1 and CaPH1, and reached a maximum value at day 21. The trend was similar for all the samples as well as for control. The highest value was noted for PPH1. The results also showed that PH1 and surface phosphorylated PH1 promotes cellular activity and accelerates osteocalcin release compared to control or calcium phosphate coated sample. The alkaline phosphatase activity of the samples decreased with time with a maximum value observed at 7 days and then decreased. The trend was same in all cases. The highest activity was observed for PPH1.

The *in vivo* toxicological response of the surface phosphorylated as well as *in vitro* calcium phosphate coated polymer as per ISO 10993. The efficacy of surface phosphorylated and apatite coated poly(HEMA-co-MMA) to initiate bone bonding by was assessed by short-term bone implantation in rabbit as per ISO 10993-6: 1994(E): Test for local effects after implantation, *clause 6.0: Test method for implantation in bone* using'CMW1' poly(methyl methacrylate) radiopaque bone cement (DePuy, Johnson and Johnson, England) as control material.

The response to material implantation is similar in both, control and test materials (surface phosphorylated PH1 and apatite coated PH1) at one week post-implantation. At four and twelve weeks post-implantation, repair with bone formation is observed in more cases around the test materials as compared to the control. Deposition of new bone was found in more cases around surface phosphorylated PH1 as compared to that around apatite coated PH1.

In comparison with the conventional synthetic bone grafts, surface phosphorylated poly(HEMA-co-MMA) possesses favourable properties such as ability to trigger biomimetic mineralization, promote cell adhesion, growth and biomineralization in presence of HO cells, promots bone specific marker proteins and accelerate *in vivo* bone regeneration.

4.2. CONCLUSIONS

The conclusions of the present study are

i) The surface phosphorylation of poly(HEMA-co-MMA) enhances the nucleation and growth of calcium phosphate under simulated physiological condition.

ii) The composition with lowest HEMA content, designated as PH_1 having HEMA: MMA in the molar ratio 0.07:0.90 was found as the most suitable composition with respect to surface phosphorylation, biomimetic nucleation of calcium phosphate, extent of equilibrium swelling (i.e., minimum percentage swelling) and mechanical properties and hence selected for detailed evaluation.

iii) The surface phosphorylated PH1 (PPH_1) showed excellent cell viability and cell adhesion with HOS cells. PPH_1 also showed *in vitro* biomineralization in presence of HOS cells. Human osteocalcin and alkaline phosphatase estimation showed that the bone specific protein secretion is enhanced in the presence of PPH_1.

iv) Both the test materials, phosphorylated PH_1 (PPH_1) and apatite coated PH_1 ($CaPH_1$) passed the biological evaluation tests, namely hemolysis, acute systemic toxicity, intracutaneous (intradermal) irritation, maximization test for delayed hypersensitivity.

v) The short term bone implantation results proved that the response to material implantation is similar in both, control and test materials (PPH1 and CaPH1) at one week post-implantation. At

four and twelve weeks post-implantation, repair with bone formation is observed in more cases around the test materials as compared to the control. Deposition of new bone was found in more cases around PPH1 as compared to that around CaPH1.

4.3. FUTURE PROSPECTS

i) The results proved that surface phosphorylated poly(HEMA-co-MMA) is capable of inducing biomimetic mineralization of calcium phosphate under accelerated physiological conditions. Further the results showed that surface phosphorylated copolymer is biocompatible and promotes new bone formation. Hence poly(HEMA-co-MMA) microspheres could be proposed as a candidate material to substitute the commercially available product 'OSTEOPOL' used for infrabony defect filling applications. 'OSTEOPOL' is basically PMMA microspheres. Surface phosphorylated poly(HEMA-co-MMA) can certainly perform its function more effectively.

ii) Long-term implantation study of surface phosphorylated poly(HEMA-co-MMA) would throw light in understanding the long-term *in vivo* response of the material.

CHAPTER 5

REFERENCES

1. S. Mann, Biomineralization: Principles and concepts in bioinorganic materials chemistry, Oxford university press, 2001.

2. Y. Dauphin, 'Biomineralization' Encyclopedia of Inorganic Chemistry, Ed. R.B. King, Wiley & Sons 1, 2005.

3. E. Baeuerlein, Biomineralization: Progress in biology, molecular biology and application, Wiley-VCH, 2004.

4. Y. Dauphin, Biomineralization: The major link between life and geosphere, http://www.u-psud.fr

5. L. Addadi and S. Weiner, 'Control and design principles in biological mineralization', Angewandte Chemie International Edition in English, 1992; 31(2): 153-169

6. H. Shin, S. Jo. A. G. Mikos, Biomimetic materials for tissue engineering, Biomaterials, 2003; 24: 4353-4364

7. P. G. Robey, M.F. Young, L. W. Fisher, T.D. McClain, Thrombospondin is an osteoblast -derived component of mineralized extracellular matrix, J. Cell Biol 1989; 108: 719-727

8. D. T. Denhardt, X Guo, Osteopontin: a protein with diverse functions, FASB J 1993; 7: 1475-82

9. K. Anselme, Osteoblast adhesion on biomaterials, Biomaterials, 2000; 21: 667-81

10. T. Kokubo, S. Ito, Z. T. Huang, T. Hayshi, S. Sakka, T. Kitsugi, T. Yamamuro, Ca, P- rich layer formed on high strength bioactive glass ceramic A-W, J. Biomed. Mater. Res. 1990; 24(3): 331-343

11. R. L. Reis, A. M. Cunha, Treatments to induce the nucleation and growth of apatite like layers on polymeric surfaces and foams, J. Mater Sci Mater Med, 1997; 8: 897-905

12. M. Tanahashi, T. Kokubo, T.Nakamura, Y. Katsura and M. Nagano, Ultrastructural study of an apatite layer formed by a biomimetic process and its bonding to bone, Biomaterials, 1996; 17 (1): 47-51

13. P. Li, Biomimetic nanoapatite coating capable of promoting bone ingrowth, J. Biomed Mater Research, 2003; 66A: 79-85

14. N. Ozawa, T. Yao, Micropattern formation of apatite by combination of a biomimetic process and transcription of resist pattern, J. Biomed Mater Research, 2002; 62: 579-586

15. A. L. Oliveria, C. M. Alves, R.L. Reis, Cell adhesion and proliferation on biomimetic calcium-phosphate coatings produced by a sodium silicate gel methodology, J. Mater Sci Mater Med, 2002; 13: 1181-1188

16. R. Fujisawa and Y. Kuboki in ' Mechanism and phylogeny of mineralization in biological systems', S. Suga and H. Nakahara (Eds), P. 107, Pringer-Verlag Tokyo, 1991

17. R. Fujisawa, Y. Wada, Y. Nodasak and Y. Kuboki, Biochem. Biophys. Acta, 1996; 53: 1292

18. A. Bigi, B. Bracci, G. Cojazzi, S. Panzavolta, K. Rubini, *In vitro* mineralization of gelatin-poly(acrylic acid) complex matrices, J. Biomater Sci, Polymer Edn. 2004; 15 (3): 243-254

19. P. Malkaj, A. Chrissanthopoulas, E. Dalas, The overgrowth of calcium carbonate hexahydrate on new functionalized polymers, J. Crystal Growth, 2002; 242: 233-238

20. E. Dalas, A. Chrissanthopoulos, The overgrowth of hydroxyapatite on new functionalized polymers, J. Crystal growth, 2003; 255: 163-169

21. S. Koutsopolulos, and E. Dalas, The crystallization of hydroxyapatite in the presence of lysine, J. Colloid and interface science, 2000; 231: 207-212

22. S. Habelitz, D. Ford, S. J. Marshall, P. K. Den Bensten, M. Balooch, G. W. Marshall, W. Li, Amelogenin induces biomimetic mineralization at specific pH, Mat. Res. Soc. Symp proc. 2003: 774

23. E. Dousi, J. Kallitis, A. Chrissanthopoulas, E. Dalas, Calcite overgrowth on carboxylate polymers, J. Crystal Growth, 2003; 253: 496-503

24. O. Grassmann and P. Lobmann, Biomimetic nucleation and growth of calcium carbonate in hydrogels incorporating carboxylate groups, Biomaterials, 2004; 25: 277-282

25. P. Liang, Y. Zhao, Q. Shen, D. Wang, D. Xu, The effect of carboxymethyl chitosan on the precipitation of calcium carbonate, J. Crystal Growth, 2004; 261: 571-576

26. E. Dalas, S. N. Koklas, V. Papakostas, Aragonite crystallization of functionalized styrene butadiene copolymer, J. Crystal Growth, 2003; 254: 219-224

27. K. L. Mittal, Polymer surface modification-Relevance to adhesion VSP, 1996

28. A. S. Hoffman, in Biomaterials Science: An introduction to Materials in Medicine; B. D. Ratner, A. S. Hoffman, F.J. Lemons, Eds; Academic Press, San Diego, 1996, Chapter 2, p.124.

29. D. Wang, S. C. Miller, P. Kopečková and J. Kopeček, Bone-targeting macromolecular therapeutics, Advanced drug delivery reviews, 2005; 57(7): 1049-176

30. J. Christoffersen, M. R. Christoffersen, W. Kiblazyc, F. A. Andersen, J. Cryst. Growth, A contribution to the understanding of the formation of calcium phosphates, 1989; 94: 767

31. G. Goissis, S. V. S. Maginador and v.d.c. A. Martins, Biomimetic mineralization of charged collagen matrices: *in vitro* and *in vivo* study, Artif. Organs, 2003; 27 (5): 437-443

32. Y. Chen, A F T Mark, M. Wang, J. Li, Composite coating of bonelike apatite particles and collagen fibres on poly(L-Lactic acid) formed through an accelerated biomimetic coprecipitation process, J. Biomed. Mater. Research, Part B, Appl. Biomater. 2006; 77B: 315-322

33. M. Tanahashi and T. Matsuda, Surface functional group dependence on apatite formation on self-assembled monolayers in a simulated body fluid, J. Biomed. Mater. Res., 1997; 34: 305-315

34. A. L. Boskey, W. Ullrich, L. Spevak, H. Gilder, Persistence of Complexed Acidic Phospholipids in Rapidly Mineralizing Tissues is Due to Affinity for Mineral and Resistance to Hydrolytic Attack: *In Vitro* Data , Calcified Tissue International, 1996, 58(1): 45-51

35. O. N. Tretinnikov, K. Kato and Y. Ikada, *In vitro* hydroxyapatite deposition onto a film surface grafted with organophosphate polymer, J. Biomed. Mater. Research, 1994; (28): 1365-1373

36. W. L. Murphy and D. J. Mooney, Bioinspired growtht of crystalline carbonate apatite on biodegradable polymer substrate, J. Am. Chem. Soc., 2002; 124(9): 1910-1917

37. A. Peytcheva, M. Antionietti, Carving on the nanoscale: Polymers for the site-specific dissolution of calcium phosphate. Chem. Int. Ed. 2001; 40: 3380

38. J. D. Hartgerink, E. Beniash, S. I. Stupp, Self-Assembly and Mineralization of Peptide-Amphiphile Nanofibers, Science, 2001; 293: 1684

39. H. L. Lu, M.D. Kofron, S. F. El-Amin, M. A. Attawia and C.T. Laurencin, *In vitro* bone formation using muscle derived cells: a new paradigm for bone tissue engineering using polymer-bone morphogenic protein matrices, Biochemical and biophysical research communications, 2003; 305: 882-889.

40. G. H. Nancollas, The involvement of calcium phosphate in biological mineralization and demineralization processes, Pure and Appl. Chem. 1992; 64(11): 1673-1678

41. H. M. Kim, T. Himeno, M. Kawashita, T. Kokubo and T. Nakamura, The mechanism of biomineralization of bone-like apatite on synthetic hydroxypatite: an *in vitro* assessment, J. R. Soc. Interface, 2004; 1: 17-22

42. H. Takadema, H.M. Kim, T. Kokubo and T. Nakamura, The mechanism of bone-like apatite formation on bioactive titanium metal in simulated body fluid, J. biomed. Mater. Res, 2001(b); 57: 441-448

43. H. Takadema, H.M. Kim, T. Kokubo and T. Nakamura, The mechanism of bone-like apatite formation on a sodium silicate glass-TEM-EDS study *in vitro*, Chem. Mater, 2001 a; 13: 1108-1113

44. R. Xin, Y. Leng, J.Chen, Q. Zhang, A comparative study of calcium phosphate formation on bioceramics *in vitro* and *in vivo*, Biomaterials, 26; 2005: 6477-6486

45. E. Dalas, Crystallization of sparingly soluble salts on functionalized polymers, J. Mater. Chem., 1991; I (3): 473-474

46. E. Fernandez, F. J. Gil, M. P. Ginebra, F. C. M. Driessens, J. A. Planell and S. M. Best, Calcium phosphate bone cements for clinical applications. Part I: Solution chemistry, J. Mater Sci., Mat. Med., 1999; 10(3): 169-176

47. S. C. Marks Jr. and D. C. Hermey, 'The structure and development of bone' in principles of bone biology, Eds: John P. Bilezikian, Lawerence G. Raisz, Gideon A. Rodan, Academic Press, 1996

48. W. Bloom, D. W. Fawcett. A textbook of histology. 12th ed. New York: Chapman & Hall, 1994: 7-16, 40-46, 863-870

49. H. Yuehuei *in* 'Mechanical properties of Bone, Mechanical Testing of Bone and the Bone-Implant Interface' By Yuehuei H. An, Robert A. Draughn, CRC Press, 1991, page 41

50. J. D. Curry, Hard Tissue (Book reviews: Mechanical properties of bone), Science, 1974; 183 (4120): 67-68

51. J. Rossant, Experimental Approaches to Mammalian Embryonic Development, Cambridge University Press, 1989

52. J. A. Buckwalter, M.J. Glimcher, R.R. Cooper, R. Recker Bone Biology Part I, structure, blood supply, cells, matrix, and mineralization. J. Bone Joint Surg. 1995; 77-A: 1256-1275

53. P. G. Robey, 'Bone Matrix proteoglycans and Glycoproteins', in principles of bone biology, Eds: John P. Bilezikian, Lawerence G. Raisz, Gideon A. Rodan, Academic Press, 1996

54. W. T. Butler, A. L. Ridall and M.D. McKee, Osteopontin, in principles of bone biology, Eds: John P. Bilezikian, Lawerence G. Raisz, Gideon A. Rodan, Academic Press, 1996

55. G. J. Tortora, S.R. Grabowski, Principles of anatomy and physiology, 10th Ed., John Wiley &Sons, Inc, 2003, pp.175

56. P. V. Giannoudis, H. Dinopoulos, E. Tsiridis, Bone substitutes: an update. Injury 2005, Nov 36(Suppl 3) S 20-7

57. M. A. Morone, S. D. Boden, G. Hair, The Marshell R. Urist Young investigator award, Gene expression during autograft lumbar spine fusion and the effect of bone morphogenic protein, Clin. Orthop. 1998; 351: 252-265

58. V. M. Goldenberg, S. Stevenson, The biology of bone grafts: Semin Arthoroplasty, 1993; 4: 58-63

59. R. Langer and J. Vcanti, Tissue engineering, Science, 1993; 260: 920-926

60. G. J. Zipfel, B. H. Guiot, R. G. Fessel, 'Bone grafting', Neurosurg Focus, 2003; 14(2), article no:8

61. T. Albrektsson ans C. Johansson, Osteoinduction, osteoconduction and osseointegration. European Spine Journal, 2001; 10(2) 96–101

62. J. B. Park, J. D. Bronzino, Biomaterials: Principles and Applications, CRC press, 2002

63. Scott A. Guelcher, Jeffrey O. Hollinger, An Introduction to Biomaterials, CRC Press, 2005

64. L. L. Hench, Bioceramics: From concept to clinic, Am. Ceram. Soc. Bull. 1993; 72: 93-98

65. L. Yuabo, C.P.A.T. Klein, Z. Xingdong, K. de Groot, Formation of a bone apatite-like layer, on the surface of porous hydroxyapatite ceramics, Biomaterials, 1994; 15: 835-841

66. P. Ducheyne, Bioactive ceramics, J. Bone Joint Surg, 1994; 76B: 861-862

67. M. M. Pereira, A.E. Clark, L.L. Hench, Calcium phosphate formation on sol-gel derived bioactive glasses-*in vitro*, J. Biomed Mat. Res. 1994; 28: 693-698

68. S. R. Radin, P. Ducheyne, The effect of calcium phosphate ceramic composition and structure on *in vitro* behaviour. II Precipitation. J. Biomed. Mat. Res. 1993; 27: 35-45

69. K. C. Dee, and R. Bizios, Mini review: Proactive Biomaterials and Bone Tissue Engineering, Biotechnology and Bioengineering, 1996; 50: 438-442

70. M. Shrikhanazadeh, G. Q. Liu, Biocompatible delivery systems for osteoinductive proteins: Immobilization of L-lysine in micro-porous hydroxyapatite coatings, Mater.Lett., 1994; 21: 115-118

71. S. I. Stupp, J. A. Hanson, J. A. Eurell, G. W. Ciegler, A. Johnson, Organoapatites: Materials for artificial bone. III Biological testing. J. Biomed. Mater. Res. 1993; 27: 301-311

72. E. Bergsma, F. Rozema, R. Bos, and W. de Bruijin, Foreign body reaction to resorbable poly(L-lactide) bone plates and screws used for the fixation of unstable zygomatic fractures, J. Oral maxillogac. Surg., 1993; 51: 666-670

73. W. B. Lehman, A.B.Strongwater, D. Tunc, F. Kummer, D. Atar, A.D. Grant, M. Kramer, M.W. Rohovsky, Internal fixation with biodegradable plates and screws in dogs, J. Pediat. Orthop. PartB, 1994; 3: 190-193

74. K. Whang, C.H.Thomas, K.E. Healy, G.Nuber, A Novel method to fabricate bioabsorbable scaffolds, Polymer, 1995; 36: 837-842.

75. S. L. Ishaug, M. J. Yasemski, R. Bizios, A.G. Mikos, Osteoblast function on synthetic biodegradable polymers, J. Biomed. Mater. Res. 1994; 28: 1445-1453

76. C. A. Vacanti, J. P. Vacanti, Bone and cartilage reconstruction with tissue engineering tissue engineering approaches. Otolaryngol. Clin. North Am. 1994; 27: 263-276

77. Fibrous tissue -Wikipedia, the free encylocpedia

78. J. H. Boss, I. Sharawi, D.G. Mendes, The nature of the bone-implant interface. The lessons learned from implant retrieval and analysis in man and experimental animal, Med. Prog. Technol., 1994; 20 (3-4): 119-42

79. L. L. Hench, and June Wilson, An introduction to bioceramics, World scientific, 1993, pages 13-14

80. D. F. Williams, Implantable prostheses, Phys. Med. Biol. 1980; 25: 611-636

81. I. M. Schakeneraad, H. J. Busscher, C.R.H. Wildevuur, J. Arends, J. Biomed Mat. Res. 1986; 20: 773-784

82. F. Grinner, Cellular adhesiveness and extracellular substrata, Int. Rev.Cytol. 1978; 53: 65-144

83. P. Van der Valk, A. W. J. Pelt, H. J. Busscher, H. P. de Jong, C. R. H. Wilderuur and J. Arends, Interaction of fibroblasts and polymer surfaces: relationship between surface free energy and fibroblast spreading. J. Biomed Mat. Res. 1983; 17: 807-817

84. O. V. Salata, Applications of nanoparticles in biology and medicine (Review), Journal of nanobiotechnology, 2 (3) 2004, pp 1-6

85. N. C Nguyen, W. J. Maloney and R. H. Dauskardt, Reliability of PMMA bone cement fixation: fracture and fatigue crack-growth behaviour, J. Mat. Sc. Mat. Med. 1997; 8: 8-12

86. C. Lee, The Mechanical Properties of PMMA Bone Cement in The Well-Cemented Total Hip Arthroplasty, Springer Berlin Heidelberg, 2005

87. R. P. S. Chaplin, A. J. C. Lee R. M. Hooper And M. Clarke, The mechanical properties of recovered PMMA bone cement: A preliminary study, J. Mat. Sci, Mat. Med., 2006; 12:17

88. C. Minari, L. Cristofolini, F. Baruffaldi, L. Pierotti, Radiopacity and Fatigue Characterization of a Novel Acrylic Bone Cement with Sodium Fluoride, Artificial Organs 2000; 24 (9): 751–757

89. H. Wahling, E. Dingeldein, R. Bergmann, K. Reuss, The release of gentamicin from polymethyl methacrylate beads, J. Bone Jt. Surg. 1978; 60-B: 270-277

90. V. Vecsei, A. Barquet, Treatment of chronic osteomyelitis by necretomy and gentamicin-PMMA beads. Clin Orthop Relat Res 1981; 159: 201-217

91. J. J. Klawitter, A. M. Weinstein and L. J. Peterson Fabrication and characterization of porous-rooted polymethylmethacrylate (PMMA) dental implants, Journal of Dental Research, 1997; 56: 385-393

92. G. Lewis, Properties of acrylic bone cement: state of art Review, J. Biomed. Mater. Res., 1997; 38(1): 155-182

93. J. A. Roether, S. Deb, The effect of surface treatment of hydroxyapatite on properties of bioactive bone cement, J. Mater. Sc. Mat. Med., 2004; 5 (4): 413-418

94. J. M. Yang, H.M. Li, M. C. Yang, C. H. Shin, characterization of acrylic bone cement using dynamic mechanical analysis, J. Biomed. Mater. Res., 1999; 48(1): 52-60

95. A. Mori, C. Ohtsuki, T. Miyazaki, A. Sugino, M. Tanihara, K. Kuramoto, A. Osaka, Synthesis of bioactive PMMA bone cement via modification with methacryloxy propyltri-methoxysilane and calcium acetate, J. Mater. Sc. Mat. Med., 2005; 16(8): 713-718

96. T. Sukeoka, M. Suzuki, C. Ohtsuki, A. Sugino, Y. Tsuneizumi, J. Miyagi, K. Kuramoto, H. Moriya, mechanical and histgological evaluation of a PMMA-based bone cement modified with gamma-methacryloxypropyltrimethoxysilane and calcium acetate, Biomaterials, 2006; 27(21): 3897-903

97. H. K. Varma, K. Sreenivasan, Y. Yokogawa, A. Hosumi, *In vitro* calcium phosphate growth over surface functionalised PMMA film, Biomaterials, 2003; 24: 297-303

98. Porous composite materials, United States Patent 6867240

99. M. Abboud, L. Casaubieilh, F. Morvan, M. Fontanille, E. Duguet, PMMA-based composite materials with reactive ceramic fillers: IV. Radiopacifying particles embedded in PMMA beads for acrylic bone cements, J. Biomed. Mater. Res., 2000; 53(6): 728-736

100. P. Li, C. Ohtusuki, T. Kokubo, T. K. Nakanishi, N. Soga, T. Nakamura, T. Yamamuro, Process of formation of bone like apatite layer on silica gel, J. Mater Sci., mater. Med., 1993; 4: 127-131

101. M. R. Mucalo, Y. Yokogawa, M. Suzuki, Y. Kawamoto, F. Nagata, K. Nishizawa, Growth of calcium phosphate on ion exchange resins presaturated with calcium or hydrogenphosphate ions: an SEM-EDX and XPS study, J. Mater Sci. Mater Med, 1995; 6: 409-419

102. H. K. Varma, Y. Yokogawa, E. F. Espinosa, Y. Kawamoto, K. Nishizawa, F. Nagata, T. Kameyama, *In vitro* calcium phosphate growth over functionalized cotton fibres, J. Mater. Sci. Mat. Med., 1999; 10: 395-400

103. K. Hato, T. Kokubo, T. Nakamura, T. Yamamura, Growth of a bone like apatite layer on a substrate by a biomimetic process, J. Am Ceram Soc, 1995; 78(4): 1049-1053

104. C. Ohtsuki, T. Miyazaki and M. Tanihara , Development of bioactive organic–inorganic hybrid for bone substitutes, Materials science and Engineering C, 2002; 22(1): 27-34

105. Y. Abe, T. Kokubo, T.Yamamura, Apatite coating on ceramics, metal and polymers utilizing a biological process, J Mater Sci Mat Med, 1990; 1: 233-238

106. T. Sakaguchi, T. Hirokoshi, A. Nakajima, Adsorption of uranium by chitin phosphate and chitosan phosphate, Agric Biol Chem 1981; 45 (10): 2191-2195

107. M. R. Mucalo, Y. Yokogawa, M. Toriyama, T. Suzuki, Y. Kawamoto, F. Nagata and K. Nishizawa, J. Mater. Sci. Mater. Med. 1995; 6: 597-582

108. H.K. Varma, Y. Yokogawa, E. F. Espinosa, Y. Kawamoto, K. Nishizawa, F. Nagata, T. Kameyama, Porous calcium phosphate coating over phosphorylated chitosan film, Biomaterials, 1999; 20: 879-884

109. S. Li, Q. Liu, J. de Wijn, J. Wolke, B. Zhou, K. de Groot, In vitro apatite formation on phosphorylated bamboo, J. Mater. Sci. Mater. Med., 1997; 8: 543-549

110. M. Suzuki, T. Yoshida, S. Kobayashi, T. Koyama, M. Kimura, K. Hanabusa, H. Shirai, Proton conduction in new polymer hydrogel films consisting of cross-linking partially phosphorylated poly(vinyl alcohol), Phys. Chem. Chem. Phys., 1999; 1: 2749-2753

111. P. L. Granja, L. Pouysegu, D. Deffieux, G. Daude, B. De Jeso, C. Labrugere, C. Baquey, M. A. Barbosa, Cellulose phosphates as Biomaterials. II. Surface chemical modification of regenerated cellulose hydrogels, J. Appl. Polym Sci, 2001; 82: 3354-3365

112. P. L. Granja, B. De Jeso, R. Bareille, F. Rouais, C. Baquey, M. A. Barbosa, Cellulose phosphates as biomaterials. *In vitro* biocompatibility studies, Reactive and Functional polymers, 2006; 66: 728-739

113. R.E. Ferrel, H. S. Olcott, H. Fraenkel-Conrat, Phopshorylation of proteins with phosphoric acid containing excess phosphorous pentoxide, Journal of the American Chemical Society, 1948; pp: 2101

114. CMW1 Radiopaque bone cement instruction leaflet, DePuy, Johnson and Johnson, England

115. I. P. Montheard, J. Kahovec and D. Chappard, Homopolymers and copolymers of 2-hydroxyethyl methacrylate for biomedical applications, in *Desk reference of Functional polymers: Synthesis and Applications*, Ed: R. Arshady, Americal Chemical society, 1997,Washington, DC

116. O. Wichterle, D. Lim, Hydrophilic gels for biological use, Nature, 1960; 185: 117-118

117. H. S. Bennet, A. D. Wyricks, S. W. Lee, H. J. Mc Neil, Science and art in preparing tissues embedded in plastic for light microscopy, with special reference to glycol methacrylate, glass knives and simple stains, Stain Technol., 1976; 51: 71-97

118. S. Uno, E. Asmussen, Marginal adaptation of restorative resin polymerized at reduced rate Acta Odontol. Scand., 1991; 49: 297-300

119. T. Seki, K. Sugibayashi, K. Juni, Y. Monimoto, Percutaneous absorption enhancer applied to membrane permeation-controlled transdermal delivery of nicardipine hydrochloride, Drug Des Delivery, 1989; 4: 69-71

120. I. Cifkova, E. Brynda, R. Holusa, M. Adam, Calcification of poly(2-hydroxyethyl methacrylate)-collagen composites implanted in rats, Biomaterials, 1987; 8: 30-34

121. R. Menace, C. Skorpik, M. Juchem, W. Scheidel, R. Schranz, J. Cataract Refract. Surg., 1989; 15: 264-268

122. J. Kopecek, J. Jokl, D. Lim, Mechanism of Three-Dimensional Polymerization of Glycol Methacrylates, J. Appl. Polym Sci. part C, 1968; 16: 3877-3881

123. A. G. Casella Farbwerke Mainkur, Dutch Patent 6603510, 1966, Chem. Abstr. 1967; 66: 55-59

124. R. Z. Greenley, An expanded listing of revised Q and e values, J. Macromol. Sci. Chem, 1980; 14A: 427-431

125. I. K. Varma, S. Patnaik, Copolymerization of 2-Hydroxyethyl Methacrylate with Alkyl Acrylates, Eur. Polym. J. 1976; 12: 259-263

126. C. H. Crooks, J. A. Douglas, R. L. Broughton, M.V. Seflon, Microencapsulation of mammalian cells in a HEMA-MMA copolymer: Effects on capsule morphology and permeability, J. Biomed. Mat. Res. 1990; 24(9): 1241-1262

127. G. D. M. Wells, N. M. Fisher, M.V. Sefton, Biomaterials, 1993; 14(22); 615-620

128. M. Feng and M. V. Sefton, Hydroxyethyl methacrylate–methyl methacrylate (HEMA–MMA) copolymers for cell microencapsulation: Effect of HEMA purity, J. Biomaterials: Polymer ed. 2004; 11(5): 537-545

129. C. D. Vianna-Soares, C. Kim, M.R. Borenstein, HEMA/MMA/ EGDMA packing material evaluation for size exclusion chromatography (SEC), Materials research, 2005; 8: 1

130. C. D Vianna-Soares, Kim C.J., Borenstein M R, J. Porous mater: 2002; 9: 67-75

131. B.M. Pogell, A new synthesis of fructose-l-phosphate with phosphorus pentoxide, Journal of Biological Chemistry, 1953, 645-650

132. J. D. H Strickland and T. R. Parsons, Determination of reactive phosphorus. In: *A Practical Handbook of Seawater Analysis*. Fisheries Research Board of Canada, Bulletin, 1968; 167, 49–56

133. D. Benayahu, I. Shur, R. Marom, I. Meller, J. Issakov, Cellular and molecular properties associated with osteosarcoma cells, J. Cell. Biochem. , 2002; 84 (1): 108-114

134. D. F. Williams, Techniques of biocompatibility testing, vol. 1, Ed. CRC press, 1986, Page: 48-51

135. J. D. Bancroft and M. Gamble, Theory and Practice of histological techniques, Churchill Livingstone, Edinburgh. 5th Ed., 2002

136. C. Maniatopoulos, D. A. Deport and A. Melcher, An Improved method for preparing histological section of metallic implants, International Journal of Oral and Maxillofacial implants, 1986; 15: 193-196

137. J. A. Brydson, Plastic materials, 7th Ed. Butterworth, 1999, pp: 59

138. Sartomer application bulletin: Glass transition temperature of sartomer products, Oaklands Corporate Center, 502 Thomas Jones Way, Exton, PA 19341

139. M. S. Choudhary, I. K. Varma, Thermal behaviour of 2-hydroxyethyl methacrylate - methyl methacrylate- copolymers, Angewandte Makromolekulare Chemie, 2003; 87(1): 75-85

140. N. A. Peppas, B. D. Barr-Howell, In Hydrogels in Medicine and Pharmacy: Fundamentals; N. A. Peppas, Ed.; CRC Press: Boca Raton, FL, 1986; Vol. I

141. A. V. Tobolsky, Stress Relaxation and Dynamic Properties of Polymers, Textile Research Journal, 1951; 21(6): 404-411

142. J. M. Tan, An Overview of PHEMA Properties, Applications, and Future Progress, Biomaterials, 2000; 4: 24

143. D. J. Aaunkia and P. M. A. Sherwood, Valance band X-ray photoelectron spectroscopic studies of vanadium phosphate and the formation of oxide –free phosphate films on metallic vanadium, J. Vacuum Sci. and Tech A: Vacuum, Surfaces and Films, 2003; 21(4): 1133-1138

144. B. D. Ratner, P. K. Weathersby, A. S. Hoffman, M. A. Kelly, L. H. Scharpen, Radiation-grafted hydrogels for biomaterial applications as studied by the ESCA technique, J. Apl. Polym. Sci., 1978; 22 (3): 643-664

145. M. Yamaguchi, Rheological properties of linear and crosslinked polymer blends: Relation between crosslink density and enhancement of elongational viscosity, J Polym Sci B: Polym Phys 39: 228-235, 2001

146. P. Zhu, Y. Masuda and K. Koumoto, The effect of surface charge on hydroxyapatite nucleation, 2004; 25(17): 3915-39-21

147. S. Mann, 'Biomimetic materials chemistry', John Wiley and Sons,1997

148. J. Chandrasekhar and W. L. Jorgansan, The nature of dilute solutions of sodium ion in water, methanol, and tetrahydrofuran, The Journal of Chemical Physics, 1982, 77(10): 5080-5089

149. L. Hermitte, F. Thomas, R. Bougaran, C. Martelet, Contribution of the comonomers to the bulk and surface properties of methacrylate copolymers, J Colloid Interface Sci. 2004 Apr 1; 272(1): 82-89

150. X. Liu, C. Ding Reactivity of plasma sprayed wollastonite in simulated bodyfluid. J Biomed Mater Res 2002; 59(2): 259–64

151. G. K. Hunter, and H. A. Goldberg, Modulation of crystal formation by bone phosphoproteins: role of glutamic acid-rich sequences in the nucleation of hydroxyapatite by bone sialoprotein, Biochem. J. 1994; 302: 175-179

152. D. H. Schlesinger and D. I. Hay, Complete covalent structure of statherin, a tyrosine-rich acidic peptide which inhibits calcium phosphate precipitation from human parotid saliva, J. Biol. Chem., 1977; 252: 1689-1695

153. H. H. Li, S. R. Pollack, P. Ducheyne, Temporal zeta potential variations of 45S5 bioactive glass immersed in an electrolyte solution, J. Biomed Mater. Res., 2000; 51(1): 80-87

154. E. C. Moreno, T. M. Gregory, W. E. Brown, J. Res. Natl. Bur. Stand. 1968; 72A: 773-787

155. G. H. Nancollas, M. S. Mohan, Arch. Oral Biol. 1970; 15: 731-745

156. N.C. Blumenthal, A.S. Posner, Calcif. Tissue Res. 1973; 13: 235-243

157. E.D. Eanes, Calcif. Tiss. Res. 1976; 20: 75-89

158. P. Calvert, Biomimetic Mineralization in and on Polymers, Chem. Mater. 1996; 8: 1715-1727

159. N. Eliaz, M. Eliyahu, Electrochemical processes of nucleation and growth of hydroxyapatite on titanium supported by real-time electrochemical atomic force microscopy, 2006 Wiley Periodicals, Inc. J Biomed Mater Res, 2007; 80A: 621–634

160. I. A. Aksay, M. Trau, S. Manne, I. Honma, N. Yao, L. Zhou, P. Fenter, P.M. Eisenberger, S.M. Gruner, Biomimetic pathways for assembling inorganic thin films, Science, 1996; 273: 892–898

161. M. J. Dalby, M. O. Riehle, D. S. Sutherland, H. Agheli and A. S. G. Curtis, Morphological And Microarray Analysis Of Human Fibroblasts Cultured On Nanocolumns Produced By Colloidal Lithography, European Cells and materials, 2 0 0 5; 9: 1 - 8

162. J. M. Rice, J. A. Hunt, J. A. Gallagher, P. Hanarp, D.S. Sutherland, J. Gold, Quantitative assessment of the response of primary derived human osteoblasts and macrophages to a range of nanotopography surfaces in a single culture model *in vitro*, Biomaterials, 2003; 24: 4799-4818

163. A. S. Andersson, F. Bäckhed, A. von Euler, A. Richter-Dahlfors, D. S. Sutherland, B. Kasemo, Nanoscale features influence epithelial cell morphology and cytokine production, Biomaterials, 2003a; 24: 3427-3436

164. M. J. Dalby, M. O. Riehle, D. S. Sutherland, H. Agheli, A.S.G. Curtis Changes in fibroblast morphology in response to nano-columns produced by colloidal lithography, Biomaterials, 2004c, 25: 5415-5422

165. M. J. Dalby, S. J. Yarwood, M. O. Riehle, H. Johnstone, S. Affrossman S, ASG Curtis, Increasing fibroblast response to materials using nanotopography: Morphological and genetic measurements of cell response to 13 nm high polymer demixed islands. Exp Cell Res, 2002c 276: 1-9

166. K. Ogata, S. Imazato, A. Ehara, S. Ebisu, Y. Kinomoto, T. Nakano, Y. Umakoshi, Comparison of osteoblast responses to hydroxyapatite and hydroxyapatite soluble calcium phosphate composites, J. Biomed. Mater. Res. 2005; 72A: 127-135

167. D. D. Deligianni, N. D. katsala, P. G. Koutsoukos, Y. F. Missirlis, Effect of surface roughness of hydroxyapatite on human bone marrow cell adhesion, proliferation, differentiation and detachment strength, Biomaterials, 2001; 22: 87-96

168. K. Hatano, H. Inoue, T. Kojo, T. Matsunaga, T. Sujisawa, C. Uchiyama, Y. Uchida, Effect of surface roughness on proliferation and alkaline phosphatase expression of rat calvarial cells cultures on polystyrene, Bone, 1999; 25: 439-445

169. M. Lampin, C. Warocquier, C. Legris, M. Degrange, M. F. Sigot-Luizard, Correlation between substratum roughness and wettability, cell adhesion and cell migration, J. Biomed. Mat. Res., 1997; 36: 99-108

170. A. Harris, Behaviour of cultured cells on substrata of variable adhesiveness, EXP. Cell. Res. 1973; 77: 285-297

171. P. C. Letourmeau, Cell-to-substratum adhesion and guidance of axonal eleongation, Dev. Biol. 1975; 44: 92-101

172. K. D. Chesmel, C. C. Clark, C. T. Brighton and J. Black, Cellular responses to chemical and morphologic aspects of biomaterial surfaces II, The biosynthetic and migratory response of bone cell populations, J. Biomed. Mater. Res. 1995; 29: 1101-1110

173. D. Riveline, E. Zamir, N. Q. Balaban, U. S. Schwarz, T. Ishizaki, S. Narumiya, Z. Kam, B. Geiger and A. D. Bershadsky, Focal Contacts as Mechanosensors: Externally Applied Local Mechanical Force Induces Growth of Focal Contacts by an mDia1-dependent and ROCK-independent Mechanism, The Journal of Cell Biology, 2001; 153(6): 1175-1186

174. M. J. Dalby, L. Di Silvio, E. J. Harper, W. Bonfield, Increasing hydroxyapatite incorporation into poly(methylmethacrylate) cement increases osteoblast adhesion and response, Biomaterials, 2002; 23(2): 569-576

175. M. Yamauchi, T. Yamaguchi, H. Kaji, T. Sugimoto and K. Chihara, Involvement of calcium-sensing receptor in osteoblastic differentiation of mouse MC3T3-E1 cells, Am J Physiol Endocrinol Metab, 2005; 288: 608-616.

176. Y. Takuwa, Y. Ohune, N. Takuwa, K. Yamashita, Endothelin-1 activates phospholipase C and mobilizes Ca2+ from extra and intracellular pools in osteoblastic cells, Am. J. Physiol, 1989; 257 E: 797-803

177. I. A. Silver, J. Deas, M. Erecinska, Interaction of bioactive glasses with osteoblasts *in vitro*: Effects of 45S5 Bioglass, and 58S and 77S bioactive glasses on metabolism, intracellular ion concentrations and cell viability, Biomaterials, 2001; 22: 175-185

178. E. A. Cowles, M. E. DeRome, G. Pastizzo, L. L. Brailey, G. A. Gronowicz, Mineralization and expression of matrix proteins during *in vivo* bone development, Calcif. Tissue Int., 1998; 62: 74-82

179. J. Y. Martin, Z. Schwartz, T. W. Hummert, Effect of surface roughness on proliferation, differentiation and protein synthesis of human osteoblast like cells (MG63), J. Biomed. Mater. Res., 1995; 29: 389-401

180. K. Anselme, Osteoblast adhesion on biomaterials, Biomaterials, 2000; 21: 667-681

181. G. R. Beck, E.C. Sullivan, E. Moran, B. Zerler, Relationship between alkaline phosphatase levels, osteopontin expression and mineralization in differentiating MC3T3-E1 osteoblasts, J. Cell Biochem, 1998; 68: 269-280

182. J. E. Aubin, F. Liu, L. Malaval, A. K. Gupta, Osteoblast and chondroblast differentiation, Bone, 1995; 17 (2 Suppl): 77S-83S

183. L. Malaval, F. Liu, P. Roche, J. E.Aubin, Kinetics of osteoprogenitor proliferation and osteoblast differentiation *in vitro*, J. Cell Biochem, 1999; 74: 616-627

184. Y. Zhu, X. Wang, F. Z. Cui, *In Vitro* Cytocompatibility and Osteoinduction of Phosphorylated Chitosan with Osteoblasts, Bioactive and Compatible Polymers, 2003; 18 (5), 375-390

185. E. M. Ooms, J. G. C. Wolke, J. P. C. M. van der Waerden, J. A. Jansen. Trabecular bone response to injectable calcium phosphate (Ca-P) Biomaterials, 2003; 24: 989-100

G. S. SAILAJA

Personal

Permanent Address (Residence)	Jungle House, Manvila, Kulathur P.O Thriruvananthapuram-695 583 Inidia
Date of Birth :	30. 05 1975
e-mail:	sailajags@yahoo.com

Educational Qualifications:

B. Tech Polymer Science and Rubber Technology 1999
Cochin University of Science and Technology, Kochi, India

M. Tech Polymer Technology 2001
Cochin University of Science and Technology, Kochi, India

ACADEMIC DISTINCTIONS

- **Second prize- Best poster award** in the **Indo-Australian conference** on Biomaterials, Implant devices, Tissue engineering and Regenerative Medicine **BITE and RM-2007** January **2007**

- **Best paper award** in the **National conference** on Ceramic materials for medical applications, held at Indian Institute of Technology Chennai, September, **2005**

- **Best poster presentation award** in **Indo-Australian conference** on Biomaterials, Implant devices and Tissue engineering, **BITE-2005** January **2005**

- **First** in the All India examination on Biomaterials, held by Society for Biomaterials and Artificial organs, (SBAOI, India) in January **2005**

- **Associate membership,** Society of Biomaterials and Artificial Organs, India, **2005**

- **Young scientist award** for the best paper in ***Health science*** section, in **Kerala Science congress,** January **2004**

- **Senior Research Fellowship,** Council of Scientific and Industrial Research, Govt. of India **(CSIR) 2002**

- **SCTIMST Fellowship,** Sree Chitra Tirunal Institute for Medical Sciences and Technology **2001**

- **First Rank, M. Tech** Polymer Technology, Cochin University of Science and Technology **2001**

- **Book chapters**

---

1. **G.S. Sailaja,** T.V. Kumari, Yoshiyuki Yokogawa, H.K. Varma, ***In*** *Vitro* Mineralization and Cell Adhesion on Surface Modified Poly (2 - hydroxy ethyl methacrylate-co-methyl methacrylate, **Bioceramics 18**, p.493

- **Journal articles**

---

1. **G.S. Sailaja**, P Ramesh, H.K. Varma, Hydroxyapatite mouldable formulations using Natural rubber latex as a binder, ***J. Biomedical materials research, part B*, Applied Biomaterials** (online: 20, Dec, 2006)

2. **G.S. Sailaja**, P Ramesh, T.V.Kumary, H.K. Varma, Human osteosarcoma cell adhesion behaviour on hydroxyapatite integrated chitosn- poly(acrylic acid) polyelectrolyte complexes, ***Acta Biomaterialia***, 2, 2006, 651-657

3. **G.S. Sailaja**, P Ramesh, T.V.Kumary, H.K. Varma, Biomimetically modified poly(2-hydroxy ethyl methacrylate-co-methyl methacrylate) bone Augmentation ***Trends Biomater. Artif organs***, vol (20) 1, 2006, pp 3-6

4. **G.S. Sailaja**, P Ramesh, T.V.Kumary, H.K. Varma, *In vitro* mineralization and cell adhesion on surface modified poly(2-hydroxy ethyl methacrylate-co-methyl methacrylate), ***Key engineering materials,*** vol. 309-31, 2006, pp 493-496

5. **G.S. Sailaja**, P Ramesh, H.K. Varma, swelling behaviour of hydroxyapatite filled chitosn-poly(acrylic acid) polyelectrolyte complexes, ***J. applied polymer science,*** vol. 100, 2006, 4716-4722

6. **G.S .sailaja**, S. Velayudhan, M. C. Sunny, K. Sreenivasan, H.K. Varma, P. Ramesh, *Hydroxyapatite filled chitosan-poly(acrylic acid) polyelectrolyte complexes*, ***J. Mater. Sci,*** 38 (17) 2003, 3653-3662

- **Conference papers**

---

1. **G.S. Sailaja**, P. Ramesh, K. Sreenivasan, T.V. Kumary and H.K. Varma, *In vitro* calcium phosphate coating on surface functionalized polymer: Ultrastructural and cell adhesion study, Indo-**Australian conference** on Biomaterials, Implant devices, Tissue engineering and Regenerative Medicine, BITE-2007, Jan. 11-13, **2007,** Thiruvananthapuram (received the **Second prize -best poster award**)

2. **G.S. Sailaja**, T.V.Kumary, Y. Yokogawa, H.K. Varma, *in vitro* mineralization and cell adhesion on surface modified poly(2-hydroxy ethyl methacrylate-co-methyl methacrylate), at International conference on ceramics in medicine (**Bioceramics-18**), Dec-6-8**, 2005,** Kyoto, *Japan.*

3. **G.S. Sailaja**, T.V.Kumary, H.K. Varma, Biomimetically modified poly(2-hydroxy ethyl methacrylate-co-methyl methacrylate) bone Augmentation **National conference on Ceramic materials for medical applications**, held at Indian Institute of Technology, Sept 16-17, **2005** Chennai, ,*India* (Received the **best paper award** for scientific content)

4. **G.S. Sailaja**, P. Ramesh, K. Sreenivasan, T.V. Kumary and H.K. Varma, *Biomimetic growth of hydroxyapatite on a novel functionally modified poly(2-hydroxy ethyl methacrylate-co-methyl methacrylate)*, pp. 94-97, **Indo-Australian conference** on Biomaterials, Implant devices and Tissue engineering, BITE-2005, Jan.19-21, **2005,** Thiruvananthapuram (received the **best poster award** in BITE-2005)

5. **G.S. Sailaja**, P. Ramesh, T. V. Kumary, H. K. Varma, *Hydroxyapatite integrated polyelectrolyte complexes for bone regeneration,* page: 321 **7th world biomaterials congress**, 17-21, May **2004**, Sydney, *Australia*

6. **G.S.Sailaja**, P. Ramesh, H. K. Varma, *A novel biodegradable composite system for bone regeneration,* 16th session of **kerala Science Congress**, January 29-31**, 2004** at CWRDM, kozhikode (**best paper award** in the Health science section)

7. **G S Sailaja**, P. Ramesh and H. K. Varma *Synthesis of novel hydroxyapatite microspheres with interconnecting porosity for controlled drug delivery'* by in the **International seminar on Advances in Polymer Technology** – (APT-04) held at Cochin university of science and Technology, Cochin, India during January 16- 17, **2004**

8. **G.S. sailaja**, P Ramesh, H.K. Varma, *Natural rubber latex as a binder for the processing of hydroxyapatite implant materials*, **Indian science congress**, at Bangal Jan 3-7, **2003**

9. **G.S. Sailaja**, P. Ramesh, H.K. Varma *Porous hydroxyapatite microspheres prepared using natural rubber latex as binder*, **Macro-2002**, at IIT Kharagpur, December 9-11, **2002**

- **Other publications**

---

1. R. Sreekumar, **G.S. Sailaja**, H.K. Varma, *Morphological studies of cell adhesion behaviour on hydroxyapatite* [illegible] *egrated polymer composite* **F**[illegible] **lletin**, Vol. 5, No.1, pp 9-12, July **2004**